Titre: Title:	The impact of varying the apex angle on static cone penetration measurements in simulated Champlain clays
Auteur: Author:	Yasser M. H. Fahmy
Date:	1993
Type:	Mémoire ou thèse / Dissertation or Thesis
Référence: Citation:	Fahmy, Y. M. H. (1993). The impact of varying the apex angle on static cone penetration measurements in simulated Champlain clays [Master's thesis, Polytechnique Montréal]. PolyPublie. https://publications.polymtl.ca/57021/

UNIVERSITÉ DE MONTRÉAL

The Impact of Varying the Apex Angle on Static Cone Penetration Measurements in Simulated Champlain Clays

Par

Yasser M. H. FAHMY
DÉPARTEMENT DE GÉNIE CIVIL
ÉCOLE POLYTECHNIQUE

MÉMOIRE PRÉSENTÉ EN VUE DE L'OBTENTION
DU GRADE DE MAÎTRE ÈS SCIENCES APPLIQUÉES (M.Sc.A.)
(GÉNIE CIVIL)
Mars 1993

ISBN 0-315-86457-5

Nom YASSER, M.H. FAHMY

Dissertation Abstracts International est organisé en catégories de sujets. Veuillez s.v.p. choisir le sujet qui décrit le mieux votre thèse et inscrivez le code numérique approprié dans l'espace réservé ci-dessous.

Génie Civil — SUJET

0543 — CODE DE SUJET

U·M·I

Catégories par sujets

HUMANITÉS ET SCIENCES SOCIALES

COMMUNICATIONS ET LES ARTS
Architecture 0729
Beaux-arts 0357
Bibliothéconomie 0399
Cinéma 0900
Communication verbale 0459
Communications 0708
Danse 0378
Histoire de l'art 0377
Journalisme 0391
Musique 0413
Sciences de l'information 0723
Théâtre 0465

ÉDUCATION
Généralités 515
Administration 0514
Art 0273
Collèges communautaires 0275
Commerce 0688
Économie domestique 0278
Éducation permanente 0516
Éducation préscolaire 0518
Éducation sanitaire 0680
Enseignement agricole 0517
Enseignement bilingue et multiculturel 0282
Enseignement industriel 0521
Enseignement primaire. 0524
Enseignement professionnel 0747
Enseignement religieux 0527
Enseignement secondaire 0533
Enseignement spécial 0529
Enseignement supérieur 0745
Évaluation 0288
Finances 0277
Formation des enseignants 0530
Histoire de l'éducation 0520
Langues et littérature 0279
Lecture 0535
Mathématiques 0280
Musique 0522
Orientation et consultation 0519
Philosophie de l'éducation 0998
Physique 0523
Programmes d'études et enseignement 0727
Psychologie 0525
Sciences 0714
Sciences sociales 0534
Sociologie de l'éducation 0340
Technologie 0710

LANGUE, LITTÉRATURE ET LINGUISTIQUE
Langues
- Généralités 0679
- Anciennes 0289
- Linguistique 0290
- Modernes 0291

Littérature
- Généralités 0401
- Anciennes 0294
- Comparée 0295
- Médiévale 0297
- Moderne 0298
- Africaine 0316
- Américaine 0591
- Anglaise 0593
- Asiatique 0305
- Canadienne (Anglaise) 0352
- Canadienne (Française) 0355
- Germanique 0311
- Latino-américaine 0312
- Moyen-orientale 0315
- Romane 0313
- Slave et est-européenne 0314

PHILOSOPHIE, RELIGION ET THÉOLOGIE
Philosophie 0422
Religion
- Généralités 0318
- Clergé 0319
- Études bibliques 0321
- Histoire des religions 0320
- Philosophie de la religion 0322

Théologie 0469

SCIENCES SOCIALES
Anthropologie
- Archéologie 0324
- Culturelle 0326
- Physique 0327

Droit 0398
Économie
- Généralités 0501
- Commerce-Affaires 0505
- Économie agricole 0503
- Économie du travail 0510
- Finances 0508
- Histoire 0509
- Théorie 0511

Études américaines 0323
Études canadiennes 0385
Études féministes 0453
Folklore 0358
Géographie 0366
Gérontologie 0351
Gestion des affaires
- Généralités 0310
- Administration 0454
- Banques 0770
- Comptabilité 0272
- Marketing 0338

Histoire
- Histoire générale 0578
- Ancienne 0579
- Médiévale 0581
- Moderne 0582
- Histoire des noirs 0328
- Africaine 0331
- Canadienne 0334
- États-Unis 0337
- Européenne 0335
- Moyen-orientale 0333
- Latino-américaine 0336
- Asie, Australie et Océanie 0332

Histoire des sciences 0585
Loisirs 0814
Planification urbaine et régionale 0999
Science politique
- Généralités 0615
- Administration publique 0617
- Droit et relations internationales 0616

Sociologie
- Généralités 0626
- Aide et bien-âtre social 0630
- Criminologie et établissements pénitentiaires 0627
- Démographie 0938
- Études de l' individu et de la famille 0628
- Études des relations interethniques et des relations raciales 0631
- Structure et développement social 0700
- Théorie et méthodes. 0344
- Travail et relations industrielles 0629

Transports 0709
Travail social 0452

SCIENCES ET INGÉNIERIE

SCIENCES BIOLOGIQUES
Agriculture
- Généralités 0473
- Agronomie. 0285
- Alimentation et technologie alimentaire 0359
- Culture 0479
- Élevage et alimentation 0475
- Exploitation des pâturages 0777
- Pathologie animale 0476
- Pathologie végétale 0480
- Physiologie végétale 0817
- Sylviculture et faune 0478
- Technologie du bois 0746

Biologie
- Généralités 0306
- Anatomie 0287
- Biologie (Statistiques) 0308
- Biologie moléculaire 0307
- Botanique 0309
- Cellule 0379
- Écologie 0329
- Entomologie 0353
- Génétique 0369
- Limnologie 0793
- Microbiologie 0410
- Neurologie 0317
- Océanographie 0416
- Physiologie 0433
- Radiation 0821
- Science vétérinaire 0778
- Zoologie 0472

Biophysique
- Généralités 0786
- Medicale 0760

SCIENCES DE LA TERRE
Biogéochimie 0425
Géochimie 0996
Géodésie 0370
Géographie physique 0368
Géologie 0372
Géophysique 0373
Hydrologie 0388
Minéralogie 0411
Océanographie physique 0415
Paléobotanique 0345
Paléoécologie 0426
Paléontologie 0418
Paléozoologie 0985
Palynologie 0427

SCIENCES DE LA SANTÉ ET DE L'ENVIRONNEMENT
Économie domestique 0386
Sciences de l'environnement 0768
Sciences de la santé
- Généralités 0566
- Administration des hipitaux 0769
- Alimentation et nutrition 0570
- Audiologie 0300
- Chimiothérapie 0992
- Dentisterie 0567
- Développement humain 0758
- Enseignement 0350
- Immunologie 0982
- Loisirs 0575
- Médecine du travail et thérapie 0354
- Médecine et chirurgie 0564
- Obstétrique et gynécologie 0380
- Ophtalmologie 0381
- Orthophonie 0460
- Pathologie 0571
- Pharmacie 0572
- Pharmacologie 0419
- Physiothérapie 0382
- Radiologie 0574
- Santé mentale 0347
- Santé publique 0573
- Soins infirmiers 0569
- Toxicologie 0383

SCIENCES PHYSIQUES
Sciences Pures
Chimie
- Généralités 0485
- Biochimie 487
- Chimie agricole 0749
- Chimie analytique 0486
- Chimie minérale 0488
- Chimie nucléaire 0738
- Chimie organique 0490
- Chimie pharmaceutique 0491
- Physique 0494
- PolymÇres 0495
- Radiation 0754

Mathématiques 0405
Physique
- Généralités 0605
- Acoustique 0986
- Astronomie et astrophysique 0606
- Électronique et électricité 0607
- Fluides et plasma 0759
- Météorologie 0608
- Optique 0752
- Particules (Physique nucléaire) 0798
- Physique atomique 0748
- Physique de l'état solide 0611
- Physique moléculaire 0609
- Physique nucléaire 0610
- Radiation 0756

Statistiques 0463

Sciences Appliqués Et Technologie
Informatique 0984
Ingénierie
- Généralités 0537
- Agricole 0539
- Automobile 0540
- Biomédicale 0541
- Chaleur et thermodynamique 0348
- Conditionnement (Emballage) 0549
- Génie aérospatial 0538
- Génie chimique 0542
- Génie civil 0543
- Génie électronique et électrique 0544
- Génie industriel 0546
- Génie mécanique 0548
- Génie nucléaire 0552
- Ingénierie des systèmes 0790
- Mécanique navale 0547
- Métallurgie 0743
- Science des matériaux 0794
- Technique du pétrole 0765
- Technique minière 0551
- Techniques sanitaires et municipales 0554
- Technologie hydraulique 0545

Mécanique appliquée 0346
Géotechnologie 0428
Matières plastiques (Technologie) 0795
Recherche opérationnelle 0796
Textiles et tissus (Technologie) 0794

PSYCHOLOGIE
Généralités 0621
Personnalité 0625
Psychobiologie 0349
Psychologie clinique 0622
Psychologie du comportement 0384
Psychologie du développement 0620
Psychologie expérimentale 0623
Psychologie industrielle 0624
Psychologie physiologique 0989
Psychologie sociale 0451
Psychométrie 0632

Name _____

Dissertation Abstracts International is arranged by broad, general subject categories. Please select the one subject which most nearly describes the content of your dissertation. Enter the corresponding four-digit code in the spaces provided.

SUBJECT TERM

SUBJECT CODE

U·M·I

Subject Categories

THE HUMANITIES AND SOCIAL SCIENCES

COMMUNICATIONS AND THE ARTS

Architecture 0729
Art History 0377
Cinema 0900
Dance 0378
Fine Arts 0357
Information Science 0723
Journalism 0391
Library Science 0399
Mass Communications 0708
Music 0413
Speech Communication 0459
Theater 0465

EDUCATION

General 0515
Administration 0514
Adult and Continuing 0516
Agricultural 0517
Art 0273
Bilingual and Multicultural 0282
Business 0688
Community College 0275
Curriculum and Instruction 0727
Early Childhood 0518
Elementary 0524
Finance 0277
Guidance and Counseling 0519
Health 0680
Higher 0745
History of 0520
Home Economics 0278
Industrial 0521
Language and Literature 0279
Mathematics 0280
Music 0522
Philosophy of 0998
Physical 0523
Psychology 0525
Reading 0535
Religious 0527
Sciences 0714
Secondary 0533
Social Sciences 0534
Sociology of 0340
Special 0529
Teacher Training 0530
Technology 0710
Tests and Measurements 0288
Vocational 0747

LANGUAGE, LITERATURE AND LINGUISTICS

Language
- General 0679
- Ancient 0289
- Linguistics 0290
- Modern 0291

Literature
- General 0401
- Classical 0294
- Comparative 0295
- Medieval 0297
- Modern 0298
- African 0316
- American 0591
- Asian 0305
- Canadian (English) 0352
- Canadian (French) 0355
- English 0593
- Germanic 0311
- Latin American 0312
- Middle Eastern 0315
- Romance 0313
- Slavic and East European 0314

PHILOSOPHY, RELIGION AND THEOLOGY

Philosophy 0422
Religion
- General 0318
- Biblical Studies 0321
- Clergy 0319
- History of 0320
- Philosophy of 0322

Theology 0469

SOCIAL SCIENCES

American Studies 0323
Anthropology
- Archaeology 0324
- Cultural 0326
- Physical 0327

Business Administration
- General 0310
- Accounting 0272
- Banking 0770
- Management 0454
- Marketing 0338

Canadian Studies 0385
Economics
- General 0501
- Agricultural 0503
- Commerce-Business 0505
- Finance 0508
- History 0509
- Labor 0510
- Theory 0511

Folklore 0358
Geography 0366
Gerontology 0351
History
- General 0578
- Ancient 0579
- Medieval 0581
- Modern 0582
- Black 0328
- African 0331
- Asia, Australia and Oceania 0332
- Canadian 0334
- European 0335
- Latin American 0336
- Middle Eastern 0333
- United States 0337

History of Science 0585
Law 0398
Political Science
- General 0615
- International Law and Relations 0616
- Public Administration 0617

Recreation 0814
Social Work 0452
Sociology
- General 0626
- Criminology and Penology ... 0627
- Demography 0938
- Ethnic and Racial Studies 0631
- Individual and Family Studies 0628
- Industrial and Labor Relations 0629
- Public and Social Welfare 0630
- Social Structure and Development 0700
- Theory and Methods 0344

Transportation 0709
Urban and Regional Planning 0999
Women's Studies 0453

THE SCIENCES AND ENGINEERING

BIOLOGICAL SCIENCES

Agriculture
- General 0473
- Agronomy 0285
- Animal Culture and Nutrition 0475
- Animal Pathology 0476
- Food Science and Technology 0359
- Forestry and Wildlife 0478
- Plant Culture 0479
- Plant Pathology 0480
- Plant Physiology 0817
- Range Management 0777
- Wood Technology 0746

Biology
- General 0306
- Anatomy 0287
- Biostatistics 0308
- Botany 0309
- Cell 0379
- Ecology 0329
- Entomology 0353
- Genetics 0369
- Limnology 0793
- Microbiology 0410
- Molecular 0307
- Neuroscience 0317
- Oceanography 0416
- Physiology 0433
- Radiation 0821
- Veterinary Science 0778
- Zoology 0472

Biophysics
- General 0786
- Medical 0760

EARTH SCIENCES

Biogeochemistry 0425
Geochemistry 0996
Geodesy 0370
Geology 0372
Geophysics 0373
Hydrology 0388
Mineralogy 0411
Paleobotany 0345
Paleoecology 0426
Paleontology 0418
Paleozoology 0985
Palynology 0427
Physical Geography 0368
Physical Oceanography 0415

HEALTH AND ENVIRONMENTAL SCIENCES

Environmental Sciences 0768
Health Sciences
- General 0566
- Audiology 0300
- Chemotherapy 0992
- Dentistry 0567
- Education 0350
- Hospital Management 0769
- Human Development 0758
- Immunology 0982
- Medicine and Surgery 0564
- Mental Health 0347
- Nursing 0569
- Nutrition 0570
- Obstetrics and Gynecology .. 0380
- Occupational Health and Therapy 0354
- Ophthalmology 0381
- Pathology 0571
- Pharmacology 0419
- Pharmacy 0572
- Physical Therapy 0382
- Public Health 0573
- Radiology 0574
- Recreation 0575
- Speech Pathology 0460
- Toxicology 0383

Home Economics 0386

PHYSICAL SCIENCES

Pure Sciences

Chemistry
- General 0485
- Agricultural 0749
- Analytical 0486
- Biochemistry 0487
- Inorganic 0488
- Nuclear 0738
- Organic 0490
- Pharmaceutical 0491
- Physical 0494
- Polymer 0495
- Radiation 0754

Mathematics 0405
Physics
- General 0605
- Acoustics 0986
- Astronomy and Astrophysics 0606
- Atmospheric Science 0608
- Atomic 0748
- Electronics and Electricity 0607
- Elementary Particles and High Energy 0798
- Fluid and Plasma 0759
- Molecular 0609
- Nuclear 0610
- Optics 0752
- Radiation 0756
- Solid State 0611

Statistics 0463

Applied Sciences

Applied Mechanics 0346
Computer Science 0984
Engineering
- General 0537
- Aerospace 0538
- Agricultural 0539
- Automotive 0540
- Biomedical 0541
- Chemical 0542
- Civil 0543
- Electronics and Electrical 0544
- Heat and Thermodynamics ... 0348
- Hydraulic 0545
- Industrial 0546
- Marine 0547
- Materials Science 0794
- Mechanical 0548
- Metallurgy 0743
- Mining 0551
- Nuclear 0552
- Packaging 0549
- Petroleum 0765
- Sanitary and Municipal 0554
- System Science 0790

Geotechnology 0428
Operations Research 0796
Plastics Technology 0795
Textile Technology 0994

PSYCHOLOGY

General 0621
Behavioral 0384
Clinical 0622
Developmental 0620
Experimental 0623
Industrial 0624
Personality 0625
Physiological 0989
Psychobiology 0349
Psychometrics 0632
Social 0451

UNIVERSITÉ DE MONTRÉAL

ÉCOLE POLYTECHNIQUE

Ce mémoire intitulé:

The Impact of Varying the Apex Angle
on Static Cone Penetration Measurements
in Simulated Champlain Clays

présenté par: Yasser M.H. FAHMY
en vue de l'obtention du grade de:
Maître ÈS Sciences Appliquées (M.Sc.A)
a été dûment accepté par le jury d'examen constitué de :

M. LAFLEUR Jean, Ph.D., président
M. SILVESTRI Vincent, Ph.D., membre et directeur de recherche
M. SOULIÉ Michel, D.Sc.A., membre

SOMMAIRE

A cause de son utilité in-situ, l'essai de pénétration au cône statique a gagné un grand intérêt en Amérique du Nord au cours de ces dernières années. Ainsi, actuellement, des recherches intensives sont effectuées dans le but d'élucider le phénomène de pénétration. Dans ce cadre, la présente étude se penche sur la variation de l'angle de pointe du cône en fonction des mesures de pénétration statique. Cette recherche est essentiellement un travail expérimental effectué au laboratoire sur un type d'argile rencontré fréquemment à l'Est du Canada, soit l'argile de la mer Champlain. Comme le prélèvement de gros échantillons naturels de l'argile de la mer Champlain entraînerait des problèmes techniques aussi bien que financiers, un matériau artificiel a été employé dans les essais. La composition de ce matériau est déterminée à partir d'une courbe de conception de mélange tout en permettant un contrôle sur la résistance au cisaillement non drainé du matériau. La présente étude examine la possibilité d'utiliser un tel matériau dans les analyses des tests de pénétration effectuées au laboratoire. Le matériau développé pourrait servir de moyen pour les chercheurs dans les travaux ultérieurs en Géotechnique qui concernent l'argile de la mer Champlain.

En se basant sur les mesures du laboratoire utilisant des cônes avec des angles qui varient de 7.5° à 180°, on remarque d'une part que les cônes aigus ont une faible résistance de pénétration tandis que les plus obtus ont une résistance plus élevée. D'autre part, on détermine la relation entre le facteur du cône et l'angle de pointe. Cette relation montre une corrélation proportionnelle, c'est-à-dire, que le facteur du cône augmente avec l'augmentation de l'angle de pointe, indépendamment de la profondeur. Ainsi, une simple courbe a été construite et pourrait être utilisée pour déterminer le facteur du cône à des profondeurs qui varient de 10 à 70 centimètres, pour un angle de cône donné. Les résultats de la présente analyse ont été comparés avec des travaux théoriques pertinents, ainsi que des mesures rapportées in-situ. Les développements atteints dans cette études éclaircissent, en général, le phénomène de pénétration dans les sols ainsi que l'interaction sol-pénétromètre et, en particulier, la pénétration du cône dans les argiles de la mer Champlain.

ABSTRACT

In recent years, the static cone penetration test has gained a broad recognition in North America as a useful in-situ test. Extensive research is currently being carried out aiming at elucidating the penetration phenomena. Along this line of research, the present study investigates the impact of varying the cone apex angle on static penetration measurements. The research is mainly a laboratory experimental work concerning a type of clay often encountered in Eastern Canada, namely Champlain clay. In order to reduce the high expense and the difficulties associated with large-scale sampling of natural Champlain clays, a common simulated material is used in the experimental work. The composition of the simulated material is determined based on a mix design chart developed to allow control over the strength of the simulated material. The study examines the possibility of using such simulated material in laboratory analysis of penetration tests. Such material could provide a means for researchers to facilitate further geotechnical engineering studies on Champlain clays.

Based on the laboratory measurements using cones with angles varying from 7.5° to 180°, it is shown that sharp cones have low penetration resistance while blunter ones exert higher resistance. The relationship between the cone factor and the apex angle is also determined from the laboratory measurements. This relationship exhibits a directly proportional correlation, namely the cone factor increases with increasing the apex angle, irrespective of depth. A simple chart is prepared and can be used to determine the cone factor for depths varying from 10 to 70 centimeters, given a specified apex angle. The results of the present analysis are compared with both pertinent theoretical work and reported field measurements. The developments made in this study shed more light on the penetration phenomena in soils and the soil-indenter interaction, in general, and cone penetration in Champlain clays, in particular.

RÉSUMÉ

GÉNÉRAL

Depuis son introduction dans les années 30, l'essai au pénétromètre statique a été largement utilisé pour la reconnaissance des sols en Europe (De Ruiter, 1971). Il est aussi appelé essai de pénétration statique, essai au cône hollandais, ou bien sondage profond hollandais. Malgré que l'essai pénétromètrique a été introduit depuis un demi siècle, sa popularité est restée pour longtemps limitée à quelques pays comme la Hollande et la Belgique (De Ruiter, 1981). Cependant, dans la dernière décennie, l'essai de pénétration au cône statique a gagné une approbation rapide dans le monde entier et, en particulier, en Amérique du Nord. Cette reconnaissance est due non seulement à son efficacité dans l'établissement du profil des sols in-situ, mais aussi à sa rapidité et à son coût peu élevé comparativement avec d'autres essais in-situ (Schmertmann, 1975).

L'essai de pénétration statique a été prouvé efficace pour l'identification préliminaire de profil des sols (Baligh et al., 1980, et Sanglerat, 1972). Récemment, plusieurs chercheurs ont réussi à établir des corrélations qui relient

les mesures de pénétration avec les principaux paramètres du sol, y compris la résistance au cisaillement non drainé de l'argile (Robertson et Campanella, 1983, Houlsby et Wroth, 1982, Lunne et al., 1976, Amar et al., 1975, Roy et al., 1974, et La Rochelle et al., 1973). Ces corrélations ont considérablement contribué à l'utilité de l'essai de pénétration au cône (Lunne et Kleven, 1981). Parmi les paramètres importants qui affectent les mesures de l'essai de pénétration au cône, on trouve l'angle de la pointe du cône. Malgré son importance, ce thème n'a pas été suffisamment traité dans les recherches antérieures.

En 1967, Ladanyi a développé une importante théorie appelée la théorie de l'expansion de cavité. L'avantage principal de cette théorie est qu'elle tient compte des caractéristiques de déformation actuelle du matériau pénétré. Bien que la théorie ait ses propres applications dans l'interprétation de l'essai de pénétration profonde dans les argiles sensibles (Ladanyi et Eden, 1969), la divergence existant entre les résultats obtenus à partir de cette théorie et ceux obtenus au chantier nécessite d'être étudiée. Le travail de recherche mené par Houlsby et Wroth (1982) sur la pénétration du cône dans les sols cohérents est une autre analyse théorique. Leur solution numérique tient compte, entre autres, de la variation de l'angle de pointe du cône.

Malgré qu'elle soit intéressante du point de vue analytique, leur analyse a quelques limitations:

- L'analyse emploie le théorème de la limite inférieure de la théorie de plasticité. Le théorème est surtout applicable aux matériaux rigides-plastiques; dans le cas des matériaux qui possèdent des propriétés elasto-plastiques, les déformations pourraient devenir importantes avant que la limite inférieure soit atteinte.
- L'analyse est appropriée pour des pénétrations par des pénétromètres près de la surface du sol, dont la profondeur ne dépasse pas 20 fois le diamètre.
- Les résultats de l'analyse doivent être validés par des travaux expérimentaux.

Afin de surmonter ces limitations, la présente recherche expérimentale étudie principalement l'effet de la variation de l'angle de pointe du cône sur la résistance à la pénétration statique profonde dans les argiles sensibles.

CHAMP ET OBJECTIFS DE L'ÉTUDE

La résistance au cisaillement est considérée comme une des importantes propriétés géotechniques de l'argile. Le terme "résistance" a été utilisé dans différentes terminologies liées au cisaillement, y compris la résistance au cisaillement au pic, la résistance au cisaillement

résiduelle, la résistance de fluage, et les résistances au cisaillement drainé et non drainé. La présente recherche est consacrée à l'étude de la résistance au cisaillement au pic sous des conditions non drainées.

La présente recherche a pour but d'étudier l'effet de la variation de l'angle à la pointe du cône sur la résistance à la pénétration quasi-statique. L'étude porte sur un type d'argile, souvent rencontré à l'Est du Canada, connu sous le nom d'argile de la mer Champlain, et caractérisé par une structure très fragile et une déformation extrêmement sensible.

Afin d'étudier le problème de pénétration dans les argiles de la mer Champlain, une série d'essais a été effectuée au laboratoire sur une argile reconstituée. Cette argile a été choisie par rapport à une argile naturelle pour éviter les dépenses impliquées dans l'acquisition de blocs d'argile naturelle et surmonter les problèmes de manipulation.

Les objectifs de la présente étude sont résumés comme suit:

1. développer un matériau artificiel qui simule l'argile de la mer Champlain avec ses composantes déterminées en fonction

de la résistance désirée. Un tel matériau facilite le travail expérimental au laboratoire.

2. étudier l'impact de la variation de l'angle à la pointe du cône sur les mesures de pénétration statique dans le matériau développé. Et, par la suite, déterminer une corrélation entre le facteur du cône et l'angle à la pointe, à différentes profondeurs.

3. comparer les résultats du facteur du cône obtenus à ceux rapportés dans la littérature.

PLAN DE L'ÉTUDE

Afin de mener à bien la présente recherche, le plan d'étude suivant a été établi:

1. Au chapitre 2, une revue bibliographique des travaux antérieurs a été menée afin d'étudier les paramètres qui contrôlent le phénomène de pénétration.

2. Au chapitre 3, le matériau modèle a été développé en modifiant les composantes de l'argile de la mer Champlain reconstituée. Cela permet de déterminer le mélange de l'argile reconstituée pour n'importe quelle résistance donnée.

3. Au chapitre 4, les essais de pénétration au laboratoire ont été mis en place par la préparation de l'argile de la mer Champlain reconstituée, et l'installation de l'essai de pénétration au cône quasi-statique. D'autres essais auxiliaires ont été effectués au laboratoire, dont l'essai au scissomètre et l'essai de compression simple. Les mesures expérimentales sont présentées dans ce chapitre.

4. Au chapitre 5, les mesures obtenues au laboratoire ont été analysées afin d'évaluer l'effet de la variation de l'angle à la pointe sur la résistance du cône. Les résultats de ces analyses ont été comparés à ceux des travaux antérieurs et à des mesures in-situ.

5. Au chapitre 6, des conclusions ont été tirées de la présente recherche et des recommandations sont présentées pour des études ultérieures.

CONCLUSIONS

La présente recherche a permis de mieux comprendre le phénomène de pénétration dans les argiles d'où on peut tirer les conclusions suivantes:

1. Mise en place d'une argile reconstituée de la mer Champlain à résistance contrôlée. Le matériau artificiel ne

coute pas cher et il est facilement maniable au laboratoire, ce qui facilite davantage les études géotechniques sur les argiles de la mer Champlain.

2. Développement des courbes qui présentent le facteur du cône en fonction de la variation de l'angle à la pointe, à différentes profondeurs de pénétration.

3. La présente étude éclaircit de plus le problème d'interaction sol-pénétromètre et celui de la pénétration du cône dans les argiles de la mer Champlain.

En se basant sur les résultats de la présente étude, les recommandations suivantes sont suggérées:

- Le matériau modèle utilisé pourrait être examiné de plus près afin d'établir son utilisation dans d'autres études géotechniques sur les argiles de la mer Champlain.
- Des mesures actuelles d'essai de pénétration au cône quasi-statique avec différents angles à la pointe pourraient être effectuées au chantier pour confirmer les mesures de laboratoire.
- Le développement d'une théorie plus détaillée pour élucider le phénomène de pénétration pourrait minimiser la divergence existant entre les résultats théoriques et les mesures réelles.

ACKNOWLEDGEMENTS

I wish to express my deepest gratitude and sincere appreciation to my supervisor Dr. V. Silvestri for his academic as well as financial support, valuable advice, and constructive guidance throughout all the stages of the present study.

I would like to take this opportunity to thank the professors of the Geotechnical Engineering Section for their valuable discussions and encouragement during the course of this research.

I am truly grateful to my colleagues for their constructive criticism and helpful advice throughout this study.

I also would like to thank the staff of the Geotechnical Engineering as well as the Structural Engineering Laboratory for their assistance during the experiments of this research.

TABLE OF CONTENTS

LIST OF FIGURES

LIST OF TABLES

LIST OF APPENDICES

LIST OF PHOTOGRAPHS

CHAPTER 1

INTRODUCTION

1.1 GENERAL

Since its introduction in the 1930's, the penetrometer test has been used extensively, and in many cases exclusively, for field investigations in Europe (De Ruiter, 1971). It is also referred to as the static penetration test, the Dutch cone test, or the Dutch deepsounding. Although the method was introduced nearly half a century ago, its popularity remained for a long time limited to a small number of countries such as Holland and Belgium (De Ruiter, 1981). In the past decade, however, the static cone penetration test has gained rapid acceptance all over the world, especially in North America. This recognition is due not only to its efficiency in establishing the soil profile at a site, but also to its relative rapidity and cheapness as compared to other in-situ tests (Schmertmann, 1975).

The static cone penetration test has proved to be valuable for soil profiling, as the soil type can be identified from the test measurements (Baligh et al., 1980, and Sanglerat, 1972). Important advances have recently been

made to correlate the penetrometer measurements with the main soil parameters, including the undrained shear strength of clay (Robertson and Campanella, 1983, Houlsby and Wroth, 1982, Lunne et al., 1976, Amar et al., 1975, Roy et al., 1974, and La Rochelle et al., 1973). Such correlations have greatly contributed to the usefulness of the cone penetration test (Lunne and Kleven, 1981). Among many factors affecting the measurements of the cone penetration test, there is the apex angle of the cone. This topic, in spite of its importance, has not been covered sufficiently in previous research work.

An important theory was developed by Ladanyi in 1967, namely the cavity expansion theory. The main advantage of this theory is that it takes into account the actual deformation characteristics of the indented material. Although the theory has its own applications in the interpretation of deep penetration test in sensitive clays (Ladanyi and Eden, 1969), the existing discrepancy between the results obtained from the theory and those obtained in field need to be more investigated. The research work carried out by Houlsby and Wroth (1982) is another theoretical analysis of cone indentation in cohesive soils. Their numerical solution considers, among others, the variation of the cone apex angle. In spite of being interesting from the

analytical point of view, their analysis has some limitations:

- The analysis uses the lower bound theorem of plasticity theory. The theorem applies directly to rigid-plastic materials; for materials with elastic-plastic properties the strains may become large before the lower bound is reached.
- The analysis is appropriate for indentation by penetrometers near the surface of a soil. The depth-to-diameter ratios considered are up to only 20.
- The results of the analysis need to be validated by conducting experimental works, for example.

In order to overcome such limitations, the present laboratory experimental study focuses on the subject of apex angle variation and its influence on the measurements of deep static cone penetration test in sensitive clays.

1.2 SCOPE AND OBJECTIVES

Shear strength is considered as one of the important engineering properties of clay. The term "strength" has been used in different terminology related to shear, including peak shear strength, residual shear strength, creep or yield strength, and drained and undrained shear strengths. The present research is concerned by the peak shear strength under undrained conditions.

The present study explores the effect of varying the cone apex angle of the quasi-static cone penetration test on penetration resistance. The scope of the current study concerns a type of clay, often encountered in Eastern Canada, known as Champlain clay. This specific type of clay is characterized by its very brittle and extremely strain-sensitive structure.

A laboratory experimental approach is adopted to study the problem of penetration in Champlain clays. This approach necessitates the use of a simulated Champlain clay to avoid the difficulties and expenses involved in acquiring and handling natural clay block samples of the necessary size and quantity.

The objectives of the present study can be summarized as follows:

1. to develop an artificial material that simulates Champlain clay with its components determined as a function of the desired strength. This material facilitates the laboratory experimental work,
2. to study the impact of varying the cone apex angle on the static penetration measurements in the simulated material developed. Accordingly, to develop a correlation between the cone factor and the apex angle at various depths; and

3. to compare the cone factor results obtained in this study with those reported in the literature.

1.3 THESIS OVERVIEW

In order to achieve the study objectives, the research is carried out and accordingly reported as follows:

1. In chapter 2, a literature review is conducted to identify previous related work and to study the factors governing the penetration phenomena.

2. In chapter 3, the effect of modifying the components of the simulated Champlain clay on its characteristics is investigated. Accordingly, the mixture of the simulated Champlain clay can be determined for a given strength.

3. In chapter 4, laboratory penetration tests are set up. These include the preparation of the simulated Champlain clay, and the set up of the quasi-static cone penetration test. In addition to the penetration test, some auxiliary tests, including the vane shear test and the unconfined compression test are performed in laboratory. The laboratory measurements are presented in this chapter.

4. In chapter 5, analyses are carried out on the laboratory measurements to investigate the impact of varying the apex angle on the cone resistance. The results of such analyses are compared with both pertinent theoretical work and reported field measurements.

5. In chapter 6, the contributions of the present research are concluded, and some recommendations have been drawn based on the present study findings.

CHAPTER 2

STUDIES ON MATERIAL PENETRATION AND ITS GOVERNING PARAMETERS

2.1 INTRODUCTION

The question of indentation has attracted the attention of many researchers not only because of its complexity, but also because of the variety of factors which affect this problem. One has to admit that the present progress achieved in Geotechnical Engineering to elucidate the topic of penetration in soils is greatly acknowledged to mechanics, physics, and mathematics scientists. Among the earliest studies concerned with the subject of ductile materials punching, the one carried out by Bishop et al. in 1945 constitutes one of the best. More recently, another group of researchers (Cox et al., 1961) considered the problem of the quasi-static axially symmetric plastic deformations in soils associated with the incipient penetration of a smooth, rigid, flat-ended, circular cylinder into an ideal soil. Later, researches conducted by Ladanyi in the early 1960's focused on the question of deep punching of saturated clays, resulting in his theory of cavity expansion (1967) which gained a lot of recognition since then. More recently, in

1982, Houlsby and Wroth endeavored to present a theoretical analysis of cone indentation in cohesive soils, leading to a relationship between cone resistance and undrained shear strength, where their analysis uses the lower bound theorem of plasticity theory and is appropriate only for indentation by penetrometers near the soil surface. In this chapter a survey is made on each of the previous mentioned studies, their governing parameters, and results.

2.2 INDENTATION OF DUCTILE MATERIALS

When a punch, cone, sphere or other indenting tool is forced into a ductile material, the load required to form a given indentation will depend on the following factors:

a) the shape and size of the indenting tool, and of the specimen if not sufficiently large;

b) the coefficient of friction between the indenting tool and the material; and

c) the yield point and strain-hardening properties of the material, which will depend, among others, on the rate of loading.

The problem of ductile materials indentation by cylindrical punches with conical heads was discussed by Bishop et al. in 1945. On the experimental side, experiments

have been made with both work-hardened and annealed copper. They have found that the load rises toward a maximum value which is not attained until the base of the cone has travelled four to five diameters into the copper block. Denoting this maximum load by p_o A, where p_o is the limiting pressure and A is the cross-section area of the punch, they discovered that p_o for a lubricated punch is about five times the yield stress of the work-hardened material. Bishop et al.'s (1945) theoretical approach has shown that it is possible to calculate the pressures p_c and p_s required to enlarge a cylindrical and a spherical hole respectively. They found it conceivable to assume that the limiting pressure, p_o, should be between the cylindrical pressure, p_c , and the spherical pressure, p_s , and since p_s is only slightly greater than p_c , an approximate theoretical estimate of p_o could be obtained, and hence an approximate value for the load required to force a cylindrical punch deep into a semi-infinite block of ductile material could be calculated; by deep it was meant a penetration equal to four or five times the diameter of the punch.

2.2.1 Experiments on deep punching

For the material to be indented, Bishop et al. (1945) have made use of copper blocks 9.5 cm. (3.75 in.) in diameter and 8.6 cm. (3.4 in.) in height. The copper was generally in

the strain-hardened condition, though one set of measurements was made with annealed copper. Stress-strain curves for the copper used in their experiments are shown in figure 2.1. The punches used were 0.89 cm. (0.350 in.) in diameter and had conical heads with semi-angles of 20°, 30°, and 60°. The diameter of the parallel parts of the punch was made 0.01 cm. (0.004 in.) less than the head diameter; this prevented rubbing of the parallel portion of the punch against the sides of the hole and consequent increase of load due to friction. A sketch of the punch head is shown in figure 2.2-a. Punching was carried out at a rate of approximately 0.01 mm/s. (1.5 in/hr.). In figure 2.2-a it is shown, for the hardened copper, the measured load divided by the cross-sectional area of the punch which is 0.62 cm^2 (0.096 in^2). This quantity has the dimensions of a pressure. Figure 2.2-b shows the same quantity for annealed copper. It can be seen from figure 2.2 that as the penetration increases beyond three or four times the punch diameter, the load tends to a stationary value, which, in the case of hardened copper (fig. 2.2-a), is not markedly different for the three punches. It is this maximum load which Bishop et al. (1945) attempted to calculate in their theoretical approach. It must also be noted that the maximum load for the annealed copper is less than that for hardened copper. Another remark is that there is some fall-off the punching curves, especially in the case

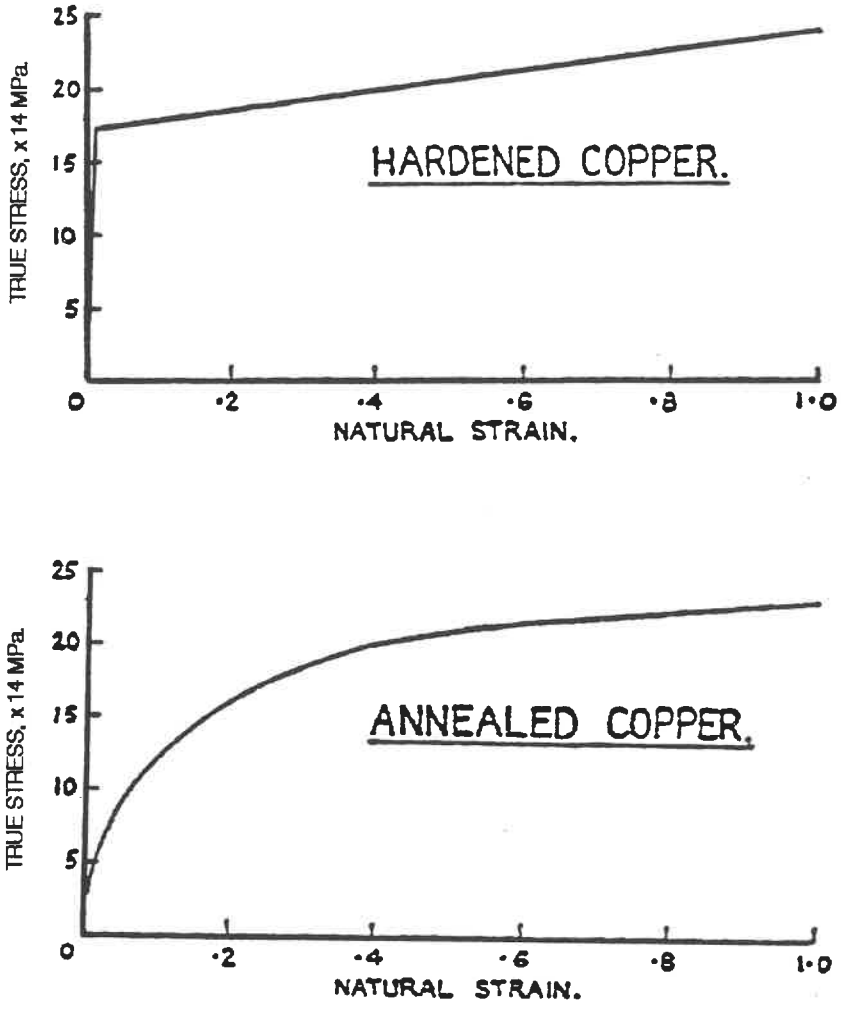

Fig. 2.1 Stress-strain curves for hardened and annealed copper (after Bishop et al., 1945).

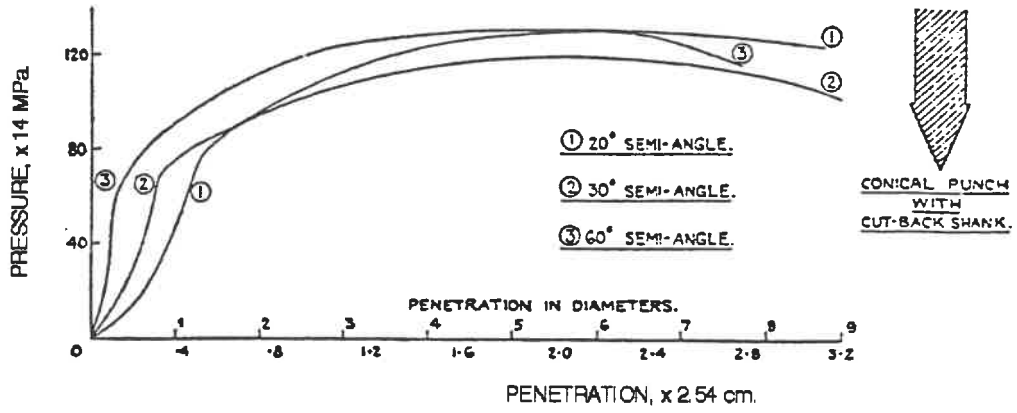

a) Hardened copper

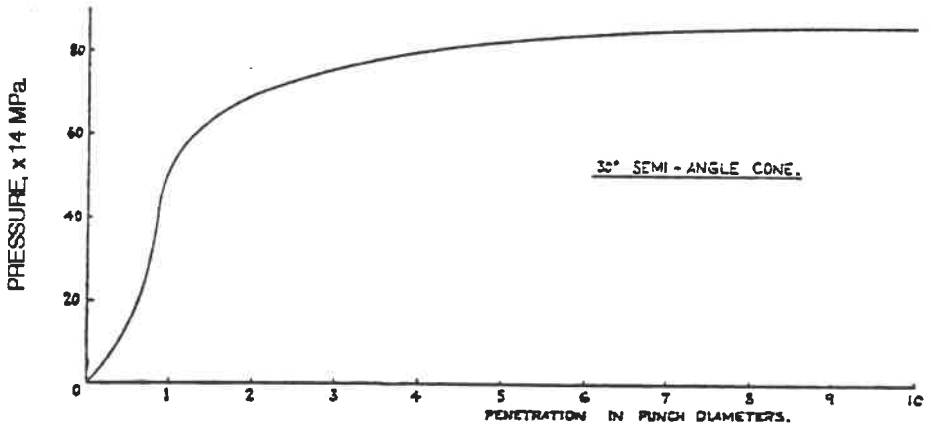

b) Annealed copper

Fig. 2.2 Unlubricated punching curves into copper (after Bishop et al., 1945).

of hardened copper (fig. 2.2-a), as the punch cones come close to the back of the specimen.

2.2.2 Theoretical estimate of the limiting pressure

An attempt of a theoretical estimation of the limiting pressure was made by Bishop et al. in 1945. Although a full theoretical solution of the equations determining the strains around the punch head has been, by that time, proved impossible, solutions of the following problems had, however, been found:

a) starting with a small hollow sphere in the body of an infinite block of a ductile material capable of work-hardening to determine the spherical pressure, p_s , which, when applied to the surface of the hole, will enlarge it indefinitely by the plastic flow of the material.

b) starting with a cylindrical hole of infinite length to find the cylindrical pressure, p_c , that will enlarge the hole indefinitely.

In both problems, Bishop et al. (1945) have assumed that the material has a yield stress Y; for stresses less than Y the material is assumed to be elastic, with Young's modulus E and Poisson's ratio ν. Above the yield stress they have assumed that in compression the true stress σ is given by:

$$\sigma = Y + f(\epsilon), \quad \sigma \geq Y \qquad [2.1]$$

where ϵ is the natural strain given by:

ϵ = ln (final area ÷ initial area of cross-section)

Also, within the plastic region they have neglected all volume changes. In addition, and in order to progress further with their problem, it was necessary to make some assumption about the stress-strain relation in the plastic region for a more general case than simple tension or compression: they have assumed that the octahedral stress is a definite function of the octahedral shear strain for all strain configurations; this is likely to be the case when the principal axes of stress and strain in a given element coincide and do not rotate during plastic flow, as in Bishop et al.'s (1945).

Following their mathematical derivation, Bishop et al. (1945) have established that for a material which its true stress σ and natural strain ϵ are connected by the relation:

$$\sigma = Y + A\epsilon \qquad [2.2]$$

where Y is the yield stress and A is the slope of the approximately linear portion of the stress-strain curve above the elastic limit, the pressure required to enlarge a cylindrical hole is given by:

$$p_c = \frac{Y}{\sqrt{3}}\left(1 + 2\log\frac{C}{a}\right) + \frac{\pi^2}{18}A \qquad [2.3]$$

with:

$$\frac{c}{a} = \left(\frac{\sqrt{3}E}{2(1+\nu)Y} \right)^{\frac{1}{2}}$$

and for a spherical hole:

$$p_s = \frac{2Y}{3}(1 + 3\log\frac{c}{a}) + \frac{2\pi^2}{27}A \qquad [2.4]$$

with:

$$\frac{c}{a} = \left(\frac{E}{(1+\nu)Y} \right)^{\frac{1}{3}}$$

Bishop et al.'s (1945) calculations showed that $p_s > p_c$, but that the difference between them is only about 15% of either. Thus the fact that p_s and p_c are nearly equal enables rather a close estimate of the limiting pressure to be made. The pressure on a lubricated punch deep in a material is likely to lie between p_s and p_c ; for a very sharp punch (i.e. small apex angles) it should approach p_c , while for a blunt punch the material is pushed away from the head of the punch in much the same way as from the neighborhood of an expanding sphere, so the pressure should be near to p_s.

2.2.3 Factors affecting indentation

As concluded from figure 2.2, the load on a punch does not reach its maximum value as soon as the head is embedded in the material, but continues to rise while the penetration increases by several diameters. On a dimensional argument the pressure would be constant while the conical head is pushed in, but the experimental results do not give such a constant pressure, and it is sometimes stated that the pressure increase after the head entry is due ONLY to the metal strain-hardening; this is certainly not true (Bishop et al., 1945), and would take place if the material did not work-harden at all. The region which is plastic round the punch head deep in a material must be very extensive, of width between 7 and 17 punch diameters, for instance in the case of copper. Near the surface, however, the constraint on the copper is less, and it can escape by forming a lip around the hole, and therefore less work per unit volume is done in making the hole. For a shallow indentation by a sphere, or by a very blunt cone, no part of the material will be highly strained; on the other hand, for a deep penetration by a sphere, or by a sharp cone, large strains will be involved and work-hardening will thus take place.

Bishop et al. (1945) have presented a figure (fig. 2.3) which shows some results obtained in the Cambridge

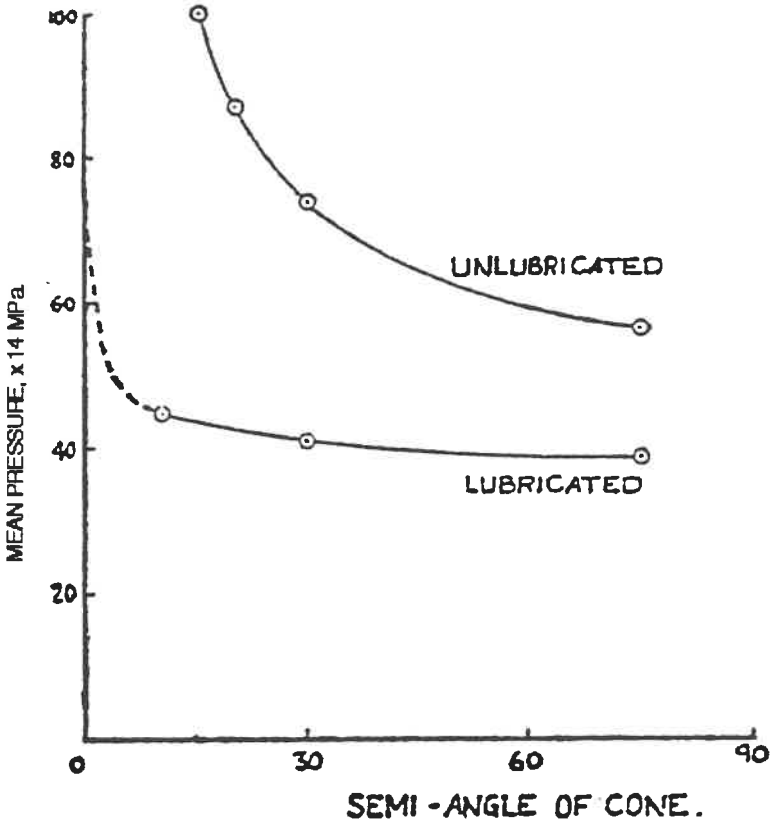

Fig. 2.3 Cones indentation tests on hardened copper (after Bishop et al., 1945).

Engineering Laboratory, UK, with lubricated and unlubricated conical punches in strain-hardened copper with a stress-strain curve as the one in figure 2.1. The punches were solid steel cones and the lubricant, which was graphite grease, was applied repeatedly as the load was increased. In figure 2.3, however, Bishop et al. (1945) have extrapolated the experimental curve for lubricated cones for zero semi-angle by making use of their developed theoretical cylindrical pressure value. It is seen, from figure 2.3, that for the lubricated punches the mean pressure increases slightly with decreasing the cone angle. Although, it is important to mention that the opposite is the case when the punch head is far from the surface, namely, the mean pressure decreases with decreasing the cone angle.

Bishop et al. (1945) have attempted to apply a simple frictional correction to their experimental results, but they have found that friction effects are not significant for the case of a blunt punch (their 60° semi-angle's cone) as this one pushes in front of itself a plug of metal which acts effectively as the indenting tool. However, they have noticed that the frictional force was large enough from being neglected in the case of cones with semi-angles of 20° and 30°; yet, they were unable to estimate this frictional force accurately.

2.3 PENETRATION INTO AN IDEAL SOIL

Cox et al. have developed in 1961 a general theory of axially-symmetric plastic deformations in ideal soils. Their theory has been applied, in particular, to discuss the problem of incipient penetration of a smooth, rigid, flat-ended, circular cylinder (henceforth referred to simply as a punch) into the plane surface of a semi-infinite mass of soil, assumed to be imponderable (in the sense that its weight is not important). Numerical solutions obtained have demonstrated that this later assumption limits the usefulness of the predicted results, in general, to punch radii of at most a few centimeters. Therefore, to achieve progress in the indentation application of the theory, it was necessary to extend the calculations to take due account of soil weight, and this was done by Cox in 1962. It is important to note that early theories of bearing capacity were normally based upon an analysis of plane strain indentation problems, and even in that case, the effects of soil weight were only discussed in an approximate manner due to the mathematical difficulty that for ponderable soils the characteristic relations for the governing differential equations cannot be integrated explicitly. However, within the past decades these effects have been investigated on a more exact basis (e.g. Lundgren and Mortensen, 1953; Spencer, 1962).

2.3.1 Axially-symmetric plastic deformations in soils

A theoretical investigation given by Cox et al. (1961) of quasi-static axially-symmetric plastic deformations in soils was concerned with ideal soils whose postulated mechanical behavior is an approximation to that of a wide class of natural soils. It seems clear that studies of theoretical soil plasticity must relate mainly to the phenomenological behavior of natural soils. In addition, owing to the variable and inhomogeneous physical structure of natural soils, it is necessary to consider ranges of values of ideal soil constants that represent certain averaged rheological properties of natural soils.

In certain circumstances (e.g. in some problems of foundation engineering), there appears to be reasonable justification for the adoption of a limit analysis approach based upon Coulomb's (1773) law of failure in soils. This law expresses the mechanical strength of a general soil in terms of certain fairly well defined physical properties, namely, cohesion due to the bonding action of water and air present between the constituent mineral particles, and friction due to forces set up at inter-particle contacts. Of course, in practical applications of theoretical studies based upon a limit analysis approach, considerable care is required in attempting to correlate values, or ranges of values, of the

ideal soil constants with the measured values of natural soils constants. Generally in theoretical soil plasticity, the difficulties of procedure are not only of a purely mathematical nature, but are also associated with incompleteness in the present knowledge of the basic physics and also with the paucity of reliable experimental data.

The yield condition on which Coulomb (1773) based his theory of earth pressure includes, as a special case, the yield condition proposed by Tresca (1868) in connexion with the plastic deformation of ductile metals. Until quite recently, an important defect in the theory of earth pressure laid in its development without reference to stress-strain relations, the theory being based upon the concept of states of limiting equilibrium satisfying Coulomb's law of soil failure in conjunction with a conjectured extremum principle. This procedure altogether neglects the important fact that stress-strain relations are an essential constituent of a complete theory of any branch of deformable solids continuum mechanics.

As remarked upon by Hill (1950), the plastic yielding of certain non-metallic materials, e.g. clay and ice, is markedly dependent upon the mean value of the principal stresses. Accordingly, a more elaborate plasticity theory is

required for such materials than is required for ductile metals for which there is not this dependence, at least under normal levels of stress intensity. The theoretical study made by Cox et al. (1961) was involved in an extension of the application of the techniques of metal plasticity theory to allow the treatment of problems relevant to plastic deformations in soils. More precisely, their research was concerned with quasi-static stress and velocity fields occurring in plastically deformed ideal soils under axially symmetric conditions. The mechanical behavior attributed to the medium was assumed to be rigid, perfectly plastic, subject to Coulomb's yield condition and associated flow rule. In suitable circumstances, the behavior of this ideal soil provides a useful approximation to that of a natural soil, say a typical clay, exhibiting both cohesion and internal friction. It should be particularly noted that Cox et al.'s (1961) analysis takes no account of effects due to elastic strain, strain-hardening or inertia. Some account of the soil weight effect, important under certain circumstances, was included later by Cox (1962). The specification of the idealized type of soil mechanical behavior considered by Cox et al. (1961) in their theoretical development involves just two parameters, namely, one representing the cohesion stress, c, and the other representing the angle of internal friction, ϕ. According to

Coulomb's law of plastic flow in soils, the shear stress, τ, must not exceed an amount that depends linearly upon the cohesion stress, c, and the normal stress, σ, i.e.:

$$\tau \leq c + \sigma \tan \phi \qquad [2.5]$$

On the basis of equation [2.5], Shield (1955 a) has correctly formulated the yield condition and associated flow rule appropriate to the general treatment of three-dimensional problems of soil plasticity. In application of his analysis, Shield considered only the approximate solution of the bearing capacity problem for a rectangular punch or footing on the plane surface of a semi-infinite mass of soil.

Now Tresca's yield criterion, which applies to ductile metals, corresponds to the particular case of Coulomb's yield criterion when there is no internal friction. In other words, Tresca's law of plastic flow in metals, which is expressed by:

$$\tau \leq k \qquad [2.6]$$

where k is the shear yield stress, is alternatively represented by equation [2.5] with $c = k$, and $\phi = 0$. The condition of equation [2.6] is simply a specialization of equation [2.5]. Fundamentally, Coulomb's yield criterion contrasts with Tresca's in its dependence upon the mean value of the principal stresses. Of course, some similarities and,

necessarily, general consistency must be expected to occur in theory and applications in analogous situations when Tresca's or Coulomb's yield criterion is adopted. To some extent, and whenever analogous physical situations of interest occur, progress in the solution of soil plasticity problems may be expected to be consequent upon progress in that of metal plasticity problems. In fact, Cox et al.'s (1961) study reflects this situation. Shield (1955 b) has developed, and applied to some problems of interest, the general theory of axially symmetric plastic flow of rigid, perfectly plastic material obeying Tresca's yield condition and associated flow rule. Detailed analysis revealed considerable variations in the structure of the field equations for the various plastic régimes. On this basis, it was conjectured that those plastic régimes agreeing with the hypothesis of Haar and von Karman (1909) were likely to be of the greatest significance in the solution of problems of interest. This heuristic principle of Haar and von Karman states, under the present axially symmetric conditions, that the circumferential principal stress is equal to one of the other two principal stresses acting in an axial plane. In this case, the stress and velocity equations are hyperbolic with the same families of characteristics, and, in addition, the stresses are statically determinate.

Essentially, Cox et al.'s (1961) analysis based upon Coulomb's yield criterion for soils may be regarded as a development of Shield's (1955 b) previous analysis based upon Tresca's yield condition for ductile metals.

2.3.2 Governing equations and numerical results

In his endeavor to carry on the calculations of the axially-symmetric plastic deformations theory in ideal soils, developed by Cox et al. (1961), to make allowance for soil weight effects, Cox (1962) has presented the differential equations controlling the stress field in a form suitable for numerical calculations. His purpose was to obtain the yield-point loads for indentation by a punch (axially-symmetric condition), but, in view of the close similarities between this problem and the corresponding one of plane strain (die indentation), equations have also been introduced for this latter case. Then, by considering a practical range for the governing parameters of the obtained equations, Cox (1962) has been able to demonstrate the resulting numerical values.

2.3.2.1 Axially-symmetric conditions

Let cylindrical polar coordinates (r, θ, z) be defined, the origin being at the centre of the smooth, rigid, flat-ended, circular punch, the radius of which is R (fig. 2.4). The soil occupies the semi-infinite region $z \geq 0$. In this

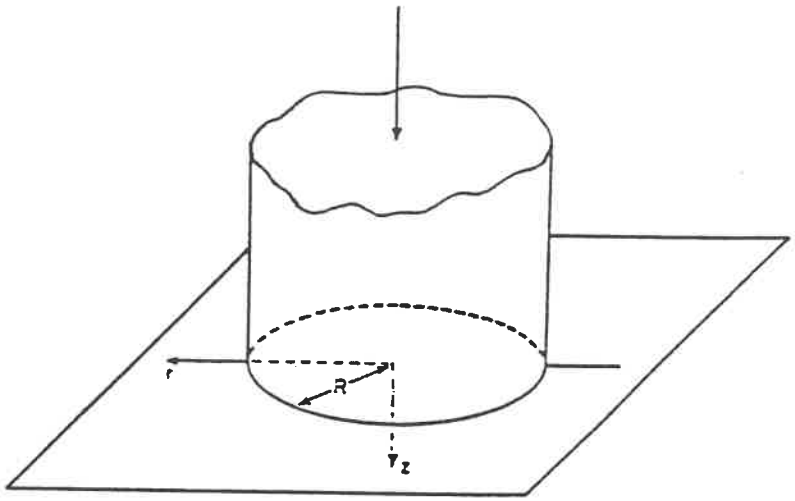

Fig. 2.4 Axially-symmetric coordinate system for punch indentation (after Cox, 1962).

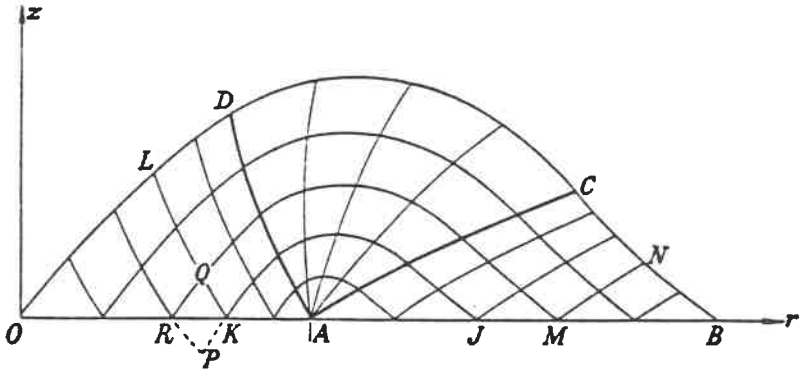

Fig. 2.5 Schematic diagram of characteristics net (after Cox et al., 1961).

coordinate system, the stress tensor components not identically zero are: σ_r , σ_θ , σ_z , and τ_{rz} ; the body force due to gravity has the components (0, 0, ρg), where ρ is the density and g is the acceleration of gravity. The idealized soil is assumed to be rigid, perfectly plastic and to obey Coulomb's yield criterion and associated flow rule. The stress boundary conditions for the problem are:

$\tau_{rz} = 0$ on $0 \leq r < R$; and

$\tau_{rz} = \sigma_z = 0$ on $r > R$ [2.7]

It is assumed that the relevant plastic régime for the problem is the one of Haar and von Karman (1909). The governing partial differential equations for the stress field are then hyperbolic, with characteristics given by:
on an α line

$$\frac{dz}{dr} = \tan\psi \qquad [2.8]$$

and on a ß line

$$\frac{dz}{dr} = \tan(\psi + \tfrac{1}{2}\pi + \phi) \qquad [2.9]$$

where: $\psi = \eta - (\frac{1}{4}\pi + \frac{1}{2}\phi)$ and η is an angle specifying the orientation of the principal stresses and the strain-rates; ϕ is the angle of internal friction; the α-line is the name

of the characteristic with slope tan ψ and the ß-line is that with slope tan $(\psi + \frac{1}{2}\pi + \phi)$. The characteristics net was expected to exhibit the geometrical features depicted schematically in figure 2.5. In this figure, the lines such as MN, AC, and KL are α lines, and those such as MQR are ß lines. In the determination of the stress distribution over the base of the circular cylinder, it was only necessary to consider that part of the field bounded by OA, AB, and BCDO, where ODCB is the ß line through O. So, the characteristic relation is the following:

on an α line and a ß line respectively

$$dA \pm 2d\psi = \left[-\frac{n}{r} \{\cos\phi \,.\, dr \pm (1-\sin\phi) \,.\, dz\} \right.$$

$$\left. \pm \frac{G}{R} (\sin\phi \,.\, dr \pm \cos\phi \,.\, dz) \exp(-A \tan\phi) \right] \qquad [2.10]$$

where: $A = \cot\phi \ln(Q/c^*)$, $Q(r, z) = \frac{1}{2}(\sigma_1 - \sigma_2) \geq 0$,

c^*, the relative cohesion, $= c + p_a \tan\phi$ with c the cohesion stress, p_a the atmospheric pressure, and ϕ the angle of internal friction;

G, the dimensionless soil weight parameter, $= \rho gR/c^*$; and

n is a numerical constant introduced for convenience and here takes the value unity.

The boundary conditions (eq. 2.7) become:

$\psi = \frac{3}{4}\pi - \frac{1}{2}\phi$ on $0 \leq r < R$; and

$\psi = \frac{1}{4}\pi - \frac{1}{2}\phi$, $A = \cot\phi \ln \cot(\frac{1}{4}\pi - \frac{1}{2}\phi)$ on $r > R$ [2.11]

with the same notations as before.

2.3.2.2 Plane strain conditions

In order to preserve notational similarity between this problem and the corresponding axially-symmetric problem discussed in 2.3.2.1, rectangular cartesian coordinates (r, z, x) were chosen, the origin being at the centre of the smooth, rigid, flat-ended die (fig. 2.6). The width of the die is 2R, and the body force has the components $(0, \rho g, 0)$ in this coordinate system. Conditions of plane strain parallel to rz-plane are assumed. It was shown by Cox (1962) that the equations governing the stress field, the well-known Kötter equations (Hill, 1950), are simply equations [2.8] through [2.10] with the same previous notations, but with the numerical constant n equals zero. Other than that, the method of solution of these plane strain equations was the same as for the axially-symmetric ones. It should be noted that the close similarity between axially-symmetric and plane strain indentation problems was a direct consequence of the assumption that the relevant plastic régime in the axially-symmetric problem is the one of Haar and von Karman (1909).

2.3.2.3 Numerical results

The most important numerical results obtained from the

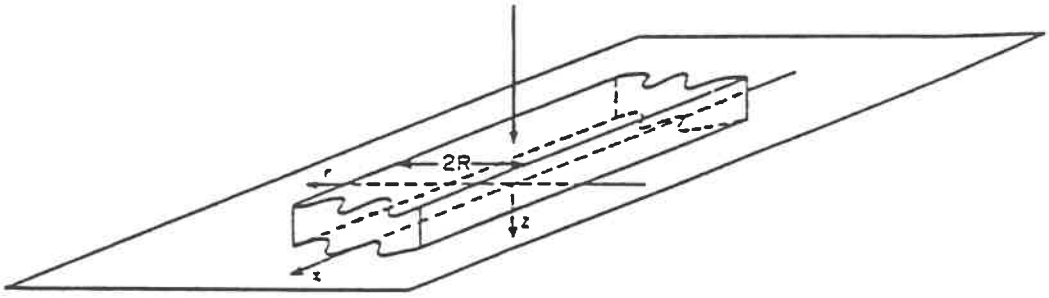

Fig. 2.6 Rectangular cartesian coordinate system for die indentation (after Cox, 1962).

study of Cox (1962) are the values of the mean yield-point pressure p_3 / c^* and p_2 / c^* for punch and die indentation respectively, where c^* is the relative cohesion previously described (sub-section 2.3.2.1), as a function of the dimensionless soil weight parameter, G, and the angle of internal friction of the soil, ϕ.

Since it is apparent from the governing equations of axially-symmetric and plane strain conditions that the corresponding dimensionless yield-point pressures p_3 / c^* and p_2 / c^*, respectively, depend upon ϕ and G, therefore Cox (1962) found it appropriate to consider the practical ranges of these parameters. His results were presented for ϕ = 0° through 40° with intervals of 10°, as for most soils ϕ lies in that range. Moreover, in order to determine the variation range of G, which is equal to $\rho gR/c^*$, it was necessary to discuss first the probable range of ρ, R, and c^*, as g was taken as a fixed value of 9.81 m/s² (32.2 ft/s²). Appropriate values for ρ are located in the range 1.6 - 2.2 t/m³ (100 - 140 lb/ft³), as it is the reliable range in which most soils could be situated. Values of R were supposed to range from zero to about 30 m. (100 ft.). The figure of 30 m. (100 ft.) was thought to represent a reasonable upper limit to the length scales of interest in practical applications. The relative cohesion of a soil, c^*, is related to the true

cohesion, c, by:

$c^* = c + p_a \tan \phi$, where p_a is the atmospheric pressure. In special cases, such as clays for which the water contents are close to the liquid limit, c and ϕ may be so small that c^* itself is small, but in general c^* may be taken as greater than 70 kN/m² (10 lb/in²). Thus the range of interest for G was taken in round figures as $0 \leq G \leq 10$, and Cox's (1962) numerical results were presented for G extending within this range. Table 2.1 presents the mean yield-point pressure values for punch indentation, p_3 / c^*, and table 2.2 demonstrates the corresponding values for die indentation, p_2 / c^*. The variation of these values with G, for a fixed value of ϕ, is shown in figure 2.7; the lines joining the calculated points being intended merely as an indication of this variation, rather than as an accurate representation.

2.4 CAVITY EXPANSIONS IN A SATURATED CLAY MEDIUM

The problem of cavity expansions in an ideal soil mass has received attention in connection with a number of geotechnical problems such as bearing capacity of deep foundation, and interpretation of both pressuremeter and quasi-static cone penetration tests. In most instances the problem has been reduced to that of an expansion of a spherical or a cylindrical cavity inside a homogeneous and

Table 2.1 Values of the mean yield-point pressure for punch indentation (after Cox, 1962).

G / ϕ	0	10^{-2}	10^{-1}	1	10
0°	5·69	5·69	5·69	5·69	5·69
10°	9·98	9·99	10·0	10·4	13·8
20°	20·1	20·1	20·3	22·4	38·8
30°	49·3	49·4	50·5	60·6	141
40°	164	165	173	237	754

Table 2.2 Values of the mean yield-point pressure for die indentation (after Cox, 1962).

G / ϕ	0	10^{-2}	10^{-1}	1	10
0°	5·14	5·14	5·14	5·14	5·14
10°	8·34	8·35	8·42	9·02	13·6
20°	14·83	14·87	15·2	17·9	37·8
30°	30·14	30·29	31·6	42·9	127
40°	75·31	76·13	83·0	139	574

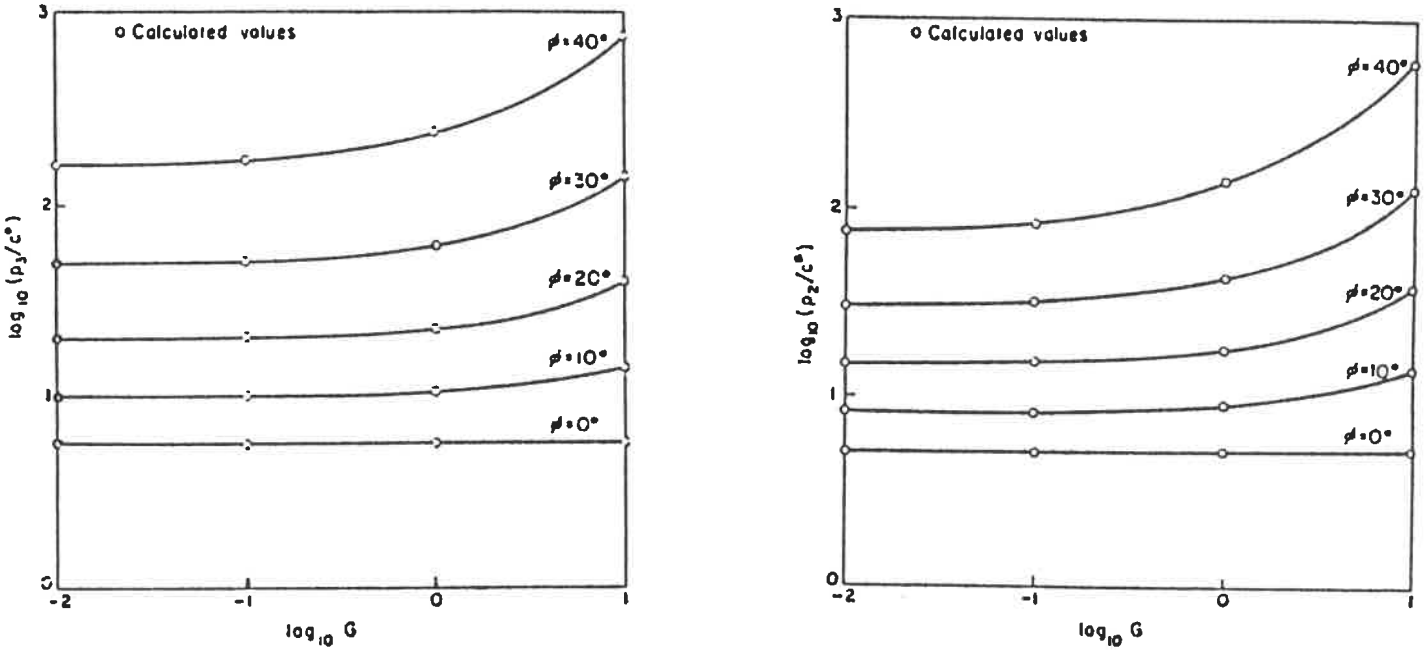

a) for punch indentation

b) for die indentation

Fig. 2.7 Variation of the mean yield-point pressure with the dimensionless soil weight parameter (after Cox, 1962).

isotropic soil mass of infinite extent. Earlier analyses consider the soil to behave as a rigid-plastic, incompressible solid in a plastic region surrounding the cavity, and as a linearly deformable solid beyond that region. In a general manner, no effects of volume change in the plastic region were considered, although attempts were made (e.g. Skempton et al., 1953) to asses their importance numerically. The introduction of volume change effects has been made possible in a systematic manner by cavity expansion analyses based on experimentally determined stress-strain and volume change-strain relationships (Ladanyi, 1961 and 1962).

2.4.1 Deep punching of sensitive clays

The problem of deep punching of saturated clays has a considerable importance in soil mechanics. Its solution is necessary, on one side for evaluating the bearing capacity of deep footings and piles in clay, and on the other side for estimating the mechanical properties of clays from the results of static deep sounding tests. It is well known that, during a quick shear test, a saturated clay behaves as a ductile material. Experimental evidence shows that when a ductile material is indented by an indenter, the load necessary for producing a given penetration depends mostly: a) on the shape of the indenter and its relative distance from the free boundaries of the indented medium,

b) on the stress-strain and strength properties of the material,

c) on the friction and adhesion between the indenter and the material; and

d) on the rate of indentation.

When Ladanyi (1967) carried out his work, it was not possible, by using the principles of the plasticity theory, to find a rigorous solution for the problem of deep punching of saturated clays. As approximate solutions, however, two alternate approaches have been proposed. The first one was obtained by extending to deep punching problems the original Prandtl's theory valid for punching at the surface (Meyerhof, 1951). As the theory is valid for a rigid plastic material, it can be applicable approximately to stiff clays and dense sands where relatively small strains are associated with shear failure. By Terzaghi's definition, this approach would cover the "general shear failure" phenomenon. The second approach which is based on the work of Bishop et al. (1945) of the indentation of ductile metals, assumes that the resistance to deep penetration is of the same order of magnitude as that necessary for expanding a small hole in the medium under the same conditions. With respect to the first one, the second approach has the advantage of being able to take into account the deformability of the indented material

and is, therefore, convenient for studying the behavior of softer and looser soils where the strains preceding failure become more and more important. In the extreme, this second approach would correspond to the notion of "local shear failure" given by Terzaghi.

Which one of the above two types of failure will be produced in reality in deep punching, can be considered to depend on the relative rigidity of the material. For relatively rigid materials, the first approach would be valid while for less rigid ones the second should be more probable. When using the second approach, most authors assume that the material behaves either as a linear elastic-perfectly plastic solid (Gibson, 1950; Osler and Peck, 1963), figure 2.8-a, or a linear-elastic-strain-hardening material (Bishop et al., 1945), figure 2.8-b. It is known, however, that the type of stress-strain behavior, shown in figures 2.8-a and b, is found approximately only in remoulded clays, and in some undisturbed clays of low sensitivity. For sensitive clays, though, showing a permanent loss of strength with remoulding after failure (fig. 2.8-c), the previous assumption may give results which are considerably in error. In fact, in terms used in the theory of plasticity, it may be said that a sensitive clay behaves as a strain-softening material. Before the solution proposed by Ladanyi (1967), no solution for deep

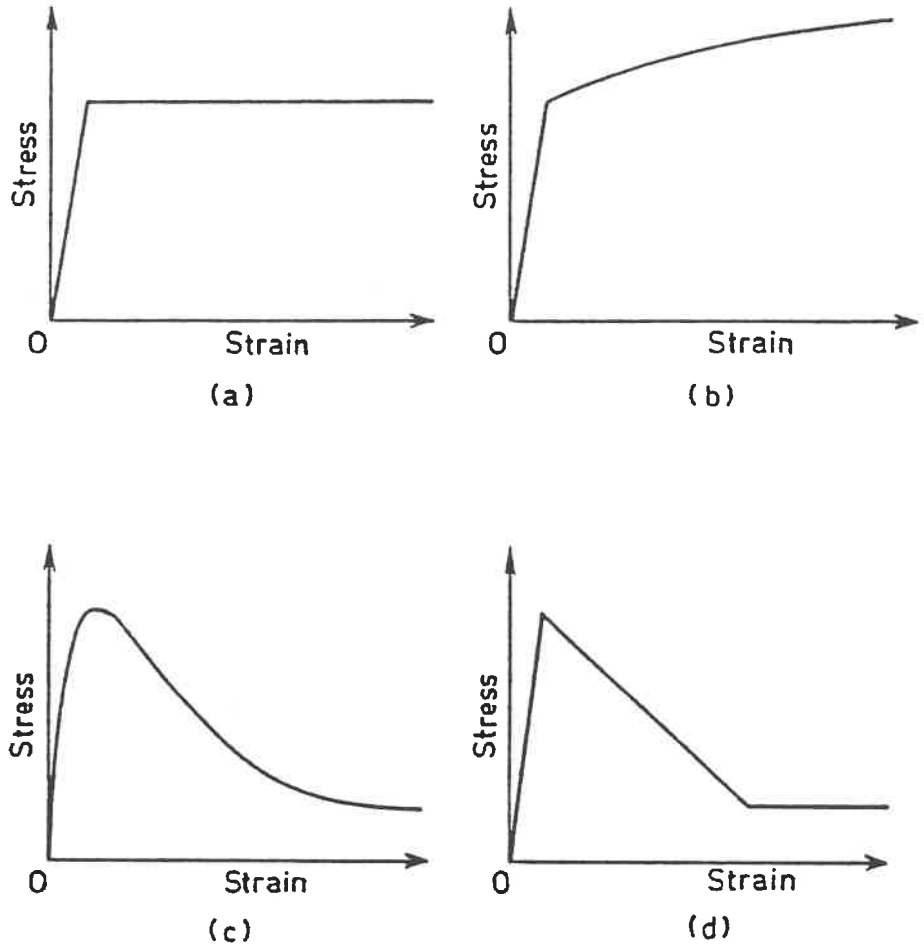

Fig. 2.8 Types of stress-strain curves (after Ladanyi, 1967).

punching based on the second approach, that would take into account the true stress-strain behavior of sensitive clays, had been presented; a solution which resulted in a formula valid for a simplified stress-strain curve such as that shown in figure 2.8-d.

2.4.2 Spherical and cylindrical cavity theory

The familiar problem in the theory of plasticity of the expansion of a spherical or a cylindrical cavity in an infinite medium has been solved by Ladanyi (1963), assuming that the medium is composed of a saturated clay, and that the expansion occurs in undrained conditions. By using a numerical integration method, the latter proposed solution enabled consideration of the real shape of the stress-strain curve of a given saturated clay as obtained in an undrained triaxial compression test.

2.4.2.1 Development of the general expressions

Ladanyi (1967) was concerned with the determination of the bearing capacity factor, N_c , for the case of punching, under undrained conditions, of a saturated undisturbed sensitive clay by a flat circular indenter. In his theoretical analysis, Ladanyi (1967) considered that the penetration of a circular punch deep into a saturated clay is equivalent to the expansion of a spherical hole in an

infinite medium composed of the same material. Moreover, it was assumed that the expansion is occurring under undrained conditions with no volume change, and that the undrained shear failure of the clay is governed by Tresca's failure criterion. The solution was obtained by integrating the differential equation of equilibrium, equation [2.12], valid for a spherical symmetry and for no body force case:

$$\frac{d\sigma_r}{dr} + 2\frac{(\sigma_r-\sigma_t)}{r} = 0 \qquad [2.12]$$

where σ_r and σ_t are the total principal stresses in the radial and the circumferential direction, respectively, while r is any radius measured from the cavity center. Furthermore, Ladanyi (1967) assumed that everywhere in the region influenced by the cavity expansion the same stress-strain law is valid. The law, which is expressed symbolically by equation [2.13], can be obtained by an undrained triaxial compression test performed on an undisturbed specimen of clay:

$$\sigma_1 - \sigma_3 = f(\gamma) \qquad [2.13]$$

where σ_1 and σ_3 are the total principal stresses, and γ is the maximum shear strain approximately equal to 1.5 times the axial strain, ϵ_1, for no volume change case. If $\sigma_r = \sigma_1$ and $\sigma_t = \sigma_3$, as was the case considered by Ladanyi (1967), so equation [2.13] could be written as:

$$\sigma_r - \sigma_t = q = f(\gamma) \qquad [2.14]$$

Equation [2.14] implies that at any point in the medium the mobilized principal stress difference depends only on the shear distortion γ at that point produced by the expansion of the cavity. Substituting equation [2.14] into equation [2.13] yields:

$$d\sigma_r = -2q \frac{dr}{r} \qquad [2.15]$$

herein, q is any mobilized value of principal stress difference, becoming equal to the undrained compression strength at failure. By respecting the continuity and the boundary conditions of the problem, and after successive integration sequences, a general equation convenient for an ordinary numerical calculation or for a computer programming was achieved by Ladanyi (1967). Comparative calculations showed that for the determination of the internal pressure, p_i , in the cavity which is able to produce an expansion failure of the medium, the actual stress-strain curve (fig. 2.8-c) can, with a small loss of accuracy for p_i , be replaced by a simpler one shown in figure 2.9, by the full line (OABC). The resulting governing equation for that simplified stress-strain curve is as follows:

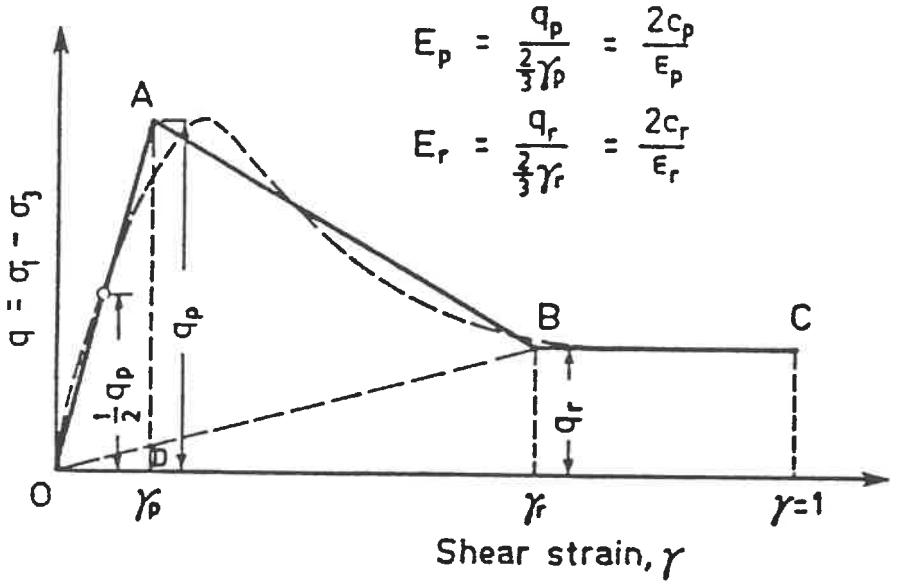

Fig. 2.9 Simplified stress-strain curve (after Ladanyi, 1967).

$$p_i = p_o' + \frac{2}{3} q_r [1 + \ln(\frac{2}{3}\frac{E_r}{q_r})]$$

$$+ \frac{2}{3} q_p \left[\frac{\frac{E_p}{E_r} - 1}{\frac{E_p}{E_r} - \frac{q_p}{q_r}} \right] \ln\left(\frac{E_p}{E_r}\frac{q_r}{q_p}\right) \qquad [2.16]$$

In this equation, p'_o denotes the original effective mean normal stress at the level of the cavity center, while the other notations are shown in figure 2.9. From the above, it can be seen that equation [2.16] could be defined by the following four parameters: two q values, the peak strength q_p and the remoulded strength q_r ; and two secant deformation moduli E, E_p corresponding to the secant passing through ½ q_p on the simplified stress-strain curve (fig. 2.9) and E_r to that passing through q_r at γ_r.

Another more convenient form of equation [2.16] to the geotechnical engineers was presented by Roy et al. (1974) as follows:

$$p_{sph} = p_o + \frac{4}{3} c_r [1 + \ln\frac{E_r}{3c_r}]$$

$$+ \frac{4}{3} c_u \left[\frac{\frac{E_u}{E_r} - 1}{\frac{E_u}{E_r} - \frac{c_u}{c_r}} \right] \ln\left(\frac{E_u}{E_r}\frac{c_r}{c_u}\right) \qquad [2.17]$$

where p_o is the total overburden pressure at the level of the test, c_u is the peak undrained shear strength and c_r is the residual undrained shear strength at large deformation, and E_u and E_r are respectively the undrained elastic and the residual undrained moduli.

The same problem of expansion of spherical and cylindrical cavities in an ideal soil, possessing both cohesion and friction in the Coulomb-Mohr sense, was treated by Vesić (1972) resulting in solutions that take into account the effects of volume change in the plastic region. The developed governing equation from Vesić's (1972) theoretical study for the problem of cylindrical cavity, introduced in an adapted shape for the present survey task, is as follows:

$$p_{cyl} = p_o + c_r[1+ \ln\frac{E_r}{3c_r}]$$

$$+ c_u \left[\frac{\frac{E_u}{E_r}-1}{\frac{E_u}{E_r}-\frac{c_u}{c_r}}\right] \ln\left(\frac{E_u}{E_r}\frac{c_r}{c_u}\right) \qquad [2.18]$$

with the same notations as for equation [2.17]. It must be mentioned that Vesić (1972) has demonstrated that the correlations between the point resistance during penetration and the undrained shear strength is a function of the soil

compressibility expressed by a rigidity index. The rigidity index, I_r, has a physical meaning: it represents the ratio of the shear modulus, G, of the soil to its initial shear strength, $\tau = c + \sigma \tan \phi$. In the present study, which is limited to purely cohesive soils (i.e. $\phi = 0°$), it would be more suitable to express the rigidity index, I_r, as follows:

$$I_r = \frac{G}{\tau} = \frac{E}{2(1+\nu)c_u} \qquad [2.19]$$

where E is the elasticity modulus of the material or Young's modulus, ν is Poisson's ratio, which is usually taken as equal to 0.5 assuming that $\Delta V = 0$ (i.e. for no volume change or for incompressible materials), and c_u is the undrained shear strength of the soil. For a comparative purpose, the governing expressions of [2.3] and [2.4] derived by Bishop et al. (1945), previously discussed through their approaching of the problem of the expansion of a spherical and a cylindrical cavity, are rewritten hereafter as were given by Roy et al. (1974):

for a spherical cavity

$$p_{sph} = p_o + \frac{4}{3}c_u[1+ \ln\frac{E}{3c_u}] \qquad [2.20]$$

and for a cylindrical cavity

$$p_{cyl} = p_o + c_u[1 + \ln\frac{E}{3c_u}] \qquad [2.21]$$

with the same notations as for equations [2.17] and [2.18].

A comparison between the two sets of equations, equations [2.20] and [2.21] on one hand, and equations [2.17] and [2.18] on the other hand, indicates that the additional terms implicated into equations [2.17] and [2.18] have been aimed to take into account the difference, in many aspects, of a natural clay behavior from that of an ideally plastic material, as was assumed in developing equations [2.20] and [2.21]. This implies that solutions, like the one obtained by Bishop et al. (1945), overlooking the importance of involving natural clay characteristics while studying the cavity expansion problem, when applied to the clay, may be considered only as rough approximations.

2.4.2.2 Probable range of numerical values

The analysis made by Ladanyi (1967) showed that the resistance of sensitive clays to deep punching does not depend only on their peak shear strength, but is also much affected by the stress-strain behavior of the clays in undrained compression both before and after failure. In particular, Ladanyi's (1967) analysis pointed out that the value of the bearing capacity factor for a deep flat circular

indenter in a sensitive clay varies within large limits in function of the shape of the stress-strain curve prior to and succeeding failure. For two typical moderately sensitive clays, namely, Ottawa clay and St. Vallier clay whose sensitivities are 16 and 13, respectively, Ladanyi (1967) found the values of the bearing capacity factor, resulting from his theory of spherical cavity expansion, to vary between 5.46 and 7.36, which is much lower than the usually assumed value of bearing capacity of 9 (Meyerhof, 1951), for non-sensitive clays. For highly sensitive clays, still lower values of bearing capacity factor may be expected, though, approaching even unity in case of extreme sensitivity.

2.5 THEORETICAL ANALYSIS OF CONE INDENTATION IN COHESIVE SOILS

Calculations have been shown by Houlsby and Wroth (1982) for the loads on a cone penetrometer in a cohesive material, with the validity of the calculations being limited to a penetrometer near the surface of the soil. The undrained strength of a cohesive soil could therefore be back-analyzed from measurements of loads on cone penetrometers. This procedure is already well established, with empirical factors being used to relate the cone load to the soil strength. These calculations were the fruit of a theoretical analysis

of cone indentation in cohesive soils made by Houlsby and Wroth (1982), which leaded to a relationship between cone resistance and undrained strength. Their analysis uses the lower bound theorem of plasticity theory, and is appropriate only for indentation by penetrometers near a soil surface; in other words, it is valid for shaft length to shaft diameter ratios, l/2r, of up to 20 (fig. 2.10). The analysis provides some indication of the cone resistance variation with the depth as well as with the apex angles of cone penetrometers, but the case of a penetrometer deeply buried in a soil is not considered.

2.5.1 Method of calculation

The calculation of the loads on the cone penetrometers, presented by Houlsby and Wroth (1982), makes use of the lower bound theorem of the plasticity theory. The lower bound theorem states that, for a perfectly plastic material with an associated flow rule, if any stress distribution can be found which:

1. is in equilibrium both internally and with the applied loads,
2. does not violate the yield condition,

then the calculated loads will be less than or equal to those required to cause failure.

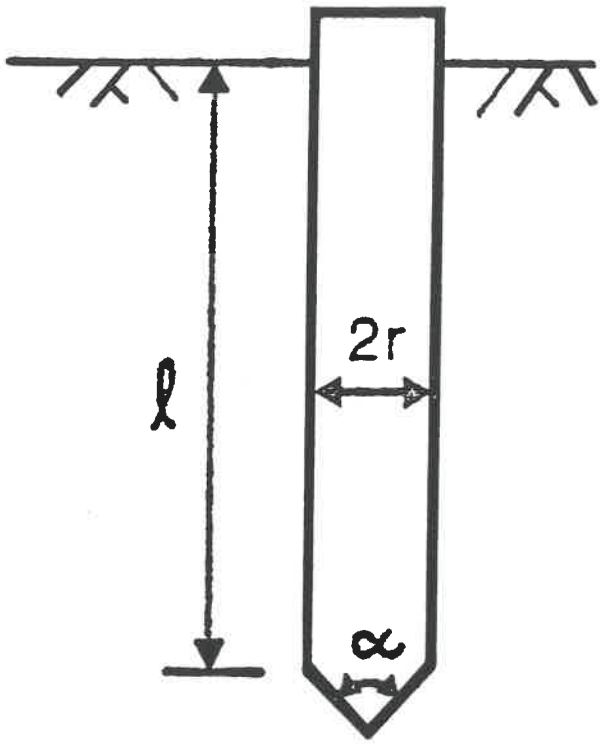

Fig. 2.10 Geometry of the cone penetrometer (after Houlsby and Wroth, 1982).

It has to be noted that the theorem applies directly to rigid plastic materials, however, for materials with elastic-plastic properties the strains may become large before the lower bound is reached. Since a cone penetrometer is bringing the soil around the tip of the cone continually to a state of failure, this theorem, according to Houlsby and Wroth (1982), may be used to provide lower bounds on the resistance of a soil to a penetrometer.

The theorem was implemented by combining the equations of equilibrium with the equation of the yield locus. The equilibrium equations are expressed in axisymmetric coordinates as:

$$\frac{\partial \sigma_{rr}}{\partial r} + \frac{\partial \tau_{rz}}{\partial z} + \frac{(\sigma_{rr}-\sigma_{hh})}{r} = 0 \qquad [2.22]$$

$$\frac{\partial \tau_{rz}}{\partial r} + \frac{\partial \sigma_{zz}}{\partial z} + \frac{\tau_{rz}}{r} = \gamma \qquad [2.23]$$

where the z-axis is taken as vertically downwards, r is the shaft radius, σ_{rr} , σ_{zz} , and σ_{hh} are the radial, axial, and hoop stress respectively, τ_{rz} is the axial-radial shear stress, and γ is the unit weight of the soil. In addition, the yield locus was considered as the Mohr-Coulomb condition with no friction (i.e. the Tresca condition):

$$(\sigma_{rr} - \sigma_{zz})^2 + 4\,\tau_{rz}^2 = 4\,c^2 \qquad [2.24]$$

with c the cohesion of the soil, and the other notations as for equations [2.22] and [2.23]. The result was a series of partial differential equations in the stresses which describe a stress field in equilibrium internally and at yield everywhere, which means that it might be expected to be the highest lower bound.

In order to solve those equations, an additional assumption had to be introduced about the value of the hoop stress, σ_{hh} . The assumption was made, after Haar and von Karman (1909), that the hoop stress is equal to either the major or the minor principal stress. It can be demonstrated that if an associated flow rule is used in connection with the Tresca yield condition, and the radial velocity is non-zero, then the Haar-von Karman assumption must be satisfied (Houlsby and Wroth, 1982). The condition arises directly from the special nature of the corners in the Tresca yield locus. In the analyses of cone indentation it is usually assumed that the soil will be displaced outwards, and so the hoop strain will be tensile. Therefore, Houlsby and Wroth (1982) have taken the hoop stress as equal to the minor principal stress.

By substituting into the equilibrium equations, Houlsby

and Wroth (1982) have obtained the following simplified form of the equations defining the stress field:

$$\sigma_{rr} = \sigma - c \cos 2\theta \qquad [2.25]$$

$$\sigma_{zz} = \sigma + c \cos 2\theta \qquad [2.26]$$

$$\tau_{rz} = c \sin 2\theta \qquad [2.27]$$

where θ is the major principal stress direction, and the other notations as previously described for equations [2.22], [2.23], and [2.24]. These resulting equations (equs. 2.25, 2.26, and 2.27) in the two variables σ and θ automatically satisfy the yield condition and are hyperbolic in form. They may be solved using the method of characteristics as applied by Cox et al. (1961) to the problem of axially symmetric plastic deformations in soils, discussed previously in 2.3. The characteristics correspond physically to the "slip surfaces", or those surfaces on which the yield condition is satisfied.

Having calculated the load P on a cone penetrometer, it is convenient to express this in a non-dimensional form. The load is non-dimensionalised by dividing it by the soil cohesion c and the cross sectional area of the cone $A = \pi r^2$ (fig. 2.10); thus, results are expressed in terms of P/cA, which corresponds exactly to a conventional end bearing capacity factor.

2.5.2 Results of cone load calculations

Houlsby and Wroth (1982) have presented (fig. 2.11) the calculated loads for smooth cones on parallel smooth shafts, with the geometry as shown in figure 2.10, not only for apex angles from 30° to 90°, but also for a flat-ended punch (i.e. 180° cone). The loads were non-dimensionalised by the soil cohesion c and the cross sectional area of the cone $A = \pi r^2$. Moreover, the loads were calculated and presented in figure 2.11 for various depths of penetration l. They have also shown similar results in figure 2.12, but for the case of rough cones with the ratio of cone surface adhesion, a, to soil cohesion, c, equals to unity (i.e. a/c = 1.0). Houlsby and Wroth (1982) have assumed that the shaft of the penetrometer in the latter case is smooth.

When comparing figures 2.11 and 2.12, it is to be noted that while for a smooth cone the lowest cone resistance is usually found to be for more pointed cones, the opposite trend is observed for rough cones, for which a blunter cone offers less resistance. This result has obvious implications for the design of driven closed ended piles.

The variation of pressure with depth for small l/2r values for the 180° cone, or a flat circular plate, are of particular relevance to the interpretation of plate loading

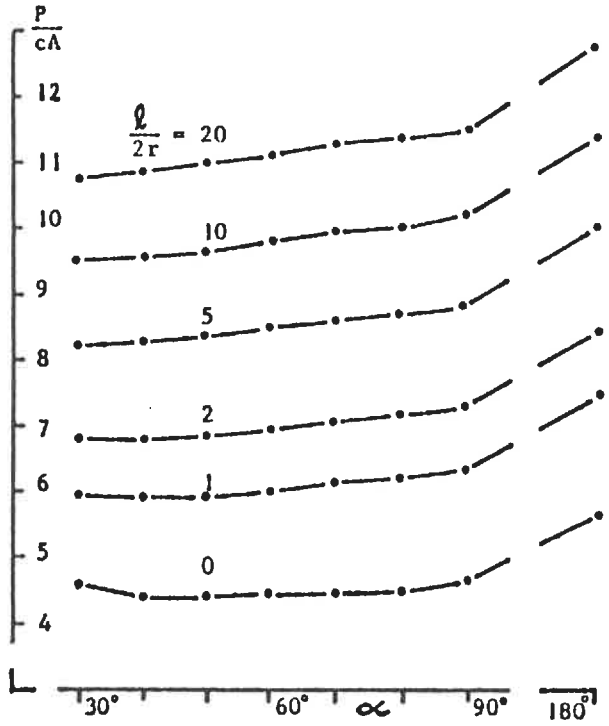

Fig. 2.11 P/cA values for smooth cones on smooth shafts (after Houlsby and Wroth, 1982).

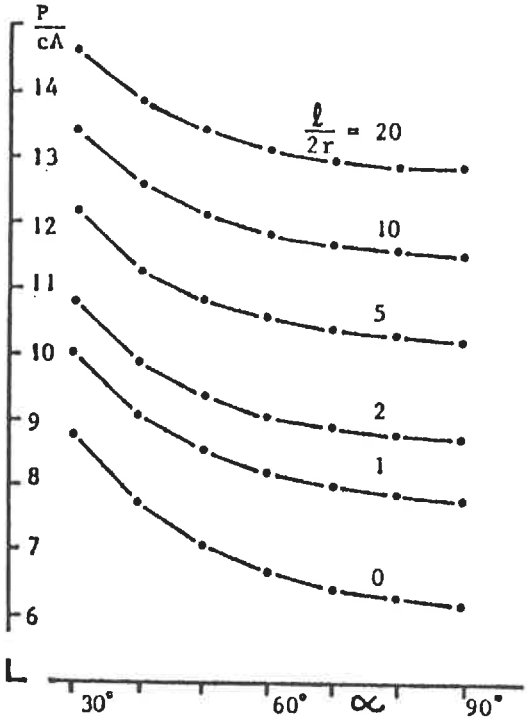

Fig. 2.12 P/cA values for rough cones on smooth shafts (after Houlsby and Wroth, 1982).

tests since these may be carried through to penetrations which are quite large compared with the diameter of the plate. It is common to take account of the penetration depth in an analysis simply by introducing an artificial overburden pressure equivalent to the penetration depth times the unit weight of the soil. However, for axi-symmetric footings this can result in a significant underestimate of the footing capacity as was shown by Houlsby and Wroth (1982). Their calculated pressure values for plate penetrations up to an 1/2r value of 1.0 are given in table 2.3. Houlsby and Wroth's (1982) calculations were carried out using the modified geometry shown in figure 2.13, which does not account for the strength of the soil actually displaced by the plate. These calculated values simply indicate the effect of change of geometry on the bearing capacity factor related to shear strength, which is equivalent to N_c. The value at 1/2r = 0.0, i.e. for the plate at the surface, is confirmed by the value of 5.69 obtained by Cox (1962) and Cox et al. (1961) using the same method of analysis, and should be compared with the value of 6.17 if one applies the well-known bearing capacity formula of Terzaghi and Peck (1967) for a circular footing at the soil surface:

$$q = 1.2\ c\ N_c \qquad [2.28]$$

with a value of $N_c = 5.14$ for a cohesive material. It has to be mentioned that if one were to use the value appropriate to

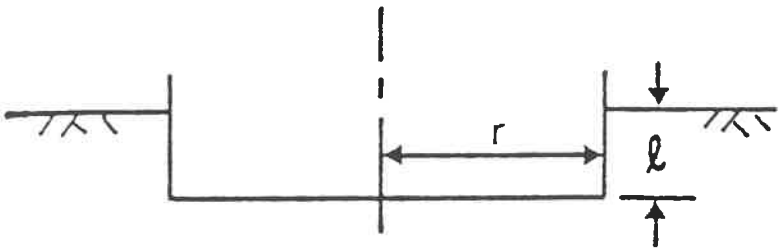

Fig. 2.13 Geometry of the plate (after Houlsby and Wroth, 1982).

Table 2.3 Values of P/cA for smooth plates on a purely cohesive material (after Houlsby and Wroth, 1982).

ℓ/2r	P/cA
0.0	5.691
0.1	5.966
0.2	6.203
0.3	6.414
0.4	6.605
0.5	6.780
0.6	6.942
0.7	7.089
0.8	7.230
0.9	7.362
1.0	7.486

the plate at the surface, the bearing capacity factor, with which the test would be back-analyzed, would be underestimated, so that the shear strength of the soil would be overestimated.

Another solution has been proposed by Sagaseta and Houlsby (1988) for the incompressible soil flow around an infinite cone; a solution which can be of application for cone penetration analyses in clay for the region around the cone tip, as that particular region plays an important role in the analysis of the stress fields during quasi-static cone penetration in clay. In their analysis, Sagaseta and Houlsby (1988) have treated the soil as incompressible elastoplastic with the Von Mises yield condition, defined by a shear modulus, $G = E/2(1+\nu)$ where E is Young's modulus and ν is Poisson's ratio, and a shear strength, c_u, in triaxial conditions ($\sigma_2 = \sigma_3$). The ratio $I_r = G/c_u$ is called the "rigidity index". In Sagaseta and Houlsby's (1988) work, the influence of cone angle and roughness, as well as soil rigidity were analyzed.

As concluded by Sagaseta and Houlsby (1988), two different flow régimes were identified, in agreement with previous numerical and experimental analyses of cone penetration. For very sharp cones, with apex angles smaller

than 20°, an elastic zone (elastoplastic case) ahead the tip was detected by Sagaseta and Houlsby's (1988) numerical formulation, as for that case the cone is acting by cutting the soil sideways. For the second régime, which was found to cover the usual range for angles of cone penetrometers (i.e. apex angles > 20°), all the soil around the cone tip was perceived to be plastic (plastic case). It is worth noting that some authors have found, as a result from numerical analyses, the difference between the two described cases. For instance, Baligh (1985) states that a blunt cone with an apex angle of 60° involves "large deformations that are clearly visible in the vicinity of the tip", while a sharp one with an apex angle of 18° acts in a different way, "cutting instead of pushing the soil ahead of the cone".

In their numerical results for the plastic case, Sagaseta and Houlsby (1988) have demonstrated for the example of a standard cone (i.e. a 60° apex angle cone), the variation of the mean pressure values defined by $(p - p_o)/c_u$, with a wide range of rigidity indices, and considering in the meantime the effect of the cone face roughness. For the condition of smooth cones (a/c = 0.0), and for a rigidity index varying from 10 to 1000, the calculated normalized mean pressure values at the cone face were ranging from 4.24 to 3.73, while for rough cones (a/c = 1.0), it was extending

from 3.24 through 2.73. It was also suggested that for rough blunt cones with angles greater than 120°, the soil would stick to the cone face and the cone roughness is only partially mobilized, sometimes producing infinite suctions instead of compressions at the penetrometer tip (Sagaseta and Houlsby, 1988).

2.5.3 Limitations of the analysis

It has to be noticed that the calculations presented by Houlsby and Wroth (1982) for the determination of the cone loads were solutions of the lower bound type, which means that the yield condition was combined with the equilibrium equations to give solutions for the cone loads which are lower bounds on the true collapse loads.

The first limitation of this calculation is that no indication of the upper bound is obtained. The experience from upper and lower bound calculations for the bearing capacity of shallow footings in plane strain would indicate that the gap between the lower and upper bound solutions for a cohesive material would probably be small, but it would be unwise to extrapolate this experience to a deep axi-symmetric footing. It may therefore be expected that the lower bound solutions will be significantly below the exact solution for a rigid-plastic material.

A second, and more serious, limitation on the calculation carried out by Houlsby and Wroth (1982) is that it gives a lower bound solution for a rigid-plastic material. Whilst it can be shown that this is also a lower bound for an elastic-plastic material, no statement can be made about the magnitude of the strains necessary to mobilise this lower bound, and for engineering purposes collapse may occur before the lower bound is reached. An extreme example of this is the solution of the pressure required to expand a cylindrical cavity in an infinite isotropic elastic-perfectly plastic cohesive material. The lower bound solution indicates that an infinite pressure is needed for failure. For this particular problem a closed form solution exists for the pressure-expansion relationship, and this shows that while an infinite pressure can indeed be reached, an infinite expansion is required to reach it. In practice, the pressure at any given expansion, even a very large one, is governed by the elastic as well as the plastic properties and bears little resemblance to the lower bound.

The behavior of a deeply buried cone may parallel this latter extreme example, in that the actual pressure on the cone is governed by elastic as well as plastic behavior, with the elastic compliance of the surrounding ground becoming increasingly important as depth increases and the problem

gradually becomes one of cavity expansion. The analysis of this second case, where the outer limit of plastic deformation depends on the elastic properties of the soil, is a considerably more complex boundary value problem, especially if one were to use the method of characteristics.

It is worth noting that the well-established end bearing capacity factor for a pile equal to 9 times the cohesion is predicted at a penetration of about 5 diameters. At this point, the mechanism becomes dominated by the compliance of the surrounding soil, although the exact value for a deeply buried cone will be expected to depend to a certain extent on the elastic stiffness.

CHAPTER 3

DEVELOPMENT OF STRENGTH-CONTROLLED SIMULATED CHAMPLAIN CLAYS

3.1 INTRODUCTION

Sensitive clays, to which the present research is limited, are a class of natural soils with unusual characteristics. The most striking feature of these clays is that they are relatively stiff and brittle in the undisturbed state, becoming virtually liquid when disturbed (Crawford, 1963).

Sensitive clays of Eastern Canada are usually characterized by a sensitivity ratio (the ratio of the peak undisturbed strength to the remolded strength at the same water content) greater than 4, are very compressible, and fail suddenly at small strains. These clays were deposited in the glacio-marine environment of the Champlain Sea that occupied the St-Lawrence and Ottawa River basins in the late Pleistocene period (Gadd, 1960). They are sometimes referred to as "Leda" clay, a name said to have been first used by Dawson (Crawford, 1968) on the basis of the Leda fossils it contained. More recently, since none of the Leda fossils were

found in many parts of these deposits, the name Champlain clay, as suggested by Gadd (1960), has become in general use.

The use of a simulated Champlain clay to conduct the laboratory penetration tests of the present study has enabled the avoidance of difficulties and expenses encountered while obtaining large quantities of such clays in an intact and undisturbed condition. In this chapter, the development of strength-controlled simulated Champlain clays is presented.

3.2 DEVELOPMENT OF THE SIMULATED CHAMPLAIN CLAY

As part of the present investigation, full scale penetrometer and vane tests had to be performed in the laboratory. Research indicating that tube sampling techniques can cause disturbances in sensitive soils are numerous (see, for example, La Rochelle and Lefebvre, 1971), so in order to perform a comprehensive investigation on sensitive Champlain Sea clays and to minimize the problems encountered when dealing with such type of clays, block samples of undisturbed clay had to be obtained. Because of the impossibility of handling natural clay block samples of the necessary size and quantity, and not talking about expenses, it was decided to develop a synthetic model material which could be easily operated in large quantities, would perfectly simulate the

mechanical properties of the Champlain clays, and finally should be attainable at low cost.

Such a model material has been defined by Tavenas et al. (1973). It consists of a mixture of kaolinite, cement, bentonite, and water. A laboratory investigation has shown that the mechanical properties of this material are very similar to those of the Champlain clays, provided it is aged for 21 days.

Unfortunately, the existing composition of the model material, selected by Tavenas et al. (1973), gives undrained cohesion of the order of 70 kPa. obtained from conventional unconfined compression tests. Since these values were considered too high to carry out the present research's penetration tests, it was decided to modify the compositions proportion of the model material, keeping in mind not to affect the modelling of Champlain clays of such modified material.

To achieve this target, a complete understanding of the role of each component of the model material had to be settled first. Then, after proposing a modified compositions proportion, a series of unconfined compression tests had to be executed to examine the influence of varying the model

material components on the peak undrained cohesion, and at the same time to ensure the retention of the imitation in stess-strain behavior between the modified model material and the natural Champlain clays.

3.3 ESTABLISHMENT OF THE MODIFIED SIMULATED CHAMPLAIN CLAY

3.3.1 Influence of the components

As a result of the development procedure described in detail by Tavenas and Chapeau (1972), the composition of the model material was selected to be consisted of kaolinite, cement, bentonite, and water.

While the kaolinite is the main solid component and it contributes to all the mechanical properties, the cement is introduced to produce the necessary peak strength and brittleness. Basically, the cement is used to simulate the supposed cementation of the Champlain clay, and it has no influence on the residual or remolded strength of the model material. It is very important to keep this in mind because it means that any attempt to alter the peak undrained shear strength will be primarily directed toward changing the cement proportion.

As the kaolinite-cement mixture exhibits a very

important brittleness and no residual strength at all, bentonite is successfully introduced in the mixture to produce the necessary residual strength. The quantities of bentonite had to be evaluated very carefully since it has a negative effect of increasing the compressibility of the material before failure.

Finally, distilled water has been first proposed, but after approving that normal tap water gave identical results, it was recommended to change over to this more economical solution (Tavenas et al., 1973).

3.3.2 Modified compositions proportion

For the reasons previously cited in studying the role of each component of the model material, attention has been mainly pointed in the direction of revising the cement percentage in the compositions proportion of the original model material.

Taking into consideration the negative effect of varying the bentonite percentage, the proposed modified proportions have been selected in such a way to obtain a satisfactory effect both in the elastic range and for the residual strength of the modified model material.

The following example demonstrate the method adopted in adjusting the components proportion for a certain cement percentage. Assuming that the required cement percentage is 12.50%, while fixing the total volume, V_t , of the model material to 100 cm^3 (i.e. a 4 cm. in diameter and 8 cm. in height cylinder specimen), and knowing that the dry unit weight, γ_d, equals 5.30 kN/m^3 (Tavenas et al., 1973):

so, the weight of solids, $W_s = V_t * \gamma_d = 53$ g.,

and the weight of cement, Cement = 12.50% of W_s = 6.625 g.;

the kaolinite/bentonite weight ratio of 8 of the original model material is kept constant to elude the influence of changing the bentonite percentage,

$$\text{Kaolinite} = 8\ \text{Bentonite} \qquad [2.1]$$

but we know that,

$$W_s = \text{Kaolinite} + \text{Cement} + \text{Bentonite} \qquad [2.2]$$

solving the above two equations to have the unknown weights of kaolinite and bentonite, we get,

$$\text{Bentonite} = \{1/9\} * \{W_s - \text{Cement}\} \qquad [2.3]$$

substituting the previously calculated values of the weight of solids and cement in equation [2.3], we get,

Bentonite = 5.153 g. (i.e. 9.72% of W_s),

and then from equation [2.1], we get,

Kaolinite = 41.222 g. (i.e. 77.78% of W_s).

For a water content at mixing of 167% (Tavenas et al., 1973), the weight of water, W_w, will be;

W_w = 167% of W_s = 88.50 g.,
which means that the needed volume of water is 88.50 cm^3

Table 3.1 groups the composition proportions of the model material at different cement percentage for a total volume of 100 cm^3, following the above mentioned method of calculation.

3.4 LABORATORY TESTS

3.4.1 Preparation of the material

All solid components: kaolinite, normal portland cement type 10, and bentonite are delivered as powders passing No. 200 sieve. The quantities of each component, following table 3.1, necessary to produce the desired volume of material are first weighed and mixed when dry. Water is added to the resulting powder while stirring with a high turbulence agitator of about 1000 revolution per minute (r.p.m.) to develop the necessary deflocculation. After all dry materials have been mixed into the water, the stirring is continued for 5 min. per liter of mixture to obtain a homogeneous slurry.

At this stage, the material is ready for casting in the appropriate molds: 5 cm. in diameter and 10 cm. in height PVC tubes, for the preparation of samples for the unconfined

Table 3.1 Compositions proportion of the model material at different cement percentage for a total volume of 100 cu.cm.

Model Material No.	Kaolinite		Cement		Bentonite		Water
	Weight, g.	%	Weight, g.	%	Weight, g.	%	Volume, cubic cm.
100	35.33	66.66	13.25	25.00	4.42	8.34	88.50
200	36.86	69.55	11.53	21.75	4.61	8.70	88.50
300	38.28	72.23	9.94	18.75	4.78	9.02	88.50
400	39.26	74.07	8.84	16.67	4.91	9.26	88.50
500	41.22	77.78	6.63	12.50	5.15	9.72	88.50
600	44.17	83.34	3.31	6.25	5.52	10.41	88.50

compression tests. After casting, and for the duration of the setting period, the material in the mold is conserved in the humid chamber to protect it from drying. A setting period of 3 weeks is usually allowed before performing the tests.

With this procedure, and provided due care is given to the casting operation, a homogeneous and isotropic material is created with properties which remain the same from batch to batch.

3.4.2 Unconfined compression tests

3.4.2.1 Purpose

A series of small-scale unconfined compression tests was performed in the laboratory on the model material specimens. The purpose of these tests was to examine the stess-strain characteristics of the modified model material which, according to our requirements, has to simulate that of the natural Champlain clay.

Another target was the investigation of the weight of changing the cement percentage on adjusting the peak undrained shear strength of the simulated Champlain clay.

3.4.2.2 Experimental apparatus and procedures

A conventional unconfined compression test apparatus with the option of selecting various rates of deformation was used. All the tests were carried out under controlled strain conditions with a rate of deformation of about 1%/min., conforming to the American Society for Testing and Materials (ASTM) recommendations (D 2166) and satisfying the expected brittle behavior of the model material.

After a minimum of trimming, specimens were sized and weighed. Then, the tests on the mounted specimens of height-to-diameter ratio of 2 were performed, while the applied load with the corresponding elapsed time was recorded through a computerized data acquisition system.

Plate C.1 in Appendix C shows a photograph of the unconfined compression test apparatus used in the present research with the specimen mounted and ready to be experimented.

3.4.2.3 Test results

Figures 3.1 through 3.3 are representative stress-strain curves obtained from the model material at 25, 12.50, and 6.25 percent of cement respectively.

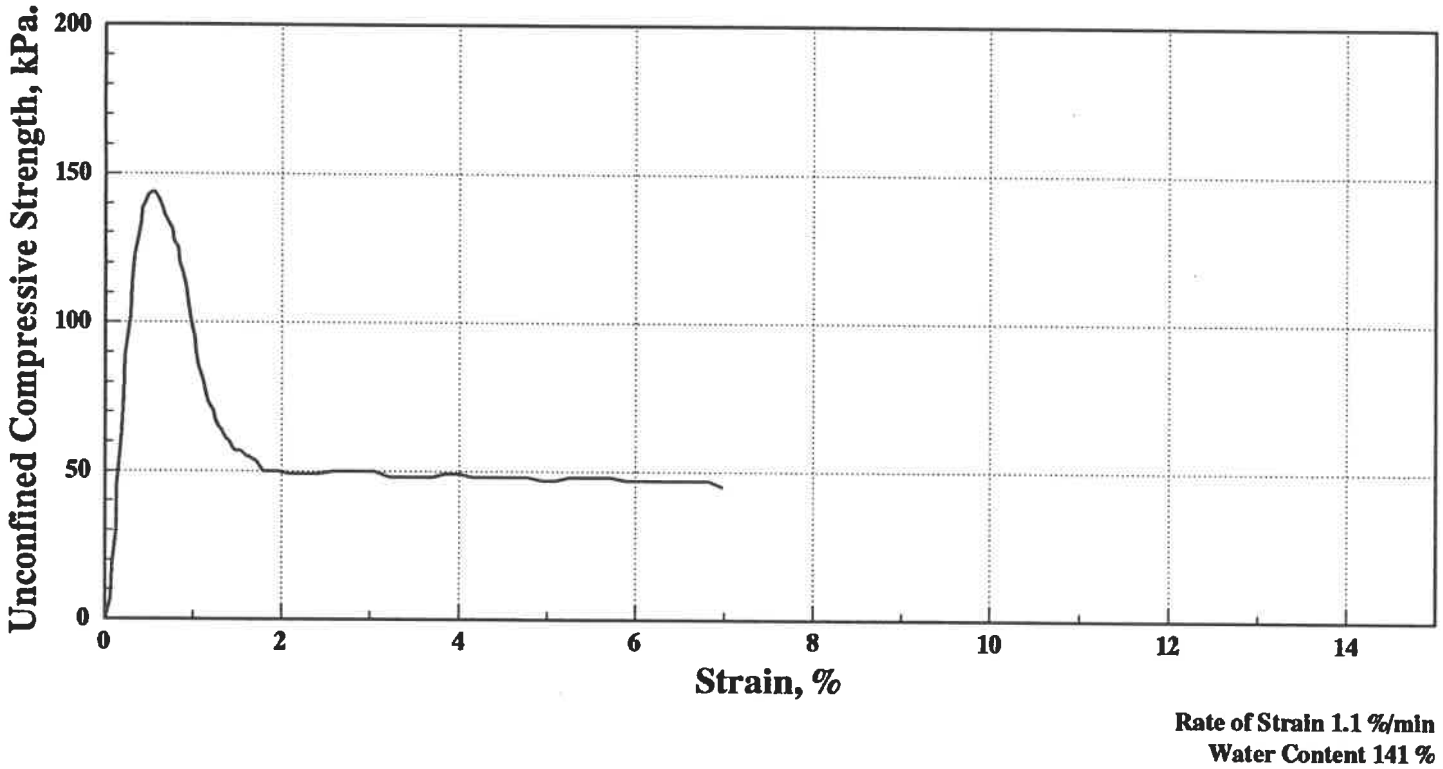

Fig. 3.1 Stress-strain curve of test 101

for model material with 25.00 % cement.

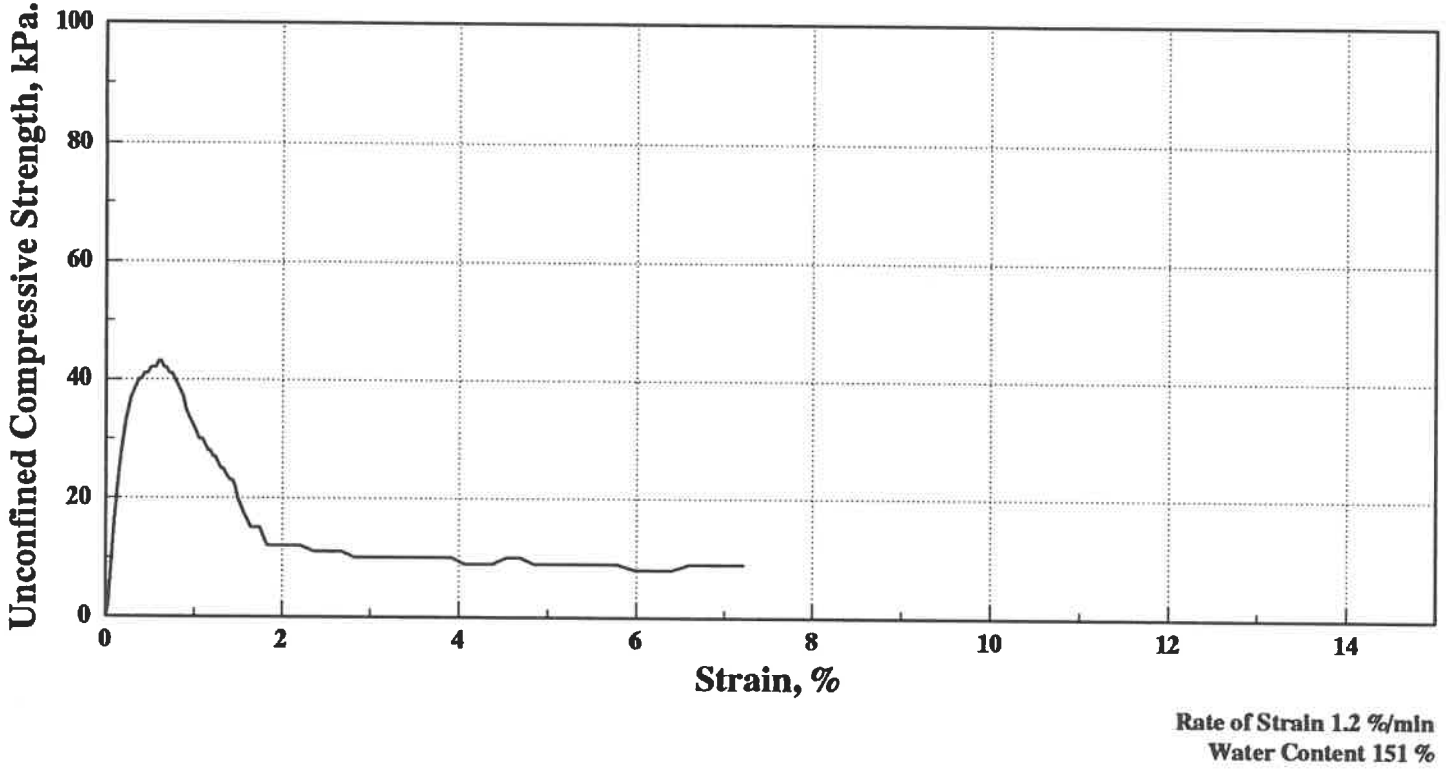

Fig. 3.2 Stress-strain curve of test 501

for model material with 12.50 % cement.

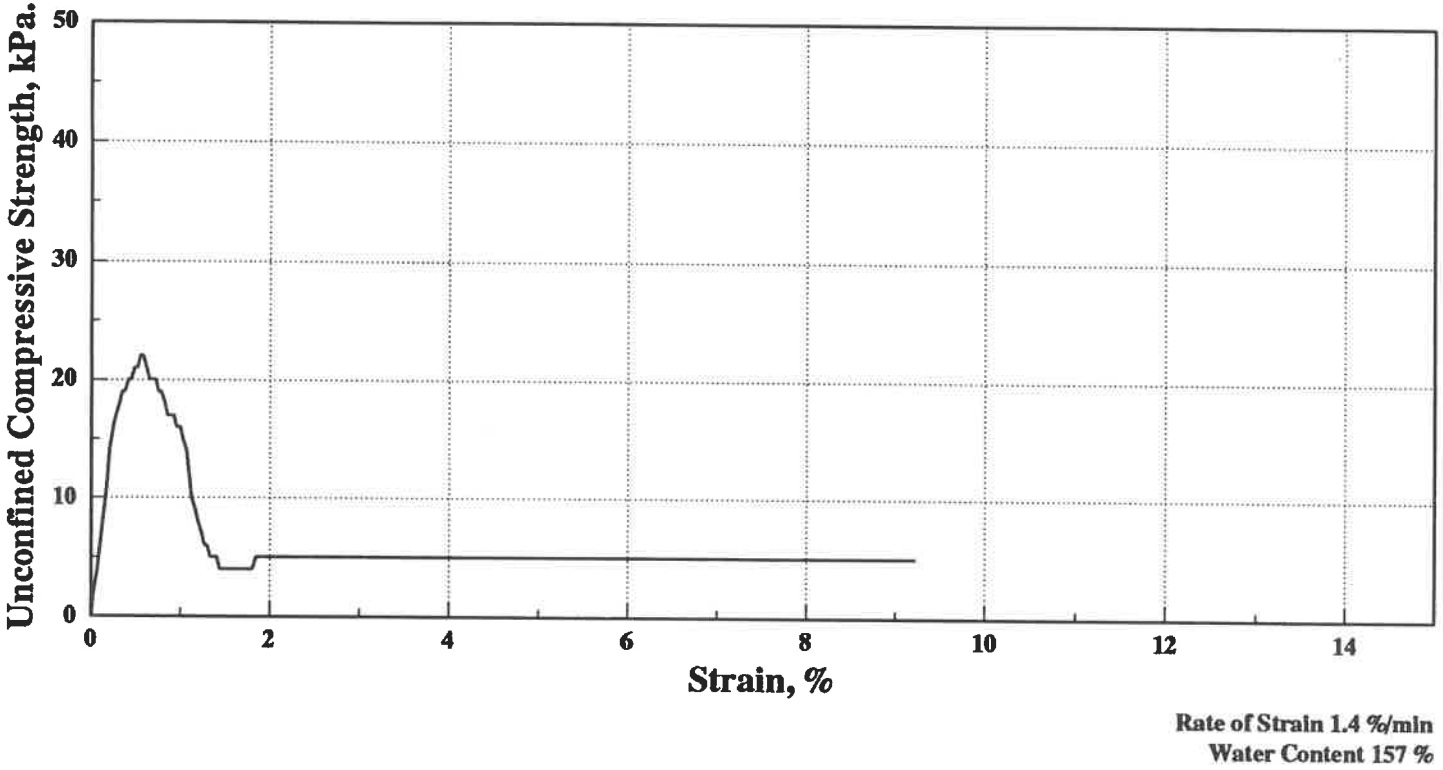

Fig. 3.3 Stress-strain curve of test 601

for model material with 6.25 % cement.

The complete set of the stress-strain curves resulting from the unconfined compression tests conducted on the model material at different cement percentage are shown in Appendix A. Furthermore, table 3.2 gathers the unconfined compression strength outcoming from all the 18-test performed. These results are presented in the form of a "best-fitting" curve (fig. 3.4) relating the 6-cement percentage accomplished in the present study to their corresponding unconfined compression strength.

3.4.3 Geotechnical properties of the selected simulated Champlain clay

Satisfying our requirement of having a simulated Champlain clay with a peak undrained shear strength in the order of 30 kPa., and ensuing the approximate chart of figure 3.4 resulted from the interpretation of the unconfined compression test results of different cement percentage, the material with the 14% cement was selected. By adopting the same calculation procedures previously described, one can get the succeeding compositions proportion of the model material with 14% cement, for a total volume of 100 cm^3:

- Kaolinite = 40.52 g. (76.45% of W_s)
- Cement = 7.42 g. (14.00% of W_s)
- Bentonite = 5.06 g. (9.55% of W_s)

with a volume of normal tap water of 88.50 cm^3.

Table 3.2 Unconfined compression test results for the model material at different cement percentage.

Cement	Test No.	Unconfined Compression Strength, KPa.
25.00%	101	144
	102	143
	103	142
21.75%	201	119
	202	123
	203	116
18.75%	301	108
	302	95
	303	112
16.67%	401	81
	402	82
	403	85
12.50%	501	43
	502	43
	503	38
6.25%	601	22
	602	18
	603	22

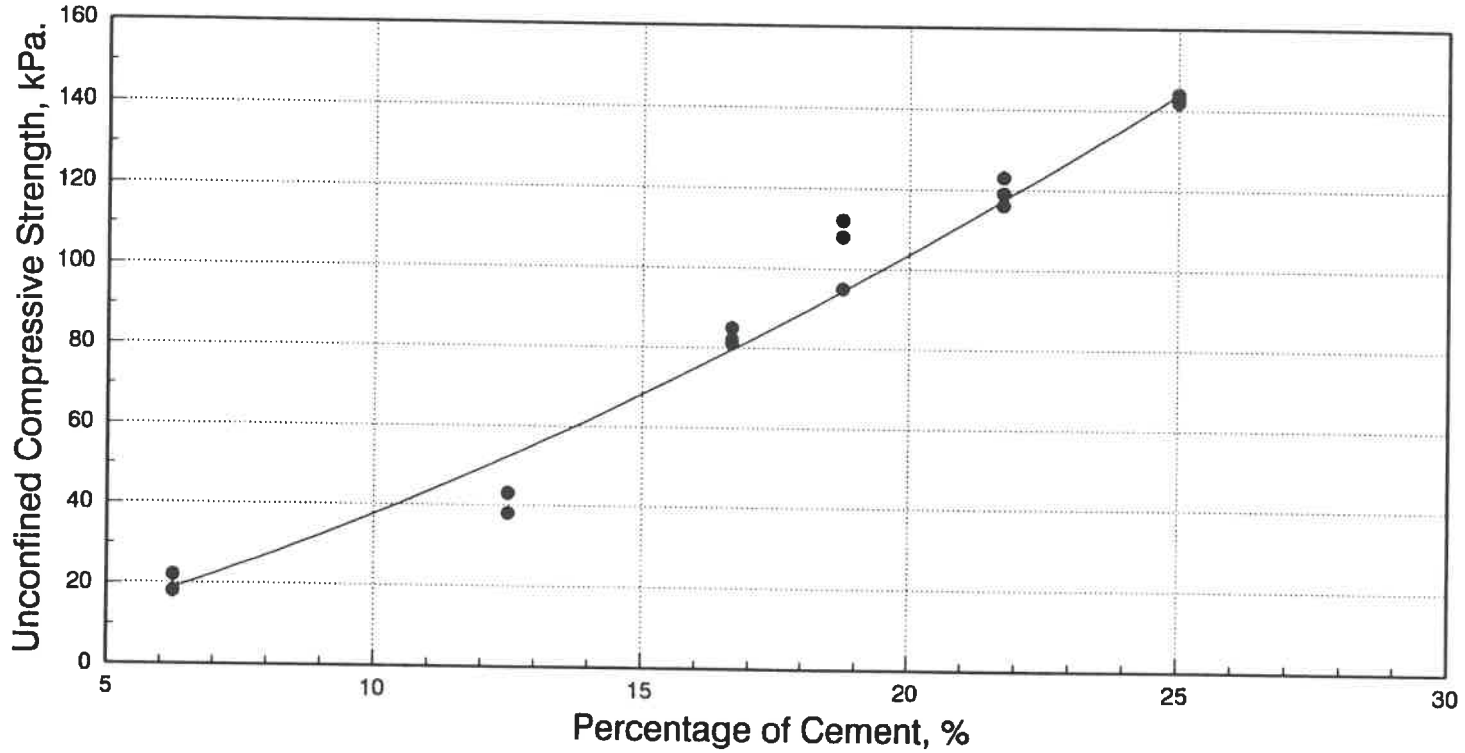

Fig. 3.4 The influence of varying the percentage of cement on the unconfined compressive strength.

This material has been subjected to conventional geotechnical tests in order to determine its properties, for instance, the water content, the consistency limits, the bulk unit weight, the dry unit weight, and the relative density. These properties and their corresponding values are illustrated in table 3.3. It has to be mentioned that all the preceding laboratory tests were conducted conforming to the ASTM recommendations, however, the determination of the liquid limit was performed by the Swedish fall-cone test rather than the traditional Casagrande method.

3.4.4 Discussion

From the results of the unconfined compression tests, it appears that the material developed is a good model of the Champlain clays in undrained shear conditions. The present laboratory investigation has shown that the mechanical properties of this material are very similar to those of the natural Champlain clays; more specifically, the stress-strain curves have the same characteristics: the material exhibits a clear peak shear strength at relatively low strain, then an almost constant post-peak residual strength at large strains.

The model material is thus fulfilling its main function as a valuable tool for understanding the behavior of sensitive cemented Champlain clays. Moreover, the developed

Table 3.3 Geotechnical properties of the 14% cement simulated Champlain clay.

Water content, w	150 ~ 154%
Liquid limit, w_L	125 ~ 130%
Plastic limit, w_P	90 ~ 100%
Plasticity index, I_P	30 ~ 35%
Liquidity index, I_L	1.5 ~ 2
Unit weight, γ	13 kN/m^3
Dry unit weight, γ_d	5.3 kN/m^3
Relative density, D_R	2.72
Unconfined compressive strength, q_u	60 ± 4 kPa
Undrained shear strength by laboratory vane, c_{uv}	23 ± 2 kPa
Sensitivity by laboratory vane, S_t	20

modified model material is proved to be an ideal simulator of sensitive, naturally cemented Champlain clays with various peak undrained shear strength; a model material which is easily handled in large quantities and whose components are available at relatively cheap prices, overcoming the difficulties and expenses encountered in adequate sampling of such type of clay.

CHAPTER 4

EXPERIMENTAL SET UP OF PENETRATION TESTS

4.1 INTRODUCTION

The adoption of a laboratory experimental approach to study the impact of varying the apex angle on the static cone penetration test measurements has raised many problems. One of these problems was the obtaining of good quality Champlain clay samples, to which the present research is limited, and by the necessary size and quantity to conduct the large scale laboratory penetrometer tests. Although this point was overcome by making use of a simulated Champlain clay, as discussed in the previous chapter, still some questions relevant to the preparation of such material with the needed size have to be answered. Another set of problems was related to the quasi-static cone penetration test, for example, the design and fabrication of penetrometers with various apex angles, and the apparatus with which the penetration tests would be carried out. The methods adopted to resolve these difficulties, as well as the presentation of the direct outcome laboratory measurements, are demonstrated in this chapter.

4.2 PREPARATION OF THE SIMULATED CHAMPLAIN CLAY

As described in chapter 3, and fulfilling our requirements, the simulated Champlain clay with 14% cement was chosen as the material upon which the penetration tests would be preformed. The same procedures of the material preparation as presented in the previous chapter were followed, however, the desired volume in this case was about 31.50 liter for each specimen, since the approved dimensions of the specimens were 20 cm in diameter and 1.00 m in height. According to that volume, and referring to the compositions proportion previously illustrated for a total volume of 100 cm^3 (chapter 3), one can determine the needed quantities of each component for preparing one specimen as follows:

- Kaolinite = 12.76 kg. (76.45% of W_s)
- Cement = 2.34 kg. (14.00% of W_s)
- Bentonite = 1.59 kg. (9.55% of W_s)

with a volume of normal tap water of 27.88 liter.

The solid components are delivered as powders passing No. 200 sieve, they are first weighed and then mixed when dry. The specific volume of water is added to the resulting powder while stirring. Stirring operation is very important and has to be done with a high turbulence agitator of about 1000 r.p.m. to assure the necessary deflocculation. A punch-

drilling machine, as the ones found in workshops, with a rotating speed of 1000 r.p.m., equipped with a special iron bar, ended with two blades and long enough to ensure the stirring of the entire volume of the mixture, was used as a convenient agitator for such huge volumes. After all dry materials have been mixed into the water, the stirring is continued for about 3 hours to obtain a homogenous slurry.

At this stage, the material is ready for casting in the appropriate mold: 20 cm in diameter and 1.00 m height PVC tube, as this kind of tubes was experienced for its perfectly water tightness. During the casting operation, three small samples, 5 cm in diameter and 10 cm in height, for the unconfined compression tests, were taken at three different depths of the 1.00 m length specimen to represent the whole height of the specimen, and by which the homogeneity of the specimen through its entire depth could be verified. After casting, and for the duration of the setting period, the material in the mold together with the three small samples, is conserved in the humid chamber to protect it from drying. A setting period of 21 days must be allowed before realizing the laboratory quasi-static cone penetration test and the other auxiliary tests.

4.3 LABORATORY QUASI-STATIC CONE PENETRATION TESTS

The basic idea of the cone penetration test remains a simple one: to advance a rod into the soil, usually vertically, measure the forces required to produce such advance, and interpret these forces in terms of shear strength, for example. In response to the variety of problems and soil conditions, engineers have developed a great variety of penetration test equipment and methods. Many types of quasi-static cone penetration test equipment and methods are described in Sanglerat's (1972) reference. Some are very sophisticated and intended for special applications. Others might have a broader usage, but for one reason or another have not caught on. In contrast, the Dutch quasi-static cone sounding systems and methods have caught on throughout the world, including the North American continent. It is worth mentioning here the difference between "truly" static and quasi-static penetration tests, which is: the continuity of penetration readings. As for the truly static test the intermittent readings are obtained at depth intervals of 20 cm, however it is possible to use smaller steps than that (e.g. 10 cm), which means that the movement of the penetrometer is interrupted before the next reading is taken. While for the quasi-static type, the rods and the penetrometer are advanced simultaneously, and hence the

penetration readings are recorded continuously.

4.3.1 Cone penetrometers and penetration apparatus

The cone penetration test does not measure shear strength directly, but measures cone bearing capacity, q_c . Depending on the cone type, it could also measure the soil-steel friction along the local friction sleeve, f_s . Moreover, the recently developed piezocone has enabled the recording of pore pressures, Δu , generated as the cone penetrates the soil. Since the present study focuses on the measurement of cone point resistance, q_c , the designed small-scale laboratory cones were not equipped with facilities for evaluating parameters as skin friction and pore pressures.

The first step in setting up the penetration test was the design of the cone penetrometers with various apex angles, as required by the present research. This design is shown in figure 4.1. All the nine cones have a base diameter of 10 mm, resulting in a projected area of 0.785 cm^2. This specific diameter was chosen in such a manner to hold a ratio of 20 between the specimen diameter, which is 20 cm, and the cone diameter. That ratio was necessary to be held in order that any possible boundary effects would be avoided. The cones, which were fabricated at École Polytechnique's

Apex Angle ß, degrees.	Height h, mm.
7.5°	76
15°	38
18°	32
22.5°	25
30°	22
45°	12
60°	9
90°	5
180°	0

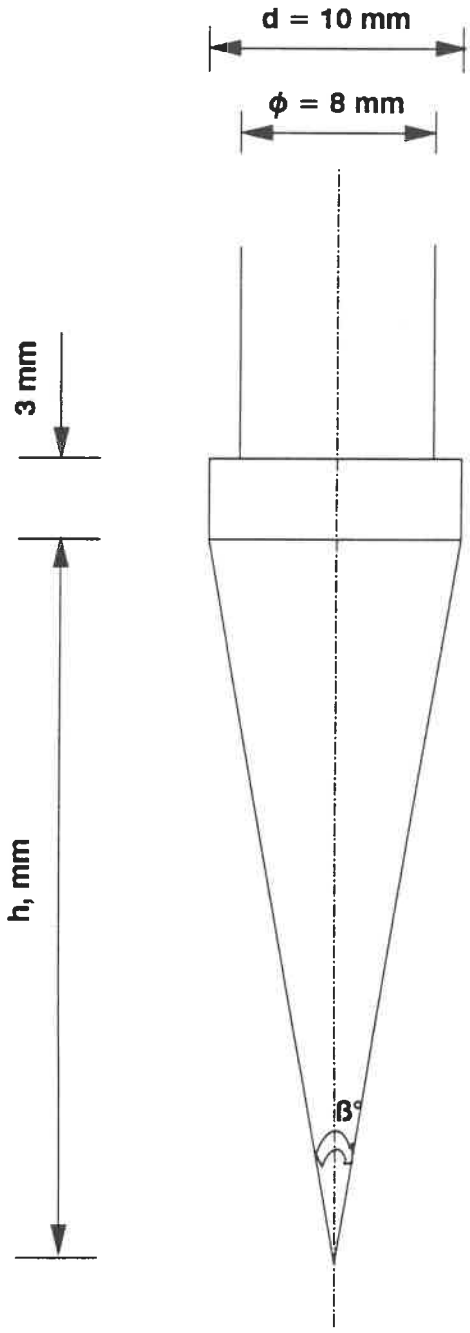

Fig. 4.1 Design of cone penetrometer and pushing rod.

workshop, were made from steel and the surfaces in contact with the simulated Champlain clay have been smoothed as possible as it could be. The push rods were made from a smooth stainless steel and had a section adequate to sustain, without buckling, the thrust required to advance the penetrometer tip. They had an outside diameter smaller than the diameter of the cone base by 2 mm (figure 4.1), to prevent the mobilization of skin friction on the penetrating rods during the penetration process.

The second problem which had to be settled before realizing the laboratory penetration tests was the adoption of a convenient jacking system. A traditional 20 kN capacity forklift truck was found to be an accepted thrust machine for pushing down the penetrometer, yet some modifications had to be made to accommodate the penetration test requirements of the present study. For instance, the rate of penetration, which was set at 0.5 cm/s (compared with the standard rate of 2.00 cm/s in field) to minimize the influence of scale effects on the measurements, had to be attained and certified throughout the tests. To achieve this target, an adjustment was made in the hydraulic pump of the forklift truck by introducing a valve controlling the hydraulic release of the forklift. Also, the installation of a light metallic structure on the movable part of the forklift truck has

enabled the gaining of extra height needed to perform the quasi-static penetration through the entire depth of the specimen. Furthermore, mounting reasonable steel weights over this light metallic structure, combined with the deadweight of the forklift truck, have proven to produce the necessary reaction required for a proper performance of the thrust machine.

4.3.2 Test procedures and measurements

After achieving the 21-day setting period of the simulated Champlain clay, the specimen of 20 cm diameter, 1.00 m height, and about 50 kg weight, in its mold, is brought from the humid chamber where it was conserved. The specimen is then placed on a wooden seat, prepared especially for the specimens' molds to prevent it from any lateral movement and to ensure its verticality. The forklift truck is moved towards the specimen so as to have the specimen under the movable part of the forklift truck. At this stage, the pushing rod along with the cone penetrometer is greased, by applying a thin layer of normal grease, before setting it up between the load cell and the specimen. The pushing rod is fitted in its vertical position in such a way to be in touch with the specimen center at one end (the cone tip), and the load cell at the other end, keeping in mind to hold the verticality of the rod. A photograph of the quasi-static cone

penetration test just before the commencement of the experiment is shown in plate C.2 of Appendix C. The load cell, which is fixed in the light metallic structure, is connected to the data acquisition system. The data acquisition system includes an electronic signal apparatus and a computer system. The electronic signal apparatus receives pulses from the load cell and transfers it to the computer system. The computer system contains an analog to digital conversion unit, a real time clock, and a disk drive unit. Figure 4.2 presents a drawing sketch of the quasi-static cone penetration test and its data acquisition system.

When starting the test, the thrust on top of the rod is applied by releasing the movable part of the forklift truck and simultaneously the recording starts. The force required to advance the conical point is transferred via the load cell to the sounding rod (figure 4.2). At the same time, the load cell transmits the measured loads, through the data acquisition system, to the recording disk which minutes also the corresponding elapsed time. Furthermore, a distometer, connected too to the data acquisition system, was used to register the penetration depths during the test.

From the measured loads, and given that the cone area is 0.785 cm^2, the cone resistance, q_c , through the 90 cm

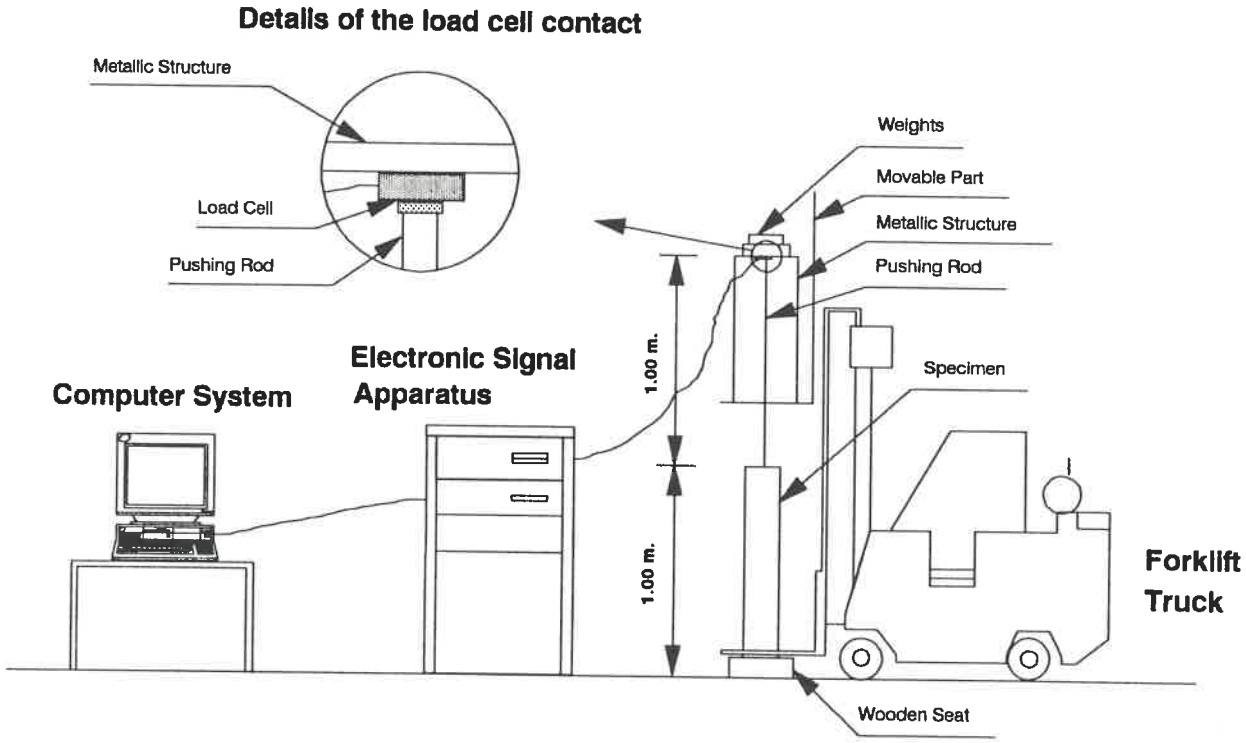

Fig. 4.2 Sketch of the quasi-static cone penetration test.

penetration depth could be determined from the following equation:

$$q_c = \frac{F}{A} \qquad [4.1]$$

where q_c = cone resistance, F = measured load, and A = cone area. The calculated cone resistance values are plotted with the measured penetration depths following the conventional graphical representation of penetrometer test data, by considering the ordinate axis to represent the penetration depth (the depth increases from top to bottom), and the abcsissa to represent the cone resistance. A representative cone resistance curve for the 30° cone apex angle is shown in figure 4.3, while the other cone resistance curves for the different apex angles considered in this study are shown in Appendix B. Another curve resulting from the measurements of the penetration tests is the rate of penetration curve. The rate of penetration is calculated as follows:

$$Rate\ of\ Penetration = \frac{measured\ depth}{corresponding\ elapsed\ time} \qquad [4.2]$$

The resulting curve verifies the respectability of the specified rate of penetration (0.5 cm/s) required for conducting the penetration tests of the present research. The rate of penetration curve for the 30° cone apex angle is

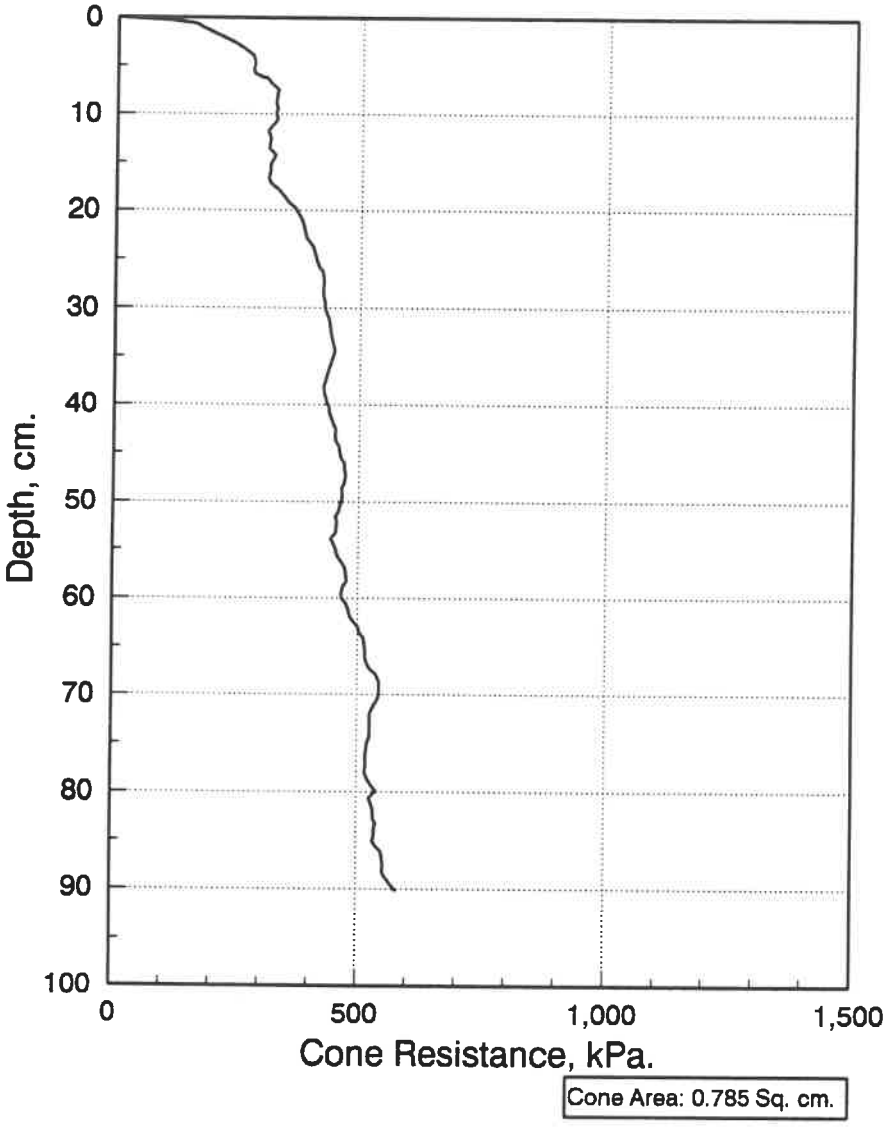

Fig. 4.3 Quasi-static cone resistance curve for 30° cone apex angle.

presented in figure 4.4 (the others are included in Appendix B).

4.4 AUXILIARY LABORATORY TESTS

4.4.1 Laboratory vane shear test

After the accomplishment of penetration test, laboratory vane shear tests were conducted on the specimen at each 5 cm depth interval. The purpose of these tests is the determination of the reference undrained shear strength needed for the analysis of the cone penetration measurements (chapter 5). The specimen was trimmed into rings 20 cm diameter and 5 cm thick. For each ring, four vane tests were carried out. The vane blades height-to-diameter ratio was 2, as the height and the diameter chosen were 25 and 12.5 mm, respectively. The tests were conducted by inserting the vane blades into four different points, equally distant from each other, located along the circumference of an imaginary circle. The center of this circle was the penetration hole resulted from the penetration test, and its radius was 5 cm. The location of the vane test points by this manner respects the ASTM recommendations (D 4648). Plate C.3 in Appendix C represents a photograph of the vane shear test carried out in laboratory.

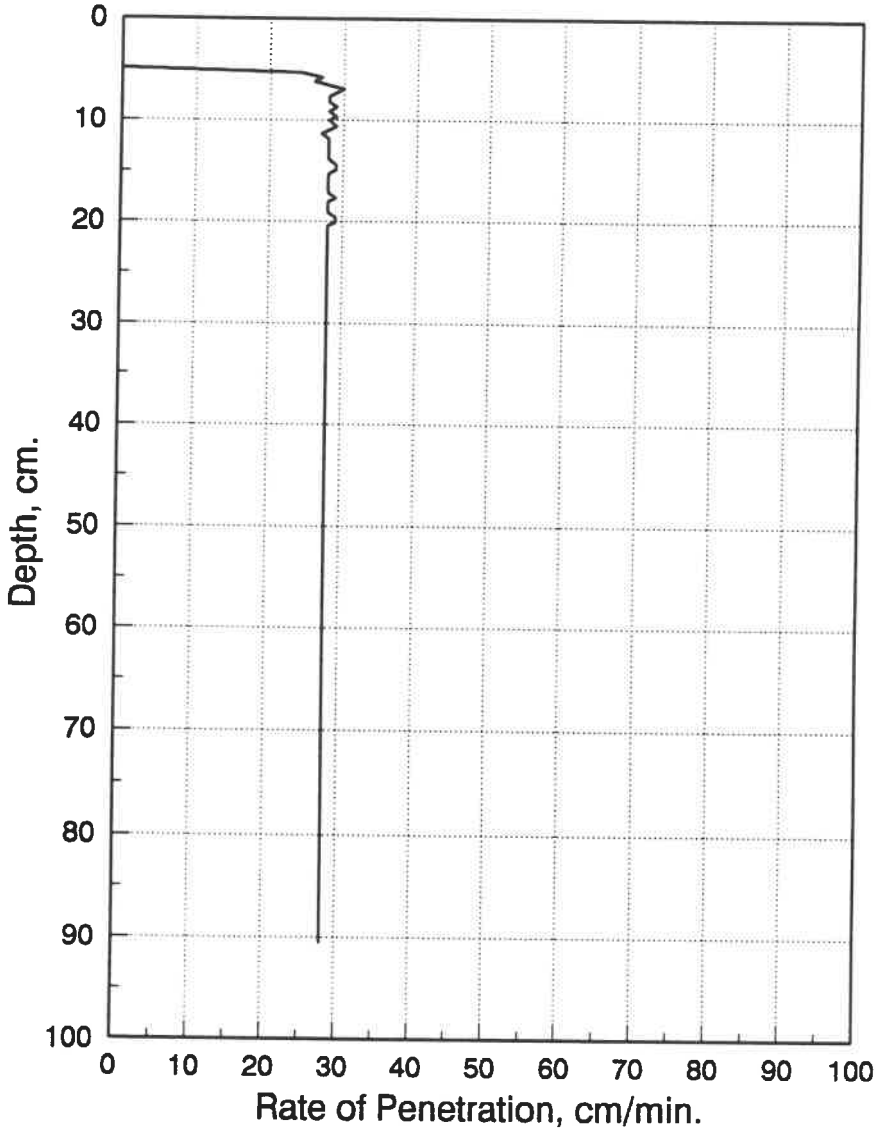

Fig. 4.4 Rate of penetration curve for 30° cone apex angle.

After the insertion of the vane blades, a torsion couple was applied with a constant speed (rate of deformation = 45°/min). The initial and final readings were recorded. For each point tested, the vane undrained shear strength, c_{uv} , was calculated from the following equation (assuming isotropic conditions and uniform shear distribution at top and bottom of vane-generated failure cylinder):

$$c_{uv} = 10 \left[\frac{M}{\pi D^3} \frac{6}{\left(\frac{3H}{D} + 1 \right)} \right] \qquad [4.3]$$

where c_{uv} is the vane undrained shear strength in kPa, M is the applied torsion moment in N.cm, H and D are the height and the diameter, respectively, of the used vane blades in cm. The applied torsion moment, M, is determined from the following:

$$M = K\,(d - d_o) \qquad [4.4]$$

in which M is the torsion moment in N.cm, K is the calibration coefficient pertinent to the spring used to produce the torsion couple in N.cm/degree, d and d_o are the recorded final and initial readings, respectively, in degrees. Given that the adopted vane blades have an H = 2.5 cm and a D = 1.25 cm, and that for the spring used in the current study K = 0.464, equation [4.3] could be rewritten,

after substituting the previous values, as follows:

$$c_{uv} = 0.648\ (d - d_o) \qquad [4.5]$$

with the same notations as before. By applying this equation, four laboratory vane undrained shear strengths have been obtained for each 5 cm depth of the specimen. The laboratory vane shear test results for the 30° apex angle penetration test specimen are presented in figure 4.5. For the remaining eight specimens, their results are shown in Appendix B.

4.4.2 Determination of water content and consistency limits

For each specimen, the water content was determined at every 5 cm depth, while the consistency limits (liquid limit and plastic limit) were determined at every 10 cm depth. The purpose of these tests is the verification of the homogeneity of the simulated Champlain clay used in the present study, throughout each specimen, on one hand, and on the other hand from one specimen to the other.

The determination of the water content, w, was done conforming to the ASTM (D 2216) recommendations and procedures. The adopted equation for calculating the water content was the following:

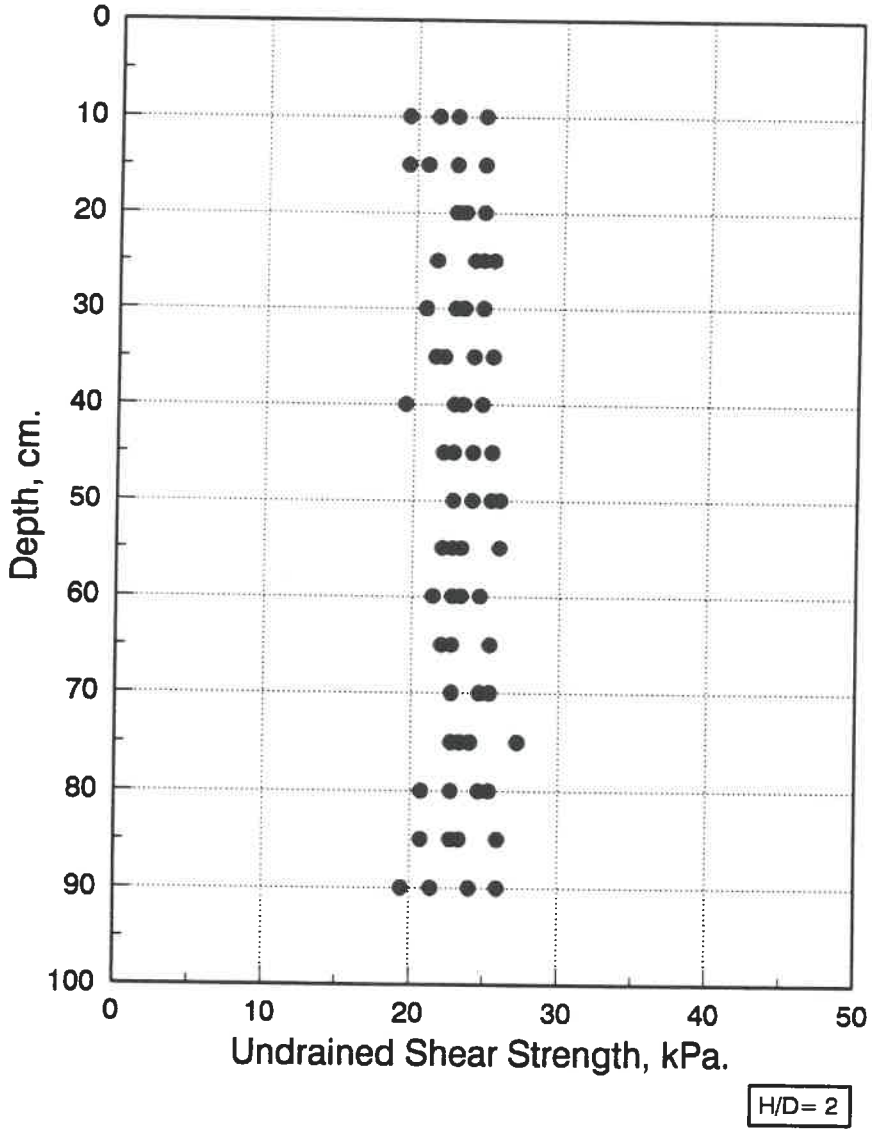

Fig. 4.5 Results of laboratory vane shear test-30°.

$$w = \frac{W_w}{W_s} \times 100 \qquad [4.6]$$

where w = water content in %, w_w = weight of water, and w_s = weight of dry sample.

For the liquid limit determination, the procedures recommended by the ASTM (D 423) were first followed, but due to numerous difficulties encountered in conducting this test (Casagrande method), it was decided to adopt the Swedish fall-cone test. The liquid limit, w_L , determined by the Swedish fall-cone test corresponds to the water content of the sample at which a penetration of 10 mm, by means of a 60° apex angle and a 60 g weight cone, is obtained. Practically, the determination of each liquid limit value necessitates at least five Swedish fall-cone tests to be conducted. These tests were carried out at various water contents in such a manner to have the penetration values ranging between 7 and 15 mm. Then, with the aid of a linear regression between penetration values and the corresponding water contents, the water content for a 10 mm penetration could be determined, which is the liquid limit value. As for the plastic limits, w_p s, the conventional procedures of the ASTM (D 424) were observed for the determination of these limits. The water content and consistency limits determined for the specimens

used in the current research are presented in Appendix B, however, these are shown in figure 4.6 for the 30° apex angle penetration test specimen.

4.4.3 Unconfined compression test

At the end of the simulated Champlain clay setting period (21 days), and in the same day of performing the penetration test, three unconfined compression tests were carried out. The main purpose of these tests is to ascertain the repeated stress-strain behavior of the simulated Champlain clay used in the present study. Moreover, the obtained stress-strain curves were useful in the analysis of the penetration measurements, for instance, the application of the cavity expansion theory (chapter 5). The tests were conducted on the three small samples taken during the casting operation of the penetration test specimen (20 cm diameter and 1.00 m height). These samples were considered to represent the entire height of the specimen, as they were taken from three different depths. Each sample had a height-to-diameter ratio of 2 (10 cm height and 5 cm diameter), following the ASTM (D 2166) recommendations. The same experimental apparatus used in the development of the strength-controlled simulated Champlain clay (chapter 3) was adopted (a photograph of this apparatus is presented in plate C.1 of Appendix C).

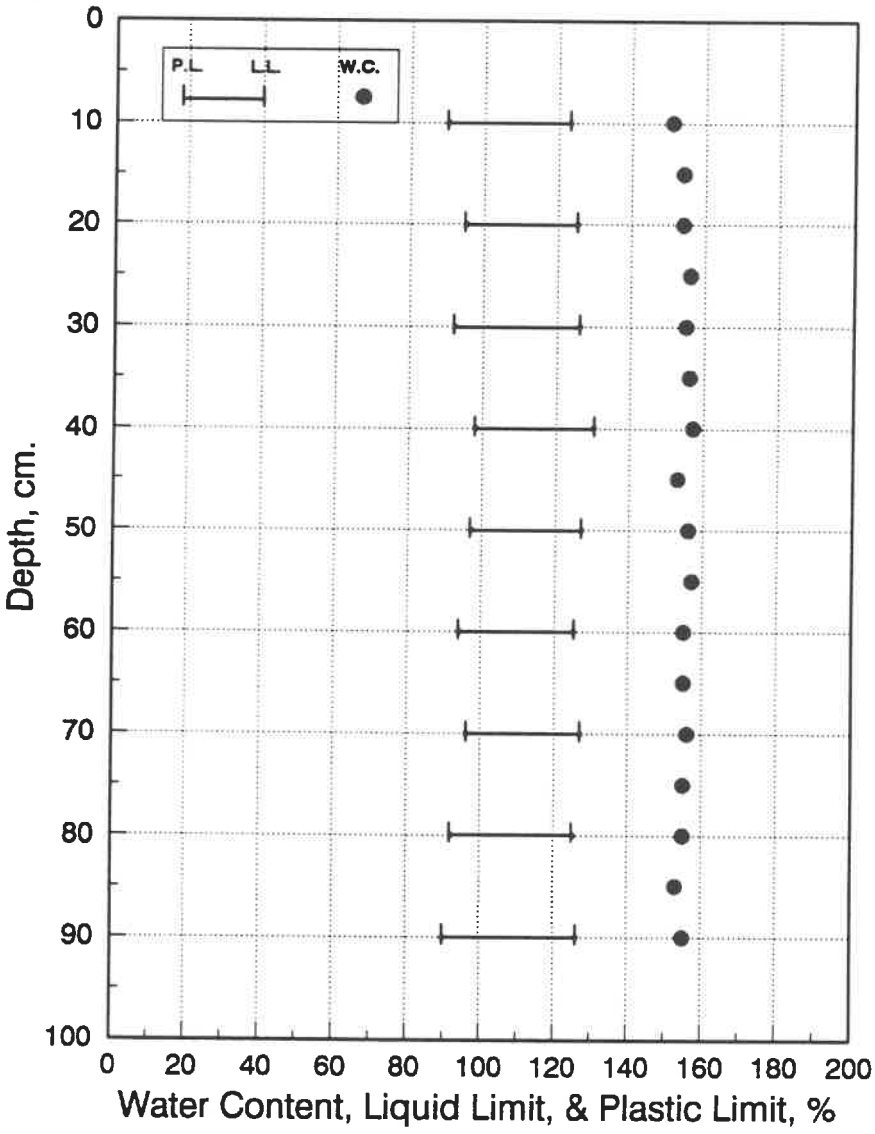

Fig. 4.6 Water content and consistency limits for penetration test-30°.

The tests were carried out under controlled strain conditions with a rate of deformation of about 1%/min, satisfying the expected brittle behavior of the simulated Champlain clay. The applied loads, along with the corresponding elapsed time, were recorded through a computerized data acquisition system. Hence, the unconfined compressive strength could be determined from the following equation:

$$q_u = \frac{F}{A} \qquad [4.7]$$

in which q_u = unconfined compressive strength, F = applied axial load (measured), and A = cross-sectional area of the sample. It has to be mentioned that as the compression load is applied to the sample, the cross-sectional area will increase a small amount. For each applied load, the increased cross-sectional area, A, has been computed by the equation:

$$A = \frac{A_o}{1 - \epsilon} \qquad [4.8]$$

where A is the increased cross-sectional area, A_o is the initial area of the sample, and ϵ is the axial unit strain. The axial unit strain was calculated by applying the following equation:

$$\epsilon = \frac{\Delta L}{L_o} \qquad [4.9]$$

with ϵ = axial unit strain, ΔL = change in length of the sample (function of the rate of deformation and the measured elapsed time), and L_o = initial length of the sample. The unconfined compressive strengths are plotted vs. the axial strains resulting in the stress-strain curves. Stress-strain curves for the 30° apex angle penetration test samples are shown in figures 4.7, 4.8, and 4.9. For the samples of the other apex angles, their stress-strain curves are included in Appendix B.

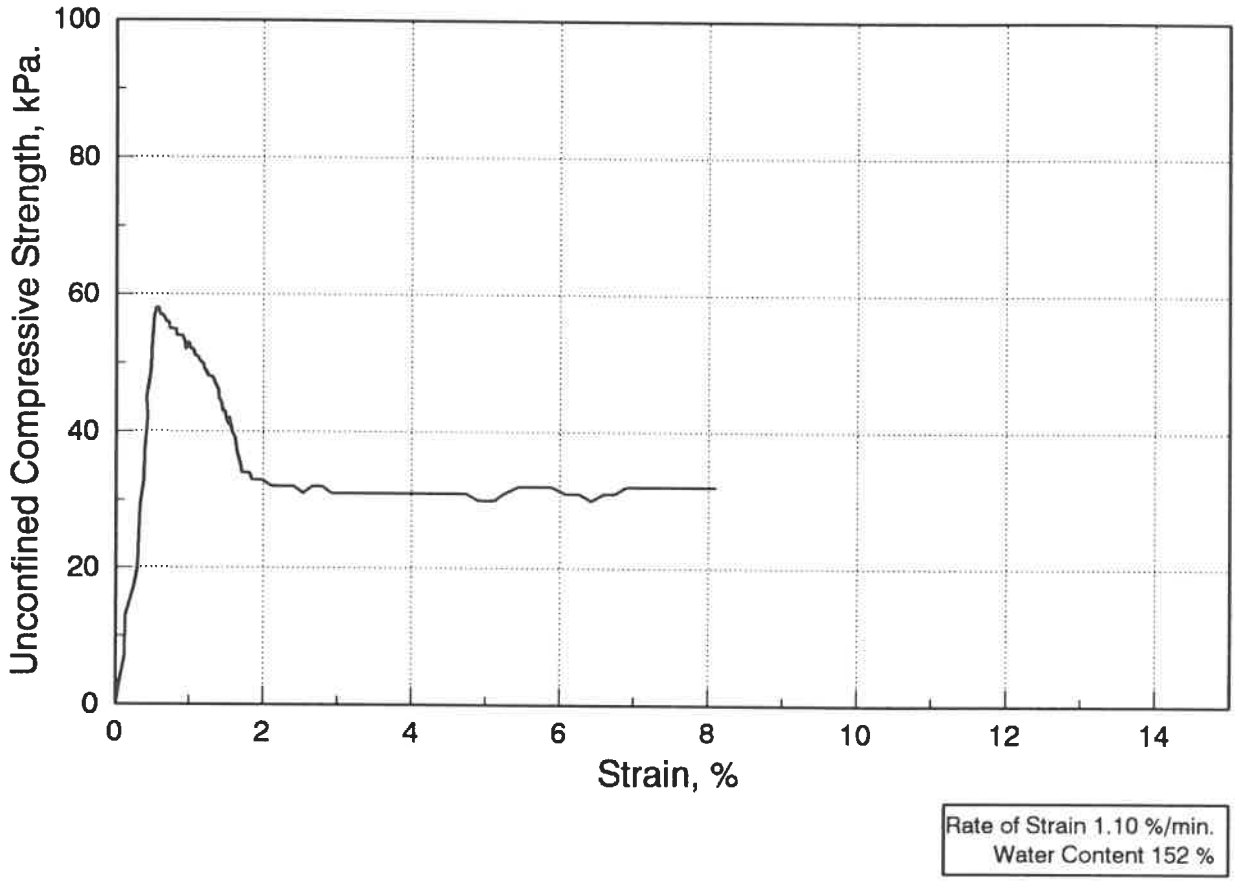

Fig. 4.7 Stress-strain curve of the unconfined compression test-30°/1.

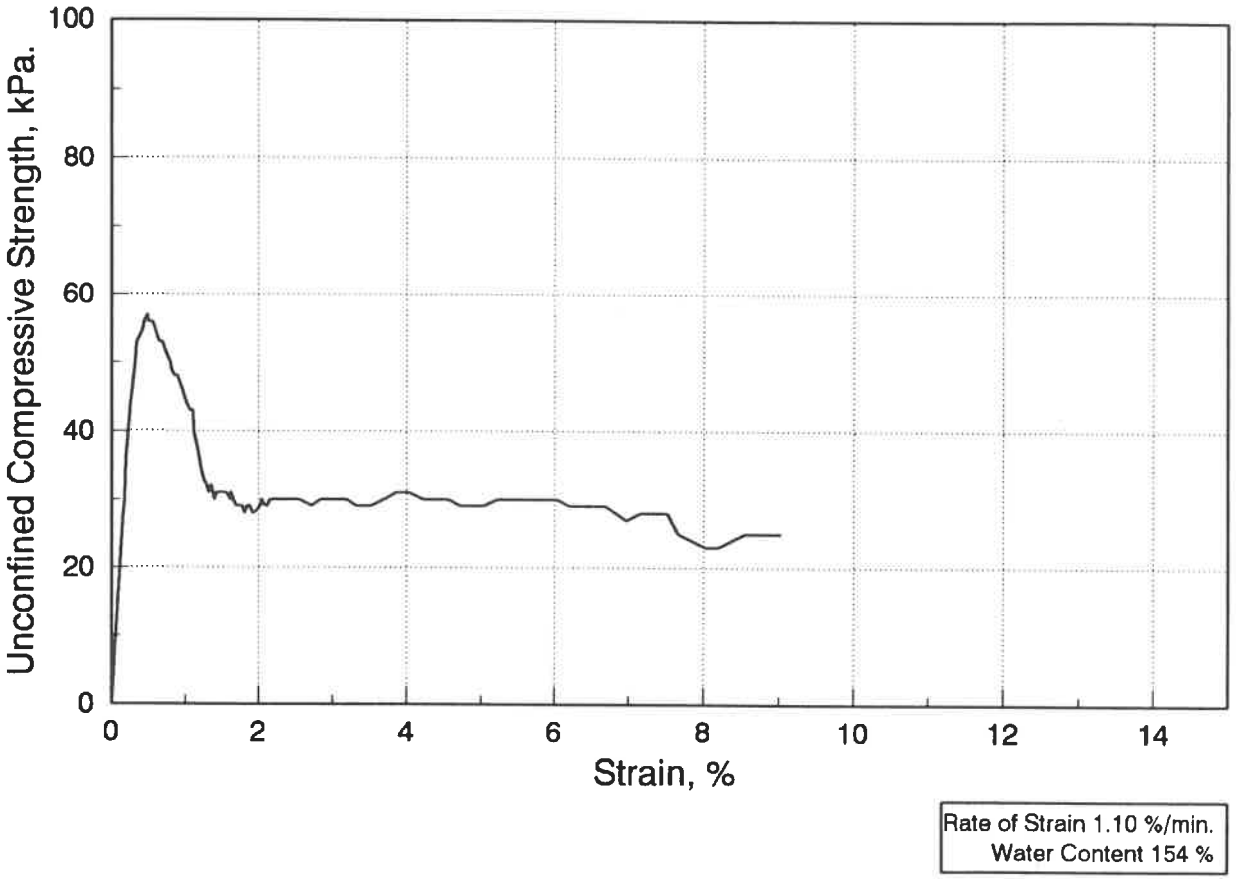

Fig. 4.8 Stress-strain curve of the unconfined compression test-30°/2.

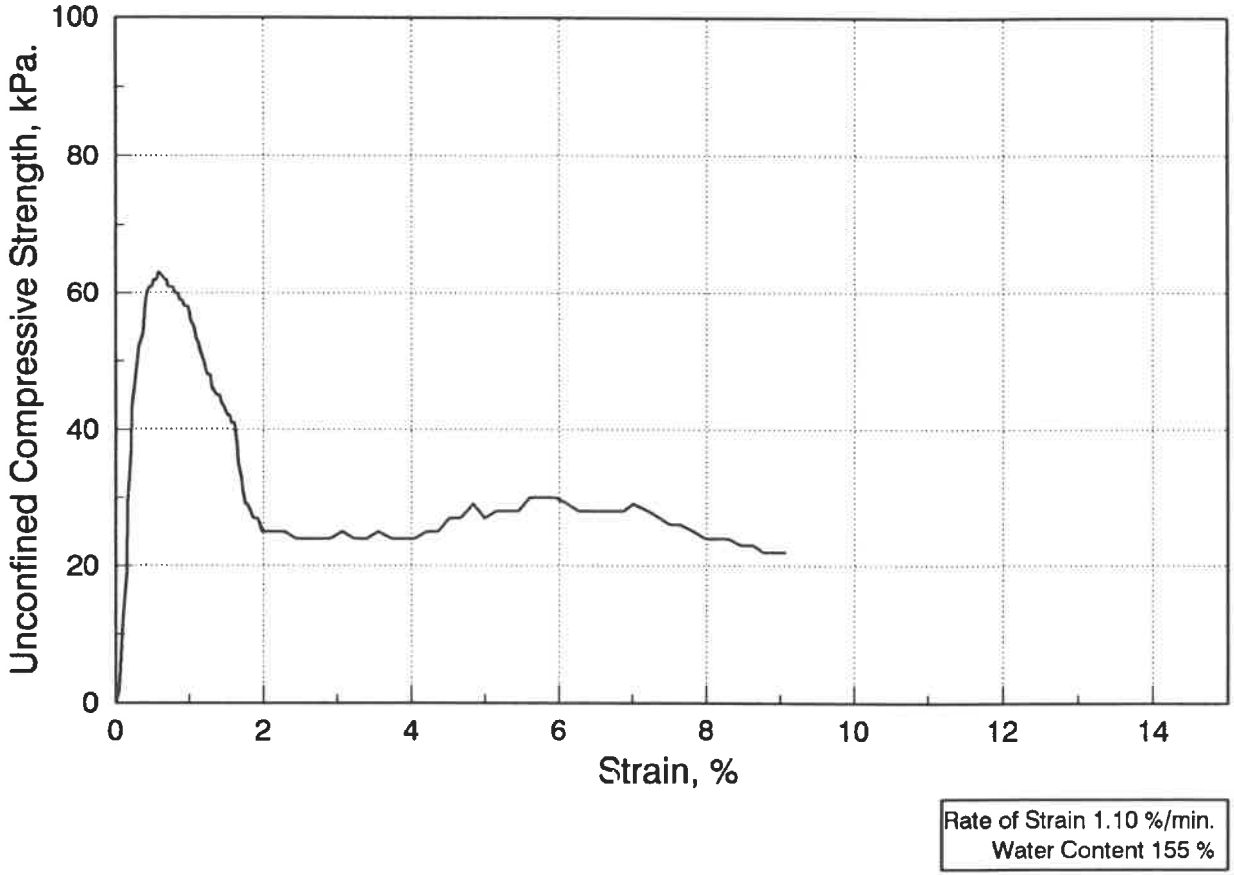

Fig. 4.9 Stress-strain curve of the unconfined compression test-30°/3.

CHAPTER 5

ANALYSIS OF APEX ANGLE VARIATION AND ITS IMPACT ON PENETRATION RESISTANCE

5.1 INTRODUCTION

In previous chapters, a simulated Champlain clay was selected as the material upon which the penetration tests would be conducted, the experimental set up of the penetration tests was described, and the laboratory measurements were presented. In this chapter, penetration test measurements are analyzed, and the results of this analysis are compared with both pertinent theoretical work and reported field measurements. Furthermore, the reliability of the laboratory penetration measurements relevant to the present analysis is discussed.

5.2 CONE FACTOR DETERMINATION

In recent years several attempts have been made to correlate the results of the quasi-static cone penetration test to the undrained shear strength of clay. Traditionally, the correlations have been undertaken using the formula originally suggested by Terzaghi (1943), rewritten as:

$$q_c = N_K c_u + \sigma_o \qquad [5.1]$$

where q_c = cone resistance, N_K = cone factor, c_u = undrained shear strength, and σ_o = total overburden pressure.

As described in chapter 4, the cone resistance values, q_c s, are obtained through the length of the specimen as a function of the cone point loads measured while performing the penetration tests in the laboratory. These values are presented in the form of curves (Appendix B) relating the cone resistance of each of the nine apex angles with the penetration depth.

The reference undrained shear strength, c_u , is often measured from the vane test, however, may in some cases taken as half the unconfined compression test. In the present study, and commonly accepted, laboratory vane test was used to directly produce the reference vane undrained shear strength, c_{uv} . These were measured, as described in chapter 4, every 5 cm along the 1.00 m depth of each of the nine specimens. At each depth interval, four values for the vane undrained shear strength, c_{uv} , were obtained and averaged to represent the reference vane undrained shear strength.

In Terzaghi's formula [5.1] the total overburden

pressure, σ_o , can be expressed as:

$$\sigma_o = \gamma\ z \qquad [5.2]$$

where γ is the total unit weight of the material, and z is the depth of penetration. The value of σ_o pertaining to the present study found to be about 12 kPa, given a 90 cm maximum depth of penetration and γ = 13 kN/m³ for the used material. Maximum and minimum cone resistance values, at penetration depth of 90 cm, are found to be 800 kPa with flat cone, and 400 kPa for the 7.5° cone apex angle, respectively. Since the overburden pressure values are low, compared with the cone resistance values, indicating the insignificant impact of σ_o on the cone factor, N_K, thus could be acceptably neglected.

Considering the effect of neglecting σ_o in Terzaghi's equation [5.1], the cone factor, N_K, can be determined from the following relationship:

$$N_K = \frac{q_c}{c_{uv}} \qquad [5.3]$$

where: N_K = cone factor, q_c = cone resistance, and c_{uv} = reference undrained shear strength obtained by laboratory vane test. In this equation the cone resistance value, q_c , which was measured during the penetration test, is divided by

the corresponding averaged vane undrained shear strength, c_{uv} , to obtain the cone factor value, N_K , for the examined apex angle at a certain penetration depth. For each angle of the nine cone apex angles considered in this study, the cone factor at every 5 cm depth was determined by following the above routine. The determined cone factor values, for each apex angle, are then plotted in the form of a curve with its corresponding penetration depth. The cone factor curves resulting from this analysis are presented in Appendix B (figures B.53 to B.60), however, a representative cone factor curve for 30° cone apex angle is shown in figure 5.1.

5.3 CONE FACTOR VARIATION WITH APEX ANGLE

5.3.1 Classification of the cone apex angles

By examining figure 5.2, in which a comparison was made between the nine cone factor curves, it is apparent that the nine cone apex angles, used in the current study, could visually be classified into four groups. The four groups identified are as follows:

1) Group 1 including cone apex angles of 7.5° and 15°,

2) Group 2 including cone apex angles of 18°, 22.5°, and 30°,

3) Group 3 including cone apex angles of 45°, 60°, and 90°; and

4) Group 4 including cone apex angle of 180° (flat cone).

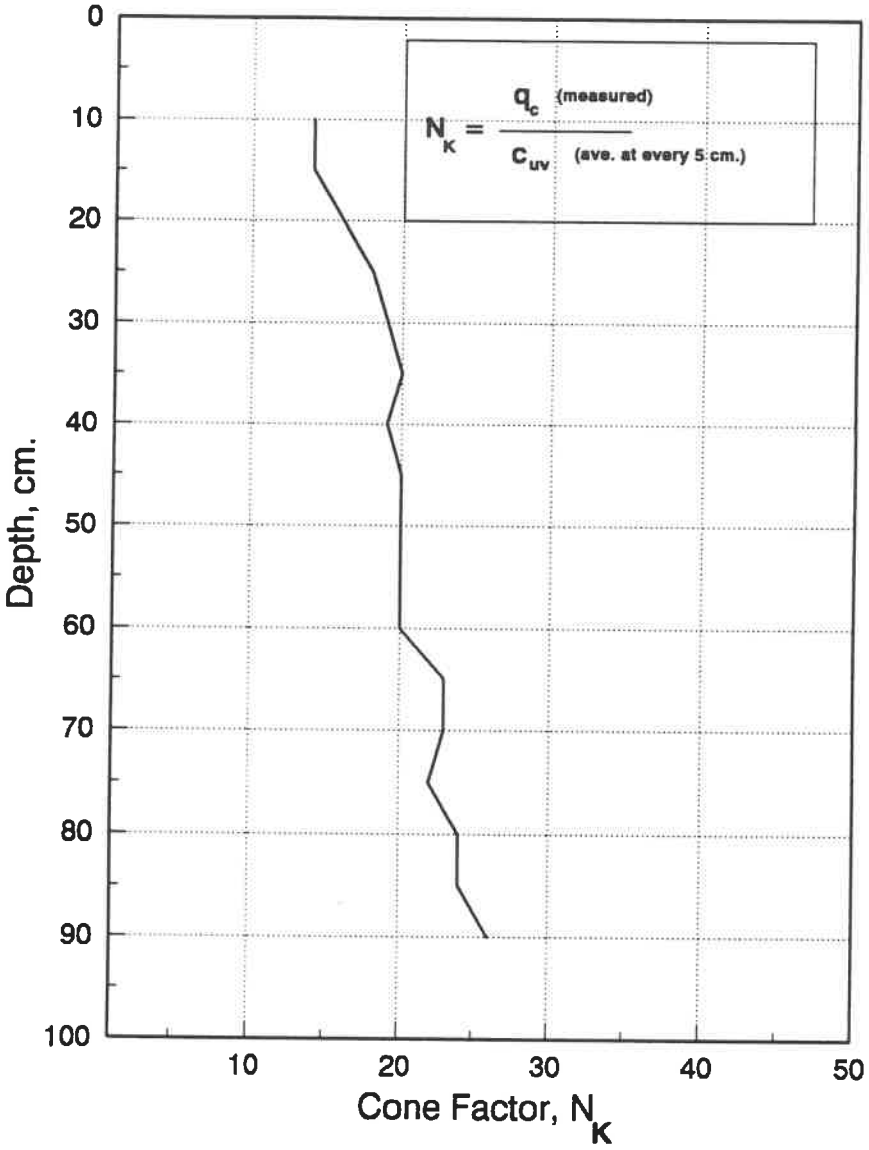

Fig. 5.1 Cone factor curve for 30° cone apex angle.

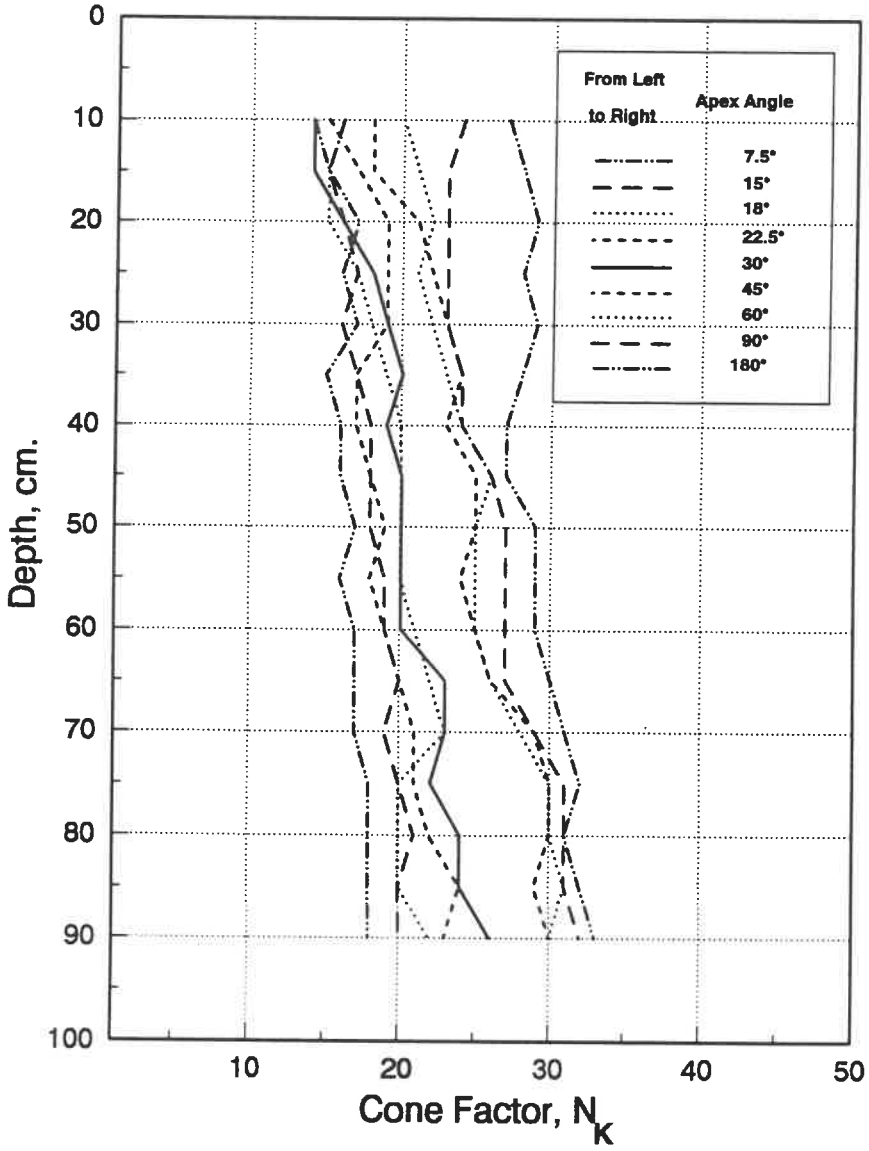

Fig. 5.2 Comparison of cone factor curves.

Figure 5.3 illustrates the trend of the four groups. In this figure, for clarification purpose, only four curves are shown, each of which is considered to represent one of the four groups, namely:

1) Group 1 is represented by the cone factor curve of the 7.5° cone apex angle,

2) Group 2 is represented by the cone factor curve of the 30° cone apex angle,

3) Group 3 is represented by the cone factor curve of the 60° cone apex angle; and

4) Group 4 is represented by the cone factor curve of the 180° cone apex angle (flat cone).

This classification is supported by the results obtained by numerous researchers who have attempted to elucidate the behavior of the soil during a quasi-static cone penetration test. For instance, the theoretical work accomplished by Sagaseta and Houlsby in 1988, has revealed two different flow régimes. The first one which has been called the elastoplastic régime, where an elastic zone ahead the cone tip was detected, concerns very sharp cones with apex angles smaller than 20°. While the second, called the plastic régime, where all the soil around the cone tip was perceived to be plastic, covers the range of apex angles greater than 20°. Another numerical analysis conducted by Baligh (1985)

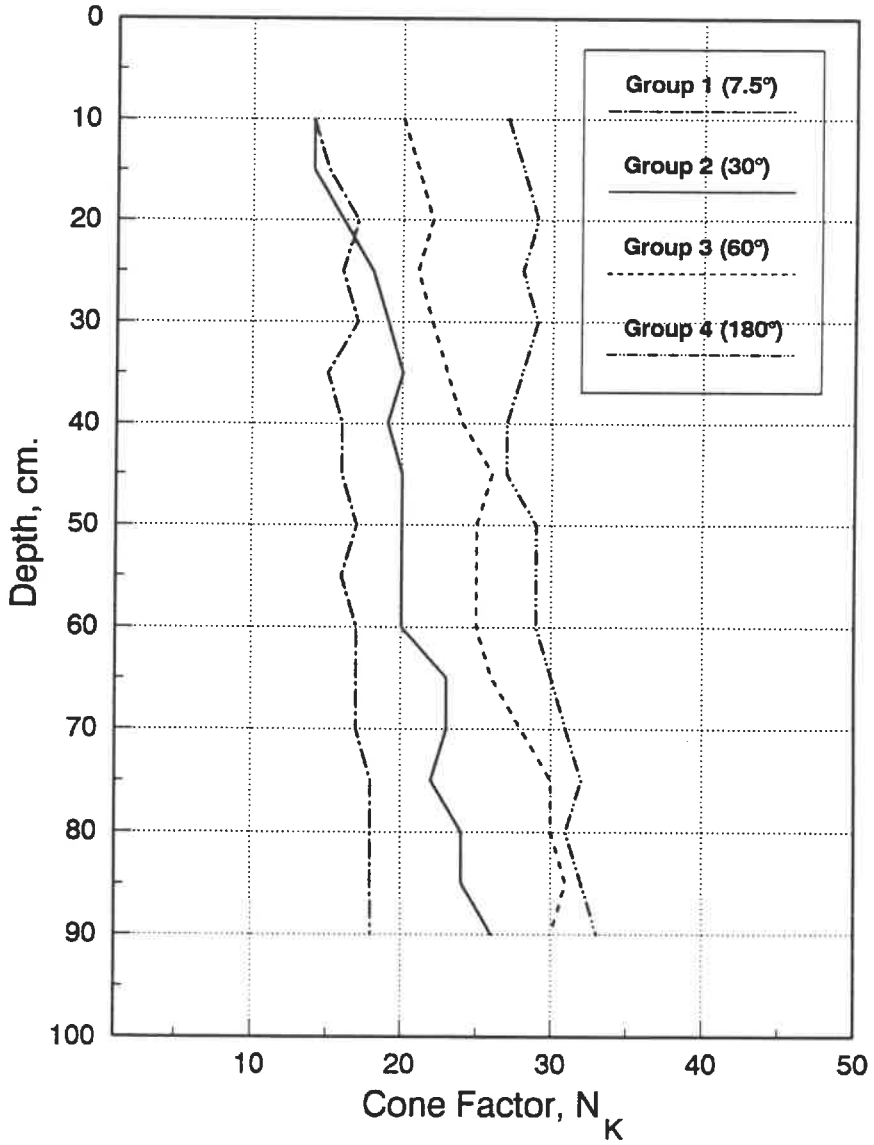

Fig. 5.3 Illustration of the cone factor curves representing the identified groups.

has made the deformations involved in the quasi-static cone penetration test carried out by a standard cone (a 60° cone apex angle), considered as a blunt one, distinctive from those involved in the same test, but for an apex angle of 18° (considered as a sharp cone). As for the latter case, the cone acts in a different way, namely, cutting instead of pushing the soil ahead of the cone.

5.3.2 The effect of skin friction

Referring to equation [5.3], the one which was adopted to interpret the cone factor curves from laboratory measurements of the quasi-static cone penetration tests, one could remark that the cone factor values are directly affected by the measurements of both the cone penetration and the vane shear tests. While the vane shear test results are almost constant with depth, with an average of about 23 ± 2 kPa for the nine 1.00 m height specimens, the cone penetration curves are constantly gaining resistance with depth, resulting in a directly proportional increase of the cone factor values with depth. The reason for that buildup of resistance with penetrating depth has been subject to an accurate investigation. The homogeneity of the material simulating Champlain clays, on which the penetration tests were conducted, through the entire length of the 1.00 m height specimens was confirmed not only by the repeated

results of the vane shear test, but also by that of the water content and consistency limits through the specimen length, as well as the repeated form of the material stress-strain curves obtained by the unconfined compression tests.

Excluding the heterogeneity of the material, one possible reason for that increase of resistance could be the mobilization of some skin friction on the penetrating rod during the penetration process. To investigate the effect of skin friction, the well-established equation for the determination of the ultimate bearing capacity, P_u, of a pile in homogeneous soil was applied. This equation may be expressed by the sum of point resistance, P_p , and skin resistance, P_s , or:

$$P_u = P_p + P_s = q_p A_p + f_s A_s \qquad [5.4]$$

in which q_p is the ultimate unit bearing capacity of pile point of area A_p , and f_s is the average unit skin friction on shaft of area A_s . Considering the penetration rod in our case, together with the cone head as a pile, and given that the average resistance gained at the end of penetration tests is around 200 kPa, one could equate the second term of equation [5.4], representing the skin resistance, with the increased resistance as follows:

$$P_s = f_s A_s = 200\ kPa. \qquad [5.5]$$

with $A_s = \pi$ b L, in which b = rod diameter = 1.00 cm, and L = the length over which skin friction is mobilized = 80 cm (assuming that the point resistance is fully attained after 10 cm penetration). These average values, representing the nine cone resistance curves, result in a unit skin friction, f_s , of the order of 0.80 kPa. For homogeneous saturated clay:

$$f_s = c_a = \alpha\ c_u \qquad [5.6]$$

where c_a = the unit shaft adhesion, α = an empirical adhesion coefficient, and c_u = the undrained cohesion. Following the previous calculations, and considering c_u = the remolded undrained cohesion = 1.20 kPa (as the average value obtained by the laboratory vane tests), we get α = 0.67. Comparing this value with the values of α for driven piles in natural clays, which range on the average roughly from unity for soft clay to one-half or less for stiff clay, one could confidently presume that the rod and the cones used in the penetration tests of the present study are almost perfectly smooth ones. However, it is sufficient to have a unit shaft adhesion, c_a , of only 0.80 kPa to increase the cone resistance by 200 kPa at 90 cm penetration depth.

5.3.3 The influence of varying the cone apex angle

The impact of apex angle variation on the cone factor is shown in figure 5.4 for different penetration depths. A linear regression analysis is conducted to identify the increasing trend of the cone factor with the apex angle, irrespective of penetration depth. Based on the trend of figure 5.4, it can be seen that sharp cones have low cone resistance, while blunter cones exhibit higher cone resistance.

Assuming the penetrating rod and cones as smooth, the trend of figure 5.4 would be in good agreement with preceding studies. For instance, the theoretical analysis carried out by Houlsby and Wroth in 1982 (figure 2.11), have illustrated similar trend in cone resistance variation. In fact, the experimental work of the present study have extended their numerical research by considering depth-to-diameter ratios greater than 20 (the limitation of their study). It has to be mentioned, however, that the penetration depths of figure 5.4 have same values as the depth-to-diameter ratios, since the cone diameter used was 1.00 cm. Earlier experimental works on ductile materials indentation (Bishop et al., 1945) have also observed a comparable trends for the cone resistance variation.

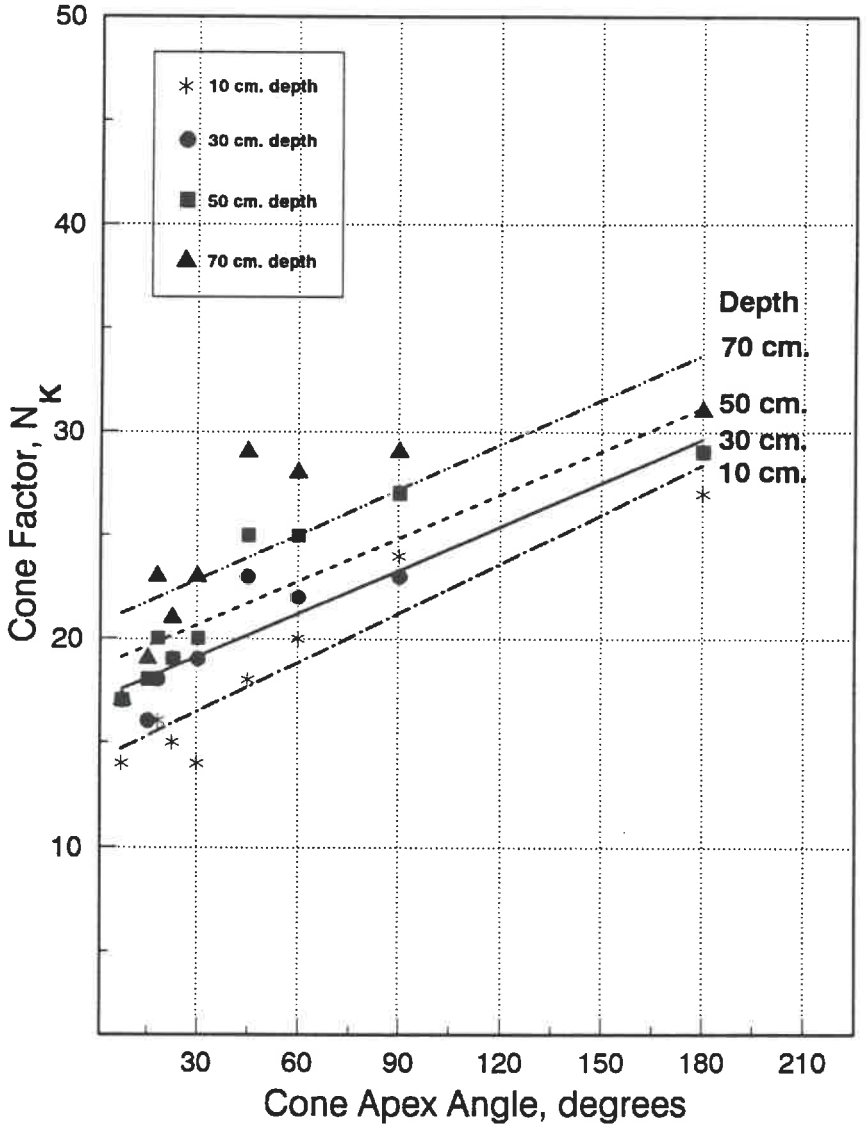

Fig. 5.4 The impact of varying the cone apex angle on the cone factor at different depths.

5.4 COMPARISON WITH PREVIOUS THEORETICAL WORK

Based on the work of Bishop et al. (1945) on the indentation of ductile metals, Ladanyi (1967) developed a solution for the ultimate spherical cavity expansion pressure (equation [2.17]), considering a simplified undrained stress-strain curve. Figure 5.5 shows the simplified stress-strain curve, represented by the full line (OABC), of the unconfined compression test-30°/2. This curve is assumed to be a fair representative for all the other 26 unconfined compression tests. The four governing parameters of equation [2.17] are obtained from figure 5.4 as follows:

$c_u = \frac{1}{2} q_p = 30$ kPa,

$c_r = \frac{1}{2} q_r = 15$ kPa,

$E_u = 2\ c_u / \epsilon_u = 24$ MPa (for $\epsilon_u = 0.25\%$); and

$E_r = 2\ c_r / \epsilon_r = 2$ MPa (for $\epsilon_r = 1.50\%$).

Substituting the above numerical values into equation [2.17], the resulting normalized spherical pressure, p_{sph} / c_u, would be 5.82.

Later in 1973, Ladanyi has determined a normalized spherical pressure considering a more simplified stress-strain curve (line OAC in figure 5.5) resulting in an expression for the bearing capacity factor of a deep circular footing, $N_{c,\ cir}$, as follows:

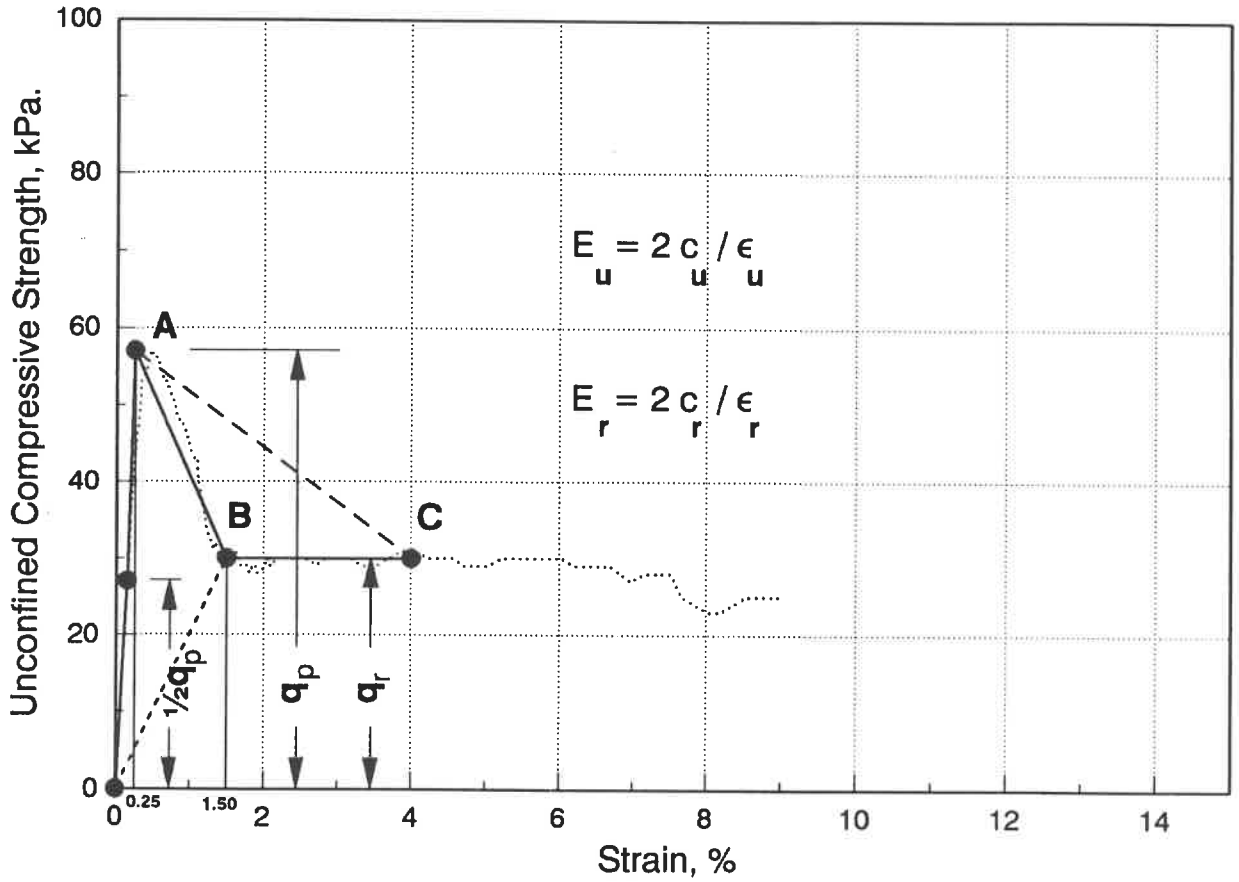

Fig. 5.5 Simplified stress-strain curve of the unconfined compression test-30°/2.

$$N_{c,cir} = \frac{C_r}{C_u} + \frac{4}{3}\left[\frac{C_r}{C_u} + \ln\frac{E_u}{3C_u}\right] \qquad [5.7]$$

using the same notations as that of equation [2.17]. Substituting the previous numerical values into equation [5.7] would result in a bearing capacity factor in the order of 8.62. Although the later result is higher than the former one for the normalized spherical pressure, yet both are much lower than the cone factors obtained from the penetration tests of the present study. The reason for this difference need to be more deeply investigated and could be a subject of future research.

5.5 COMPARISON WITH FIELD MEASUREMENTS

A study of available literature reveals that reported correlations between field measurements of quasi-static cone resistance and undrained shear strength of clay show a large scatter. Several different cone penetrometers have been used, and the undrained shear strength has been determined by different methods (unconfined compression, triaxial, pressuremeter, plate load, and vane tests). Cone factor values, N_K s, are reported to vary between 5 and 70, for instance, Amar et al. (1975), however, most of the values are in the 10 to 30 range (Bowles, 1988).

In 1973, a joint research program was started between the Norwegian Geotechnical Institute and the Dutch firm Fugro-Cesco B.V., in which an extensive quasi-static cone penetration testing program was carried out at several locations with well documented clay deposits in Norway, Sweden, and Denmark. A part of this research results was presented by Lunne et al. (1976). Since much experience exists for Scandinavian soft clays regarding the correlation between the vane shear strength and the undrained shear strength, therefore it was seemed justified to attempt to correlate the cone resistance to the vane shear strength. The tests were conducted using standard vanes with height-to-diameter ratio of 2. The Fugro cone penetrometer used in the tests has a cone area of 10 cm^2, and a 60° cone apex angle with a straight cylindrical shaft above the cone having the same diameter as the cone, which is 36 mm. The thrust required to advance the penetrometer at a rate of approximately 2 cm/s was applied to the top of the push rods, and the cone resistances were recorded directly through an electrical cable connected to the load cell in the penetrometer tip. From the results of five different sites presented by Lunne et al. (1976), in which the deposits vary from soft to medium stiff normally consolidated Scandinavian marine clays, the cone factor, N_K , has been found to vary between 13 and 24. Later in 1981, data presented by Lunne and

Kleven show that, for the normally consolidated marine clays in the North Sea, using the corrected field vane strength (i.e. Bjerrum's (1973) correction for plasticity index), the corrected cone factor, $N_{K,\ coor}$, falls between 11 and 19. A comparison between the above field measurements and the ones obtained from the laboratory measurements of the present study implies that the cone factor values obtained are within practical range, despite the scale effect and the variability in the tested clays.

Baligh (1975) has combined the two common theories for calculating the cone factor (bearing capacity theory and cavity expansion theory) in an approximate form to study the effect of clay rigidity index, I_r , of equation [2.19] on penetration resistance. The results of the cone resistance were obtained by the use of a standard Fugro-type electric cone at a penetration rate of 2 cm/s. The obtained results demonstrate that the cone factor, N_K , should not be constant for all clays. The study showed also that using a standard cone (60° apex angle and 36 mm diameter) $N_K = 16 \pm 2$ over the full range of likely rigidity index values ($10 < I_r < 500$). In the case of the simulated Champlain clay used in the present research the rigidity index, I_r ,was found to be around 150 (assuming that Poisson's ratio is equal to 0.5), while the cone factor for the 60° apex angle is in the order

of 20 at 10 cm depth, where the skin friction influence is considered negligible. The cone factor value of 20 is considered close to the field measurements of Baligh mentioned above.

5.6 THE EFFECT OF CONFINEMENT AND EXPERIMENTAL ERRORS ON PENETRATION MEASUREMENTS

As described in chapter 4, the laboratory penetration tests were conducted on specimens, 1.00 m height and 20 cm diameter, casted in PVC tubes, while the cones were 10 mm in diameter. To investigate the influence of confinement on the cone resistance curve, two unconfined quasi-static cone penetration tests, using the 30° cone apex angle, were carried out in the laboratory. In these tests, the 1.00 m height specimens were drawn out of their molds by applying a pneumatic pressure, and then the penetration test is performed by the same way and under the same conditions the other confined penetration tests were realized, to enable the comparison of the cone resistance curves. A photograph illustrating the unconfined specimen, 1.00 m height, 20 cm diameter, and about 50 kg weight, just before testing it, is shown in plate C.4 of Appendix C. Figures 5.6 and 5.7 demonstrate the obtained cone penetration curves from the two tests carried out. It has to be noticed that the slight

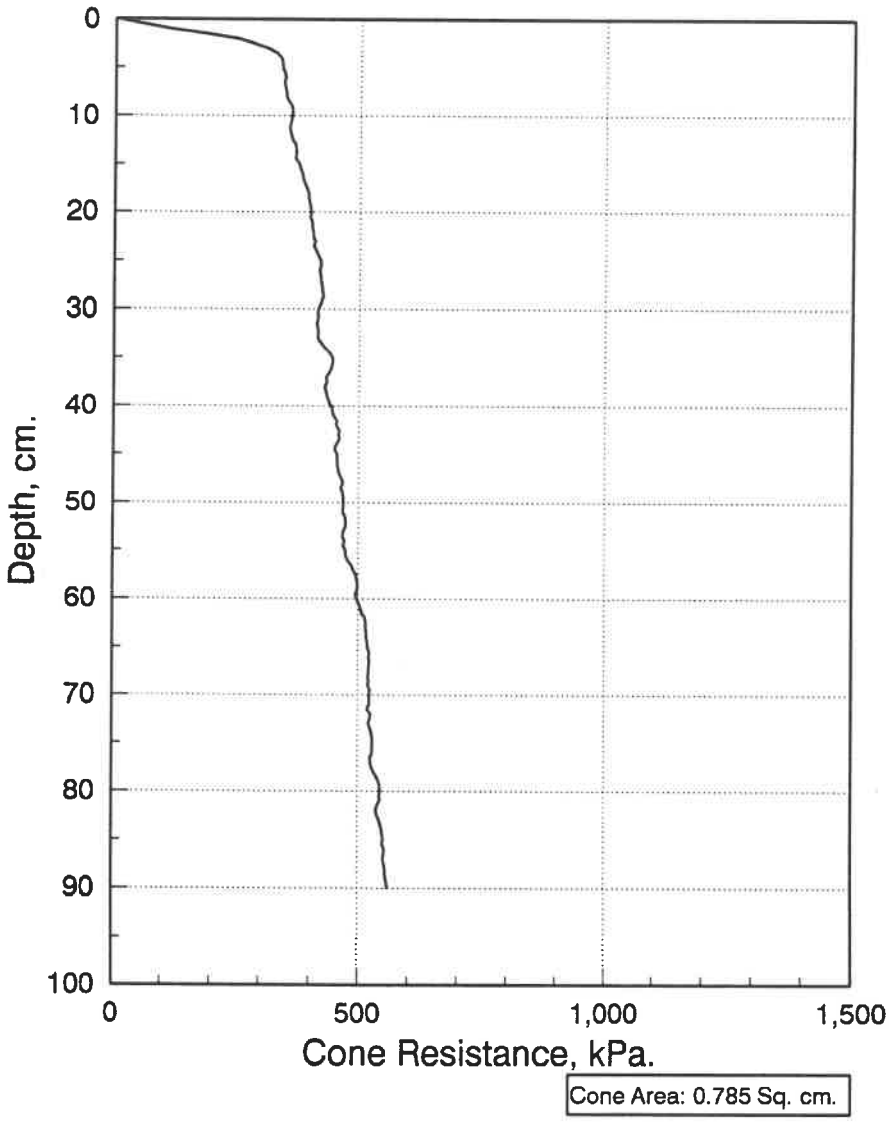

Fig. 5.6 Unconfined quasi-static cone resistance curve for 30° cone apex angle after 23 days.

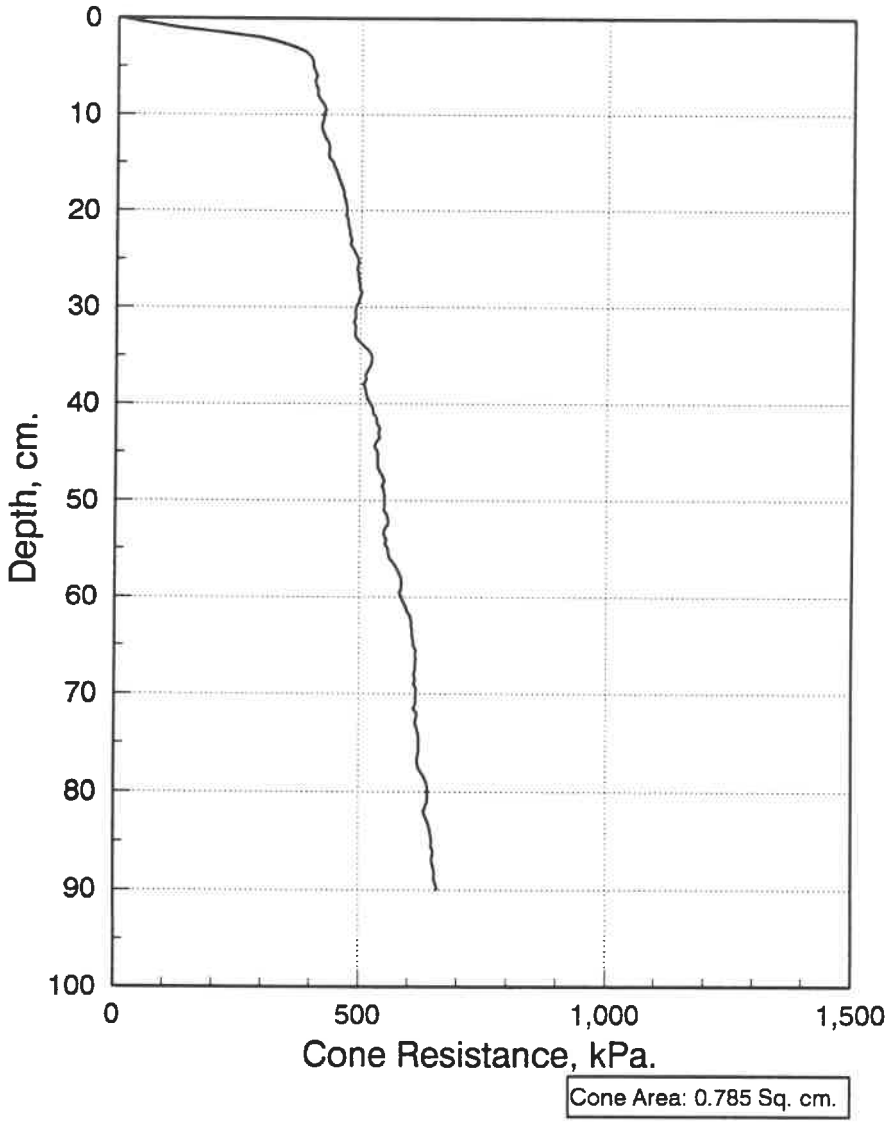

Fig. 5.7 Unconfined quasi-static cone resistance curve for 30° cone apex angle after 30 days.

difference between the cone resistance values of these two tests is due to the fact that the first one was conducted after 23 days of casting the material, and the second was performed after 30 days. This can easily be explained by emphasizing the role of cement, which is one of the model material components and in which it is introduced to produce the necessary peak strength, as it is well-known that cement gains strength with time. On the other hand, comparing figure 4.3 with figures 5.6 and 5.7 reveals that choosing a specimen with diameter of about 20 times the penetrating cone diameter, as was adopted in the current research, would avoid any possible negative effects of boundaries on the penetration measurements.

Precluding the influence of confinement, one possible source of errors could be the experimental errors involved in any laboratory research. The deviation from the vertical line during the test is one of these errors. It is believed that the great majority of all penetration tests, especially in field, is subjected to some degree of deviation and that this phenomenon is one of the most important sources of error, particularly in deep soundings. It has to be mentioned that the penetrating rods have a relatively low moment of inertia and that, consequently, they can bend considerably without suffering permanent deformation. In spite of all precautions

taken to elude the drifting of the cone, which is usually progressive once the process has started, it is often impossible to prevent errors in verticality. Serious mistakes may also result, specifically in the output readings of the tests, if a load concentration is felt by the load cell. This is the case, as in ours, if the applied thrust on top of the rods is measured by a load cell through a bearing point. Therefore, selecting this manner of load measurements must be coupled with utmost care in the choice of a convenient bearing contact. Another cause of experimental errors is the accuracy of devices and instruments used in the measurements. The precision of the load cell, for instance, could be one of the predominant origins of the penetration test results discrepancy.

CHAPTER 6

CONCLUSIONS

The present research explores the penetration phenomena in soils and soil-indenter interaction. The study focuses on the quasi-static cone penetration test. The present study concerns varying the cone apex angle. A laboratory experiment is set up and cone penetration measurements have been successfully carried out in order to investigate the impact of varying the apex angle on the quasi-static penetration measurements. The research deals with a certain type of clay often encountered in Eastern Canada, namely Champlain clay. The main characteristics of such clay reside in its very brittle and extremely strain-sensitive structure. The study investigated the reliable use of a simulated Champlain clay in laboratory analysis of penetration tests. This material provides a means for researchers to more carefully examine the inherent behavior of Champlain clays, avoiding the difficulties and expenses of acquiring and handling undisturbed natural clay samples of the necessary size and quantity.

In general, this research contributes to the understanding of the penetration phenomena in clays. The research specific contributions can also be summarized as follows:

1. The development of a strength-controlled simulated Champlain clay. The simulated material is cheap and easily handled in the laboratory, facilitating further geotechnical engineering studies on Champlain clays.
2. The demonstration of the impact of varying the apex angle on the cone factor as a function of cone resistance at different penetration depths.
3. The present study sheds more light on soil-indenter interaction and cone penetration in Champlain clays.

Based on the findings of the present study, the following recommendations could be drawn:

- The simulated material used could be further investigated to identify its appropriateness for other geotechnical engineering studies on Champlain clays.
- Actual quasi-static cone penetration test measurements with different apex angles might be conducted in field to confirm the laboratory measurements.
- The development of a more elaborate theory to elucidate the penetration phenomena could minimize the existing discrepancy between theoretical results and real measurements.

REFERENCES

AMAR, S., BAGUELIN, F., JEZEQUEL, J.F. and LE MEHAUTE, A., 1975 "In Situ Shear Resistance of Clays", Proc. ASCE Specialty Conference on In Situ Measurement of Soil Properties, Raleigh, NC, Vol. 1, pp. 22-45.

American Society for Testing and Materials, 1981 "ASTM Book of Standards", Philadelphia, Pa.

BALIGH, M.M., 1985 "Strain Path Method", Journal of Geotechnical Engineering, ASCE, Vol. 111, pp. 1108-1136.

BALIGH, M.M., VIVATRAT, V. and LADD, C.C., 1980 "Cone Penetration in Soil Profiling", Journal of the Geotechnical Engineering Division, ASCE, Vol. 106, pp. 447-461.

BALIGH, M.M., 1975 "Theory of Deep Site Static Cone Penetration Resistance", Research Report, Massachusetts Institute of Technology, Department of Civil Engineering, Cambridge, MA.

BISHOP, R.F., HILL, R. and MOTT, N.F., 1945 "The Theory of Indentation and Hardness Tests", Proc. of the Physical

Society, Vol. 57, Part 3, pp. 147-159.

BJERRUM, L., 1973 "Problems of Soil Mechanics and Construction on Soft Clays", State-of-the-Art Report, Proc. 8th International Conference on Soil Mechanics and Foundnation Engineering, Moscow, Russia, Vol. 3, pp. 109-159.

BOWLES, J.E., 1988 "Foundation Analysis and Design", 4th ed., McGraw-Hill, Inc., New York, p. 1004.

CHEN, C.K., 1972 "Wedge and Cone Indentation of Soils", Ph.D. thesis, Civil Engineering Department, McGill University.

COX, A.D., 1962 "Axially-Symmetric Plastic Deformation in Soils-II. Indentation of Ponderable Soils", International Journal of Mechanical Sciences, Vol. 4, pp. 371-380.

COX, A.D., EASON, G. and HOPKINS, H.G., 1961 "Axially-Symmetric Plastic Deformations in Soils", Philosophical Transactions of the Royal Society of London, Series A, Vol. 254, pp. 1-45.

CRAWFORD, C.B., 1968 "Quick Clays of Eastern Canada", Engineering Geology, Vol. 2 (4), pp. 239-265.

CRAWFORD, C.B., 1963 "Cohesion in an Undisturbed Sensitive Clay", Géotechnique, Vol. 13 (2), pp.132-145.

DAS, B.M. and HASSLER, P.C., 1988 "Statics and Mechanics of Materials", Prentice-Hall, Inc., Englewood Cliffs, New Jersey, p. 486.

DE RUITER, J., 1981 "Current Penetrometer Practice", Symposium on Cone Penetration Testing and Experience, Geotechnical Engineering Division, ASCE, St. Louis, Missouri, pp. 1-48.

DE RUITER, J., 1971 "Electric Penetrometer for Site Investigations", Journal of the Soil Mechanics and Foundations Division, ASCE, Vol. 97, pp. 457-472.

GADD, N.R., 1960 "Surficial Geology of the Becancour Map-Area, Quebec", Geological Survey of Canada, paper 59-8.

GIBSON, R.E., 1950 "Discussion on Paper by G. Wilson", Journal of the Institution of Civil Engineers, Vol. 34, p. 382.

HAAR, A. and VON KARMAN, 1909 "Zur Theorie der Sannungszustande in Plastischen und Sandartigen Medien",

Nachr. Ges. Wiss., Göttingen, p. 204.

HILL, R., 1950 "The Mathematical Theory of Plasticity", Clarendon Press, Oxford, p. 299.

HOULSBY, G.T. and WROTH, C.P., 1982 "Determination of Undrained Strengths by Cone Penetration Tests", Proc. 2nd European Symposium on Penetration Testing, Amsterdam, Netherlands, pp. 585-590.

LADANYI, B., 1974 "Discussion on Paper by M. Roy et al.", Proc. 1st European Symposium on Penetrartion Testing, Stockholm, Sweden, Vol. 2:1.

LADANYI, B., 1973 "Bearing Capacity of Deep Footings in Sensitive Clays", Proc. 8th International Conference on Soil Mechanics and Foundnation Engineering, Moscow, Russia, Vol. 2.1, pp. 159-166.

LADANYI, B. and EDEN, W.J., 1969 "Use of the Deep Penetration Test in Sensitive Clays", Proc. 7th International Conference on Soil Mechanics and Foundnation Engineering, Mexico, Vol. I, pp. 225-230.

LADANYI, B., 1967 "Deep Punching of Sensitive Clays",

Proc. 3rd Pan American Conference on Soil Mechanics and Foundnation Engineering, Caracas, Venezuela, Vol. I, pp. 533-546.

LADANYI, B., 1963 "Expansion of a Cavity in a Saturated Clay Medium", Journal of the Soil Mechanics and Foundations Division, ASCE, Vol. 89, pp. 127-161.

LA ROCHELLE, P., ROY, M. and TAVENAS, F., 1973 "Field Measurements of Cohesion in Champlain Clays", Proc. 8th International Conference on Soil Mechanics and Foundnation Engineering, Moscow, Russia, Vol. 1.1, pp. 229-236.

LA ROCHELLE, P. and LEFEBVRE, G., 1971 "Sampling Disturbance in Champlain Clays", American Society for Testing and Materials, STP-483, pp. 143-163.

LIU, C. and EVETT, J.B., 1984 "Soil Properties: Testing, Measurement, and Evaluation", Prentice-Hall, Inc., Englewood Cliffs, New Jersey, p. 315.

LUNDGREN, H. and MORTENSEN, K., 1953 "Determination by the Theory of Plasticity of the Bearing Capacity of Continuous Footings on Sand", Proc. 3rd International Conference on Soil Mechanics and Foundnation Engineering,

Zurich, Switzerland, Vol. 1, pp. 409-412.

LUNNE, T. and KLEVEN, A., 1981 "Role of CPT in North Sea Foundation Engineering", Symposium on Cone Penetration Testing and Experience, Geotechnical Engineering Division, ASCE, St. Louis, Missouri, pp. 76-107.

LUNNE, T., EIDE, O. and DE RUITER, J., 1976 "Correlations between Cone Resistance and Vane Shear Strength in some Scandinavian Soft to Medium Stiff Clays", Canadian Geotechnical Journal, Vol. 13, pp. 430-441.

MEYERHOF, G.G., 1976 "Bearing Capacity and Settlement of Pile Foundations", Journal of the Geotechnical Engineering Division, ASCE, Vol. 102, pp. 195-228.

MEYERHOF, G.G., 1951 "The Ultimate Bearing Capacity of Foundations", Géotechnique, Vol. 1, pp. 301-332.

OSLER, J.C. and PECK, G.M., 1963 "Bearing Capacity of Model Footings under Conditions of Local Shear Failure", Proc. Canadian Soil Mechanics Conference, Ottawa, Canada.

ROBERTSON, P.K. and CAMPANELLA, R.G., 1983 "Interpretation of Cone Penetration Tests. Part II: Clay",

Canadian Geotechnical Journal, Vol. 20, pp. 734-745.

ROY, M., MICHAUD, D., TAVENAS, F., LEROUEIL, S. and LA ROCHELLE, P., 1974 "The Interpretation of Static Cone Penetration Tests in Sensitive Clays", Proc. 1st European Symposium on Penetrartion Testing, Stockholm, Sweden, Vol. 2:2, pp. 323-330.

SANGLERAT, G., 1972 "The Penetrometer and Soil Exploration", Elsevier Publishing Co., Amsterdam, The Netherlands, p. 464.

SAGASETA, C. and HOULSBY, G.T., 1988 "Elastic-plastic Incompressible Flow around an Infinite Cone", Proc. 1st International Symposium on Penetration Testing, Orlando, pp. 933-938.

SCHMERTMANN, J.H., 1975 "Measurement of In Situ Shear Strength", State-of-the-Art Report, Proc. ASCE Specialty Conference on In Situ Measurement of Soil Properties, Raleigh, NC, Vol. 2, pp. 57-138.

SHIELD, R.T., 1955a "On Coulomb's Law of Failure in Soils", Journal of the Mechanics and Physics of Solids, Vol. 4, pp. 10-16.

SHIELD, R.T., 1955b "On the Plastic Flow of Metals under Conditions of Axial Symmetry", Proc. of the Royal Society of London, Series A, Vol. 233, pp. 267-287.

SILVESTRI, V., 1974 "Performance of Sensitive Clays under Variable Stresses", Ph.D. thesis, Civil Engineering Department, McGill University.

SPENCER, A.J.M., 1962 "Perturbation Methods in Plasticity-III Plane Strain of Ideal Soils and Plastic Solids with Body Forces", Journal of the Mechanics and Physics of Solids, Vol. 10, pp. 165-177.

TAVENAS, F., ROY, M. and LA ROCHELLE, P., 1973 "An Artificial Material for Simulating Champlain Clays", Canadian Geotechnical Journal, Vol. 10, pp. 489-503.

TAVENAS, F. and CHAPEAU, C., 1972 "Développement d'un matériau artificiel de simulation des argiles de la mer Champlain", Rapport interne No. GCS-72-02-01, Département de Génie Civil, Université Laval, Québec.

TERZAGHI, K. and PECK, R.B., 1967 "Soil Mechanics in Engineering Practice", 2nd ed., John Wiley & Sons, Inc., New York, p. 729.

TERZAGHI, K., 1943 "Theoretical Soil Mechanics", John Wiley & Sons, Inc., New York, p. 510.

VESIĆ, A.S., 1972 "Expansion of Cavities in Infinite Soil Mass", Journal of the Soil Mechanics and Foundations Division, ASCE, Vol. 98, pp. 265-290.

APPENDICES

APPENDIX A: STRESS-STRAIN CURVES.

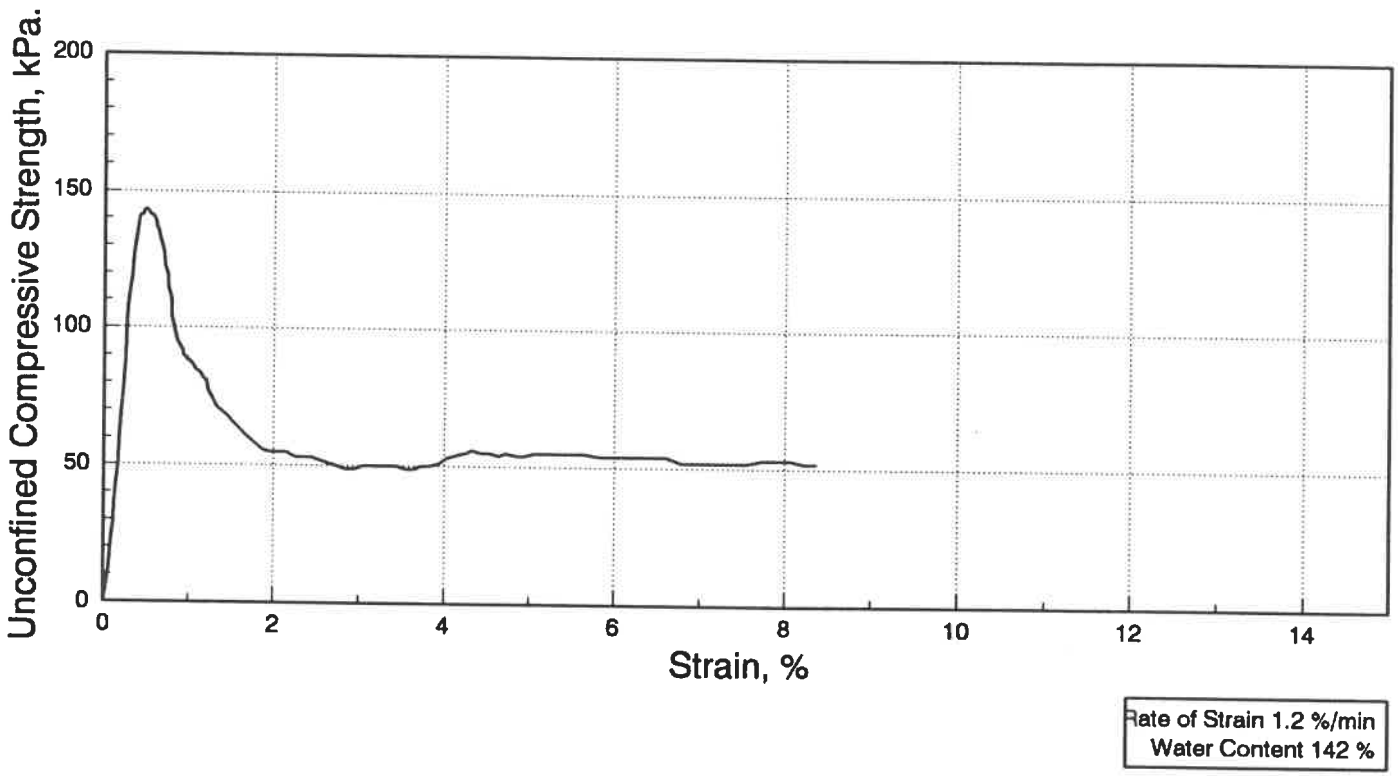

Fig. A.1 Stress-strain curve of test 102

for model material with 25.00 % cement.

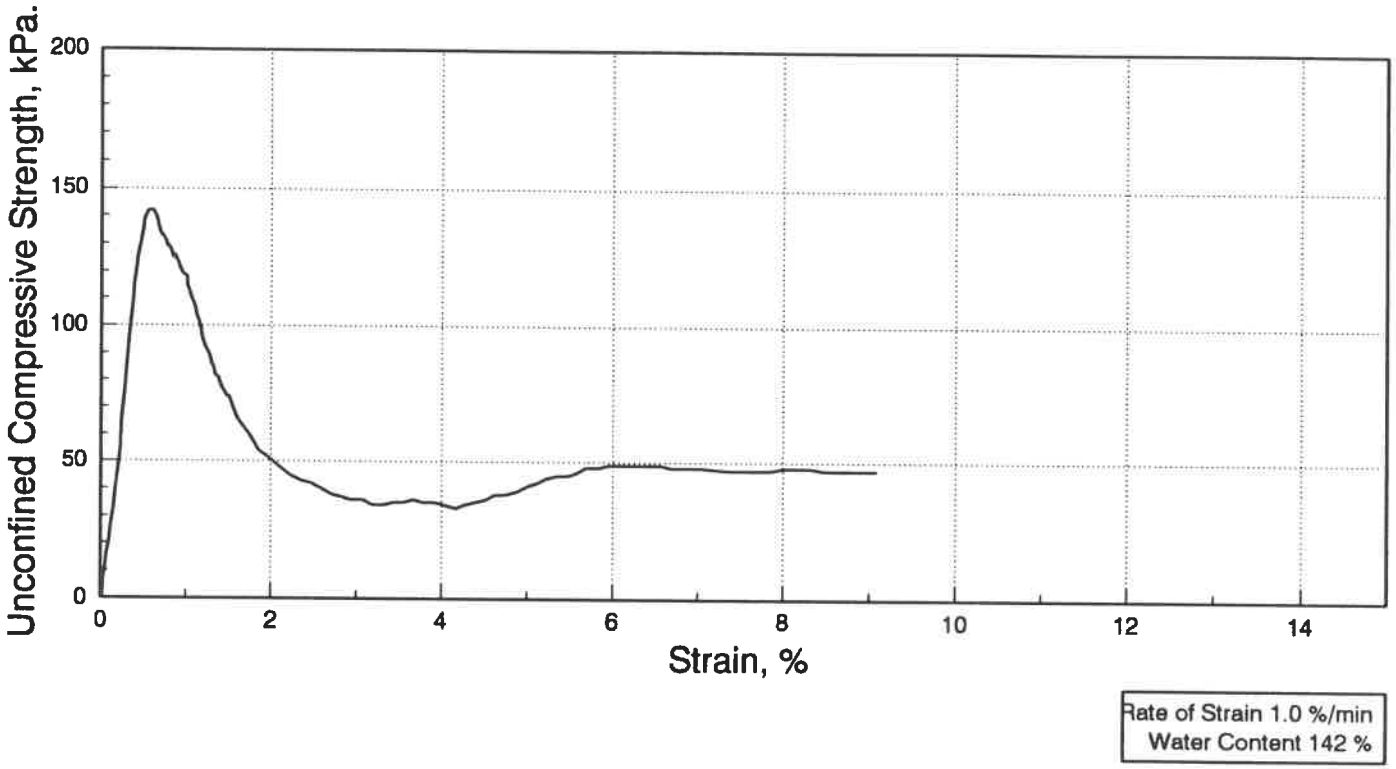

Fig. A.2 Stress-strain curve of test 103

for model material with 25.00 % cement.

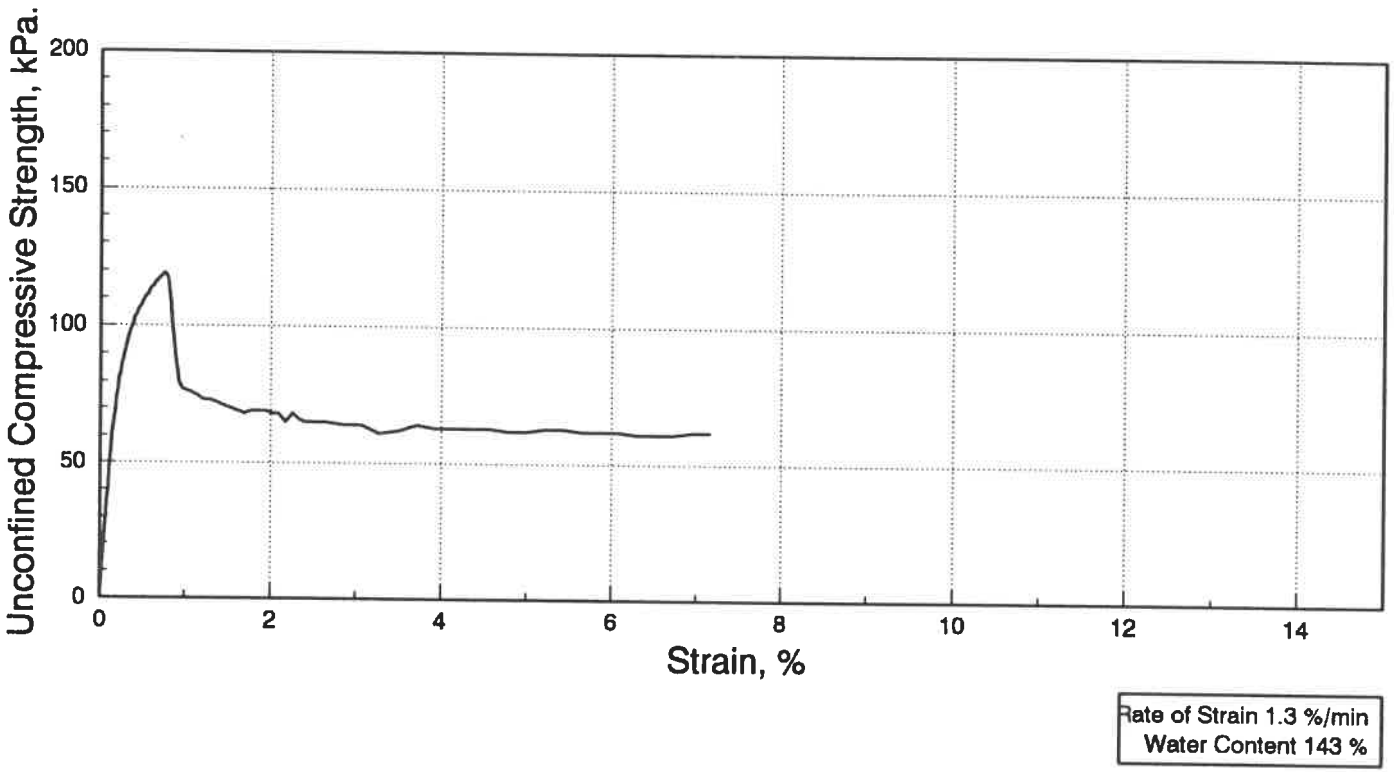

Fig. A.3 Stress-strain curve of test 201

for model material with 21.75 % cement.

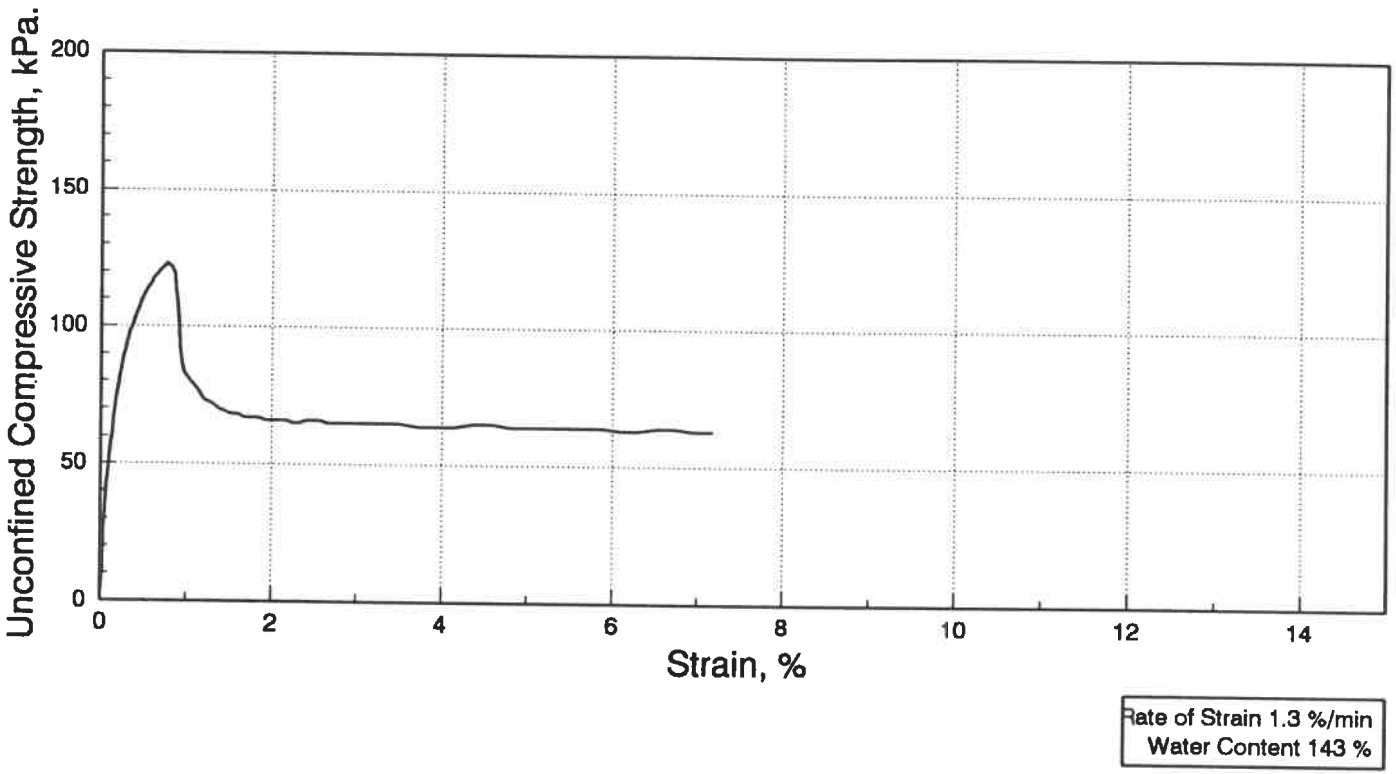

Fig. A.4 Stress-strain curve of test 202

for model material with 21.75 % cement.

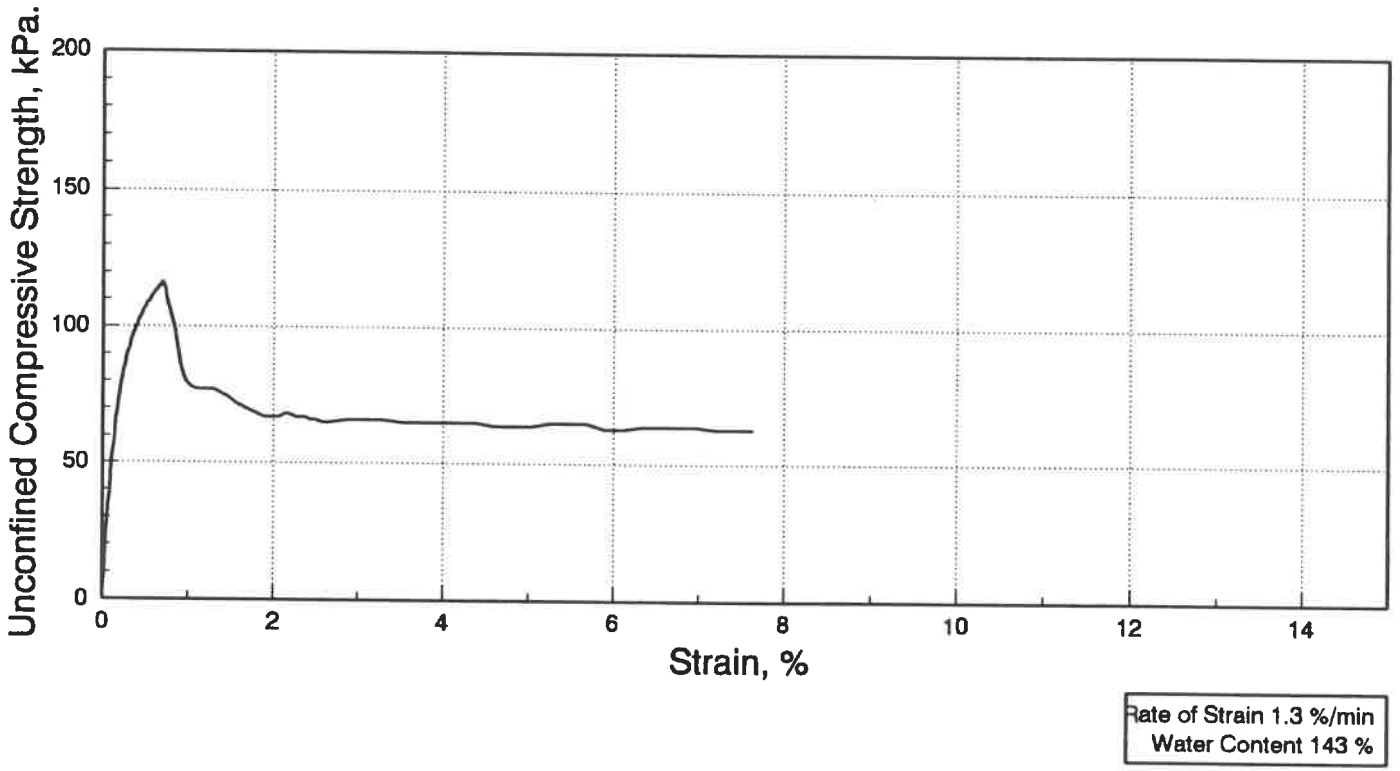

Fig. A.5 Stress-strain curve of test 203

for model material with 21.75 % cement.

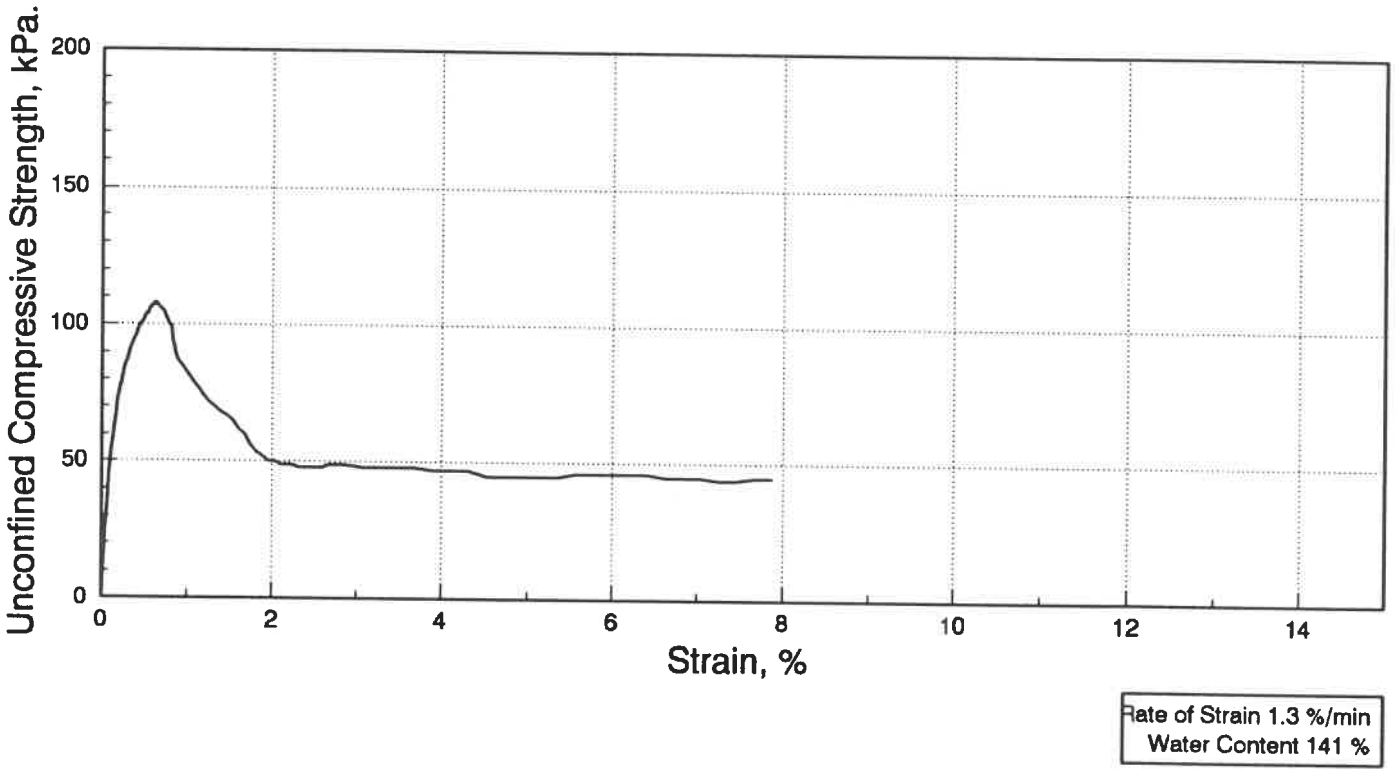

Fig. A.6 Stress-strain curve of test 301

for model material with 18.75 % cement.

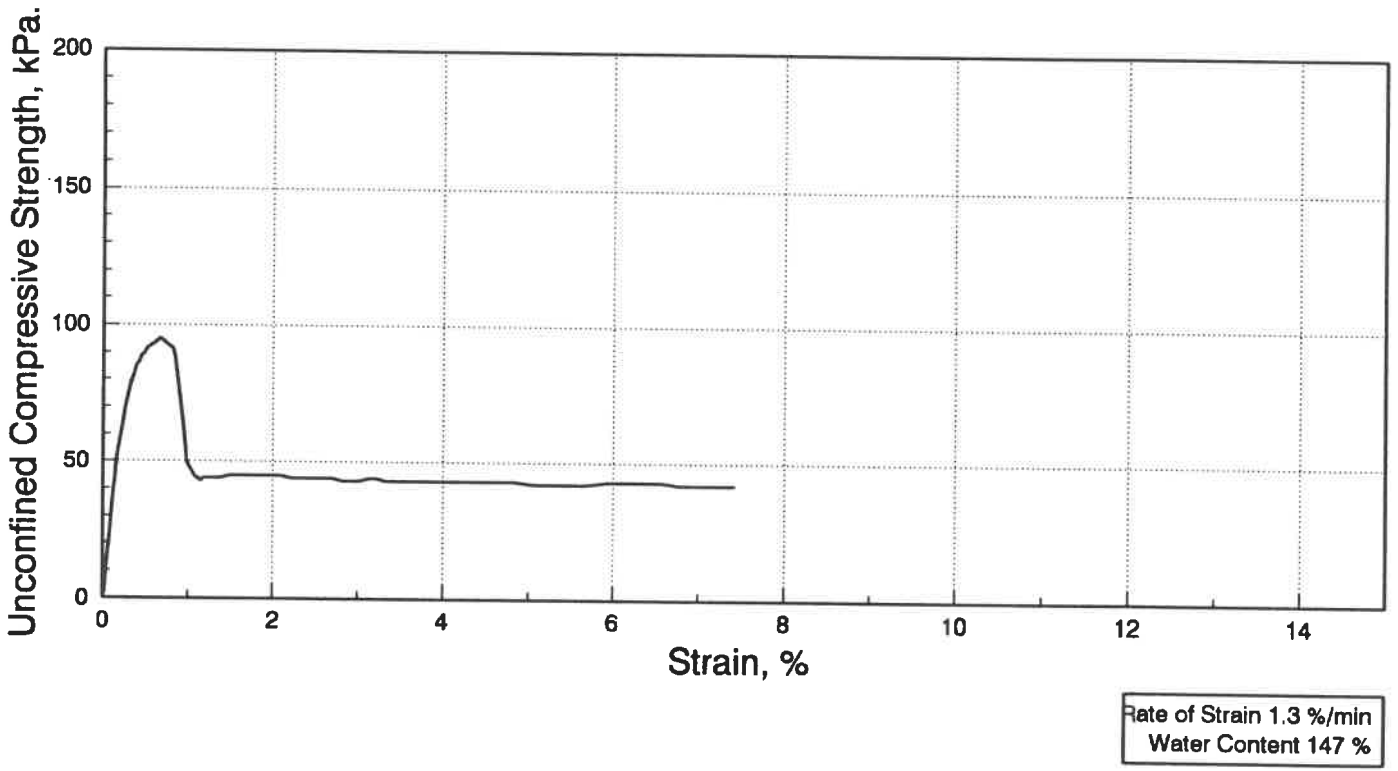

Fig. A.7 Stress-strain Curve of test 302

for model material with 18.75 % cement.

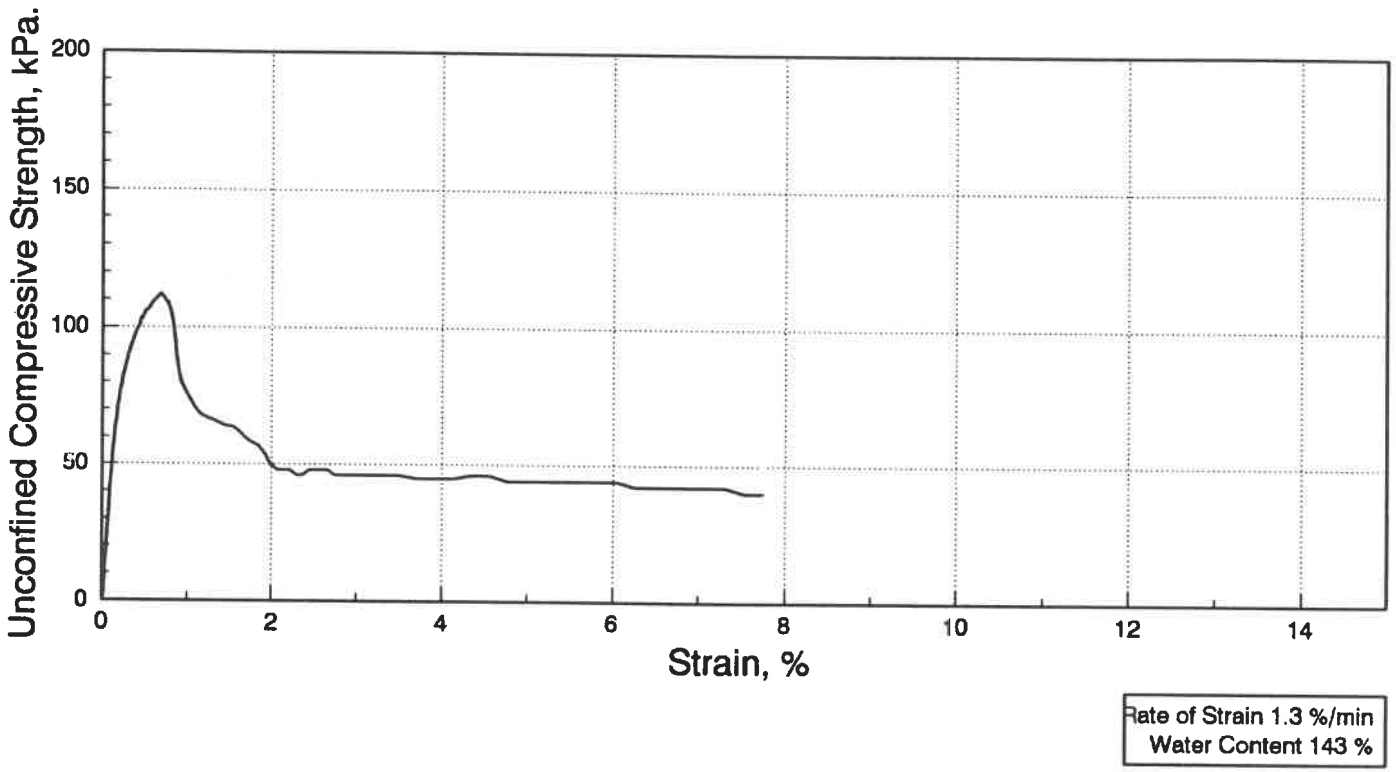

Fig. A.8 Stress-strain curve of test 303

for model material with 18.75 % cement.

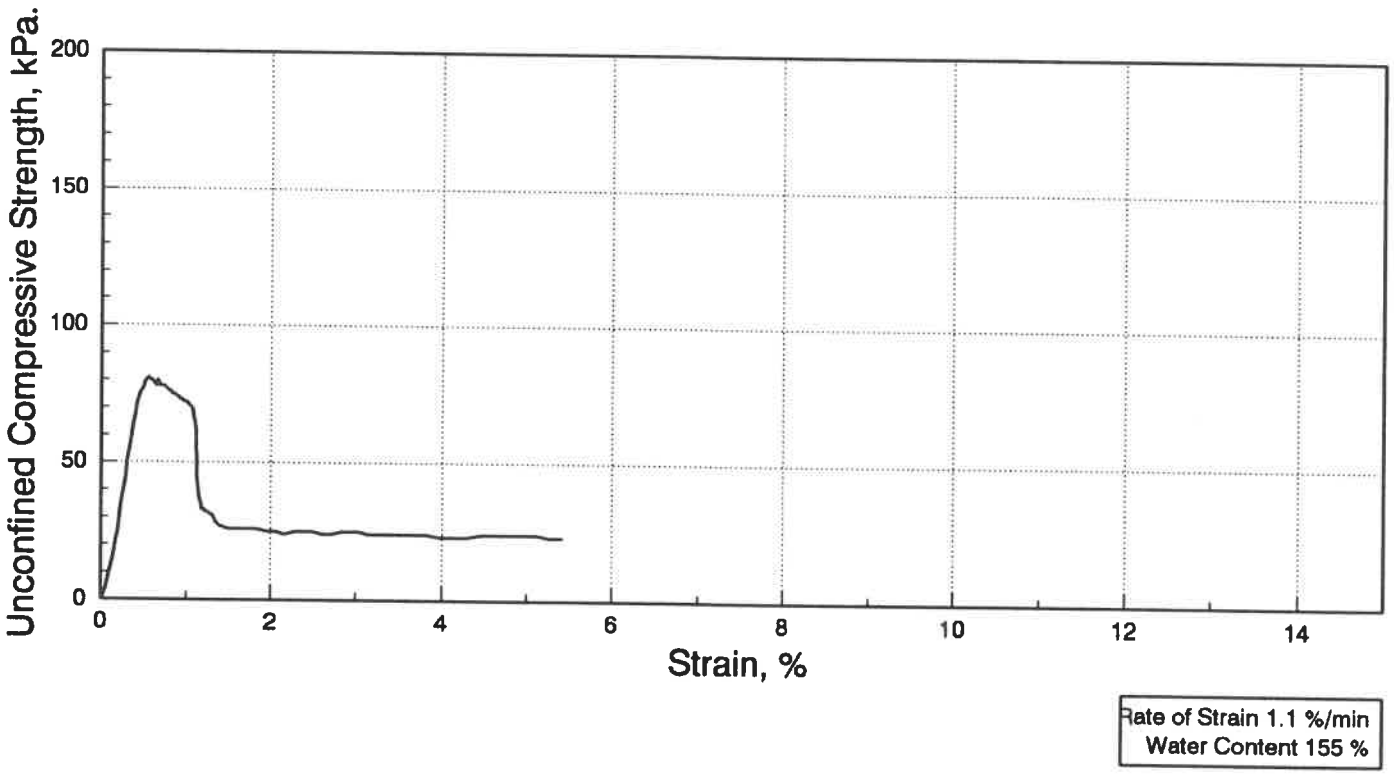

Fig. A.9 Stress-strain curve of test 401

for model material with 16.67 % cement.

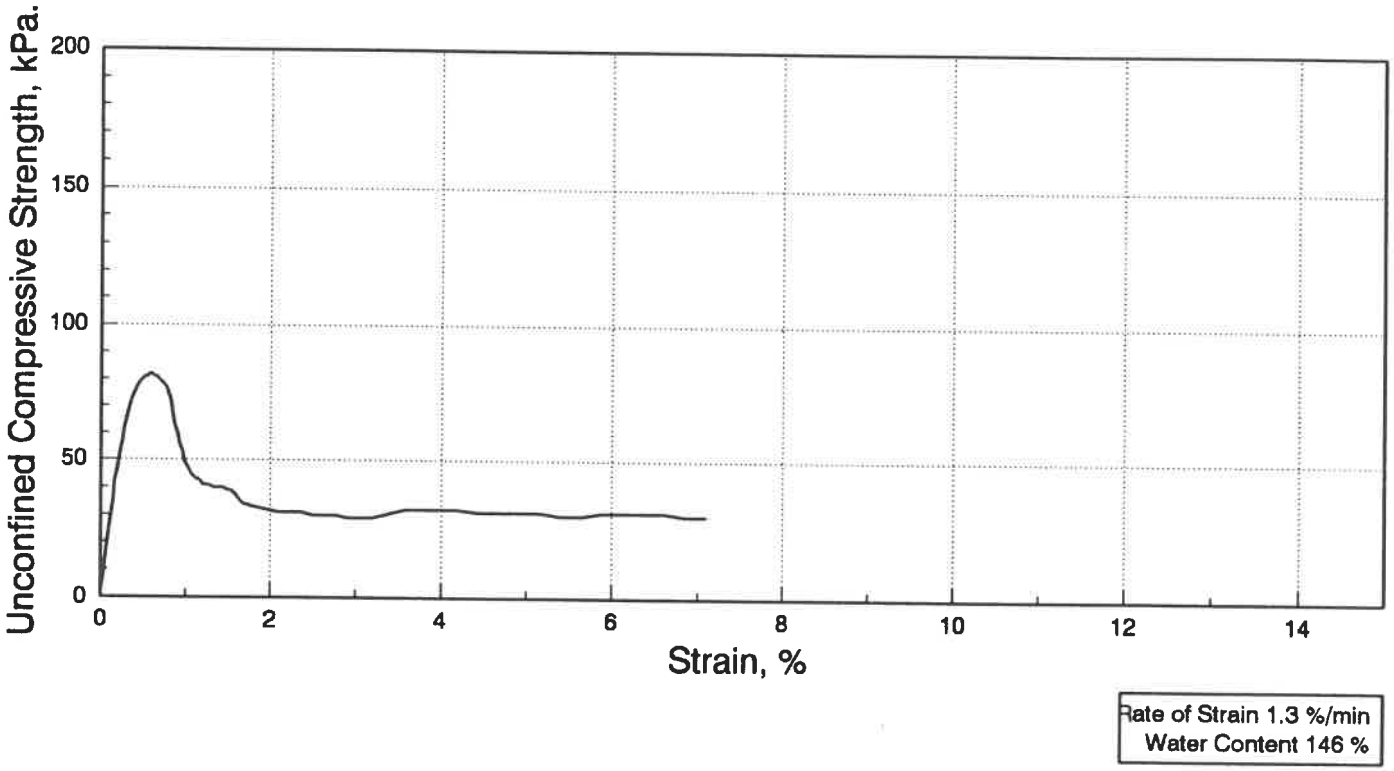

Fig. A.10 Stress-strain curve of test 402

for model material with 16.67 % cement.

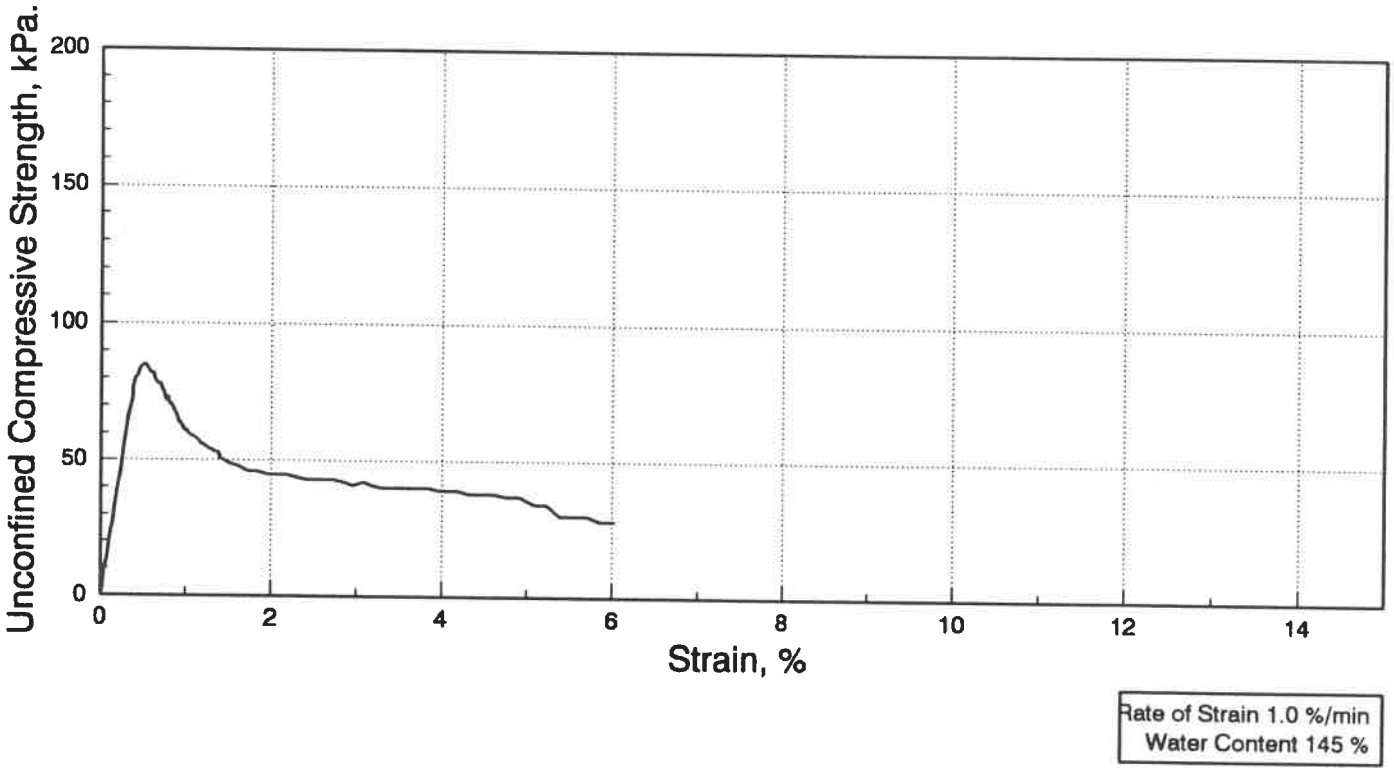

Fig. A.11 Stress-strain curve of test 403 for model material with 16.67 % cement.

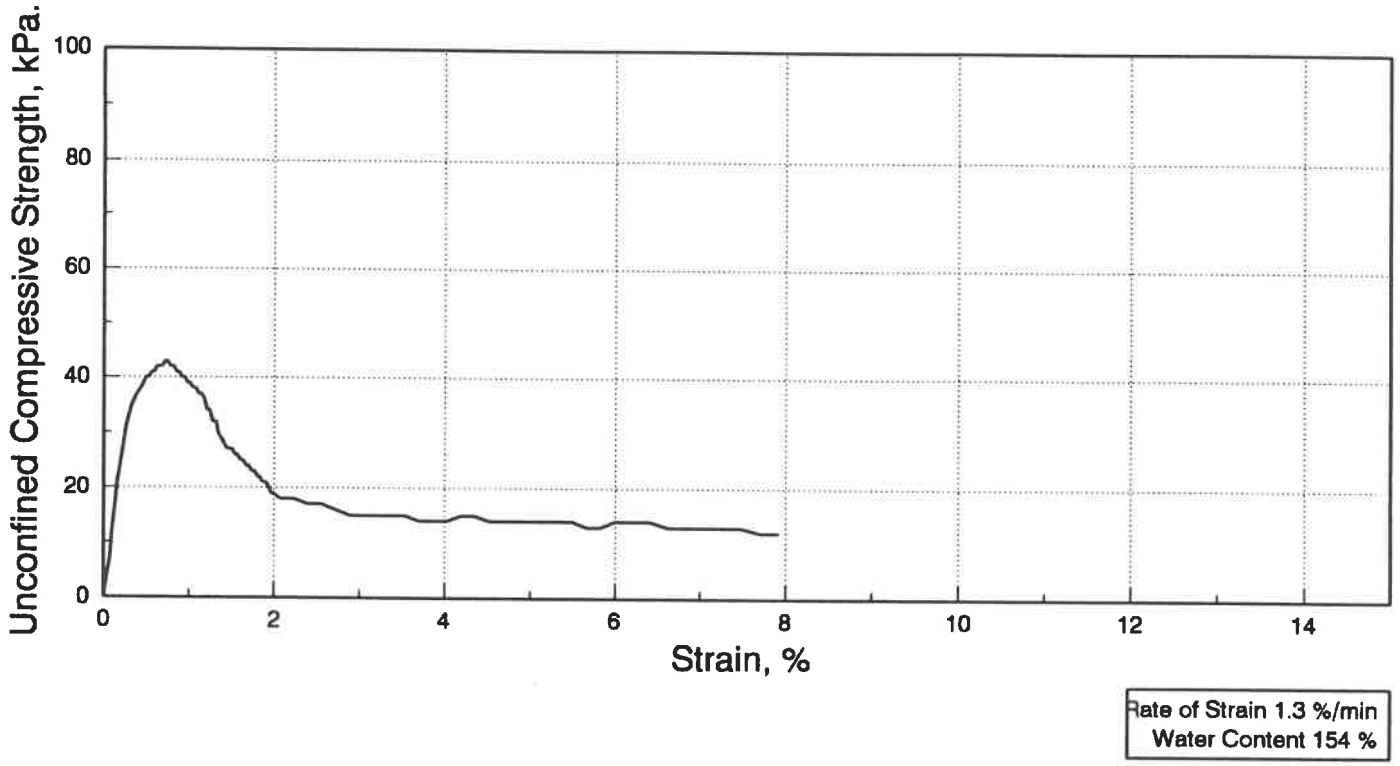

Fig. A.12 Stress-strain curve of test 502

for model material with 12.50 % cement.

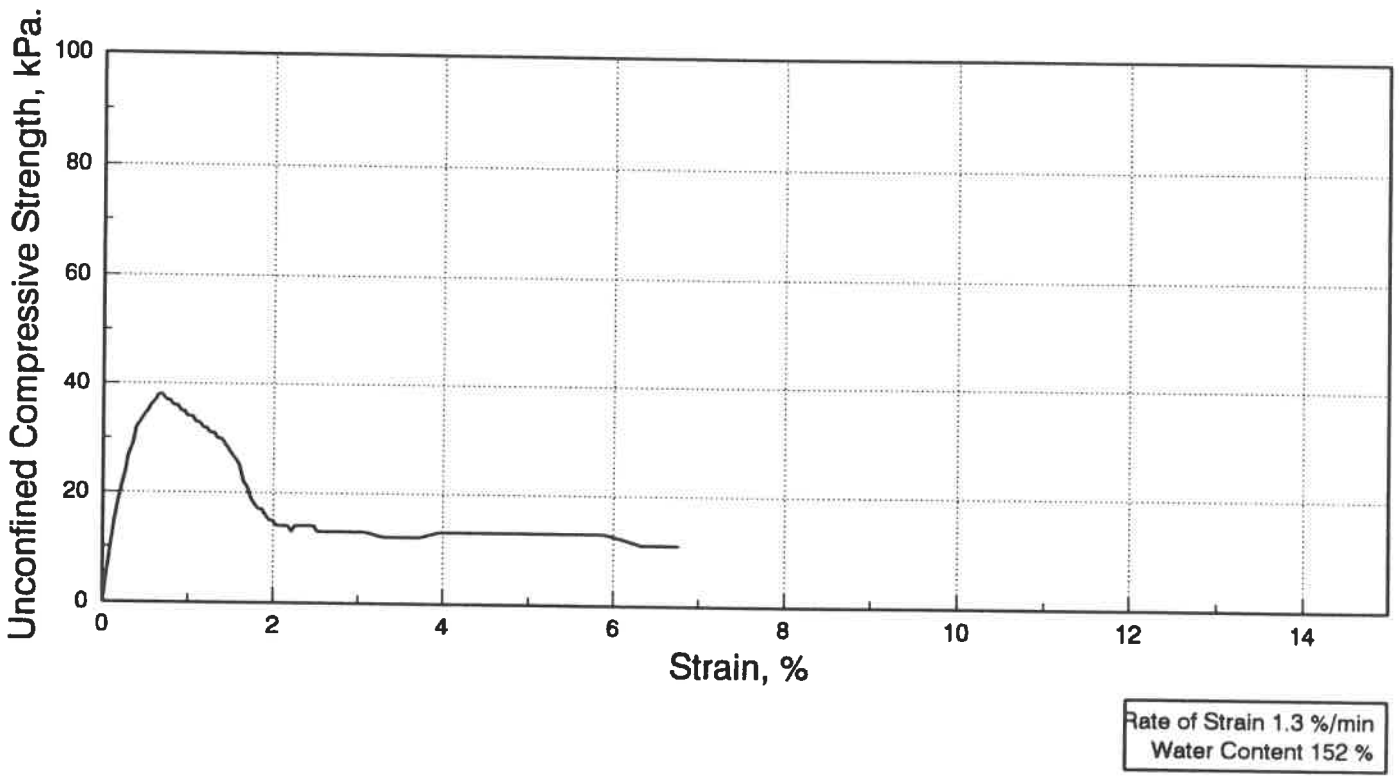

Fig. A.13 Stress-strain curve of test 503

for model material with 12.50 % cement.

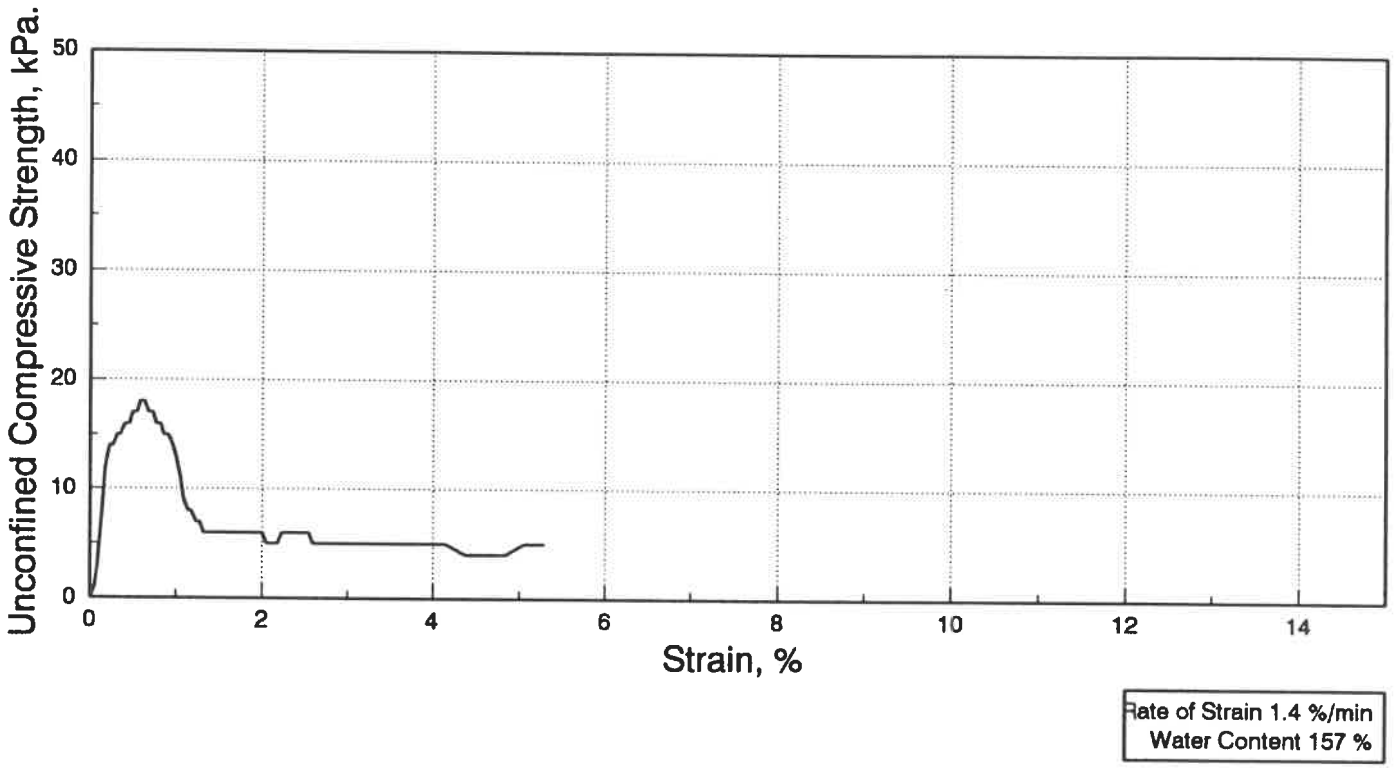

Fig. A.14 Stress-strain curve of test 602 for model material with 6.25 % cement.

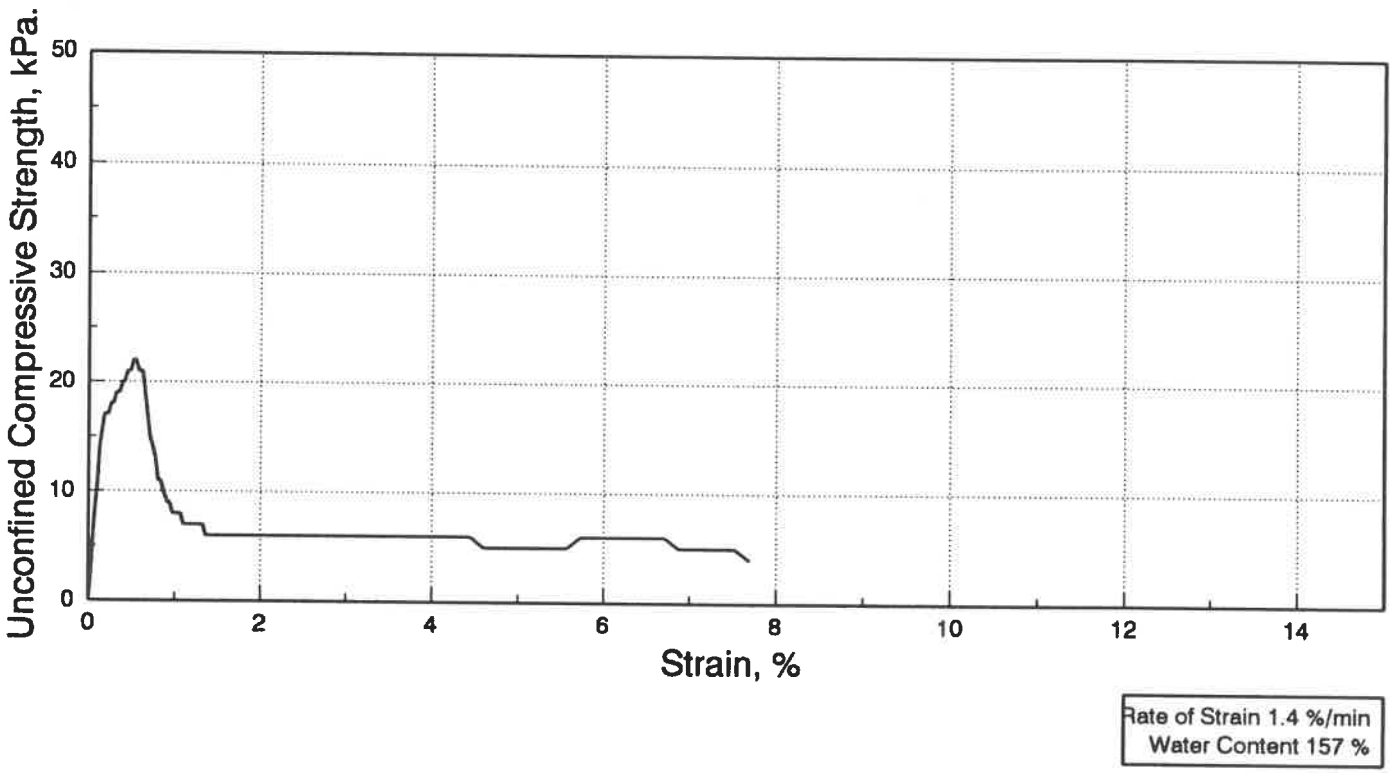

Fig. A.15 Stress-strain curve of test 603 for model material with 6.25 % cement.

APPENDIX B: LABORATORY TESTS

MEASUREMENTS.

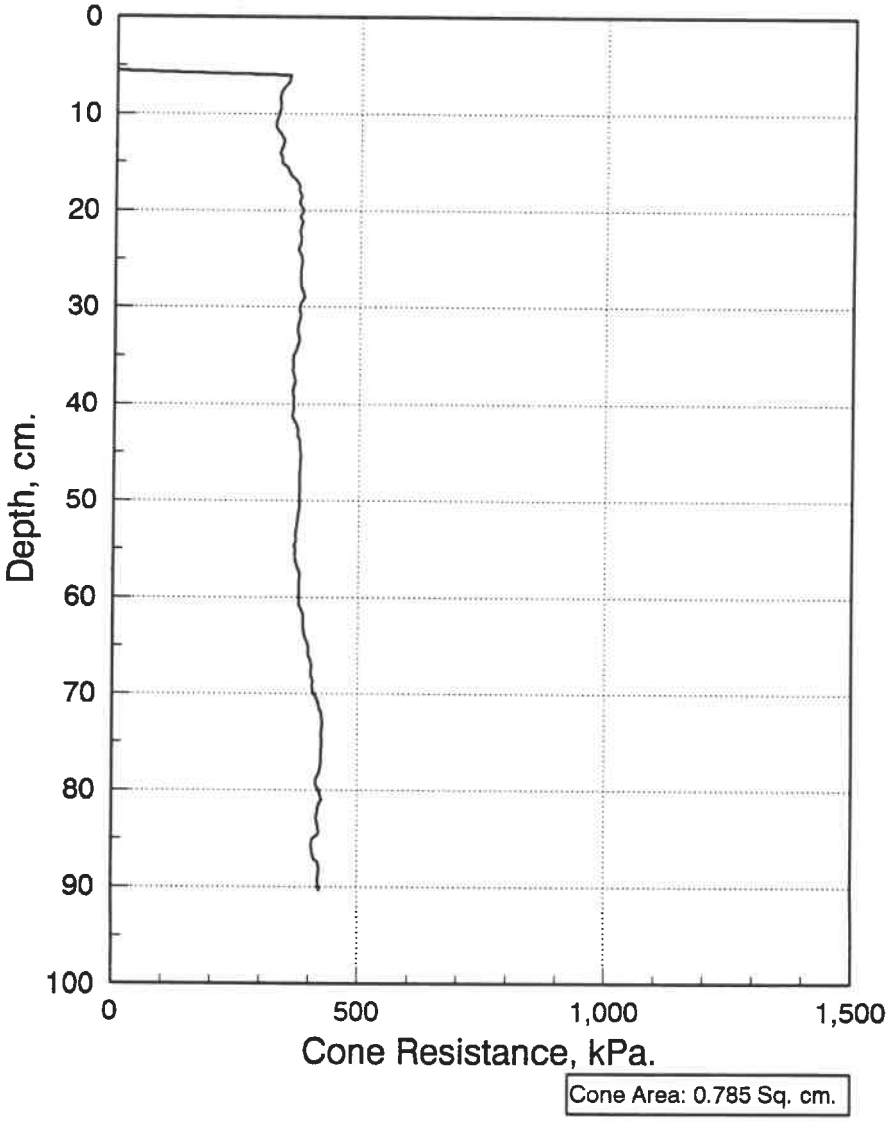

Fig. B.1 Quasi-static cone resistance curve for 7.5° cone apex angle.

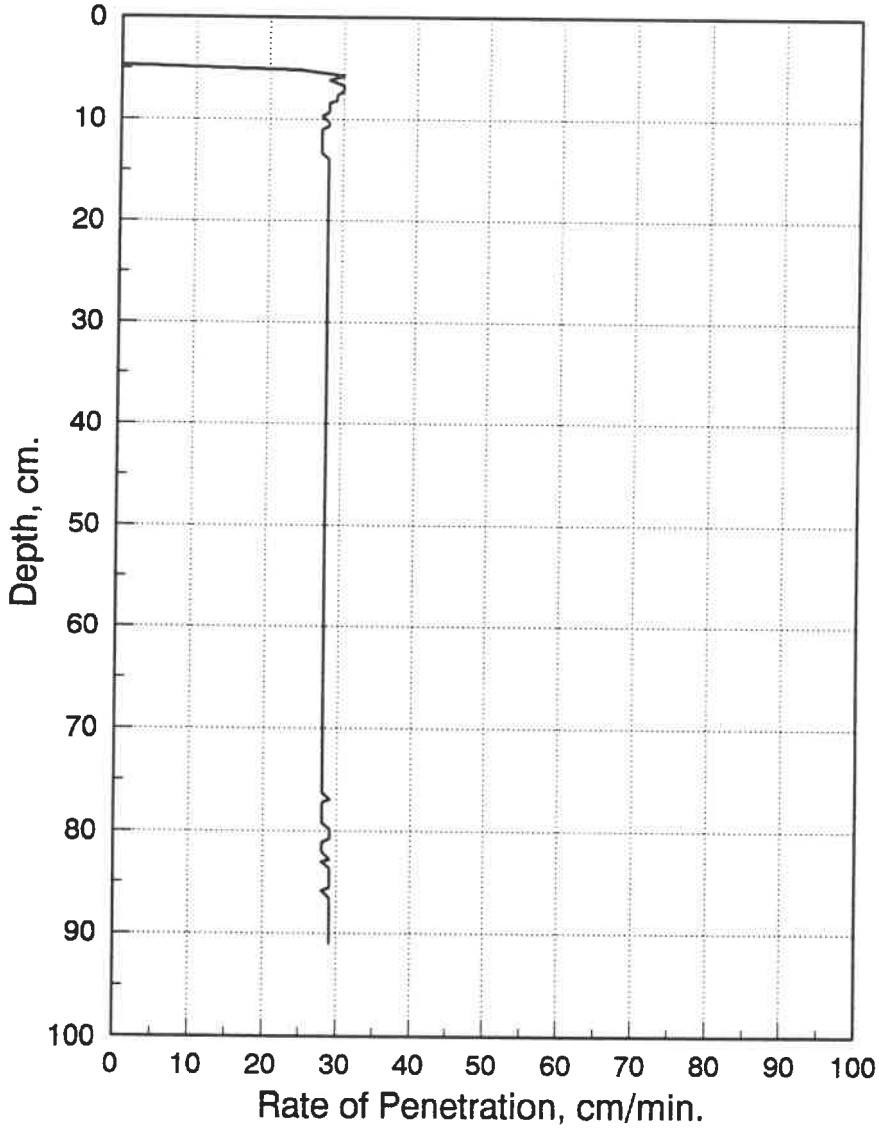

Fig. B.2 Rate of penetration curve for 7.5° cone apex angle.

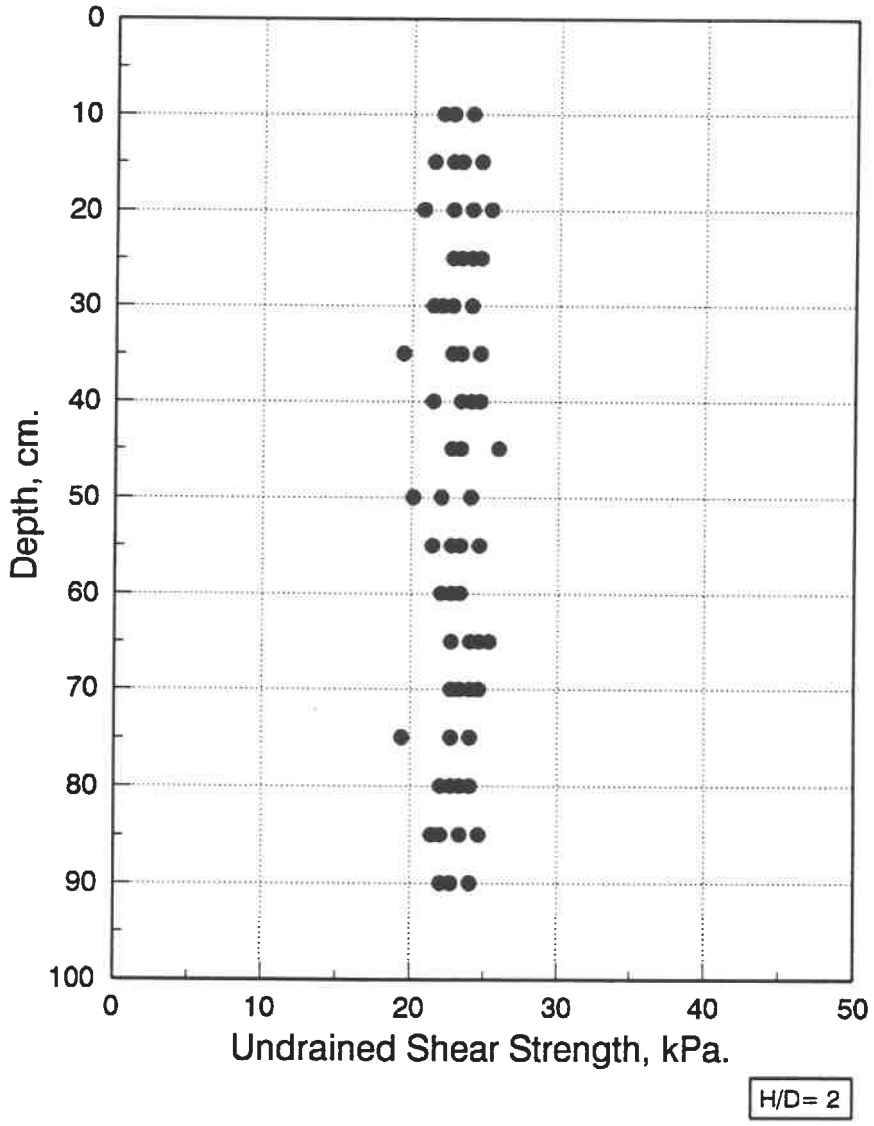

Fig. B.3 Results of laboratory vane shear test-7.5°.

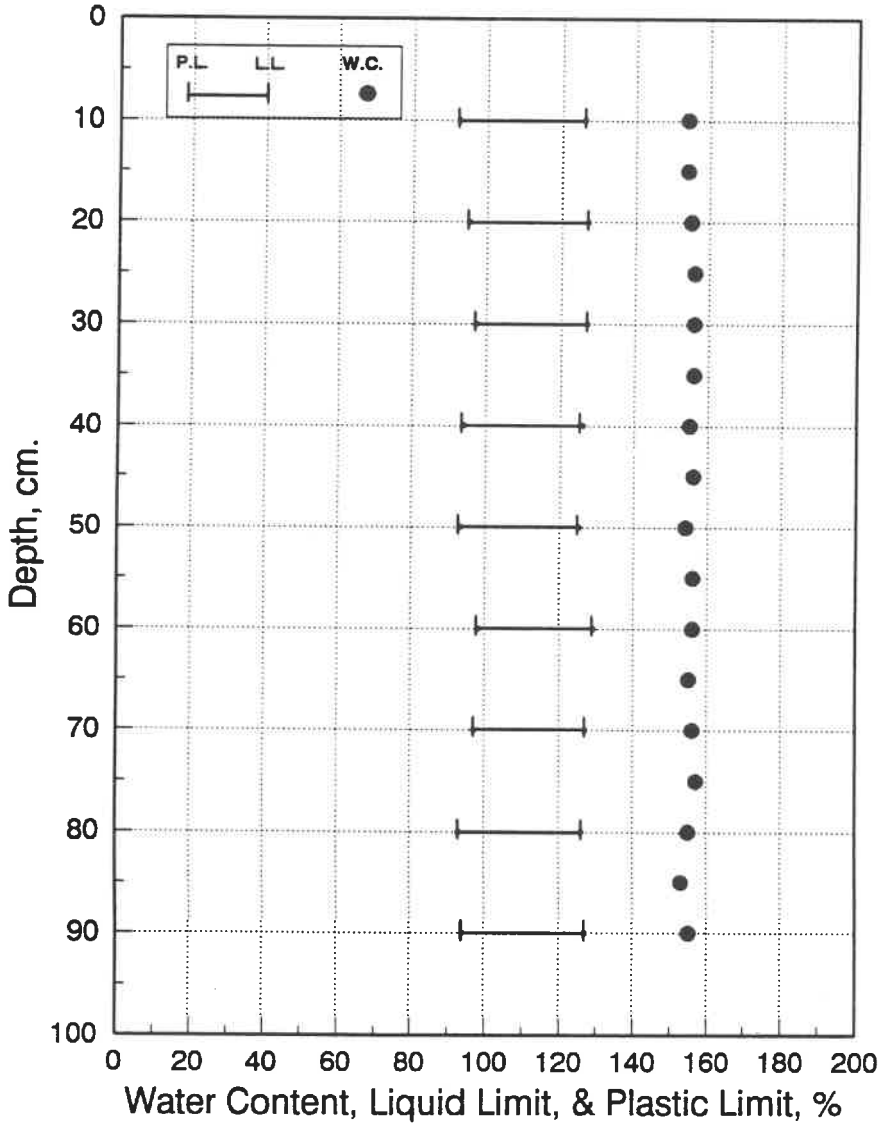

Fig. B.4 Water content and consistency limits for penetration test-7.5°.

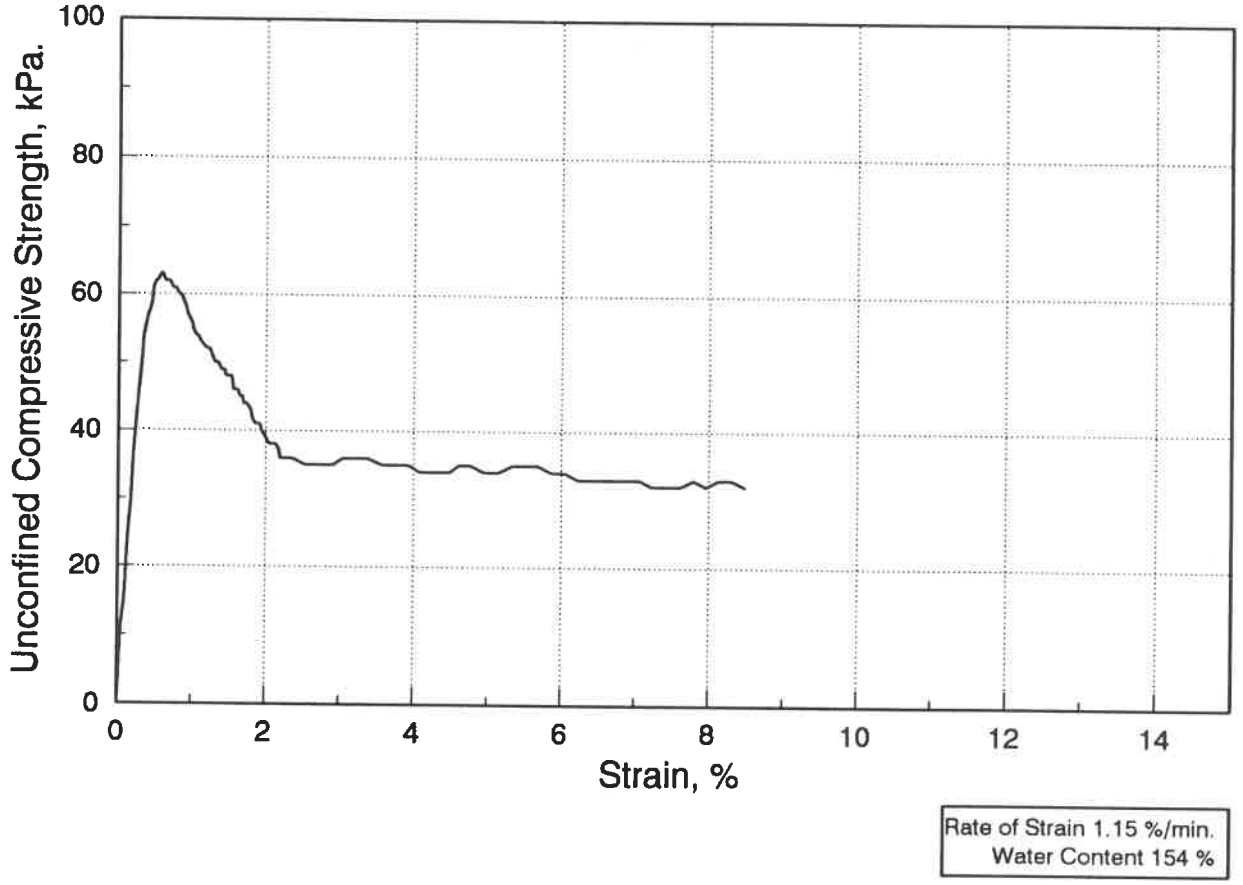

Fig. B.5 Stress-strain curve of the unconfined compression test-7.5°/1.

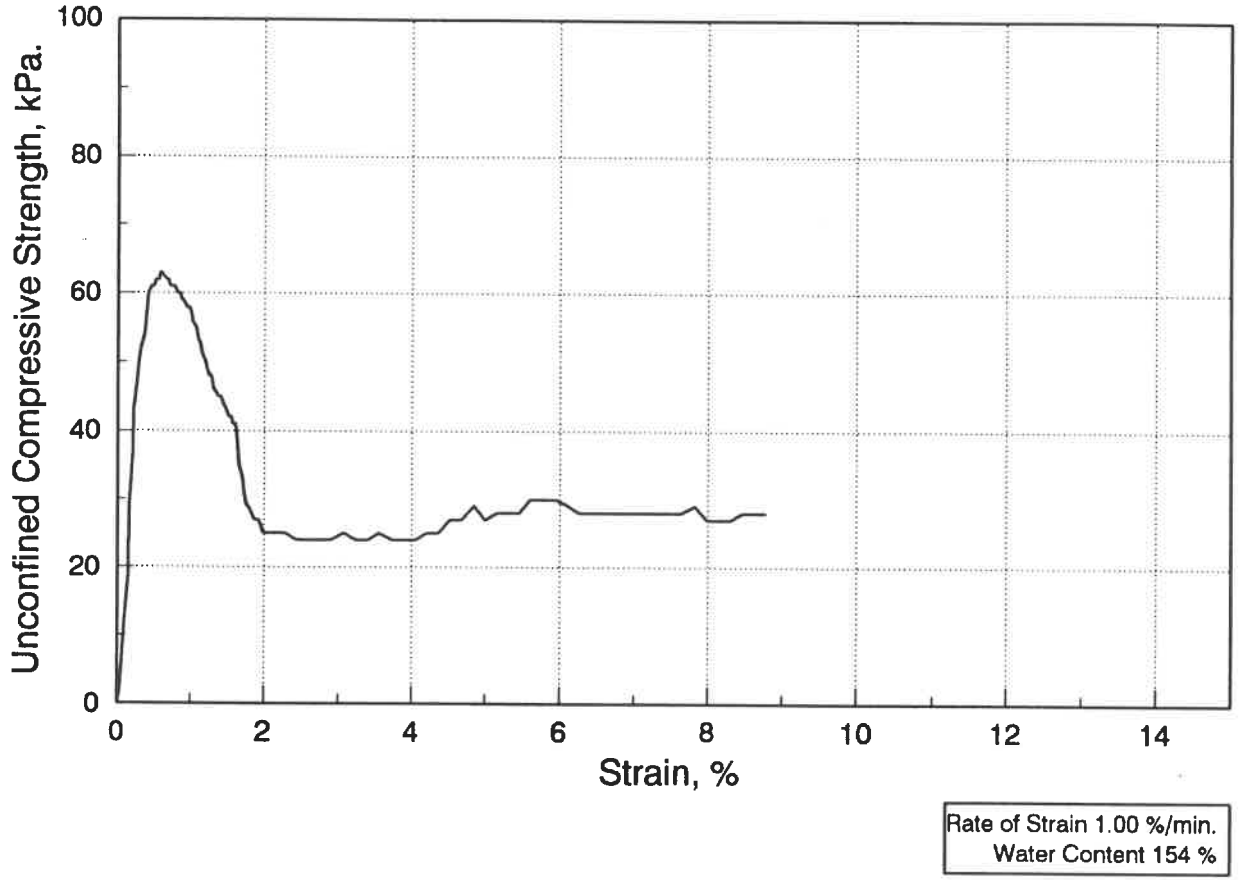

Fig. B.6 Stress-strain curve of the unconfined compression test-7.5°/2.

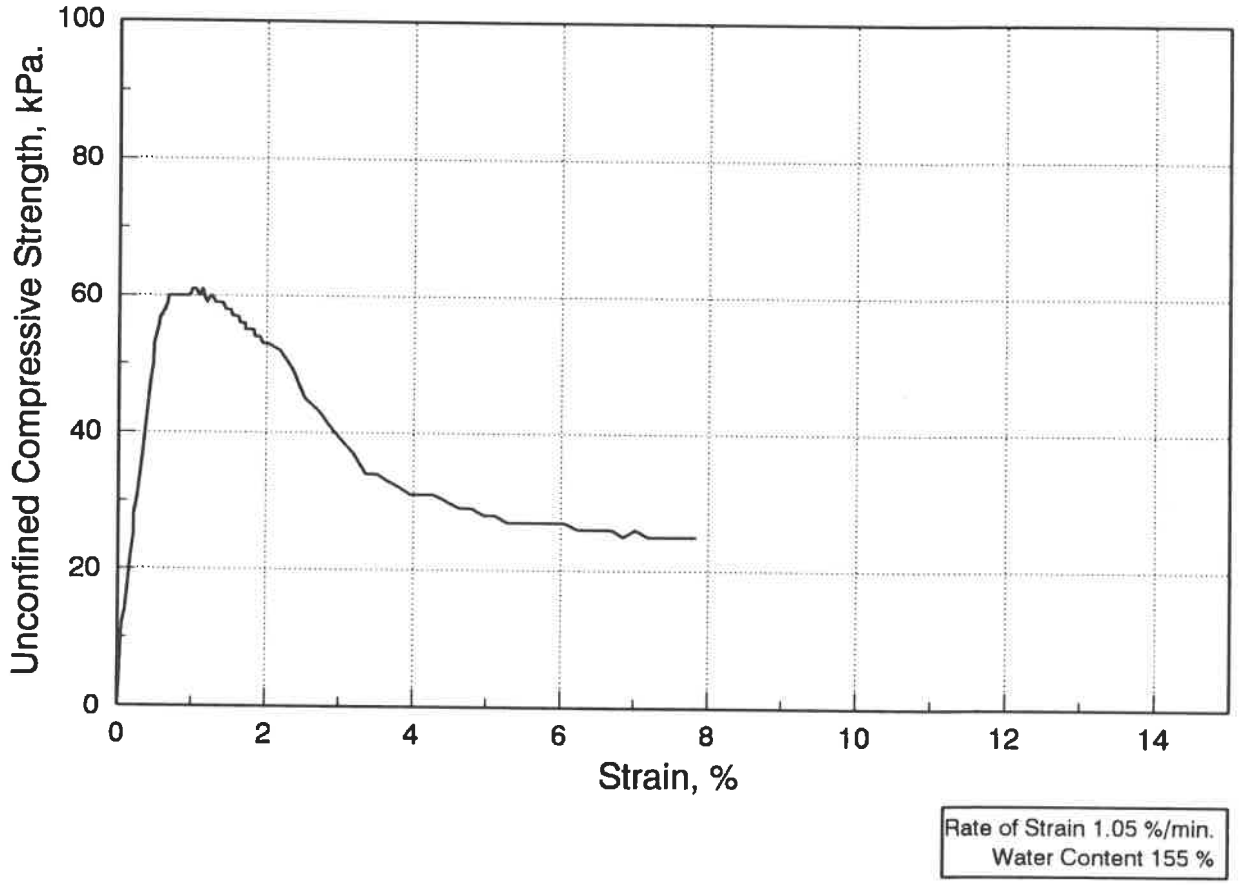

Fig. B.7 Stress-strain curve of the unconfined compression test-7.5°/3.

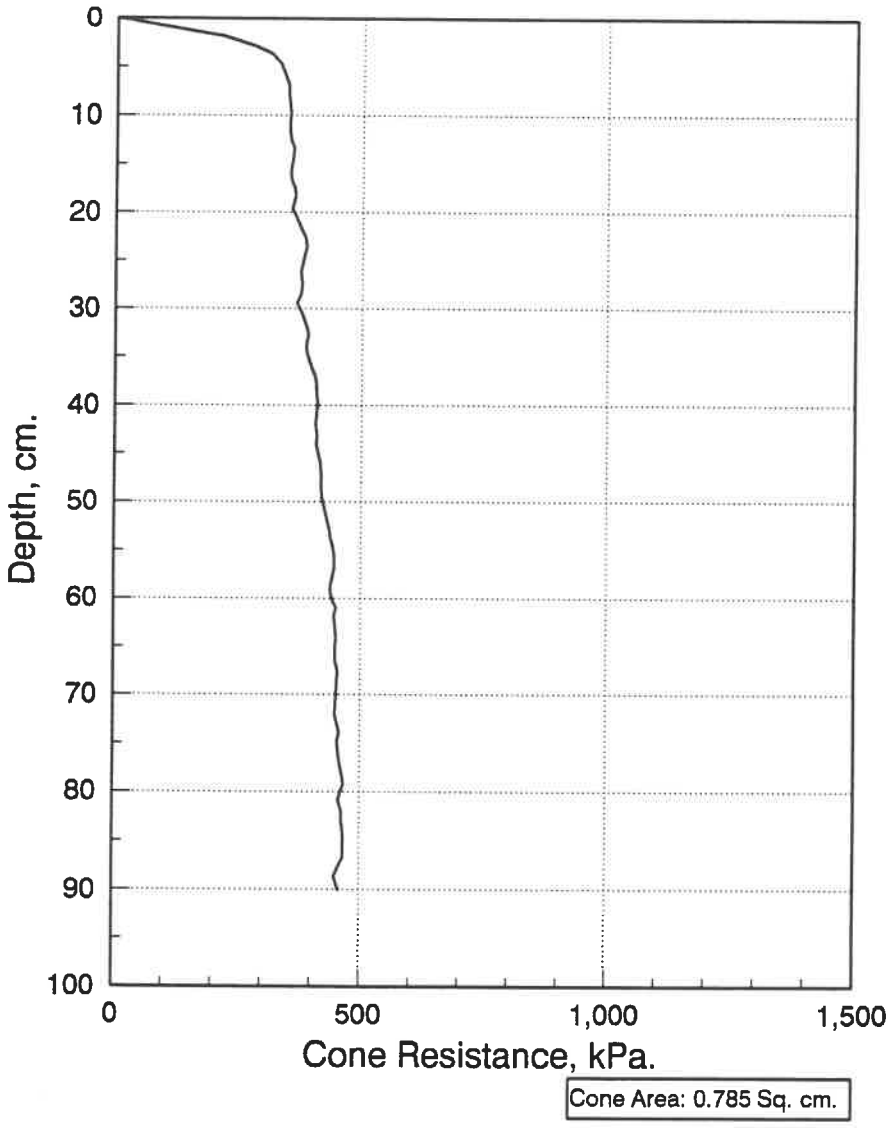

Fig. B.8 Quasi-static cone resistance curve for 15° cone apex angle.

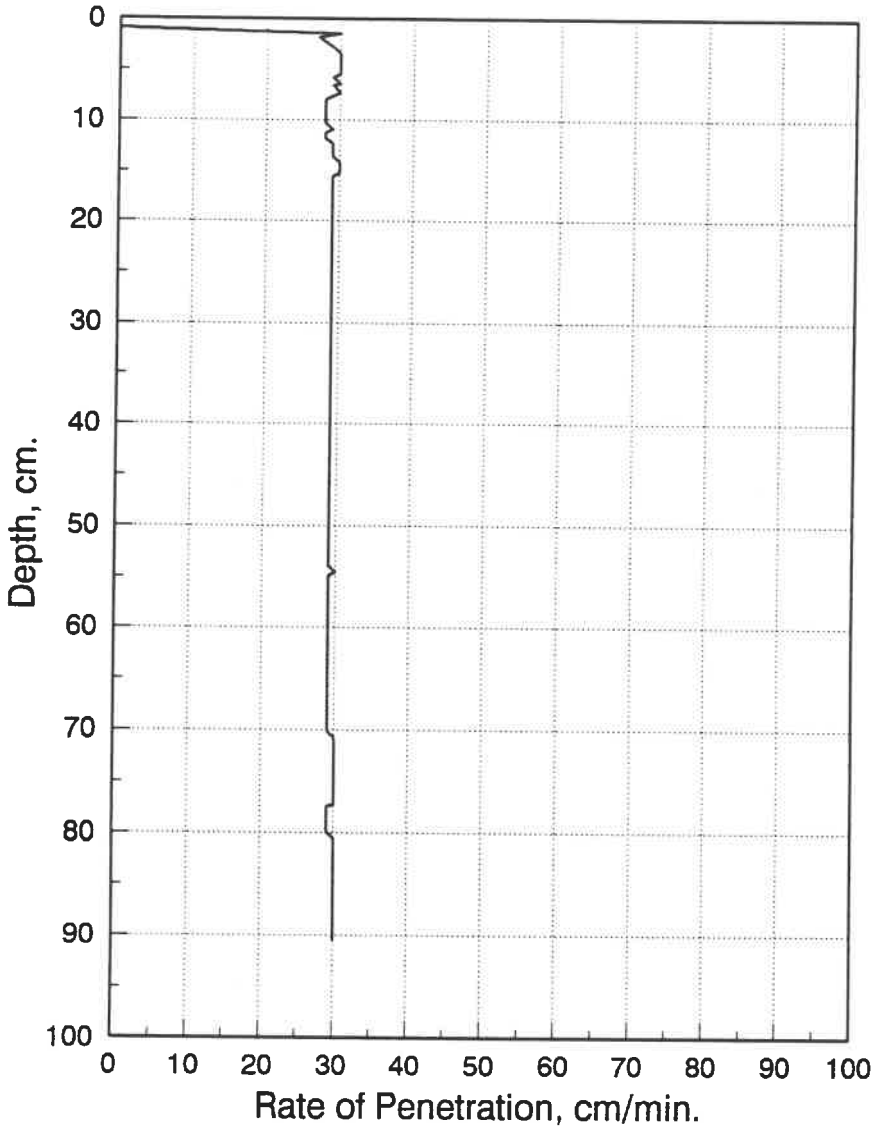

Fig. B.9 Rate of penetration curve for 15° cone apex angle.

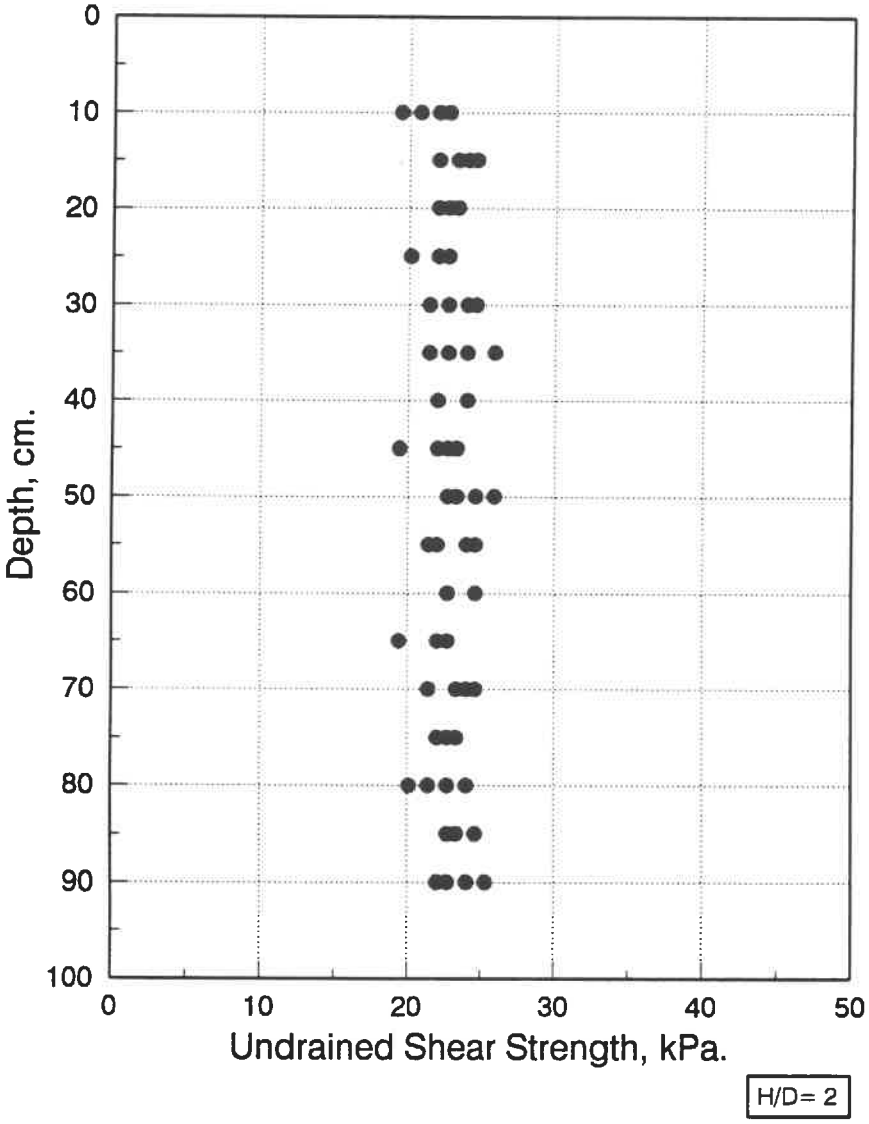

Fig. B.10 Results of laboratory vane shear test-15°.

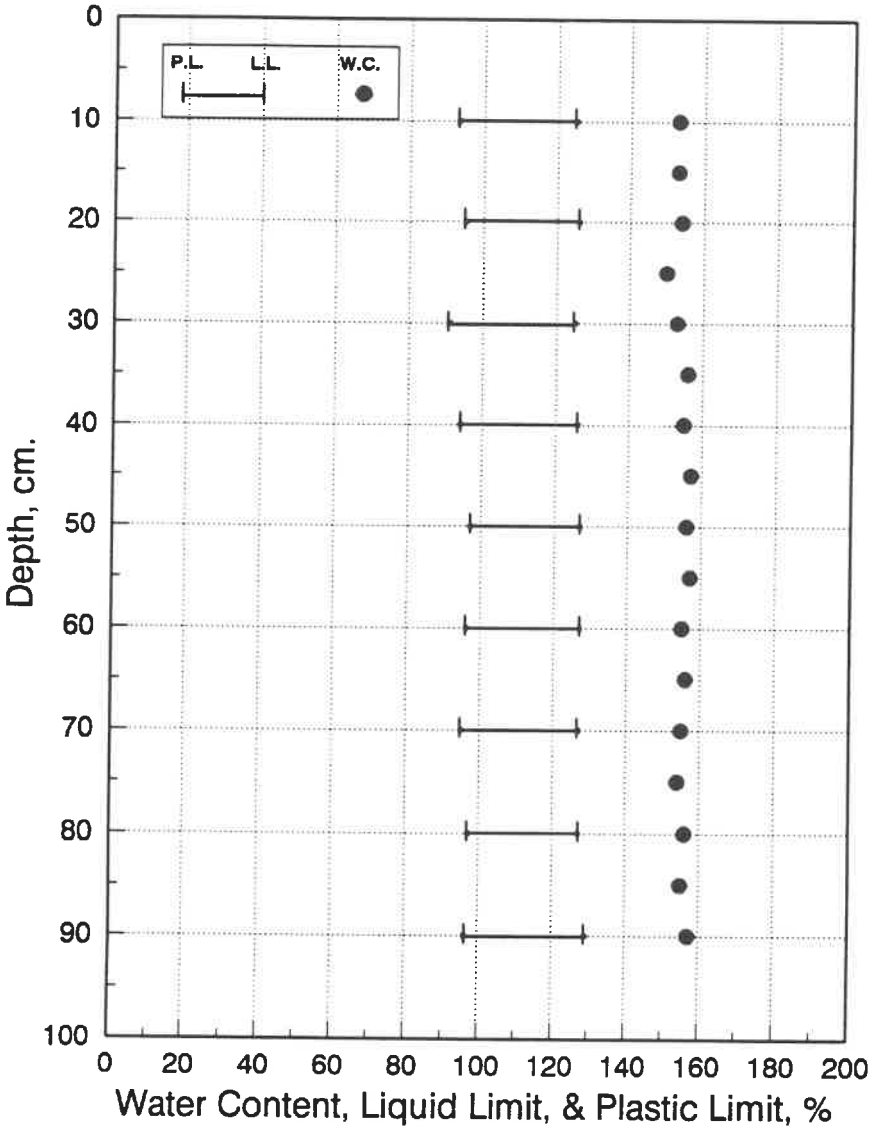

Fig. B.11 Water content and consistency limits for penetration test-15°.

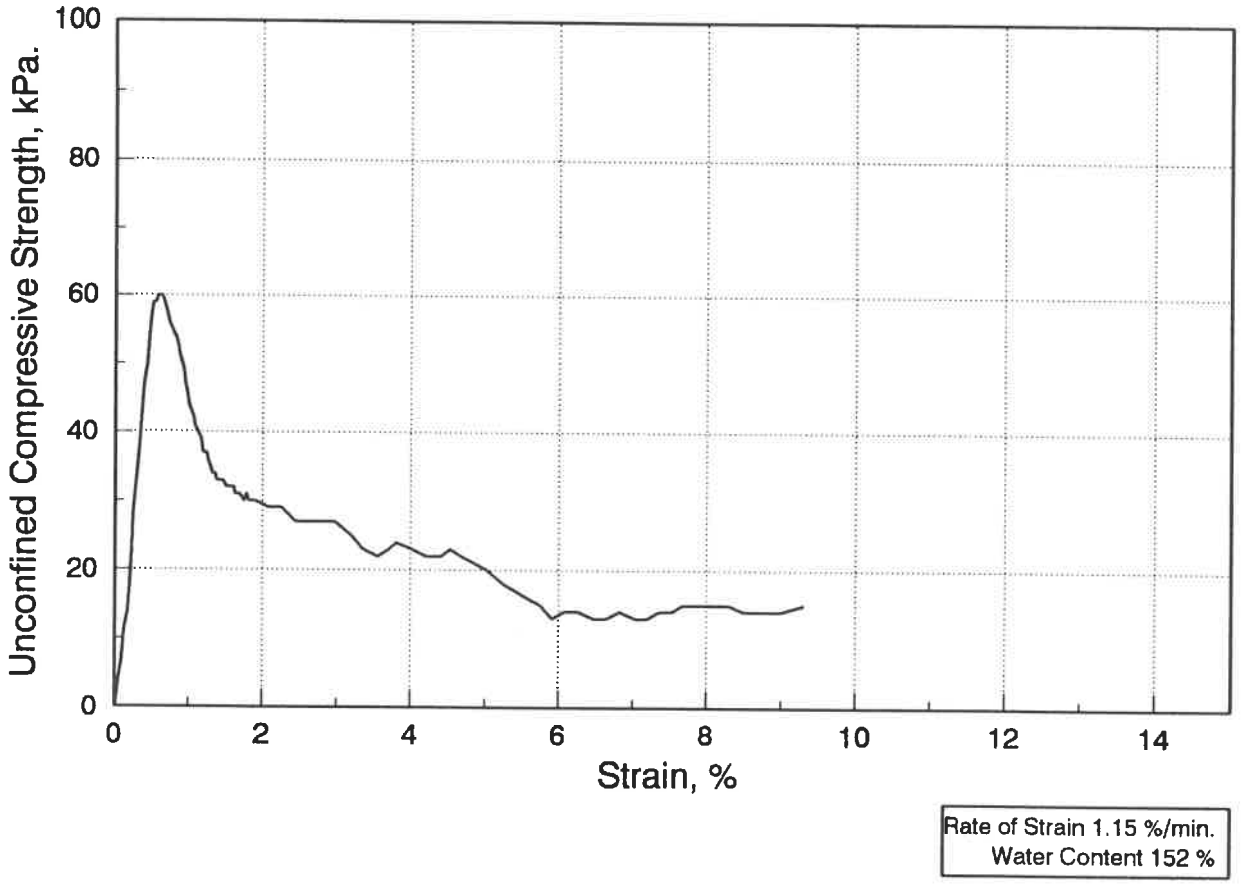

Fig. B.12 Stress-strain curve of the unconfined compression test-15°/1.

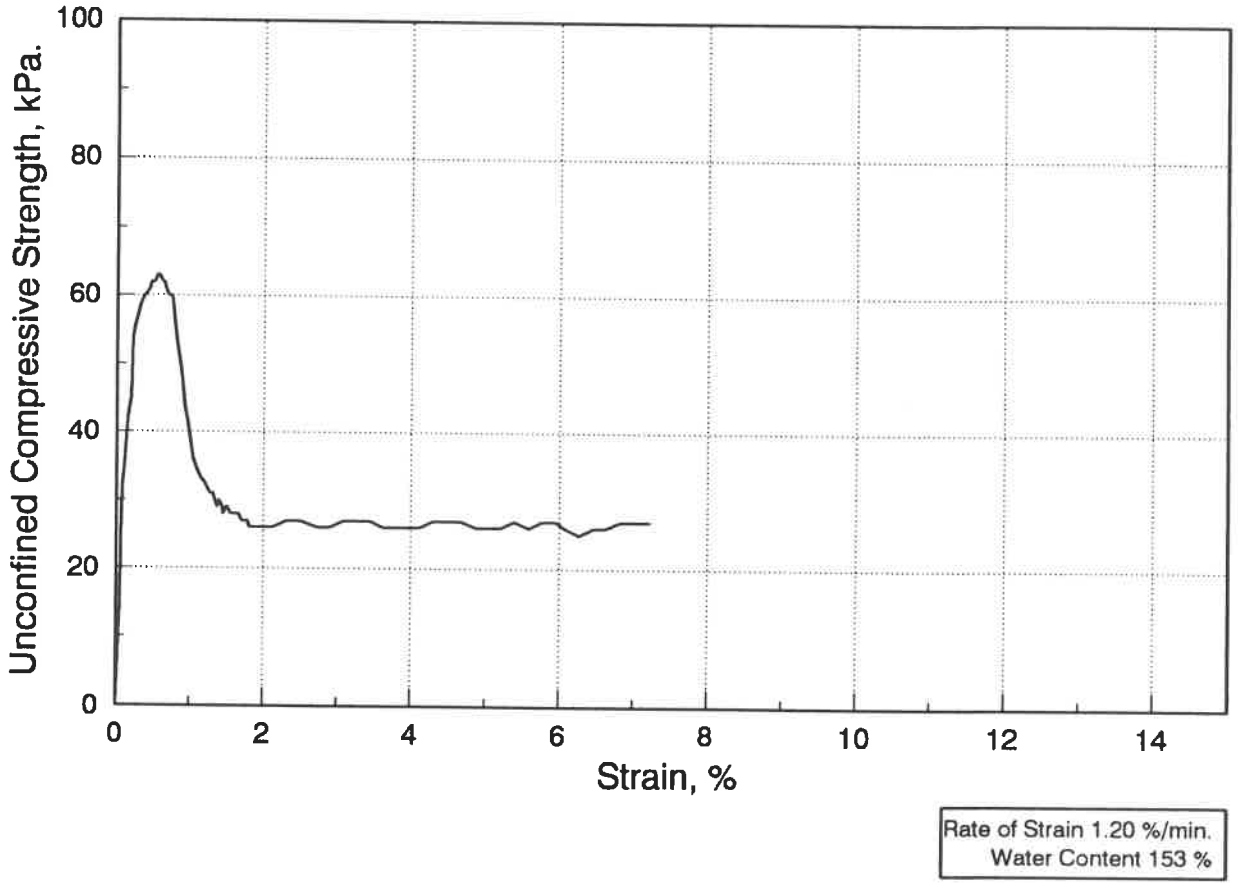

Fig. B.13 Stress-strain curve of the unconfined compression test-15°/2.

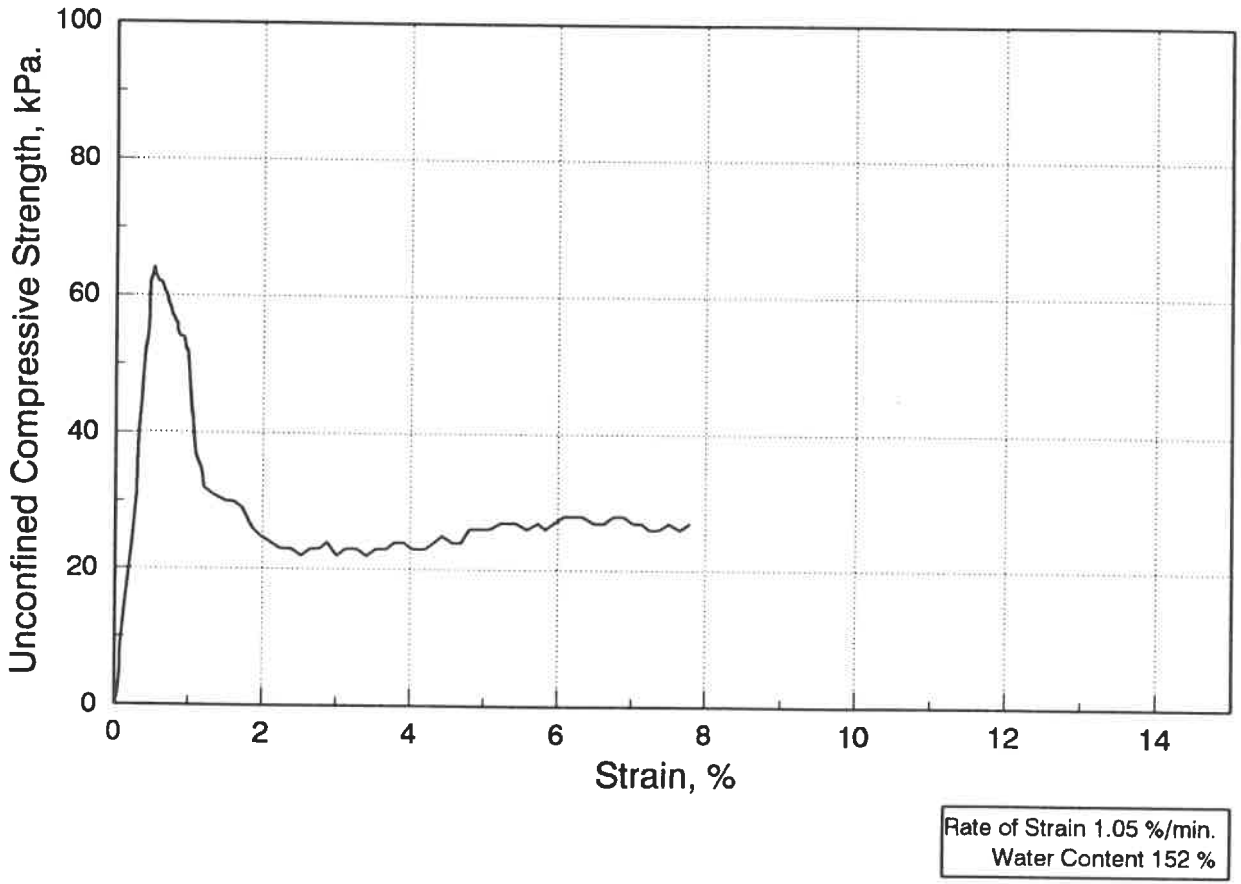

Fig. B.14 Stress-strain curve of the unconfined compression test-15°/3.

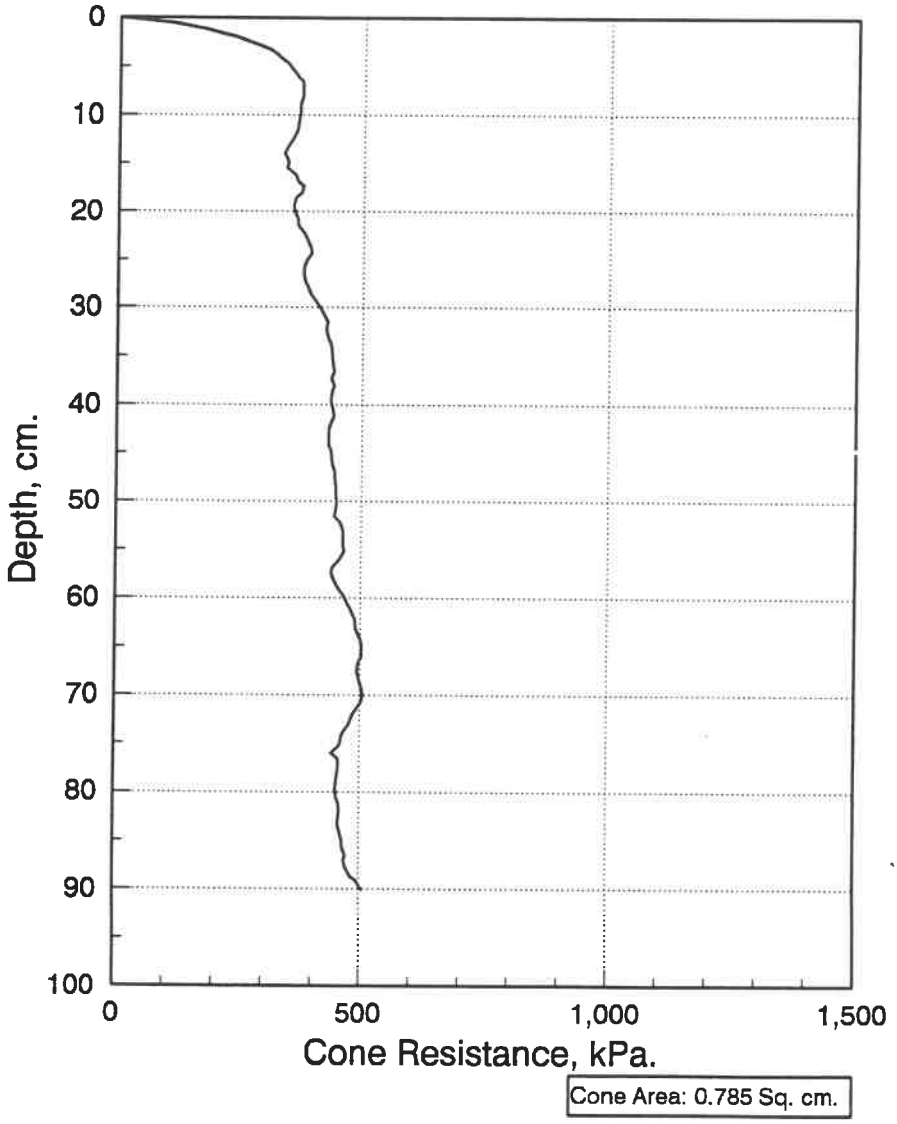

Fig. B.15 Quasi-static cone resistance curve for 18° cone apex angle.

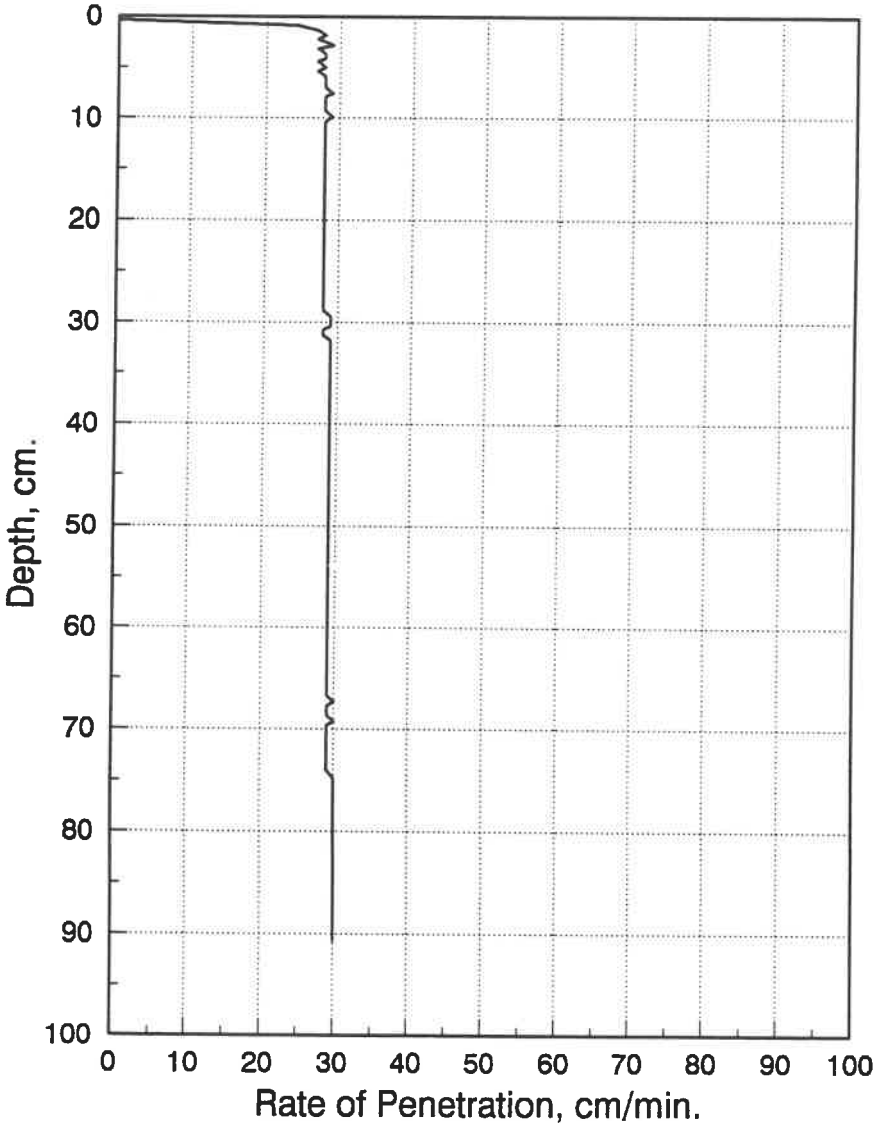

Fig. B.16 Rate of penetration curve for 18° cone apex angle.

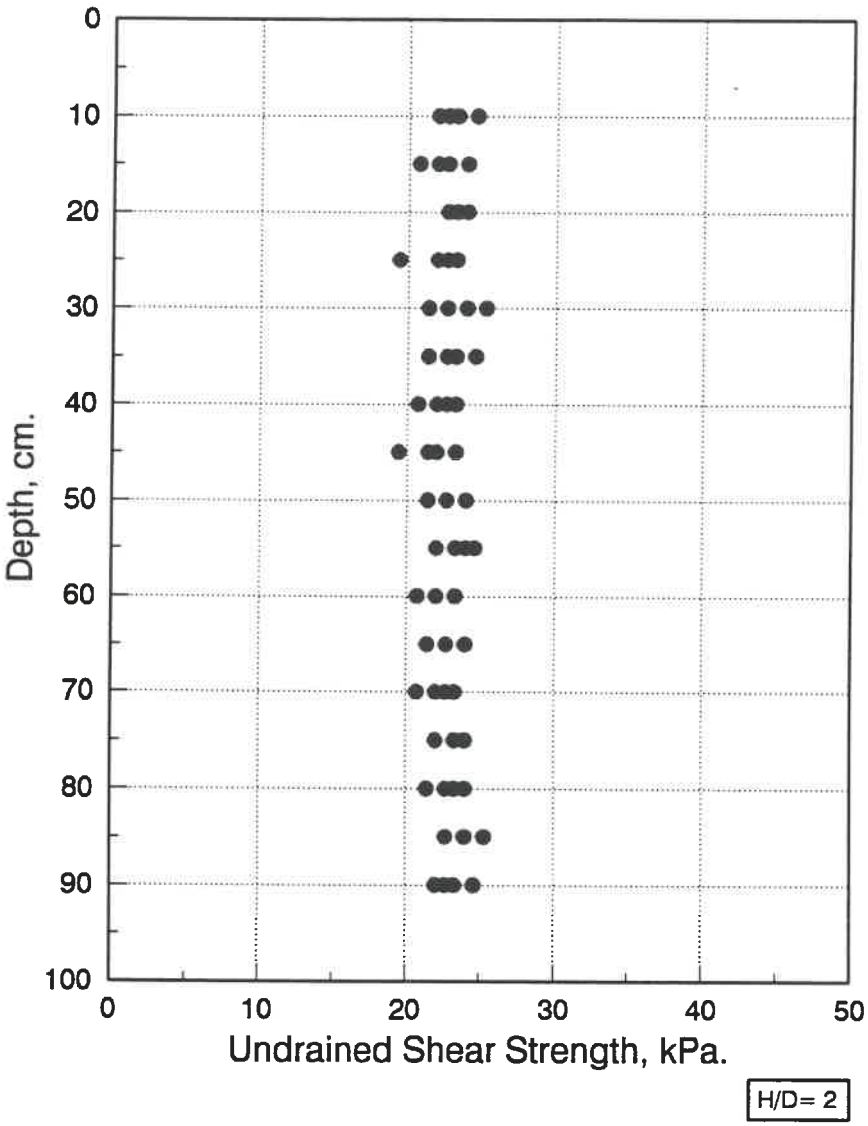

Fig. B.17 Results of laboratory vane shear test-18°.

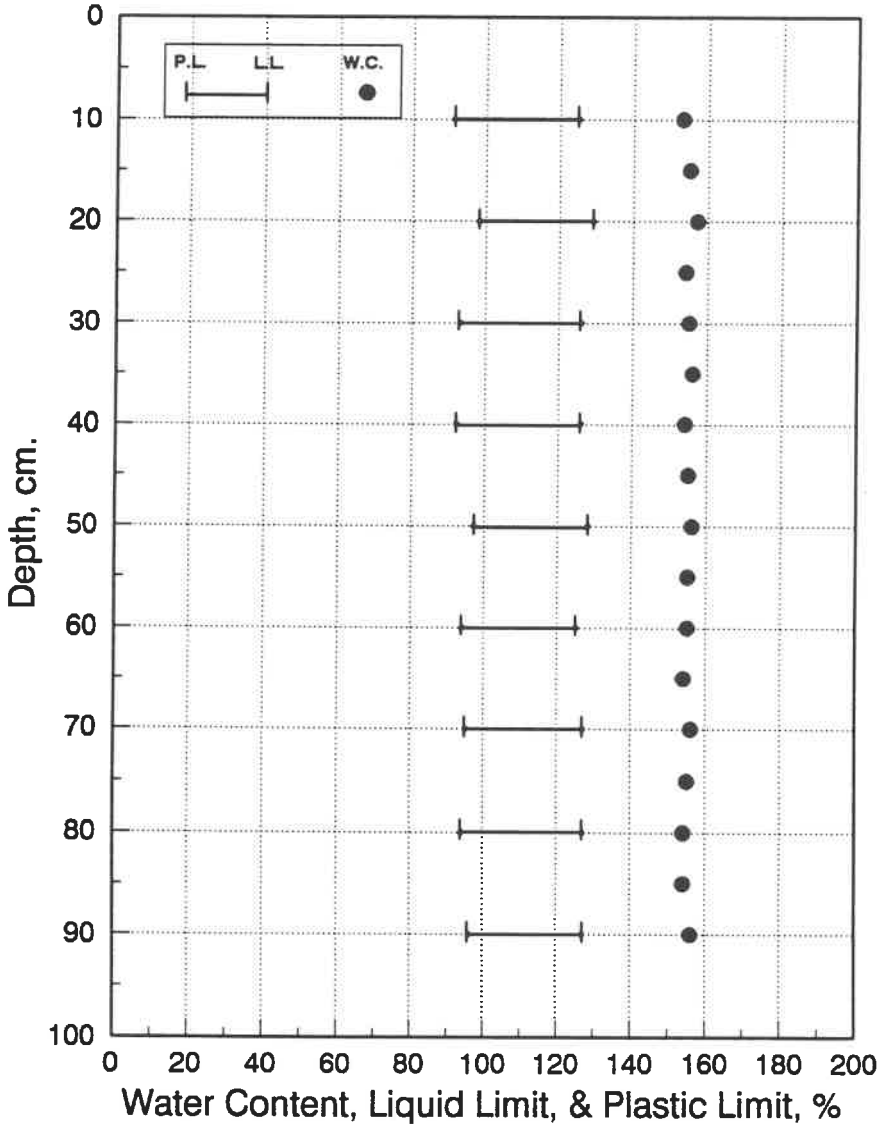

Fig. B.18 Water content and consistency limits for penetration test-18°.

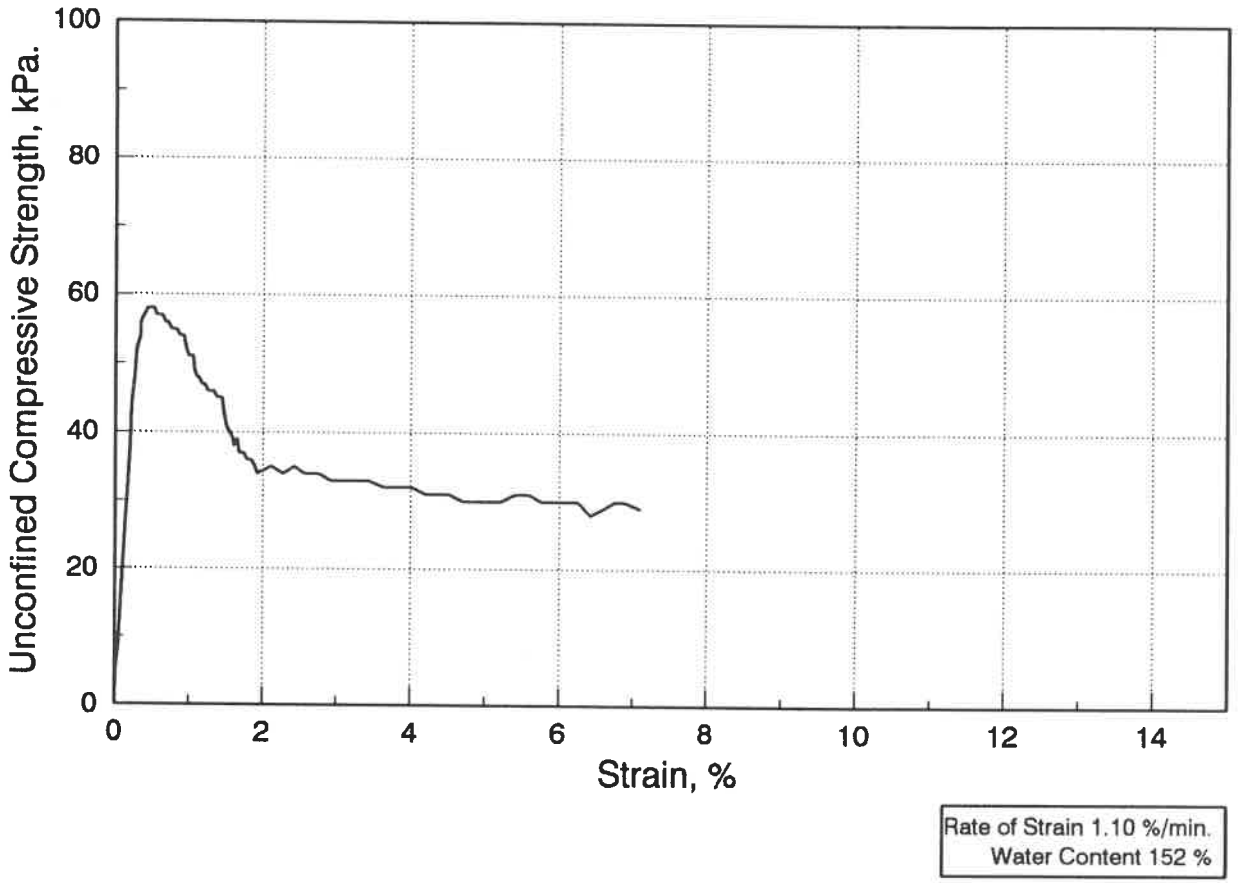

Fig. B.19 Stress-strain curve of the unconfined compression test-18°/1.

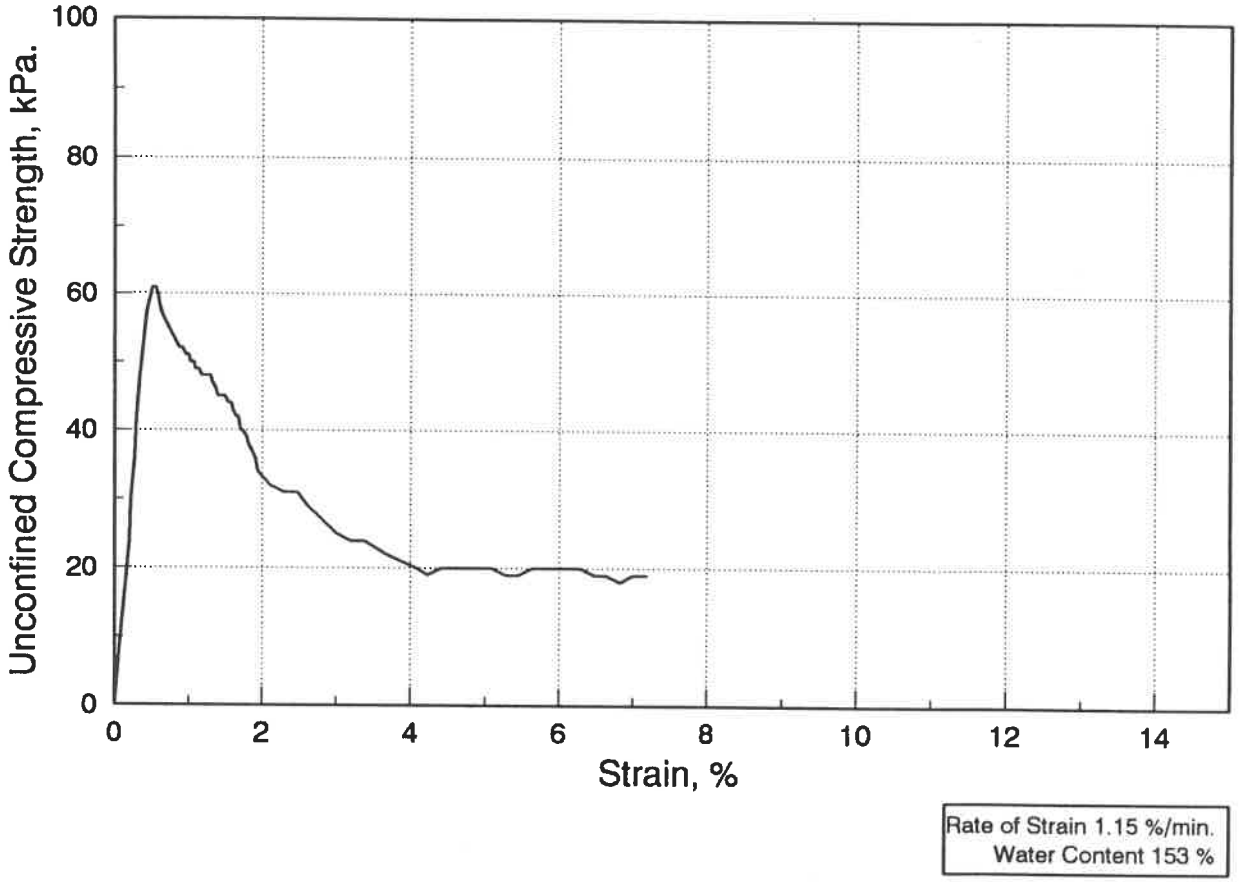

Fig. B.20 Stress-strain curve of the unconfined compression test-18°/2.

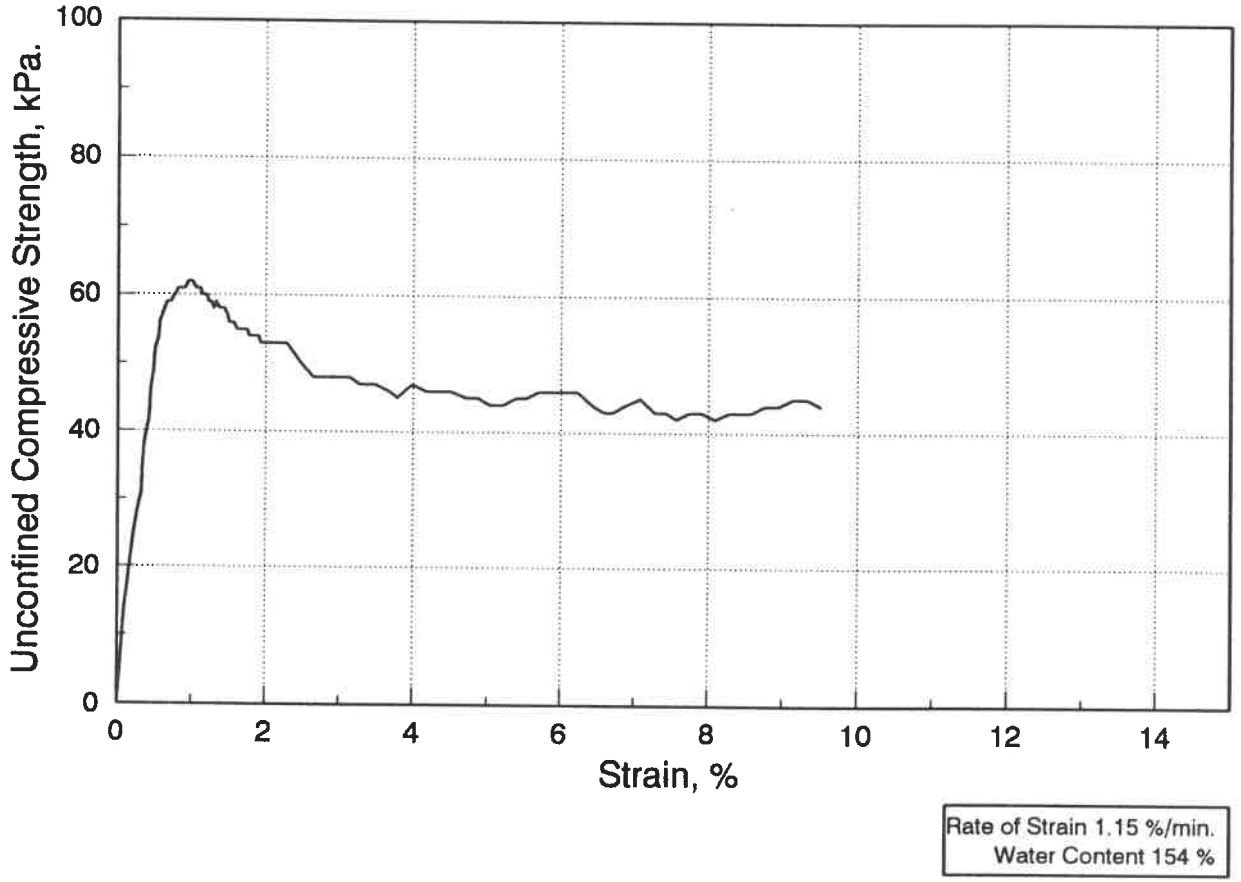

Fig. B.21 Stress-strain curve of the unconfined compression test-18°/3.

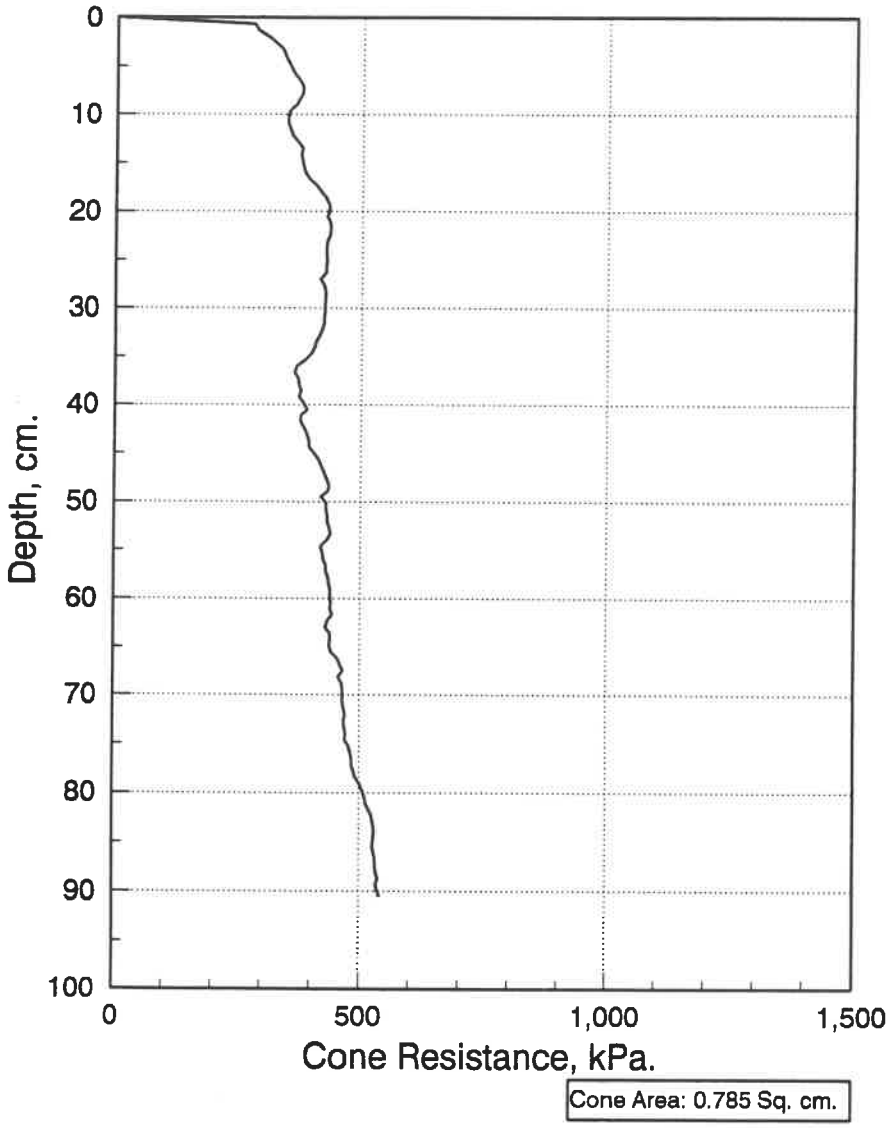

Fig. B.22 Quasi-static cone resistance curve for 22.5° cone apex angle.

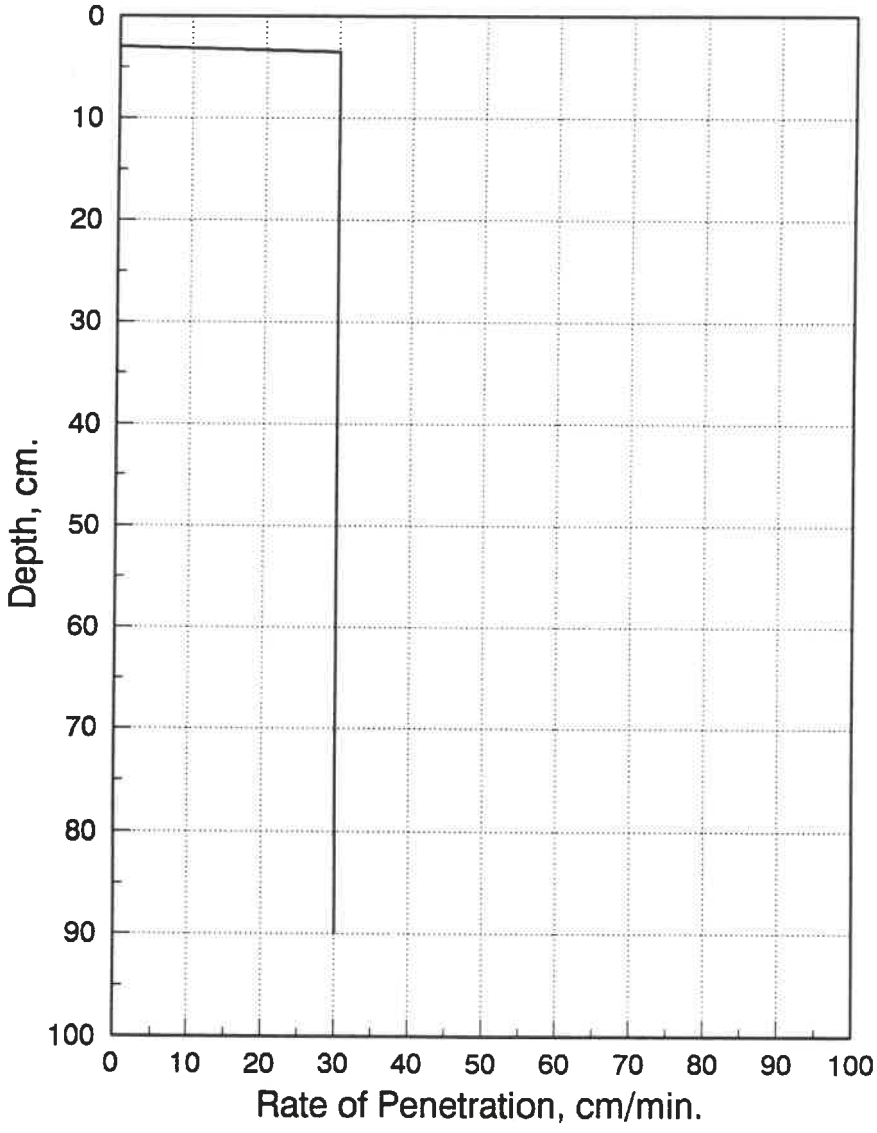

Fig. B.23 Rate of penetration curve for 22.5° cone apex angle.

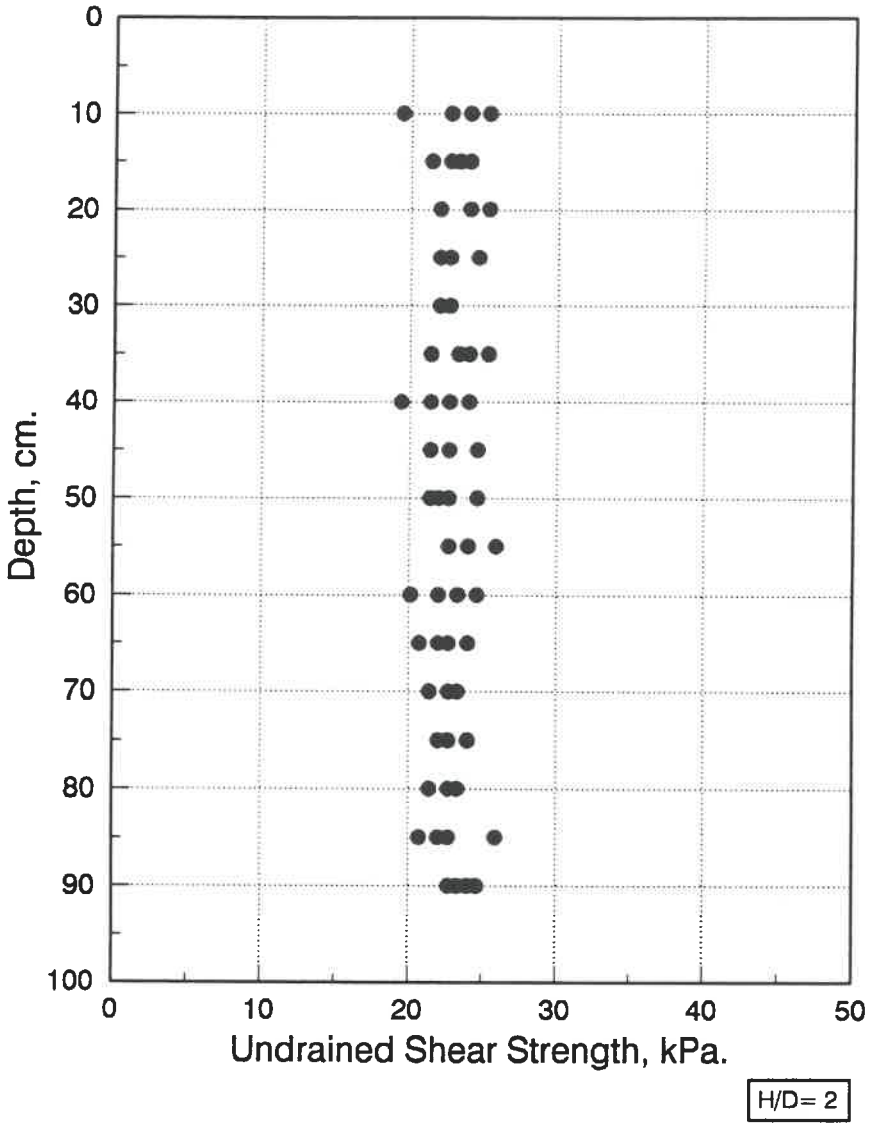

Fig. B.24 Results of laboratory vane shear test-22.5°.

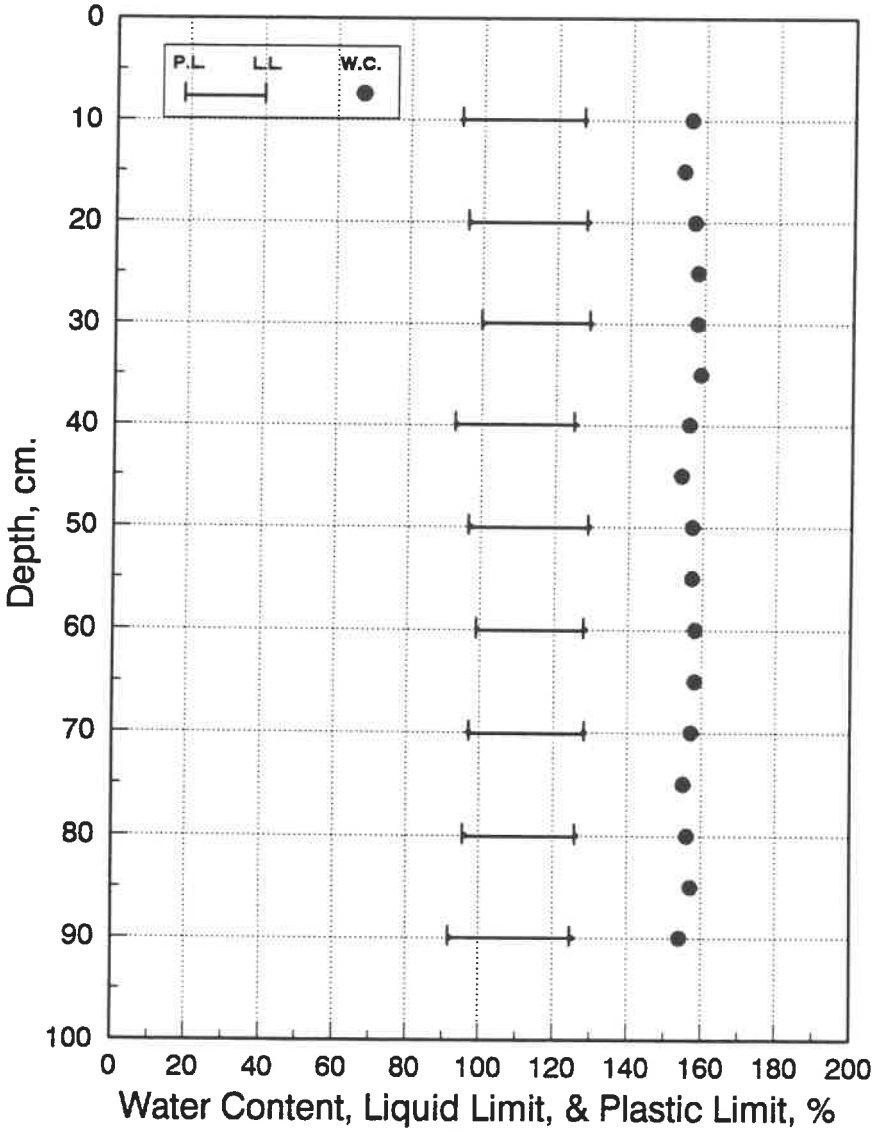

Fig. B.25 Water content and consistency limits for penetration test-22.5°.

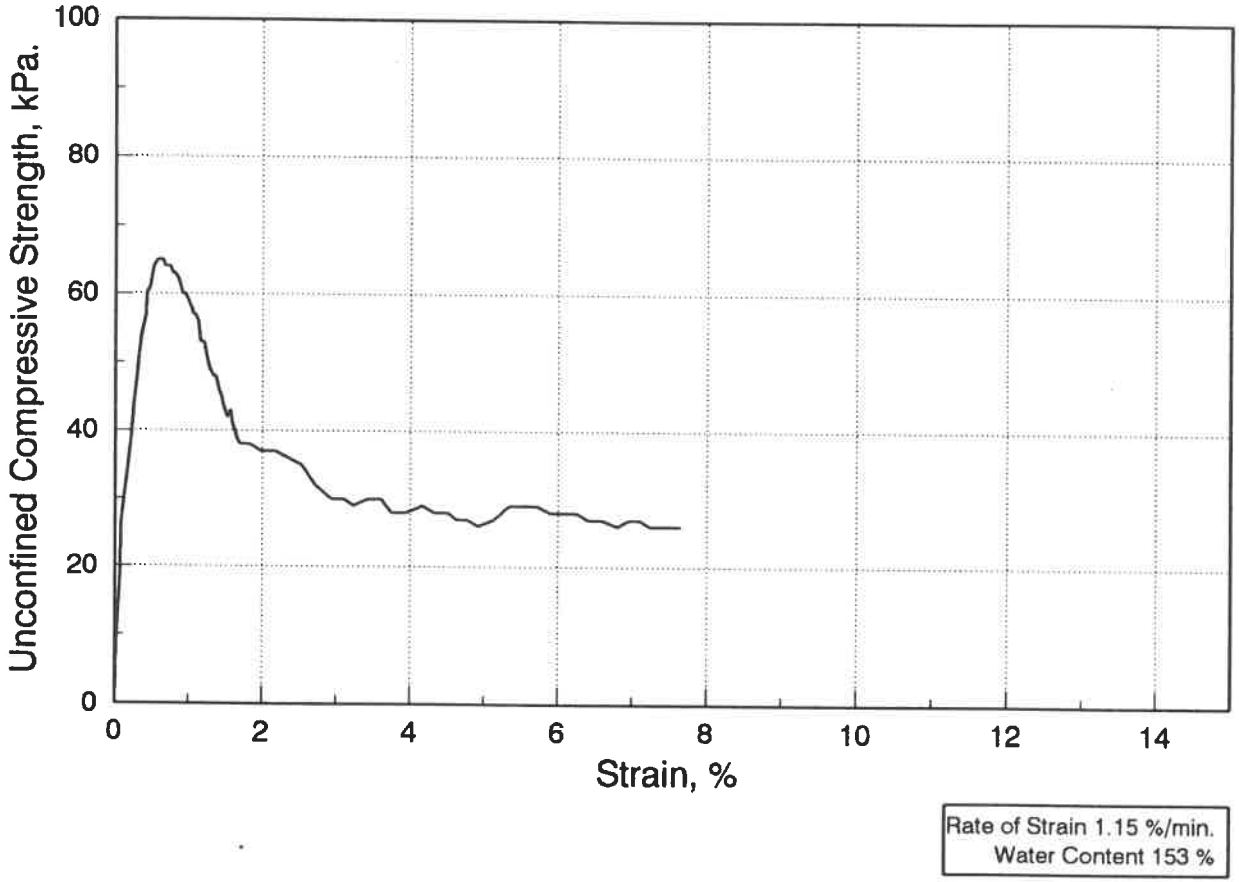

Fig. B.26 Stress-strain curve of the unconfined compression test-22.5°/1.

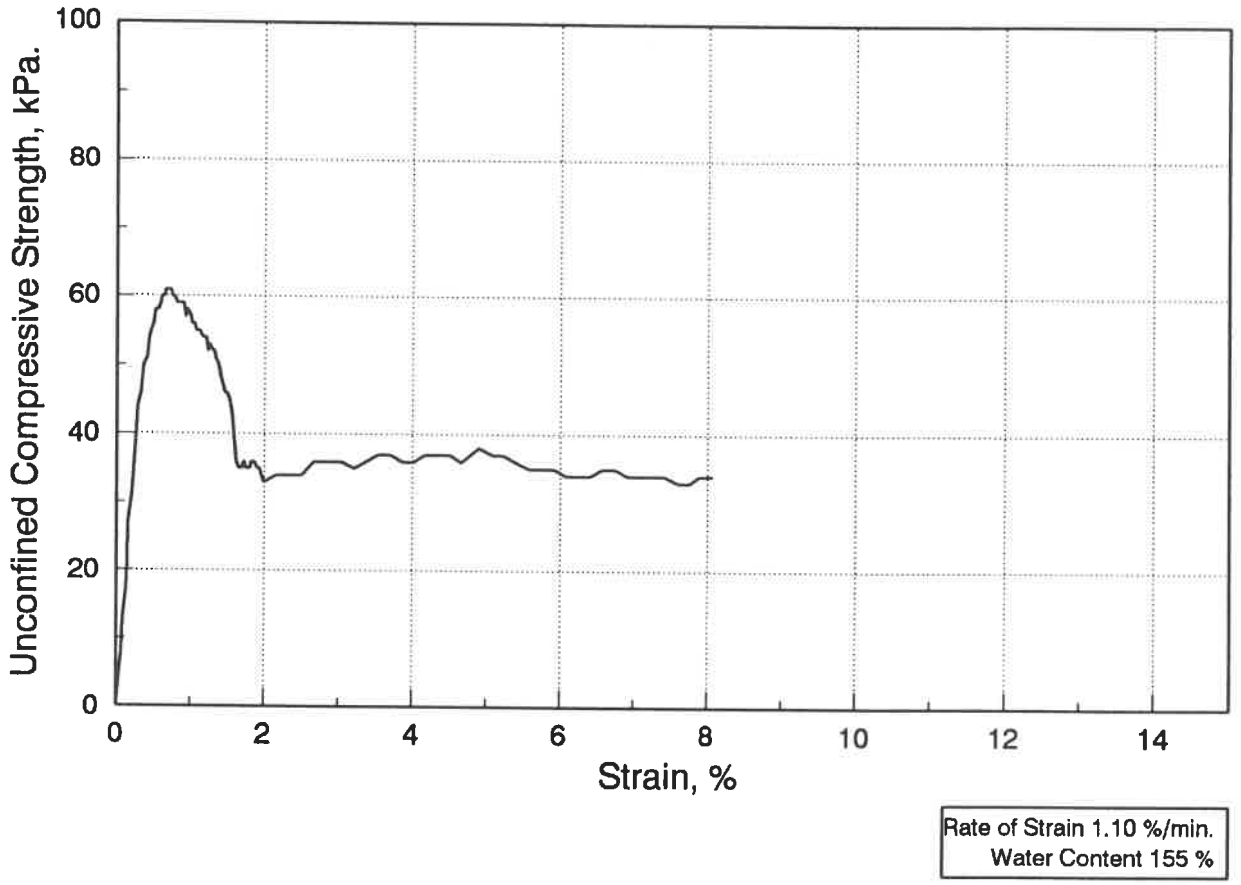

Fig. B.27 Stress-strain curve of the unconfined compression test-22.5°/2.

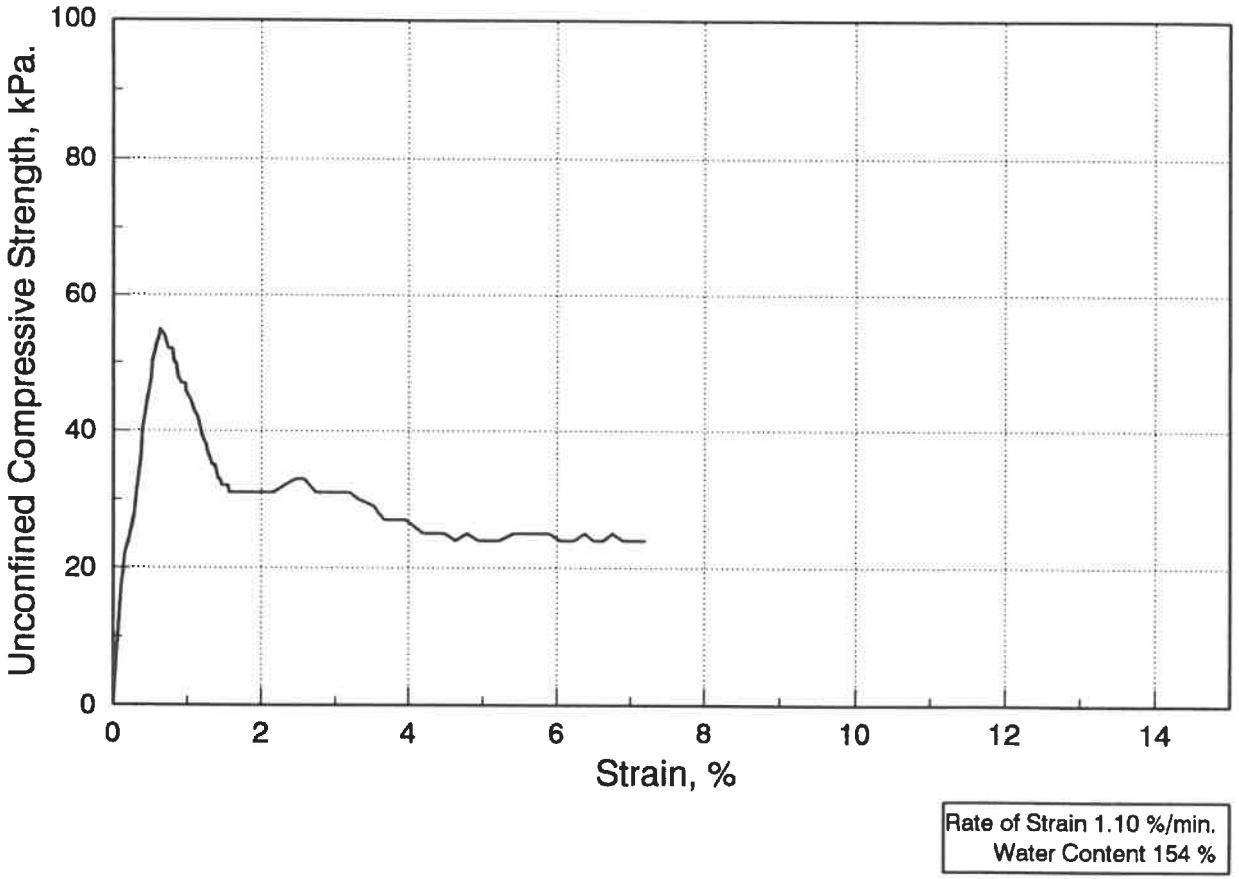

Fig. B.28 Stress-strain curve of the unconfined compression test-22.5°/3.

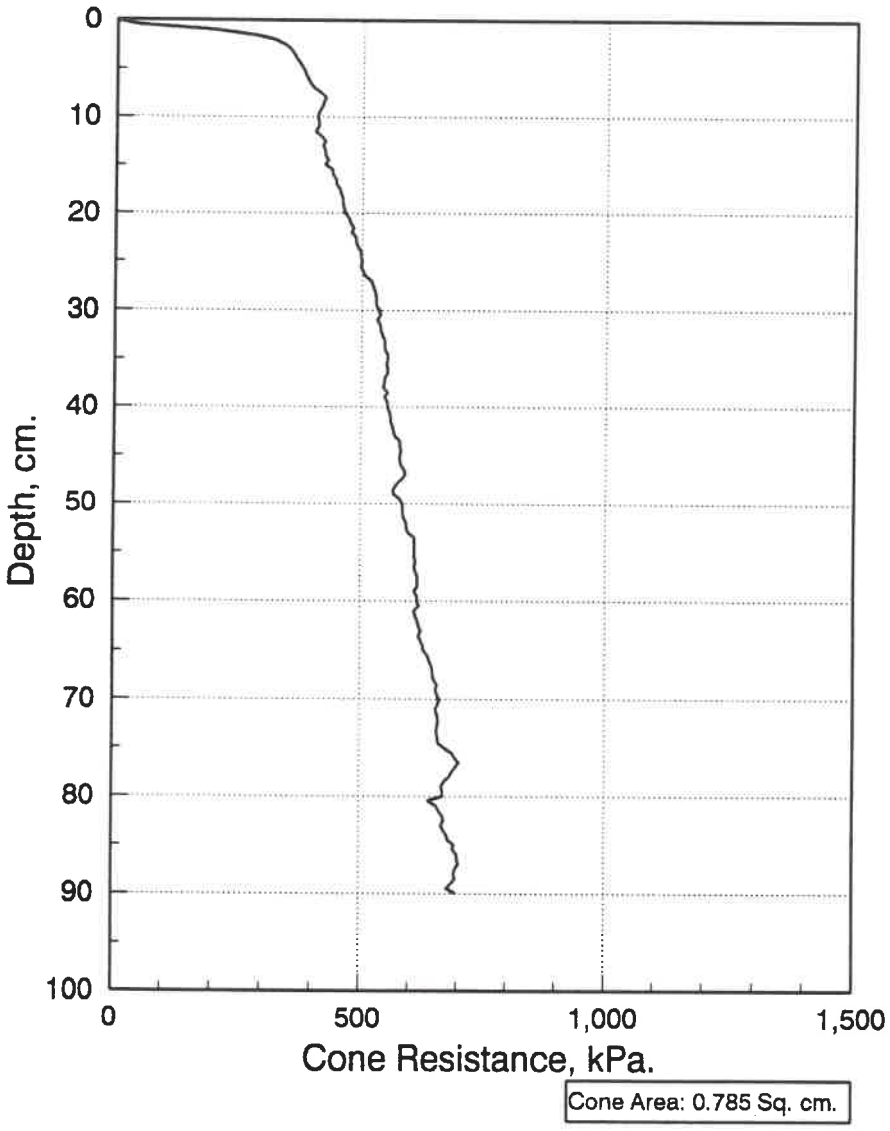

Fig. B.29 Quasi-static cone resistance curve for 45° cone apex angle.

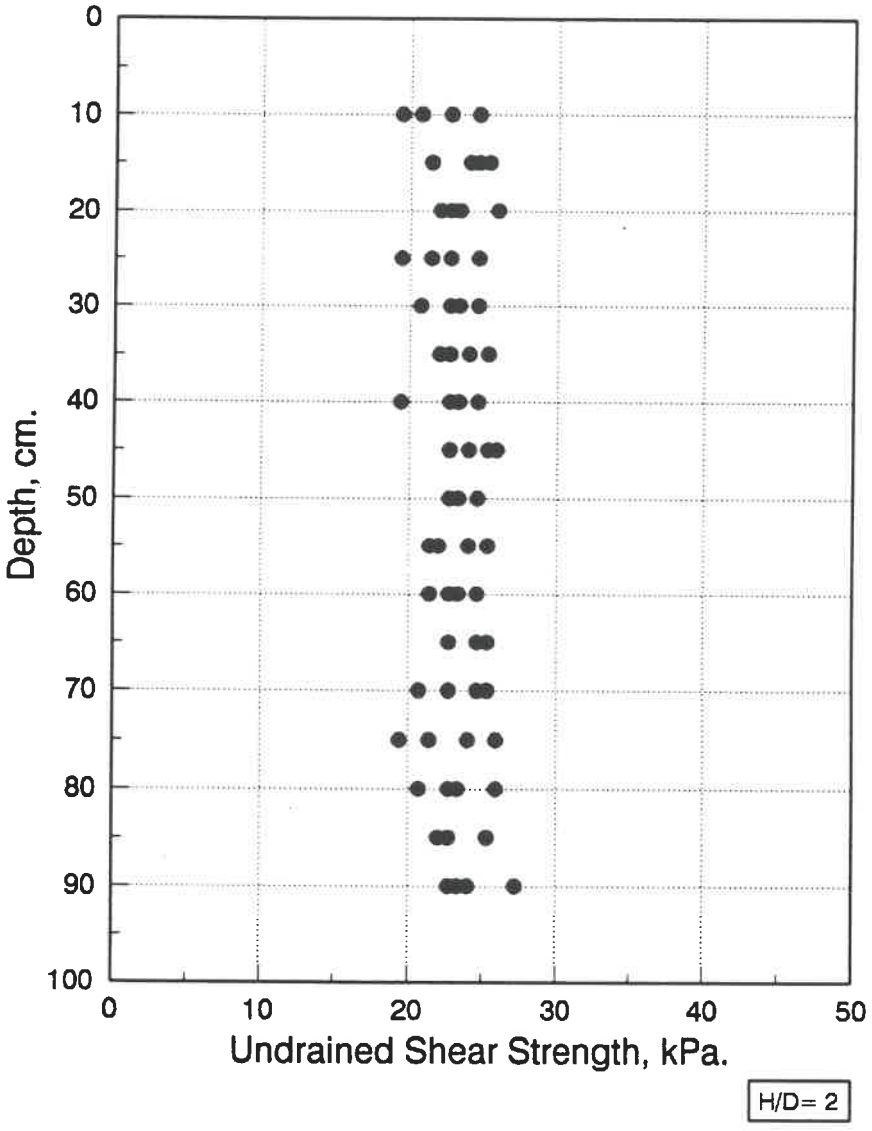

Fig. B.30 Results of laboratory vane shear test-45°.

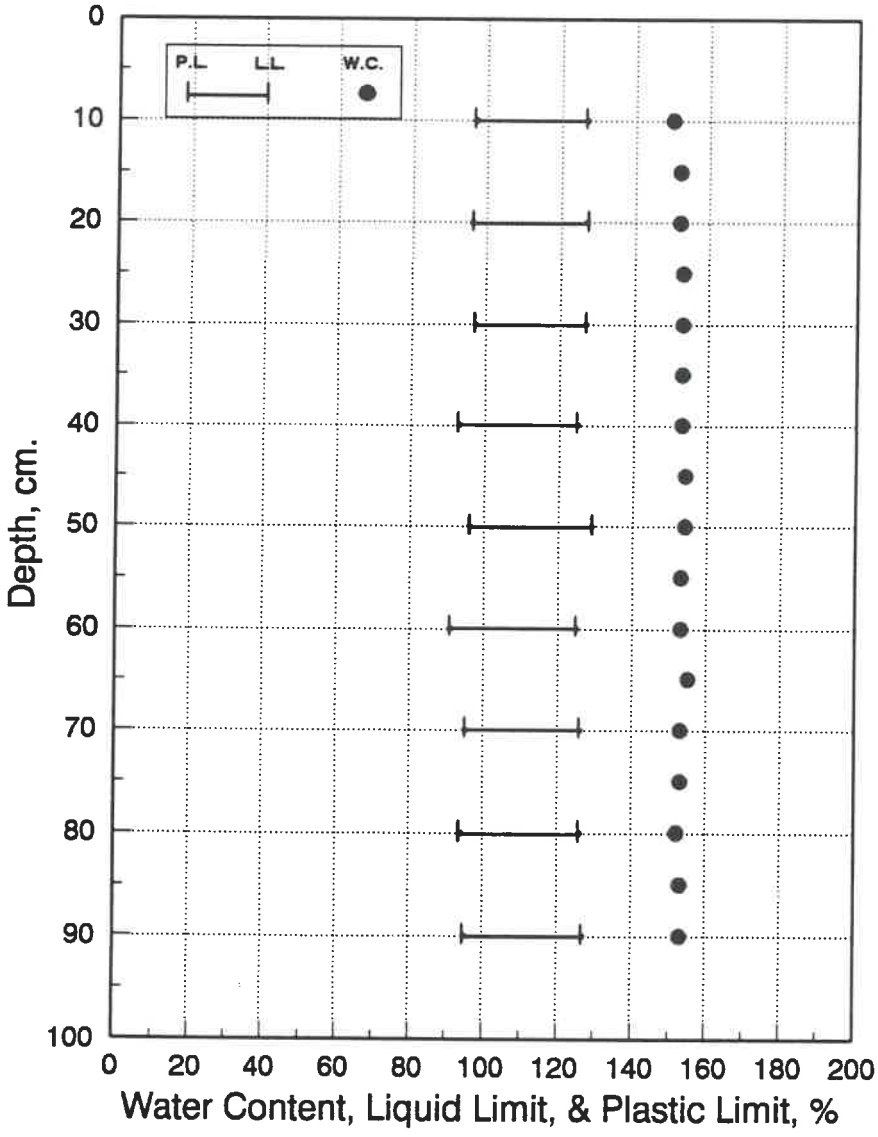

Fig. B.31 Water content and consistency limits for penetration test-45°.

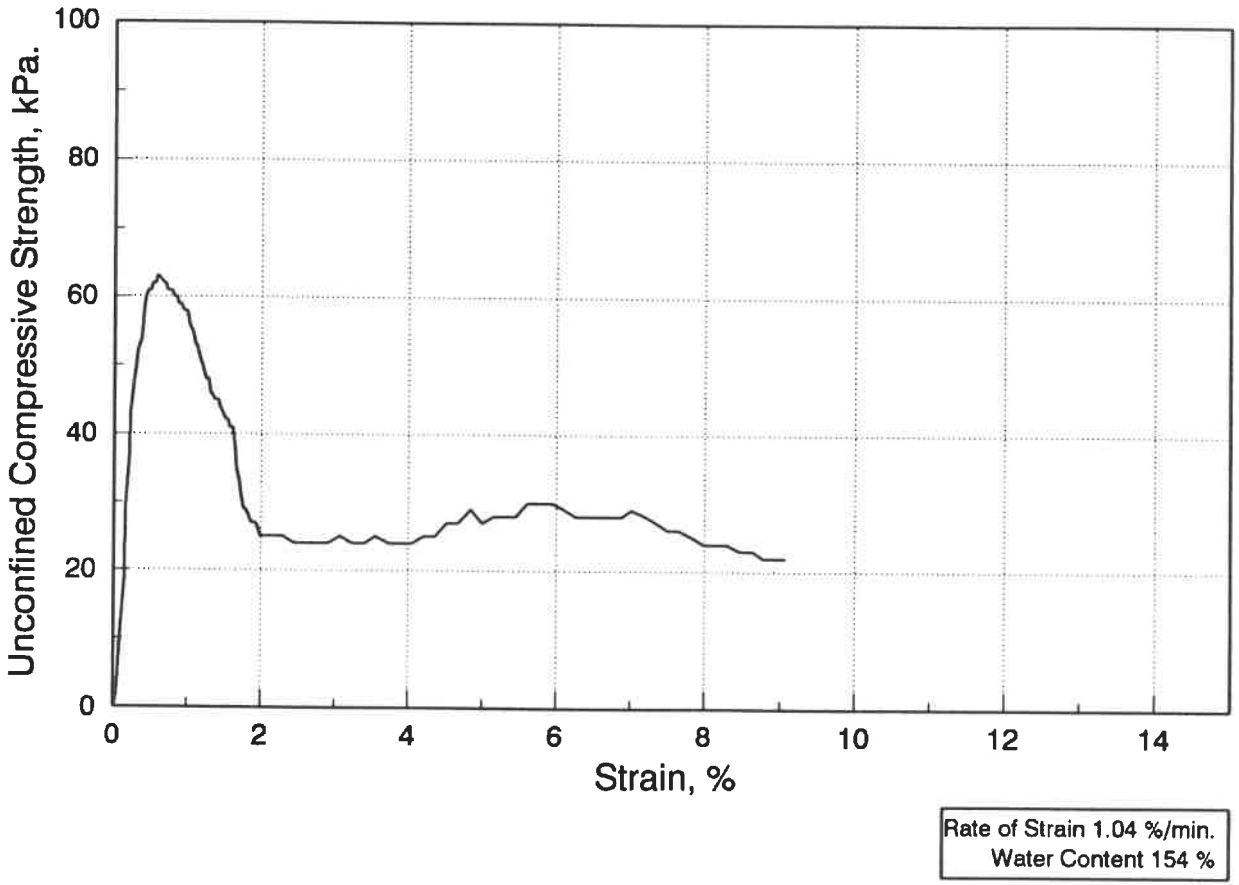

Fig. B.32 Stress-strain curve of the unconfined compression test-45°/1.

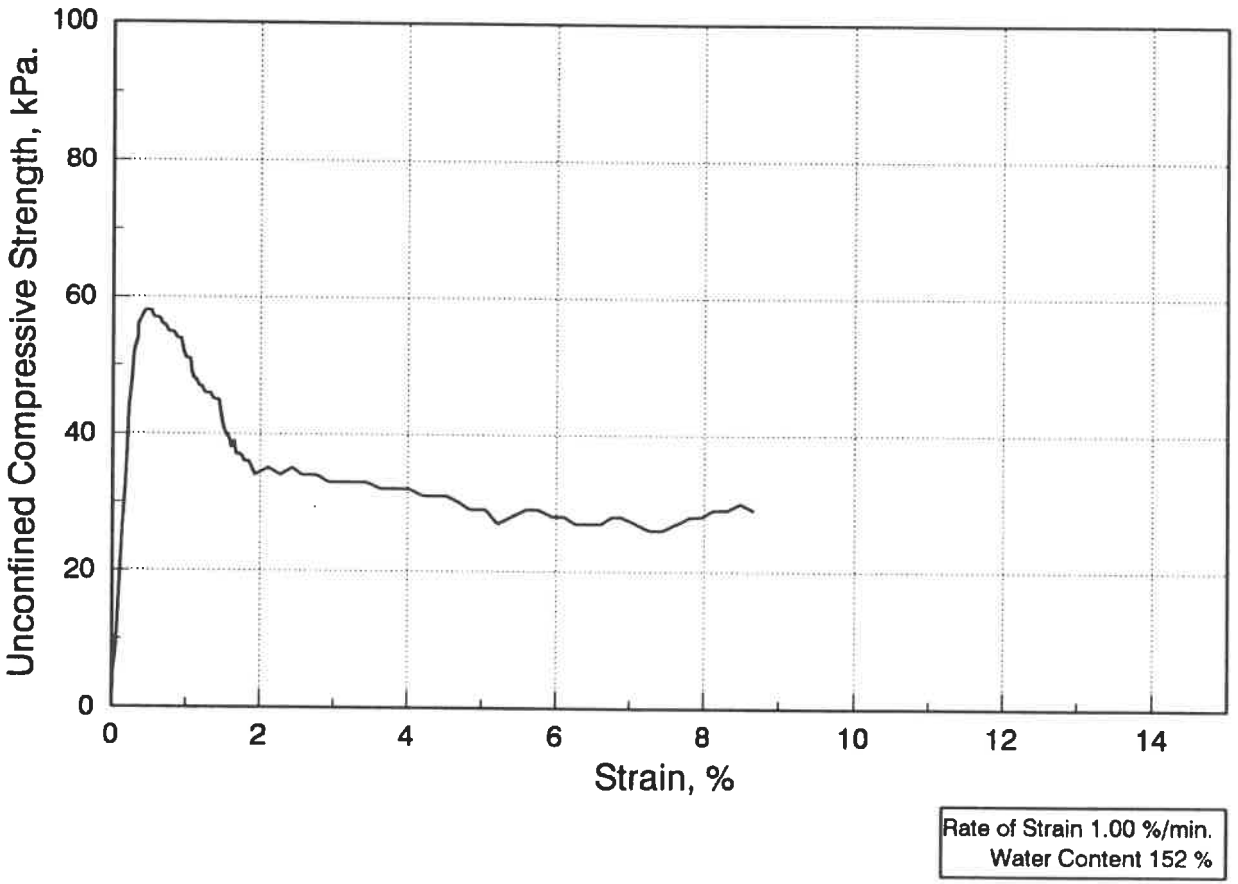

Fig. B.33 Stress-strain curve of the unconfined compression test-45°/2.

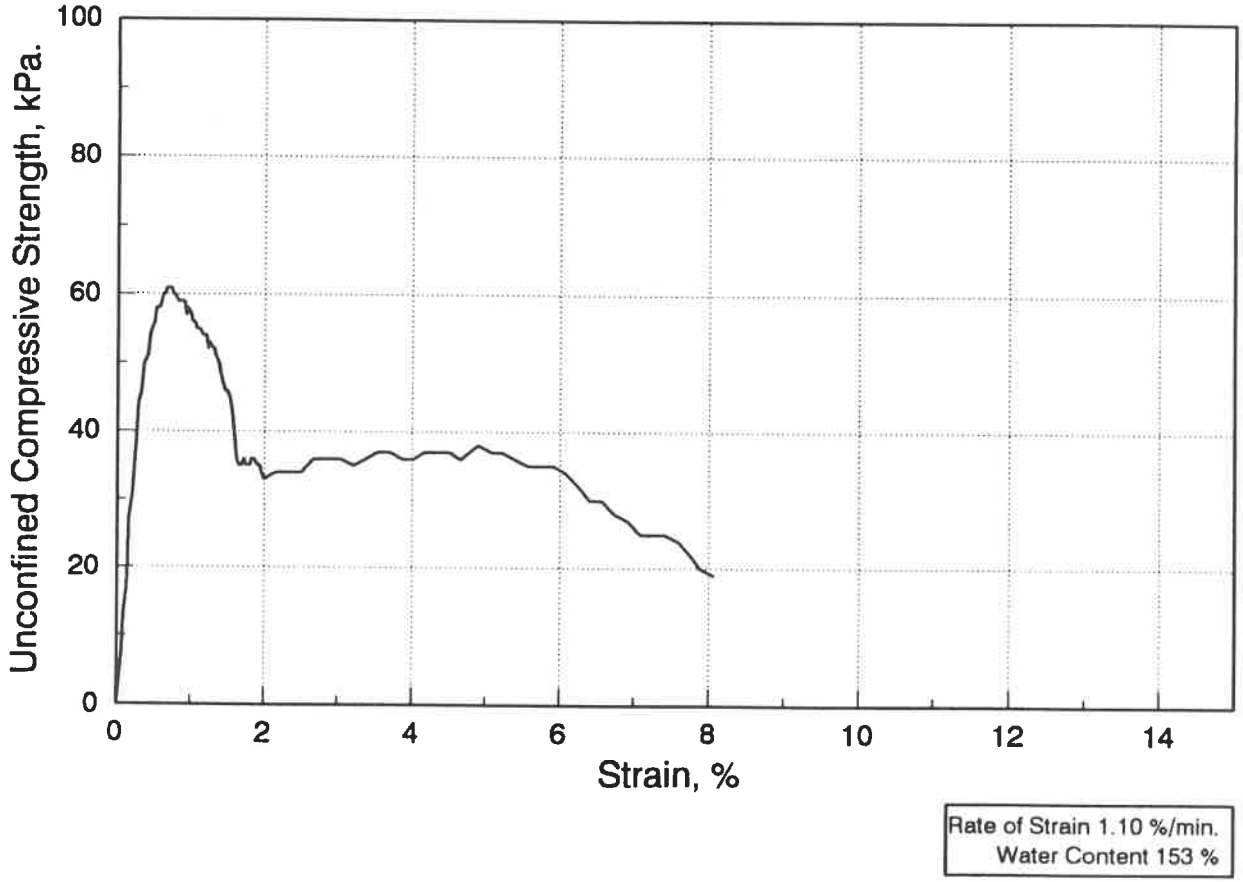

Fig. B.34 Stress-strain curve of the unconfined compression test-45°/3.

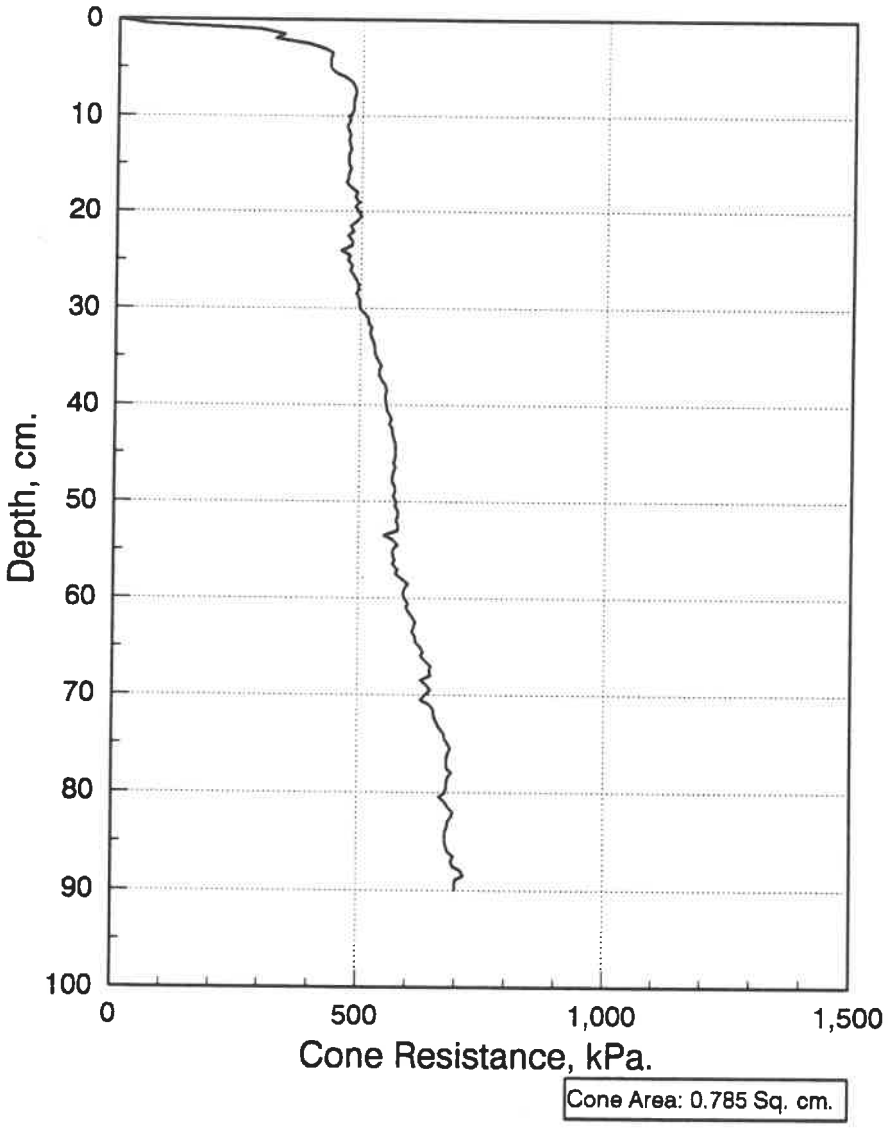

Fig. B.35 Quasi-static cone resistance curve for 60° cone apex angle.

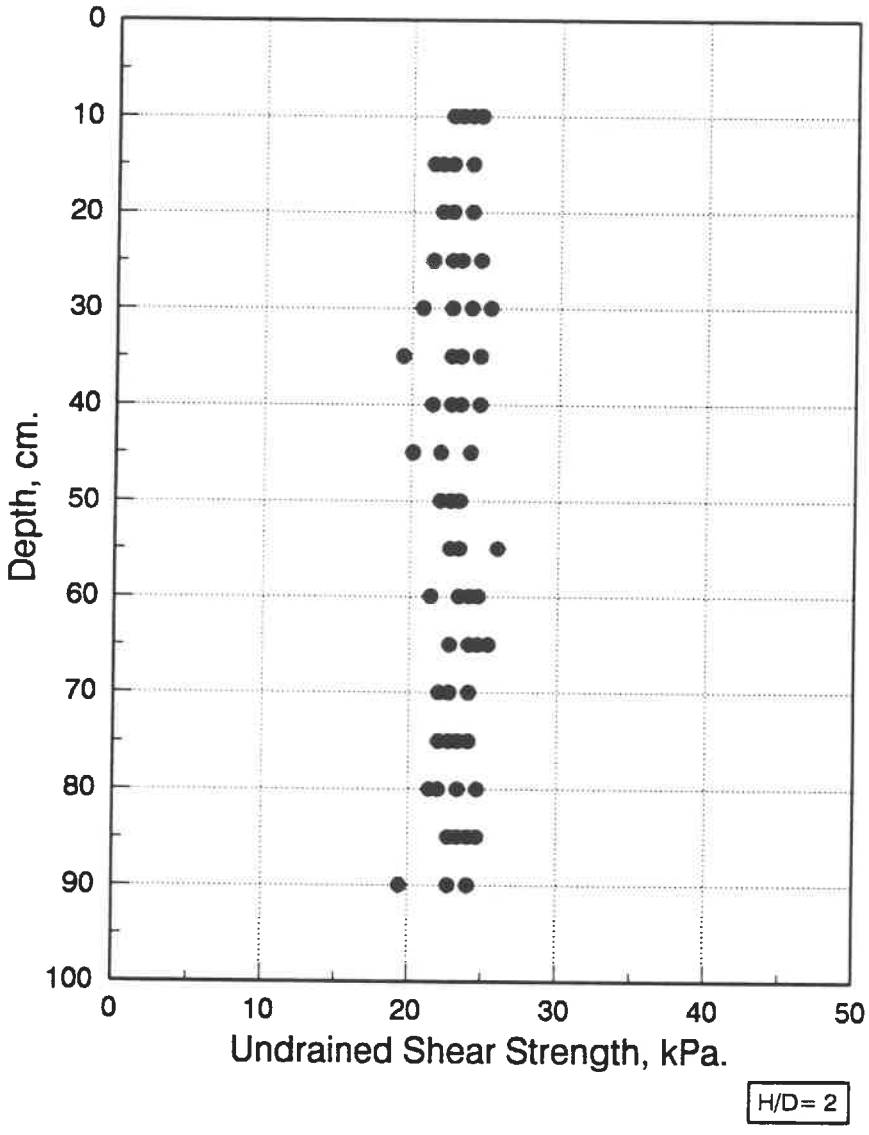

Fig. B.36 Results of laboratory vane shear test-60°.

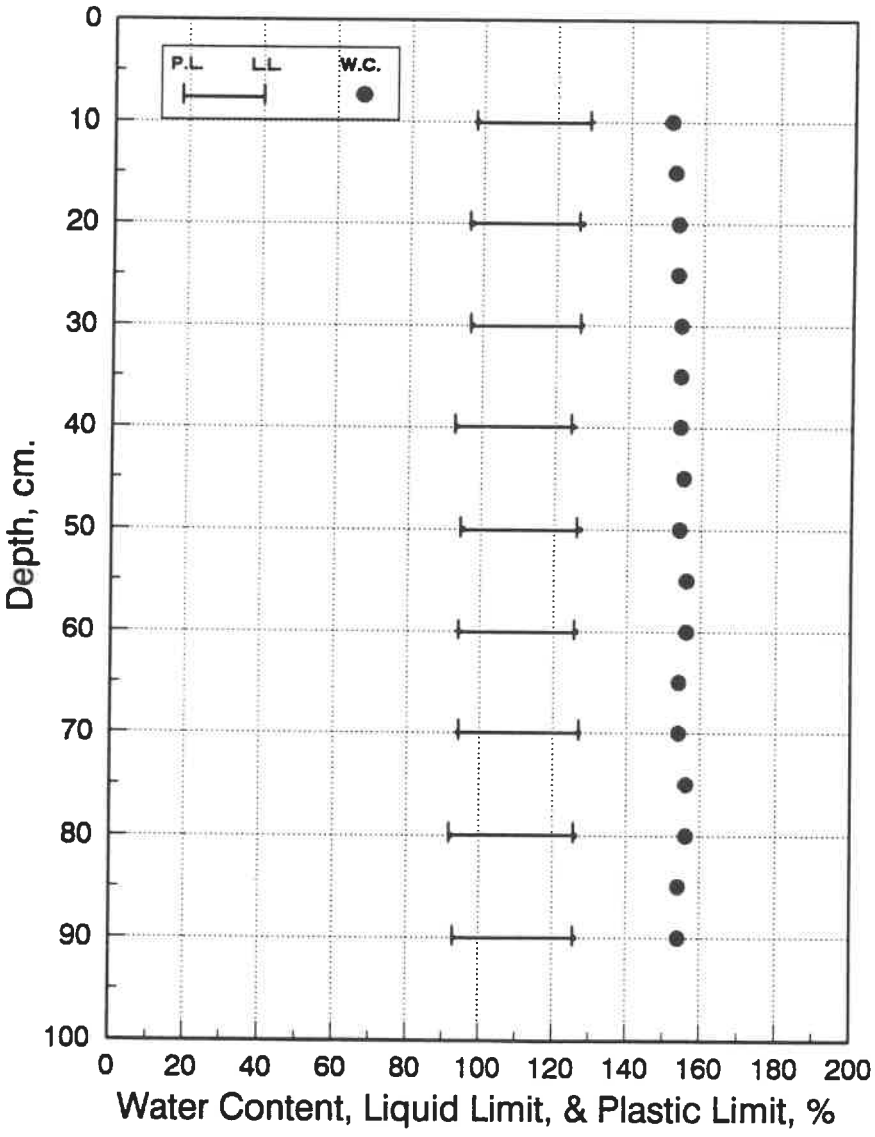

Fig. B.37 Water content and consistency limits for penetration test-60°.

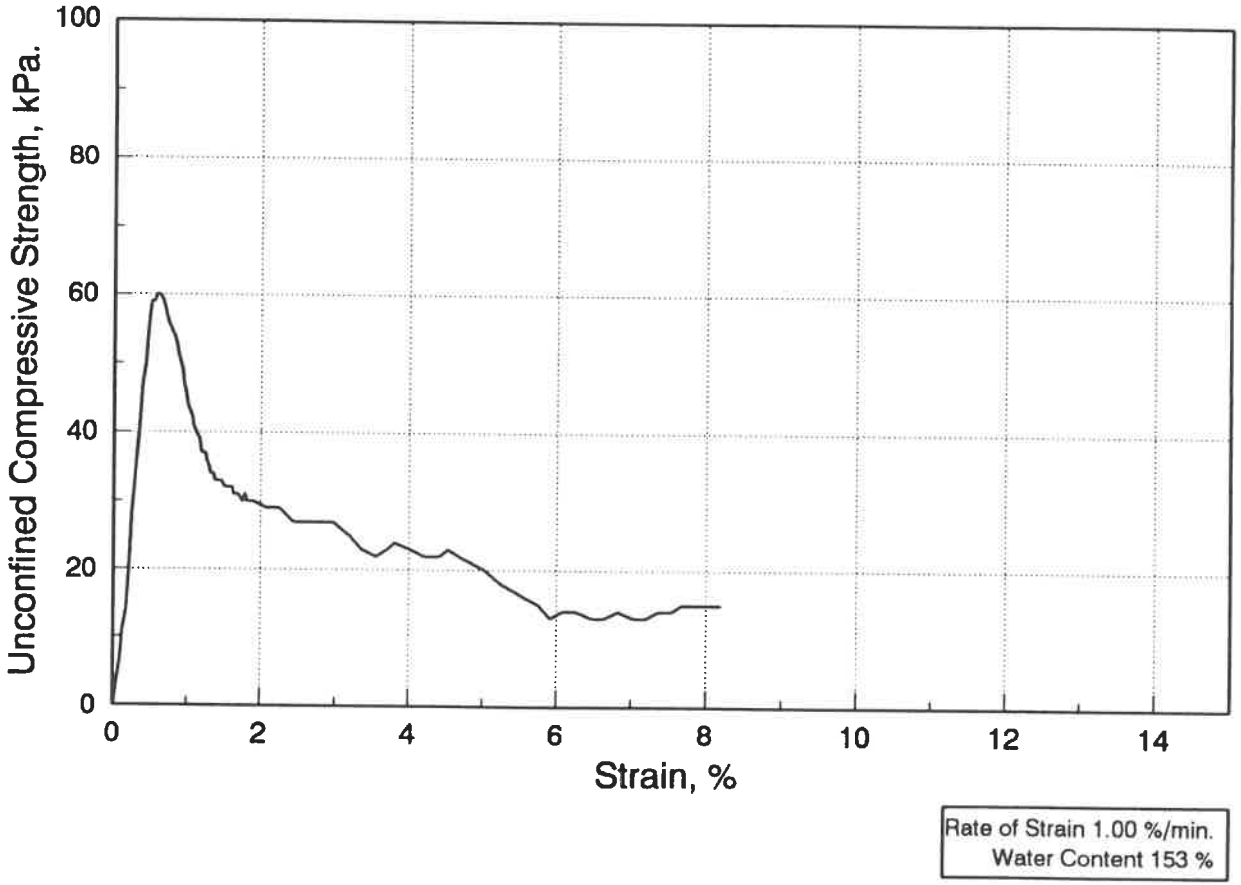

Fig. B.38 Stress-strain curve of the unconfined compression test-60°/1.

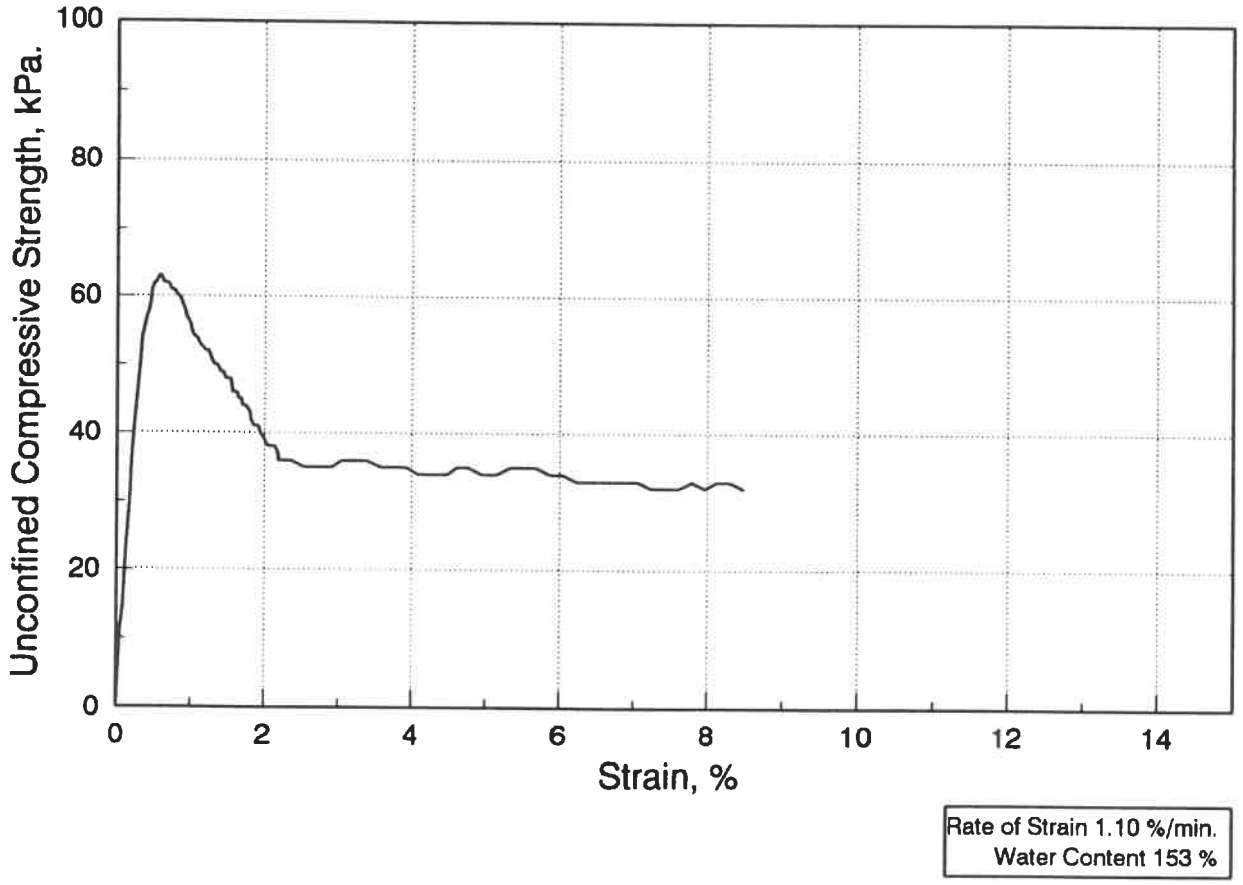

Fig. B.39 Stress-strain curve of the unconfined compression test-60°/2.

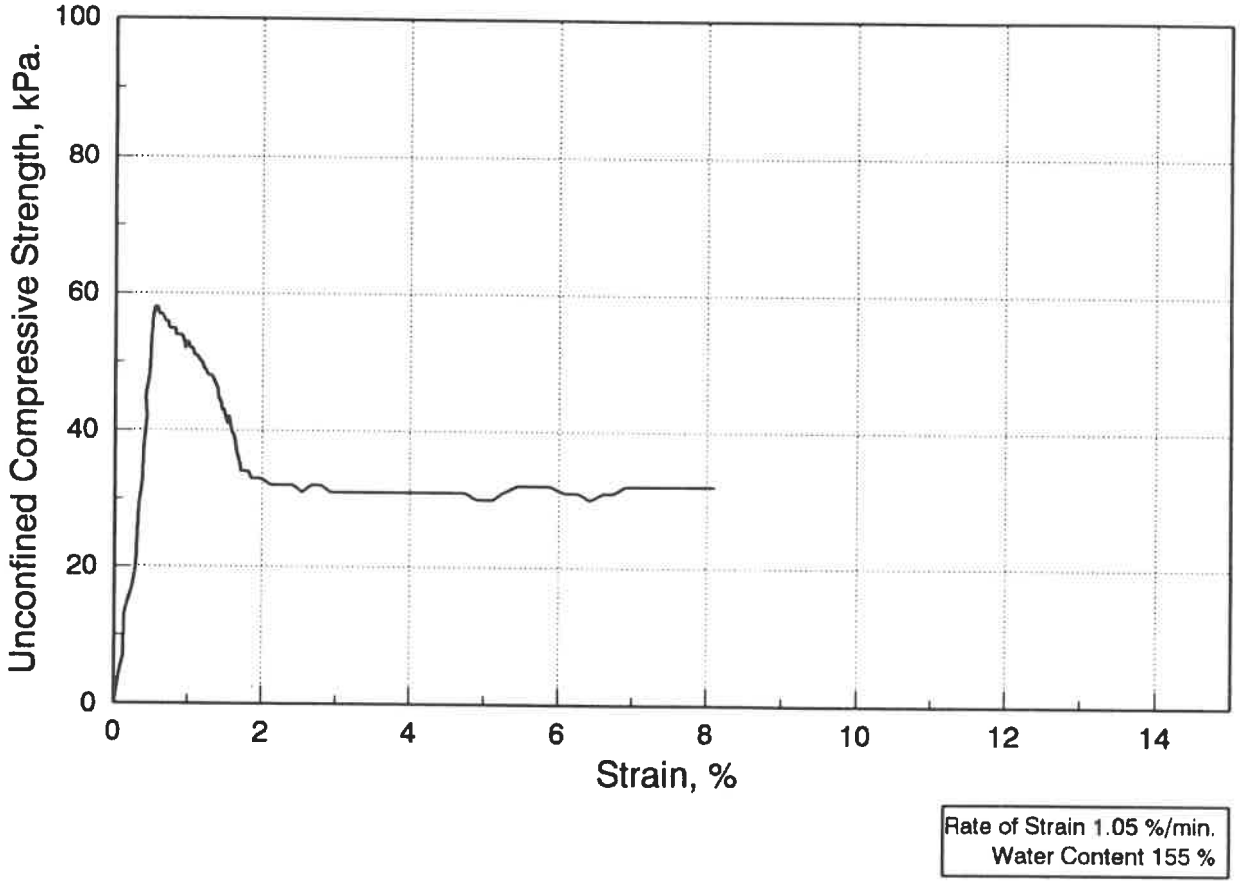

Fig. B.40 Stress-strain curve of the unconfined compression test-60°/3.

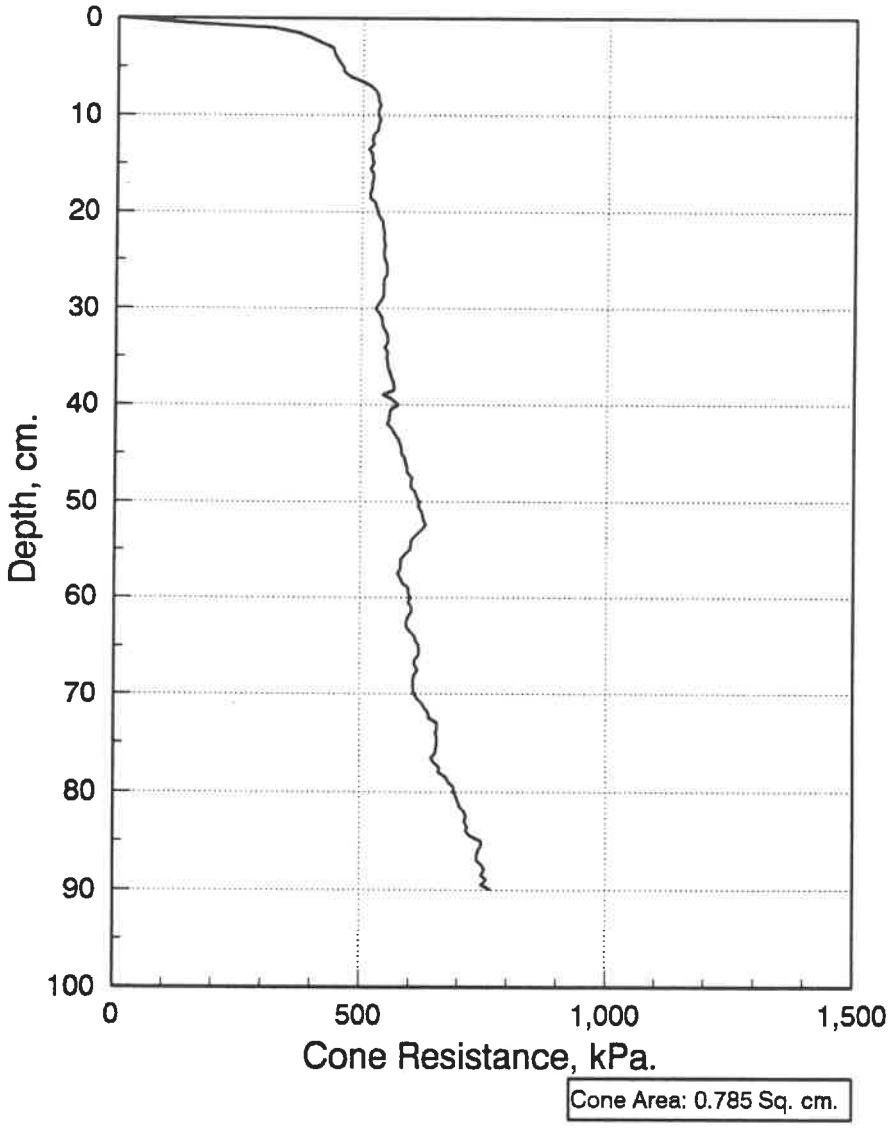

Fig. B.41 Quasi-static cone resistance curve for 90° cone apex angle.

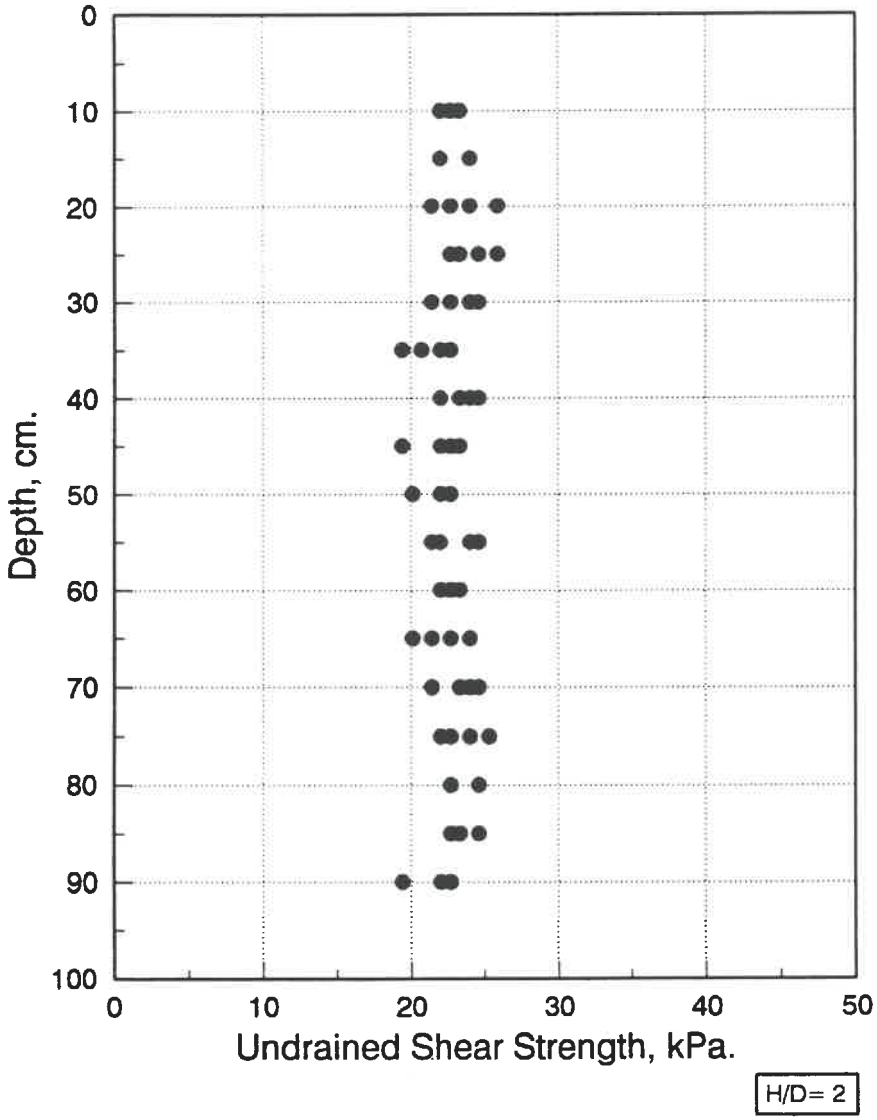

Fig. B.42 Results of laboratory vane shear test-90°.

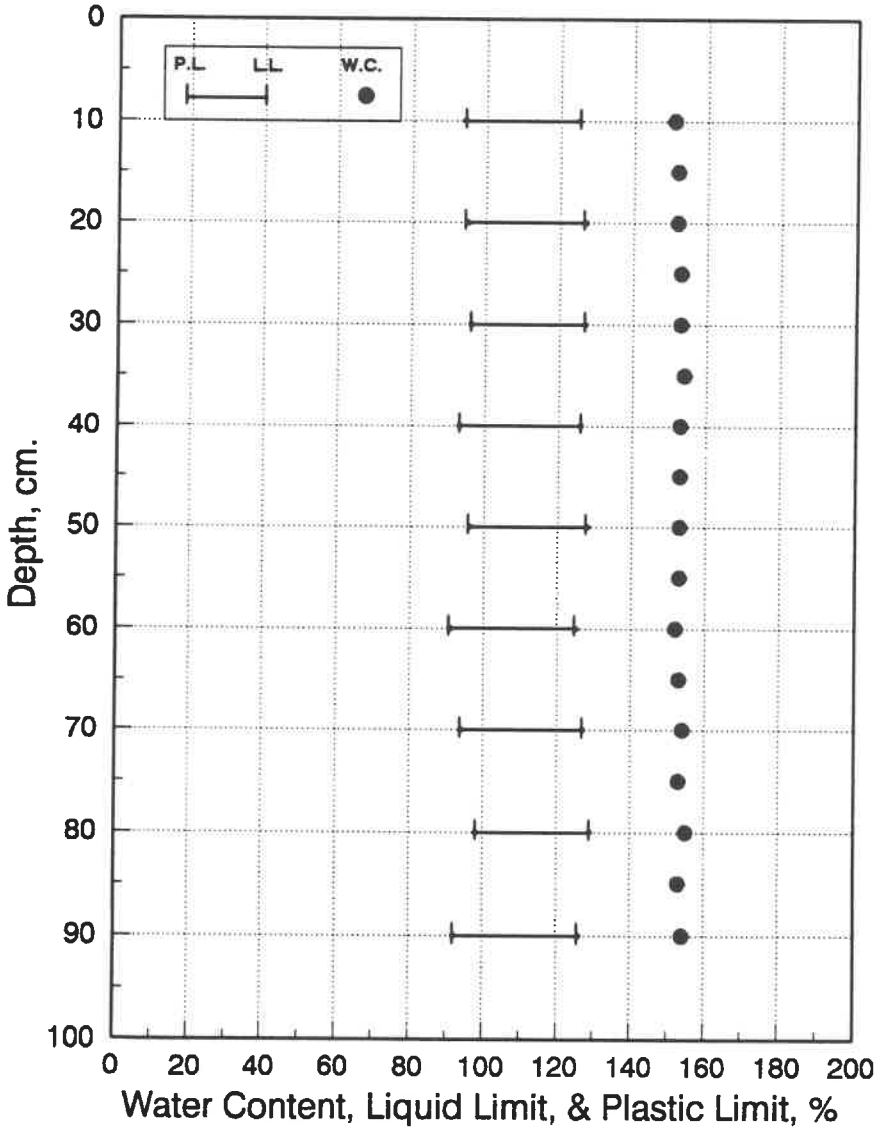

Fig. B.43 Water content and consistency limits for penetration test-90°.

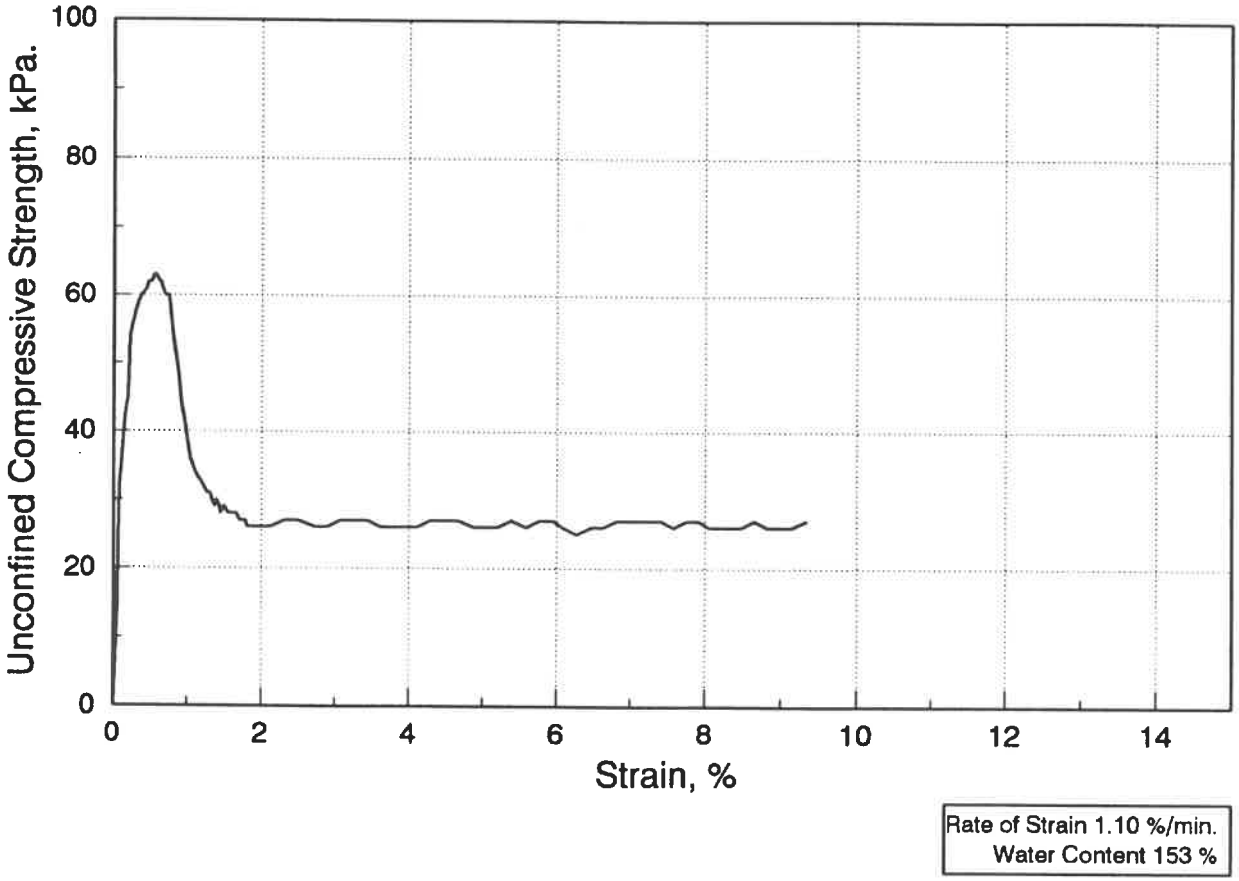

Fig. B.44 Stress-strain curve of the unconfined compression test-90°/1.

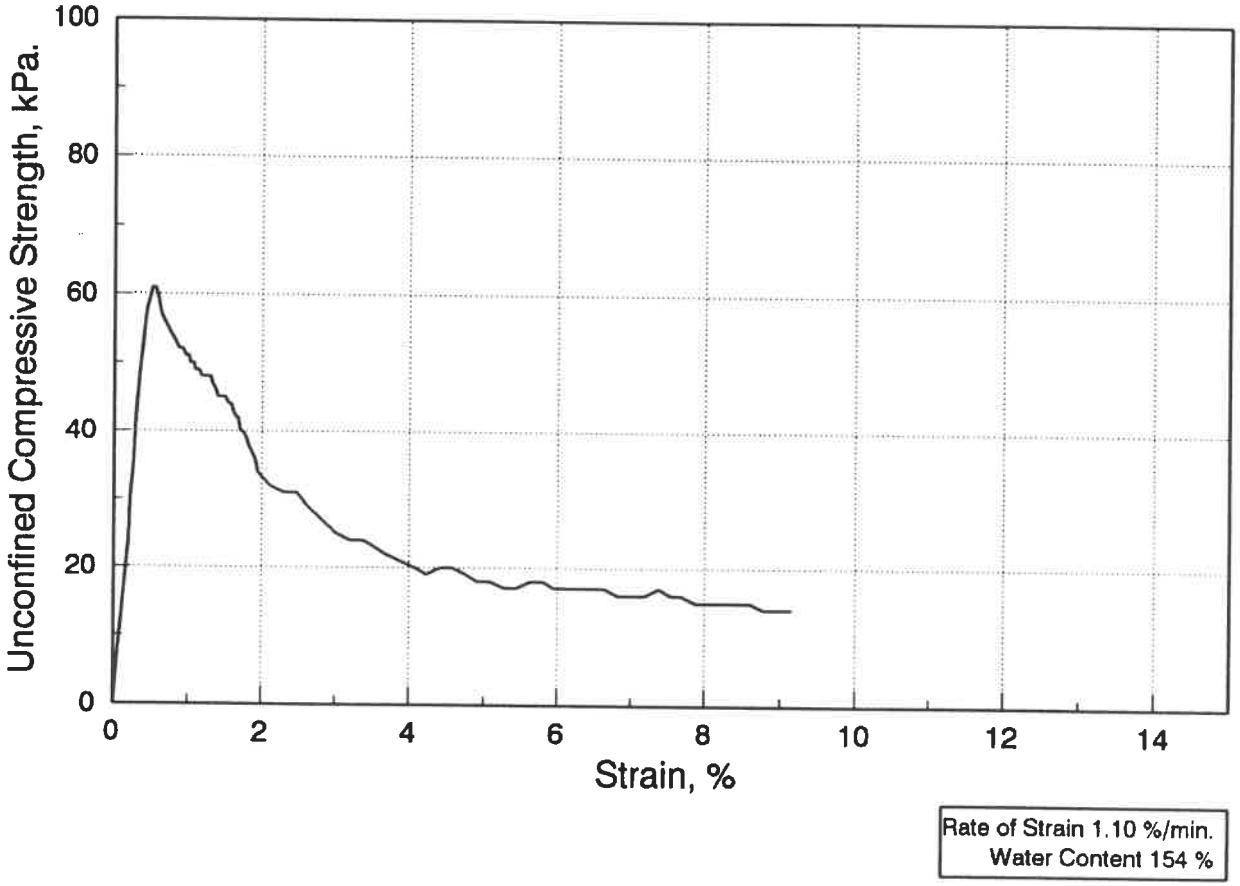

Fig. B.45 Stress-strain curve of the unconfined compression test-90°/2.

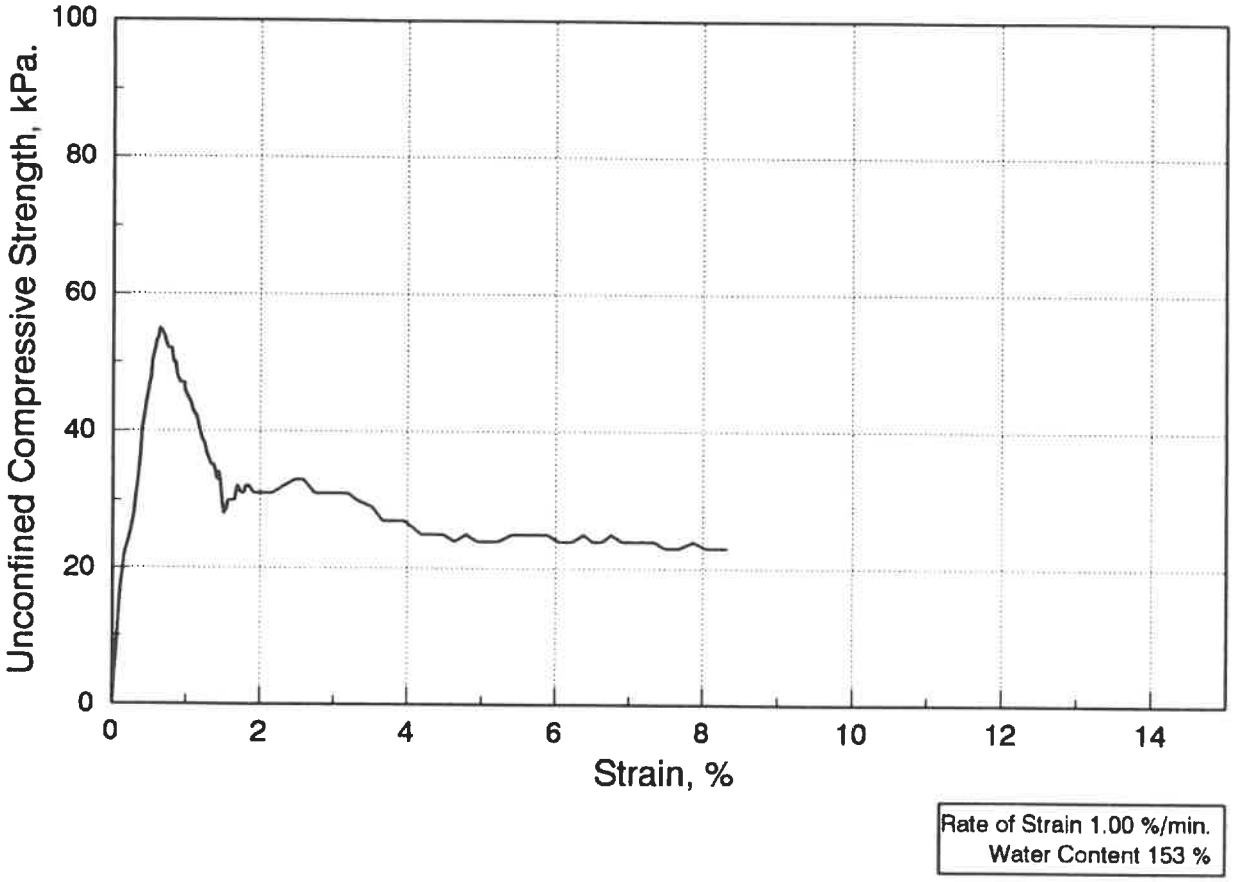

Fig. B.46 Stress-strain curve of the unconfined compression test-90°/3.

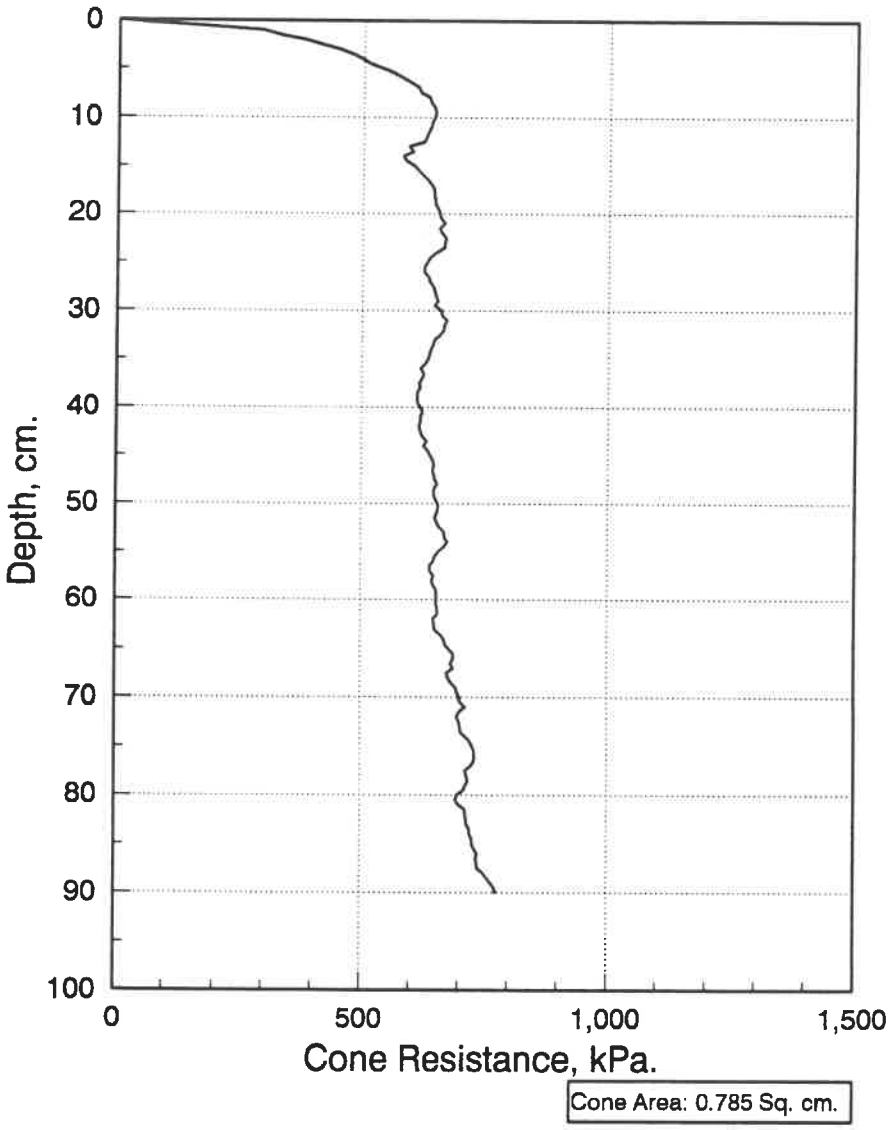

Fig. B.47 Quasi-static cone resistance curve for 180° cone apex angle.

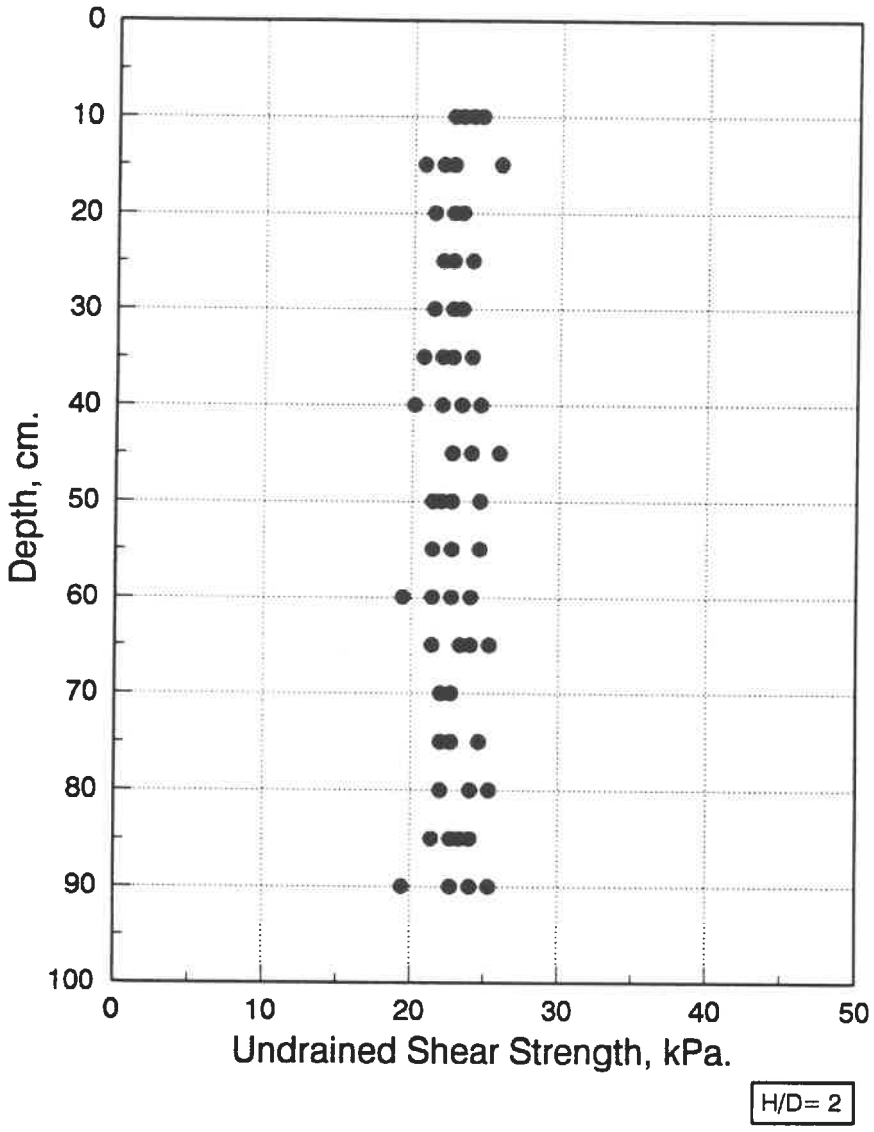

Fig. B.48 Results of laboratory vane shear test-180°.

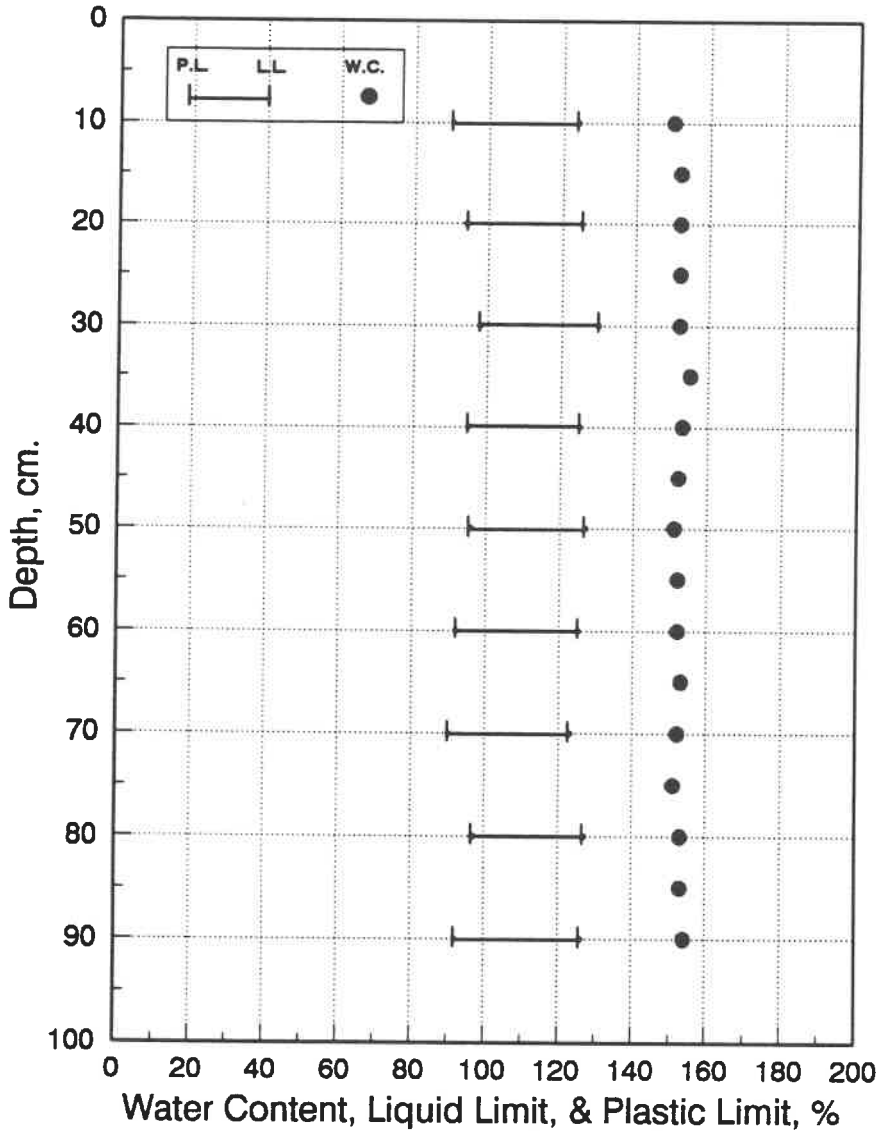

Fig. B.49 Water content and consistency limits for penetration test-180°.

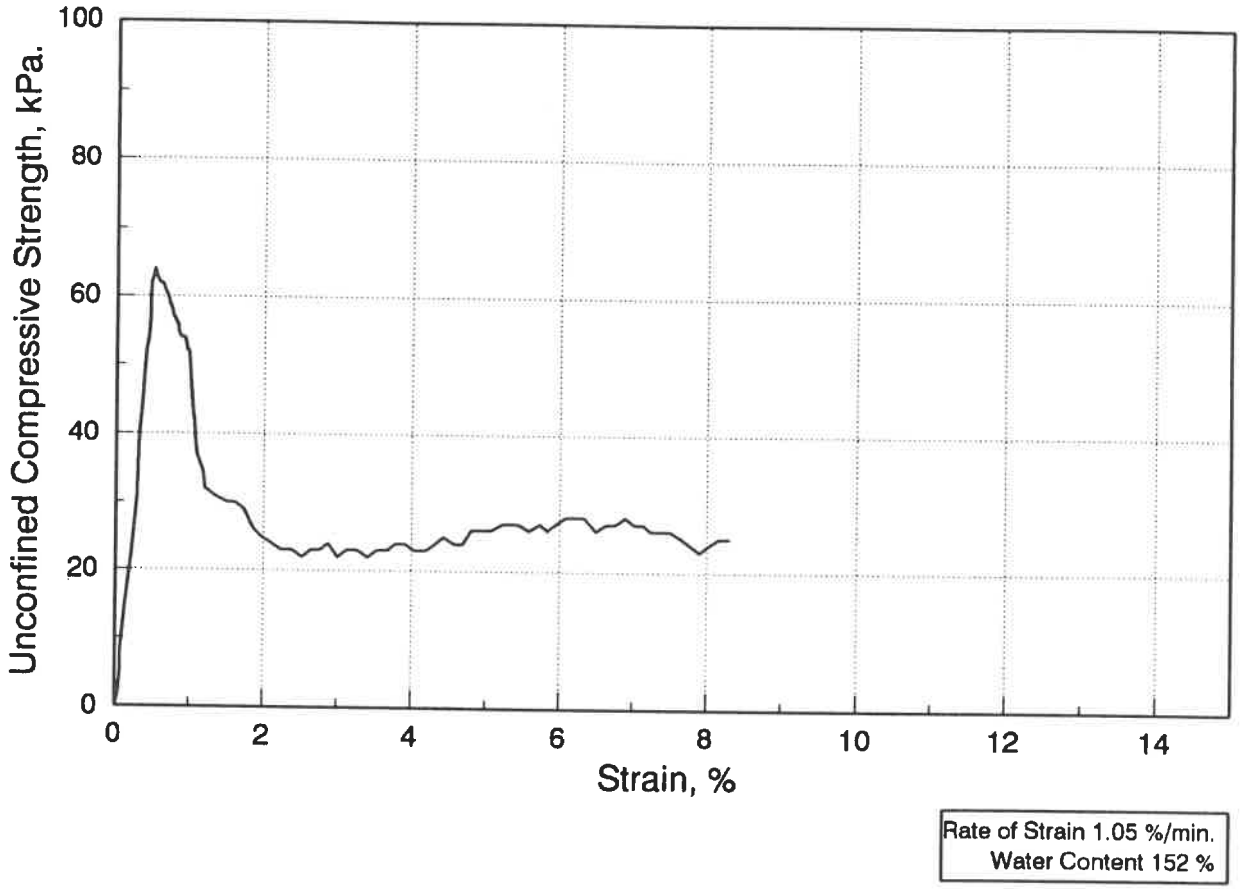

Fig. B.50 Stress-strain curve of the unconfined compression test-180°/1.

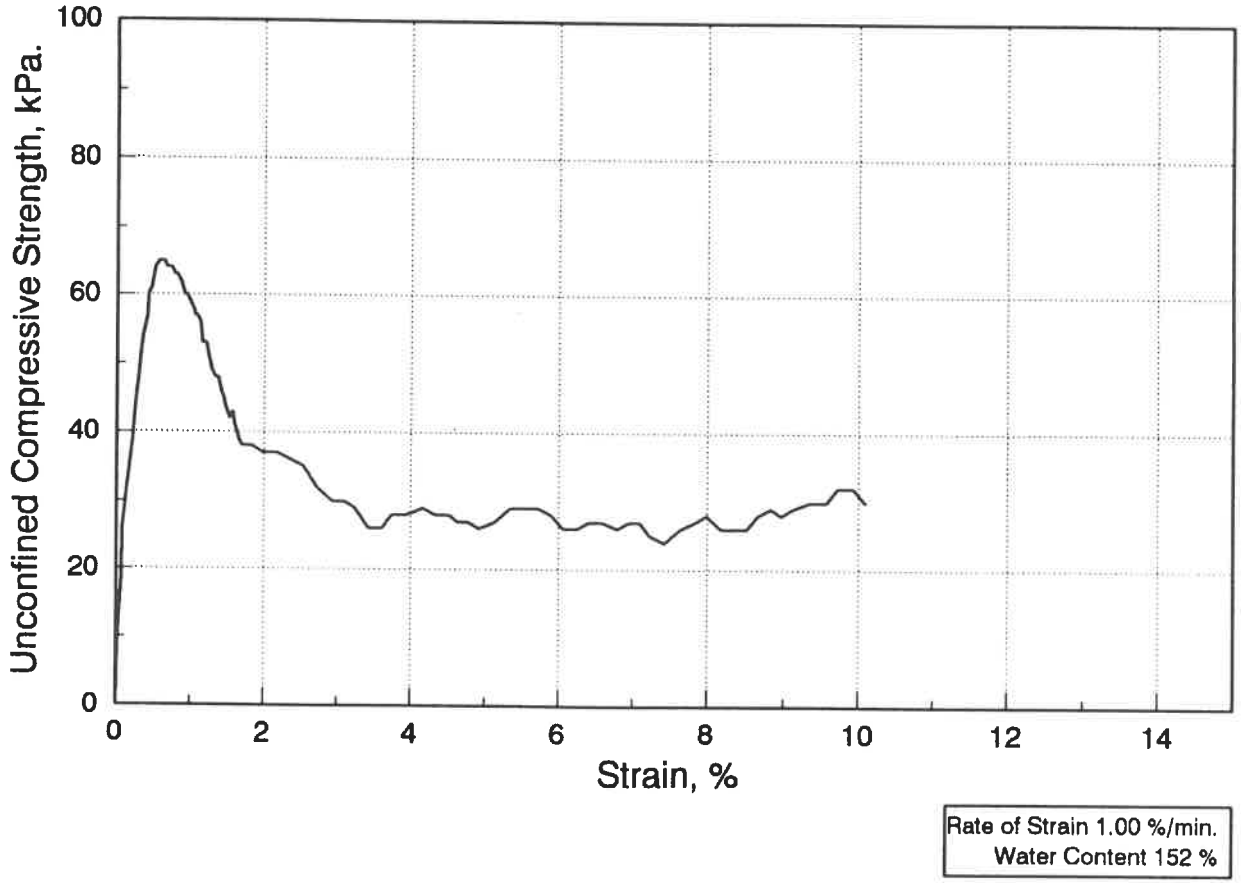

Fig. B.51 Stress-strain curve of the unconfined compression test-180°/2.

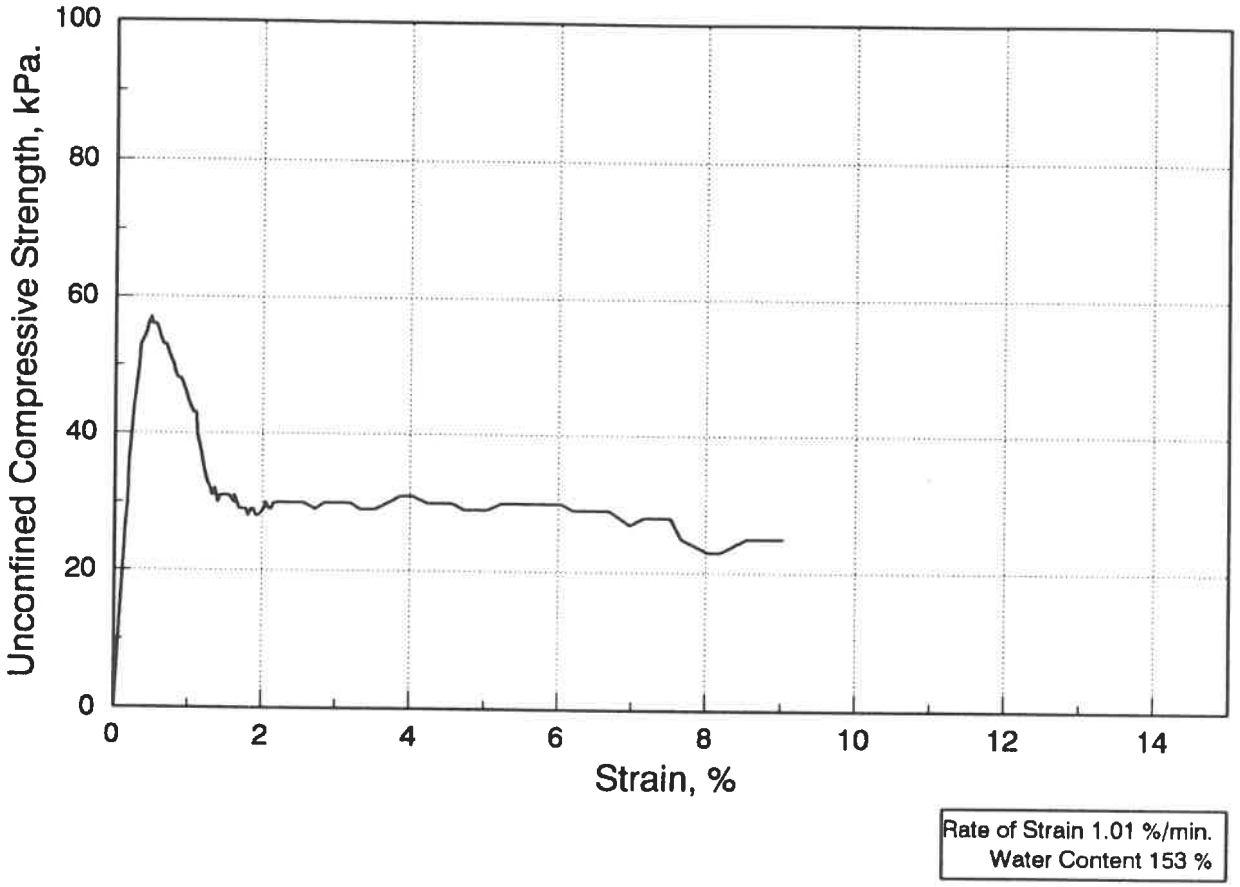

Fig. B.52 Stress-strain curve of the unconfined compression test-180°/3.

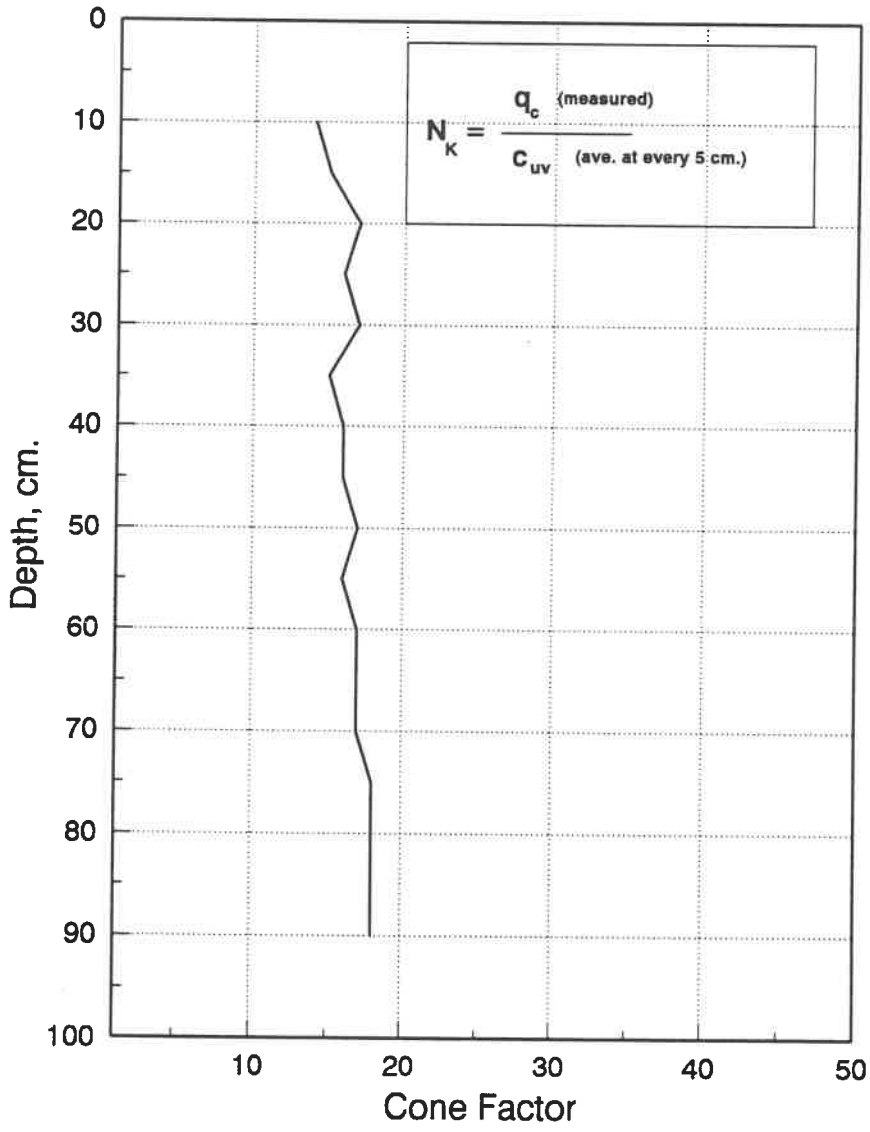

Fig. B.53 Cone factor curve for 7.5° cone apex angle.

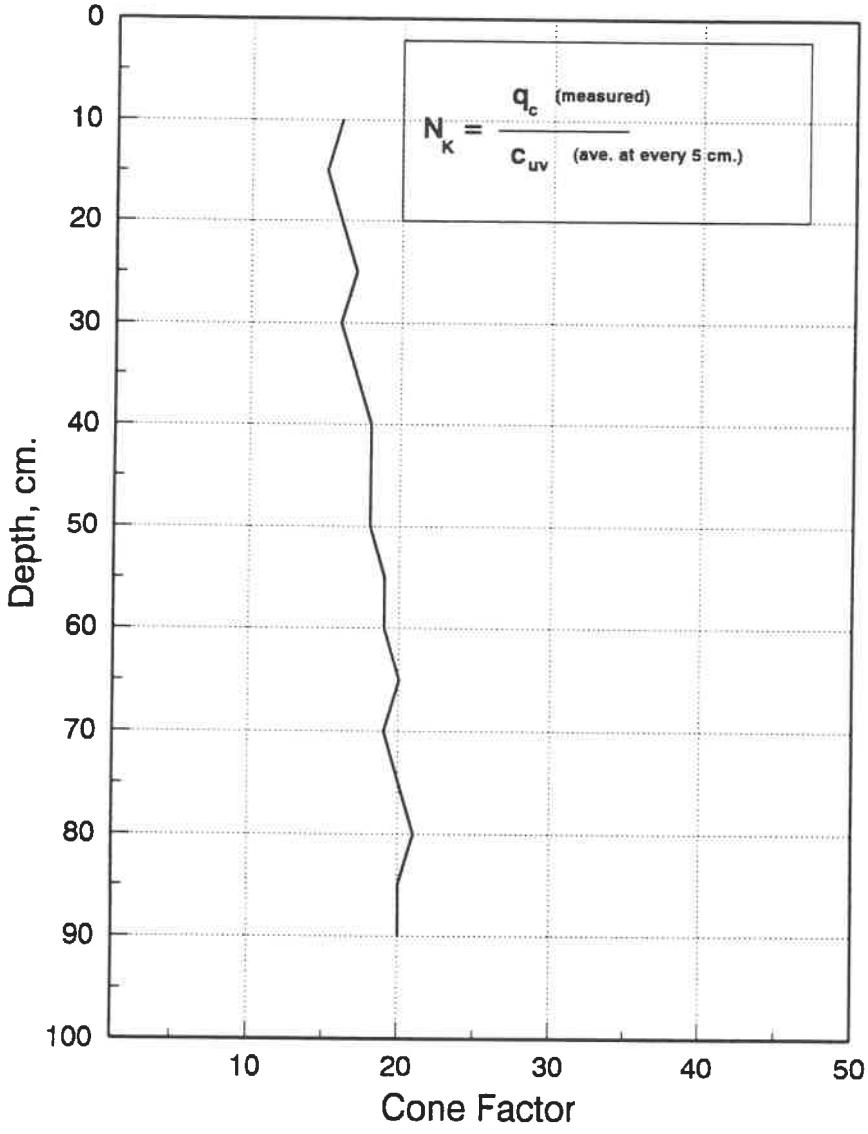

Fig. B.54 Cone factor curve for 15° cone apex angle.

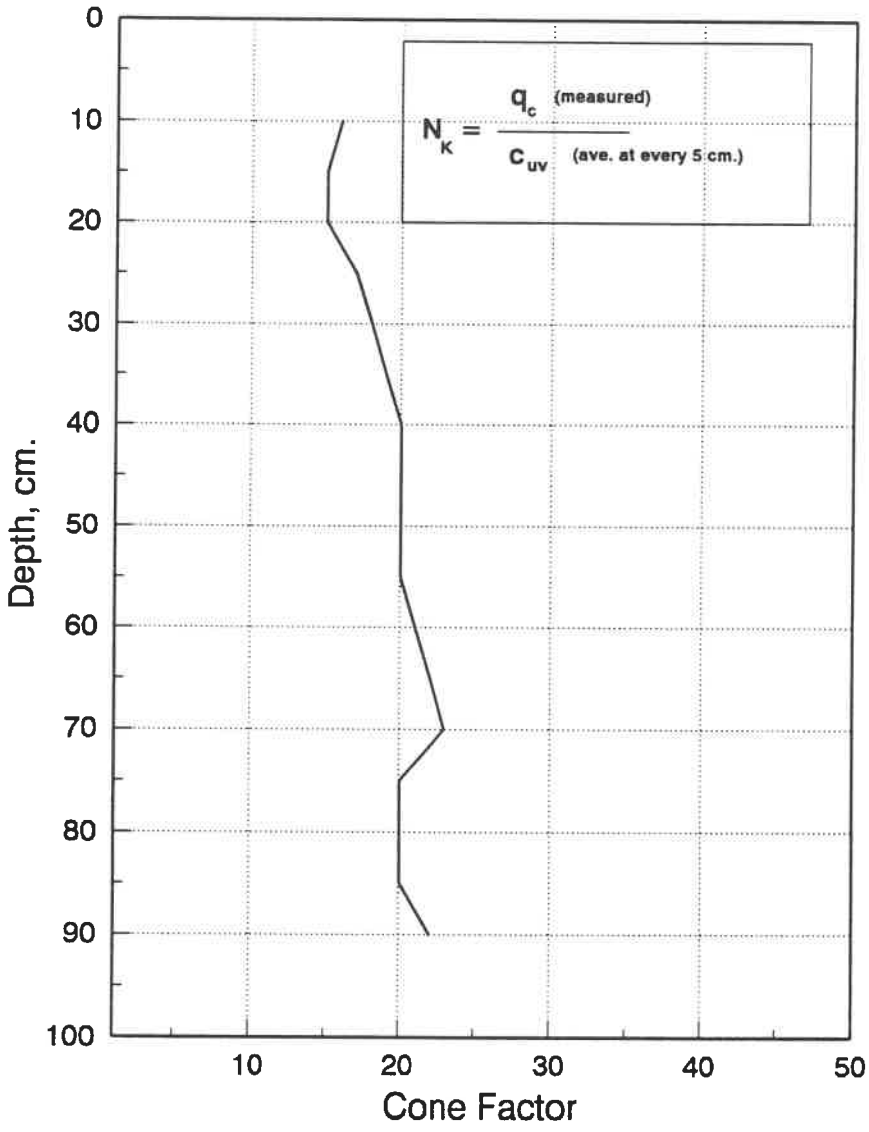

Fig. B.55 Cone factor curve for 18° cone apex angle.

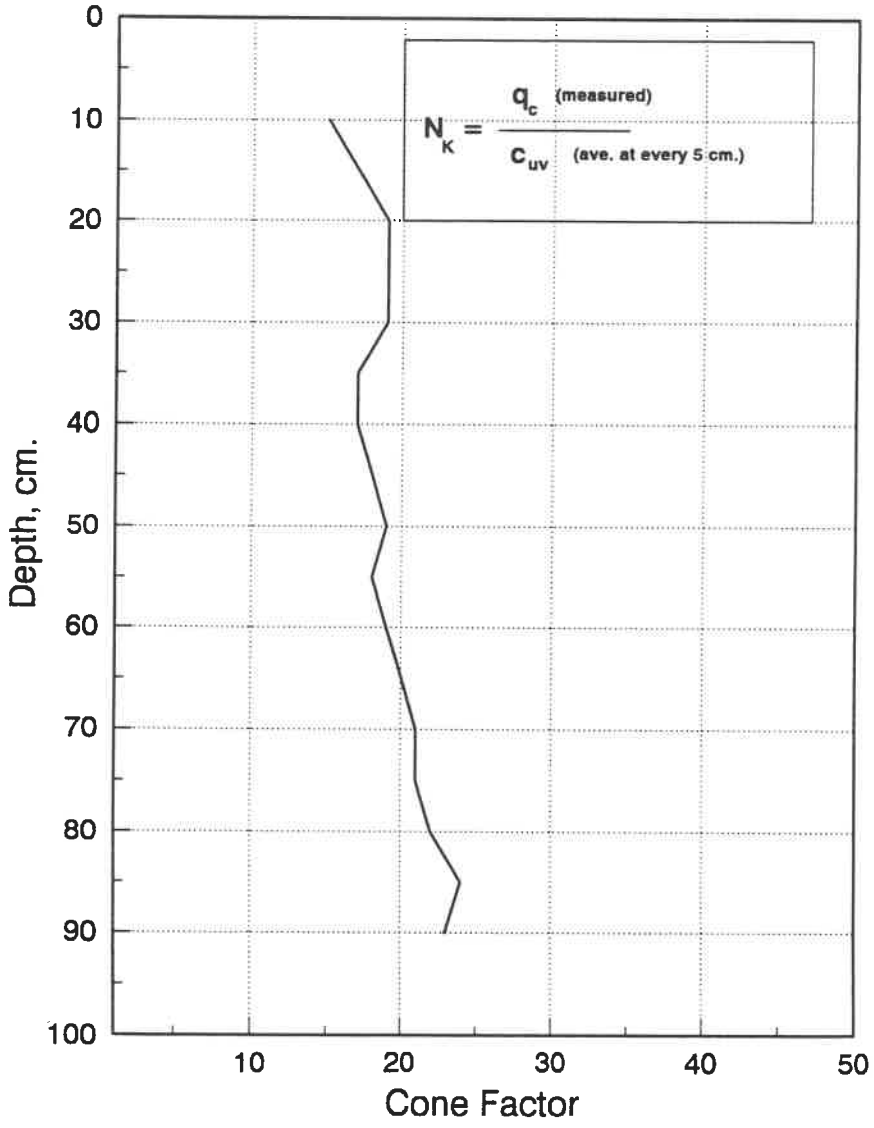

Fig. B.56 Cone factor curve for 22.5° cone apex angle.

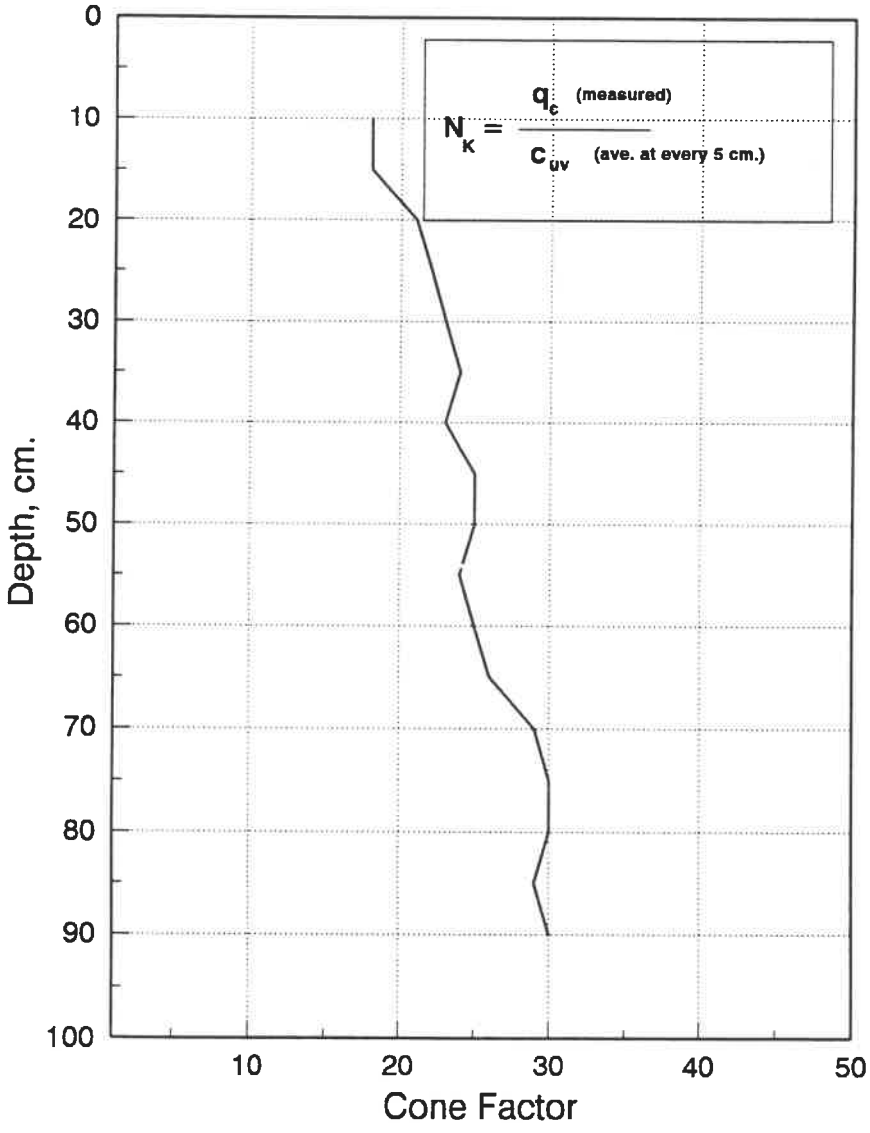

Fig. B.57 Cone factor curve for 45° cone apex angle.

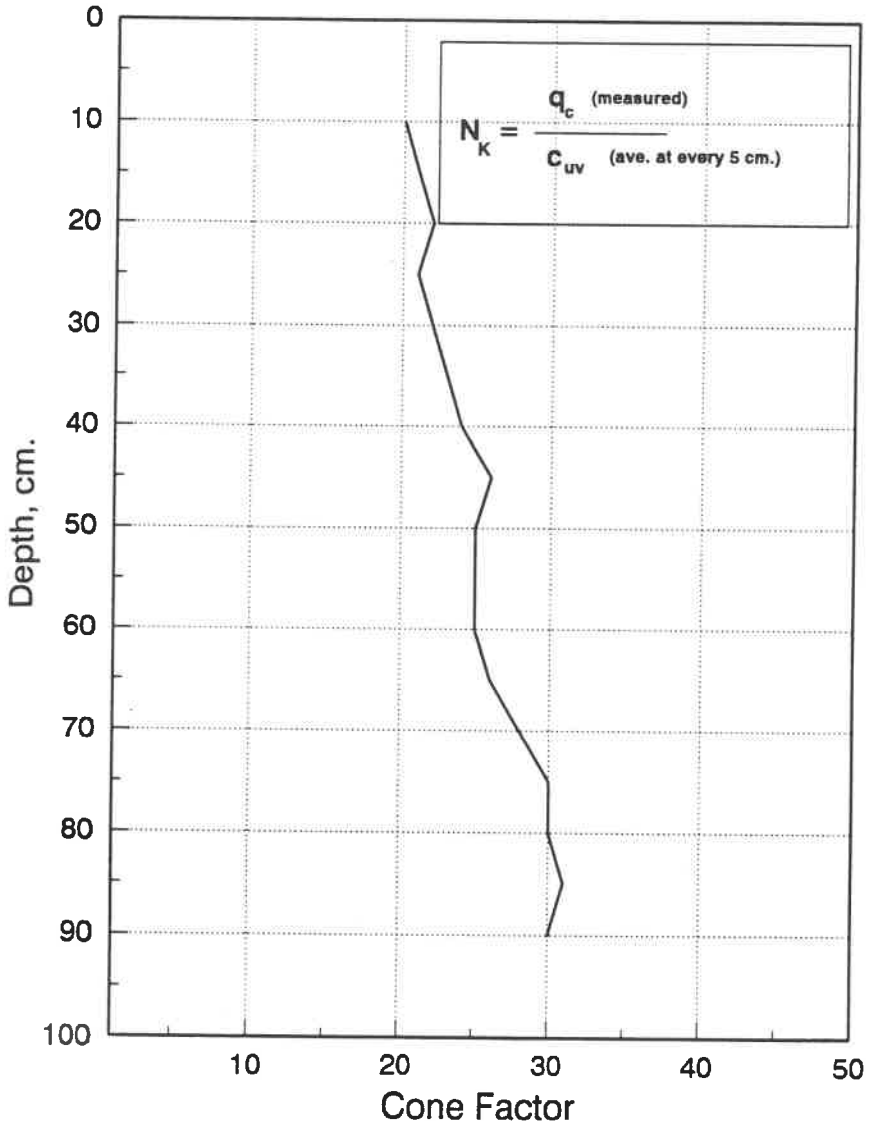

Fig. B.58 Cone factor curve for 60° cone apex angle.

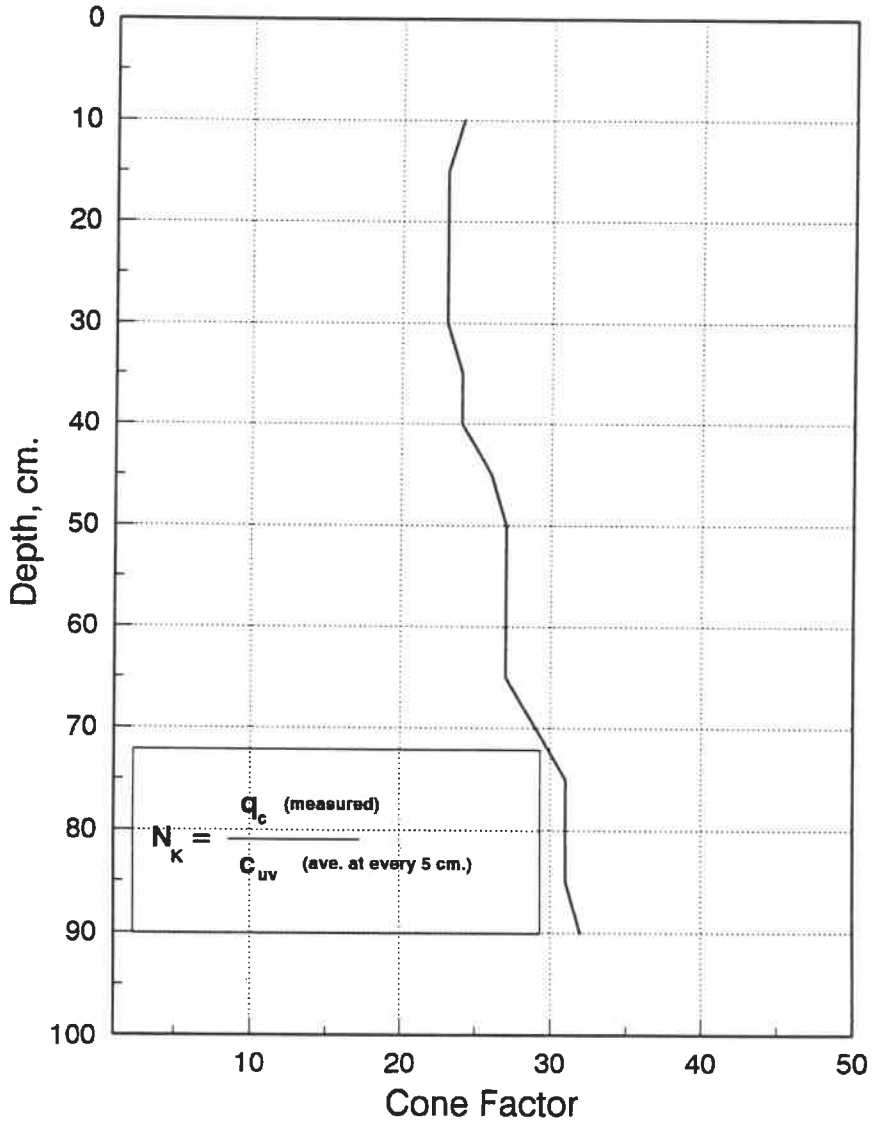

Fig. B.59 Cone factor curve for 90° cone apex angle.

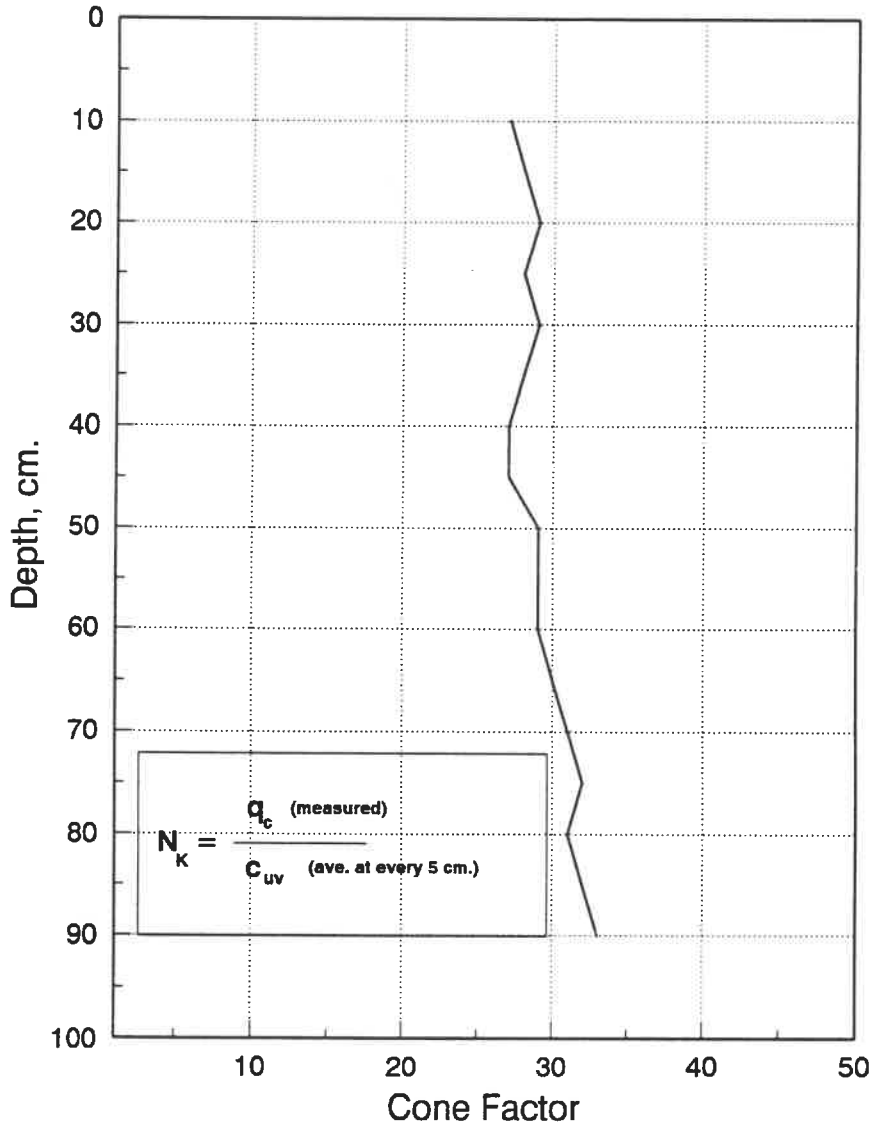

Fig. B.60 Cone factor curve for 180° cone apex angle.

APPENDIX C: PHOTOGRAPHS.

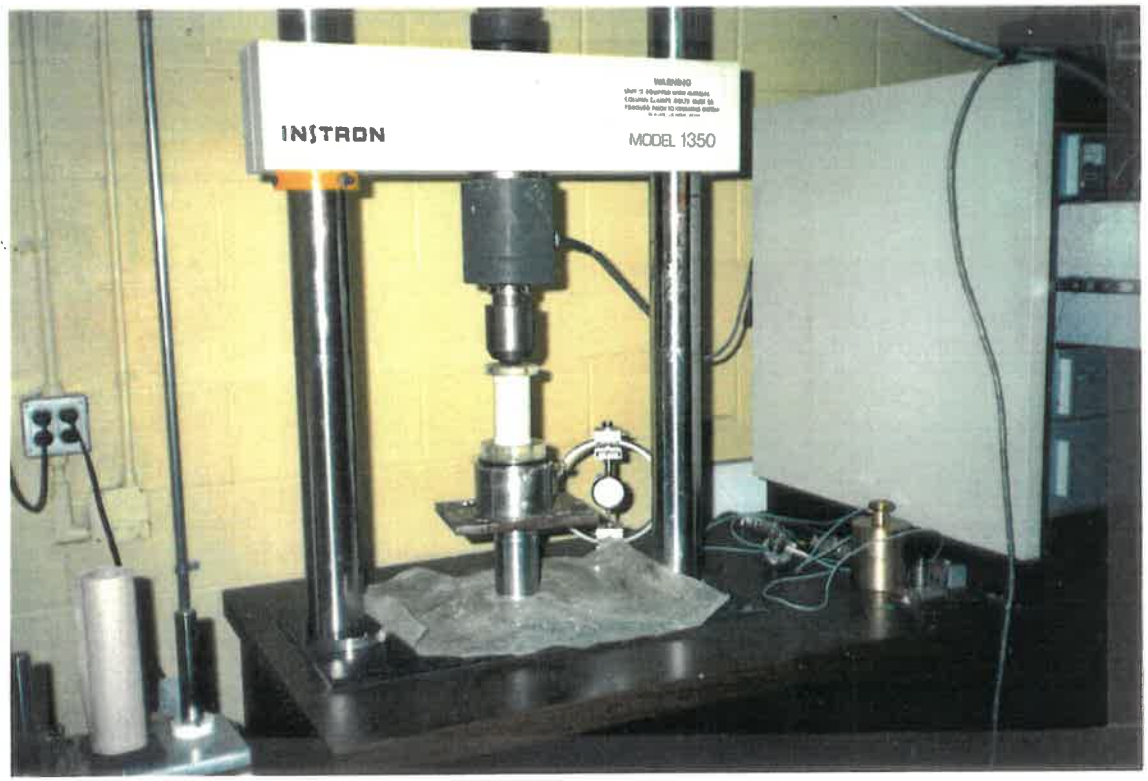

Plate C.1 General view of the unconfined compression test.

Plate C.2 Quasi-static cone penetration test.

Plate C.3 General view of the laboratory vane shear test.

Plate C.4 Unconfined cone penetration test.